3.6 COLLOIDS
(P. Vilks)

3.6.1 Introduction

The transport of radionuclides in groundwater systems can be modelled as a chromatographic process in which radionuclides are partitioned between a mobile fluid phase and an immobile solid phase. However, if radionuclides become attached to mobile solid particles to form radiocolloids, the migration of radionuclides could be increased. There is evidence that particle transport underground does occur and may affect contaminant migration (Neretnieks 1978; Kim et al. 1984; Airey 1984; McDowell-Boyer et al. 1986; Vilks and Drew 1986; Mills et al. 1991). Colloid-facilitated transport would have the greatest effect on the relatively insoluble contaminants, which are considered immobile if transport occurrs only in a dissolved state. It is useful to distinguish between the colloidal particles small enough to remain in stable suspension, and larger particles that require significant water movement and larger fracture apertures to stay in suspension and migrate. In this work groundwater particles have been classified as being either colloids, with diameters between 1 and 450 nm, or suspended particles >450 nm in diameter. Since both colloids and suspended particles can contribute to contaminant transport they have both been investigated, and in this text are often collectively referred to as particles.

Although one of the main objectives of AECL's colloid research program has been to characterize natural particles in groundwater from granite rocks, the Cigar Lake deposit offers a unique opportunity to study colloids formed in the presence of a rich uranium ore, and may be an analog to colloid transport from a used-fuel disposal vault to the geosphere. Because uranium has a low solubility within the deposit, it is an ideal element to use to test the effects of particulate transport. Since piezometers have been emplaced in key locations within the deposit, it was possible to set up a sampling program to look for evidence of colloid transport and to assess the variation of colloids within different parts of the deposit. With the on-site groundwater sampling equipment and laboratory facilities, it was also feasible to carry out detailed experiments on trace-element sorption by colloids and on the effects of groundwater sampling on measured particle concentrations.

The objective of the colloid program at Cigar Lake was to evaluate the likelihood for particle-facilitated transport within the deposit by determining whether the amount of radionuclides and trace elements attached to particles is significant, and whether particles migrate in the subsurface. In this study particle concentrations and compositions have been determined for all parts of the deposit, and trace-element attachment to particles has been investigated to evaluate the amount of a given radionuclide that is likely attached to particles in groundwater. Aspects of particle migration have been addressed by determining particle size distributions, looking for evidence of particle dispersion away from the ore zone, studying particle behaviour in a flow field, and assessing mechanisms of particle generation (Vilks et al. 1988, 1993).

3.6.2 Colloid characterization

3.6.2.1 Methods

Piezometers located in various parts of the deposit have been sampled periodically for colloids and water chemistry since 1986, using a squeeze pump with flow rates between 2 and 25 L/h. Samples for colloid characterization were collected in 50-L, polyethylene carboys that had been flushed with nitrogen to avoid contamination with the atmosphere. To collect enough material for colloid characterization, Millipore tangential-flow ultrafiltration systems were used to produce particle concentrates (2 to 6 L) from 50-L groundwater samples. These concentrates contained enough material for colloid concentration and size analysis, as well as X-ray diffraction analysis (XRD). Chemical and radiochemical analysis of particle concentrates and filtered water provided information on the association of various elements and radionuclides with colloids and suspended particles. The groundwater was not prefiltered before ultrafiltration, to avoid loss of colloids and suspended particles on the prefilter. In the first step (Figure 3.86) particles larger than about 10 nm were concentrated by filtering groundwater through a Pellicon system equipped with 100 000 nominal molecular weight limit (NMWL) polysulfone membrane packets, separated by retentate screens (Vilks et al. 1991). The concentrate (retentate) produced by the 100 000-NMWL filter was filtered with the Minitan tangential flow filtration system (Millipore), equipped with a 450-nm cut-off Durapore membrane. This produced a filtrate containing colloids between 10 and 450 nm, and a concentrate enriched in suspended particles >450 nm. Ten litres of filtrate produced by the initial 100 000-NMWL filtration were filtered through another Pellicon system, equipped with a 10 000-NMWL polysulfone filter cassette. This produced a sample of filtered water containing only dissolved species, and a concentrate enriched in colloids with a size range between 10 000 NMWL (~ 1 nm) and 100 000 NMWL (~ 10 nm). The filtrate and concentrate samples to be used for chemical and radiochemical analysis were preserved by acidifying to pH 1 with HCl.

Particle concentrations and size distributions were measured by pressure-filtering 20 to 50 mL of particle concentrates through a series of 25-mm Nuclepore polycarbonate filters with cutoff sizes of 10 000, 5000, 1000, 400, 100, 50 and 10 nm. Particle concentrations were determined by the weight of material deposited on the filters. The presence of colloidal material in the 1- to 10-nm size range was determined by comparing the chemical composition of colloid concentrates with that of filtered water. The material deposited on Nuclepore membranes was examined by scanning electron microscopy with energy dispersive X-ray analysis (SEM/EDX) to identify particle compositions and to evaluate visually the effectiveness of the particle size separation. Samples for XRD were prepared by filtering particle concentrates through a 450-nm silver membrane.

The major- and trace-element compositions of particle concentrates and filtered water were determined by atomic absorption and inductively coupled plasma spectrometry. Inorganic and organic carbon compositions were determined by the Astro 2001 carbon analyzer with a detection limit of 0.02 mg/L. Uranium concentrations were determined by fluorometry

using the Scintrex system with a detection limit of 0.05 μg/L. Uranium, Th and Ra isotope activities were determined by chemical separation and alpha spectrometry (Chiu and Dean 1984; Gascoyne and Larocque 1984).

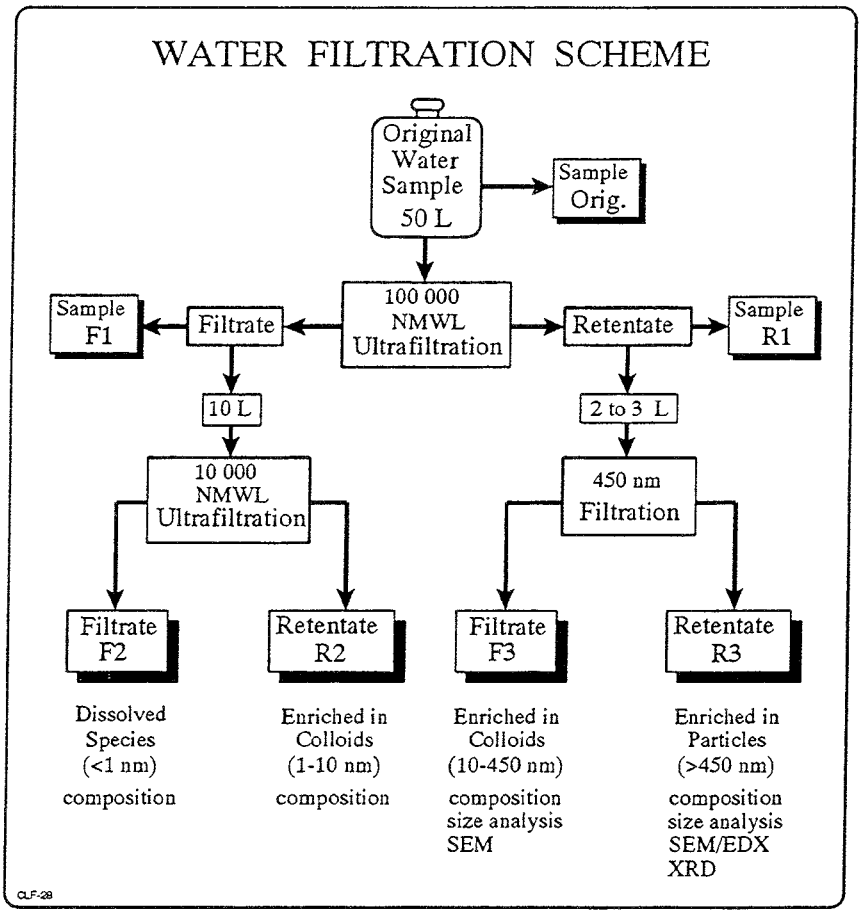

FIGURE 3.86 Diagram illustrating the scheme for fitration of groundwater samples to obtain both filtrates (F1, F2 and F3) and retentates (R1, R2 and R3).

3.6.2.2 Particle concentrations within deposit

Average particle concentrations for key parts of the deposit, including groundwaters flowing toward and away from the deposit above the unconformity, are shown in Table 3.39. As discussed in Section 3.6.3, particle concentrations are often higher when a borehole is sampled for the first time. With continued pumping from the borehole, particle concentrations decrease and fluctuate between lower values. These high initial suspended particle concentrations were not included in the calculation of average particle concentrations, since these values may have represented drilling artifacts. Boreholes shown without calculated errors have been sampled only once for colloids. Suspended particle

concentrations are determined more by the integrity of the local rock than by geological formation. For example, particle concentrations are much higher in altered basement rock (hole 199) than in well-consolidated basement rock (hole 137). In the clay zone, only borehole 91, which is connected to a fracture zone, has high concentrations of suspended particles. With the exception of two holes from the basement, colloid concentrations are fairly uniform throughout the deposit. The particle concentrations in shallow overburden waters can be much higher than in the deep groundwaters.

3.6.2.3 Particle composition

The results of SEM/EDX and XRD analysis have shown that suspended particles and colloids larger than about 50 nm consist mostly of clay minerals (illite with chlorite and kaolinite), X-ray amorphous Fe-Si precipitates, quartz, and organic particles.

The composition of colloids smaller than 50 nm must be inferred from the chemical analysis of colloid concentrates. This method does not distinguish individual types of colloids, and is not very sensitive to some elements, such as Si, which may have a high dissolved concentration. By analyzing the filtrate and retentate samples produced during groundwater filtration (Figure 3.86), it is possible to calculate the groundwater concentrations of a given element associated with dissolved species, colloids from 1 to 10 nm, colloids from 10 to 450 nm, and suspended particles larger than 450 nm. The concentration of dissolved elements is given by

$$\text{dissolved concentration} = F2 \tag{1}$$

where F2 represents element concentrations in the F2 filtrate. The groundwater concentrations of elements associated with colloids between 1 and 10 nm is given by

$$\text{colloids(1-10 nm)} = (R2-F2)/C2 \tag{2}$$

where R2 represents element concentrations in retentate R2, and C2 is the colloid concentration factor during filtration with the 10,000 NMWL membrane. The concentration factor is given by the sample volume before filtration divided by the volume of retentate. The concentrations of elements associated with colloids between 10 and 450 nm can be calculated from equation 3 or equation 4. The reported value for these concentrations is the average of equations 3 and 4.

$$\text{colloids(10-450 nm)} = (F3-F1)/C1 \tag{3}$$

$$\text{colloids(10-450 nm)} = (R1-F1)/C1 - \text{particles } (>450 \text{ nm}) \tag{4}$$

TABLE 3.39
SUMMARY OF PARTICLE CONCENTRATIONS IN
CIGAR LAKE GROUNDWATERS (1986-1991)

Hole #	Susp. Part. mg/L	Colloids mg/L	Depth m	Comments
75	0.63 ±0.14[a]	0.83 ±0.26	154-159	upper sandstone
71	1.76 ±0.42	0.73 ±0.16	243-245	lower sandstone
80	1.42	0.77	203-205	lower sandstone
67	1.90 ±0.21	1.33 ±0.30	346-348	altered sandstone
211	1.89 ±0.49	0.81 ±0.17	416-418	altered sandstone
91	4.92 ±1.48	0.60 ±0.09	407	clay zone *
134	0.61	0.94	415-417	clay zone
197	0.64 ±0.13	0.72 ±0.19	416-421	ore/clay contact
79	2.23 ±0.67	0.78 ±0.15	432	ore
198	2.86 ±0.98	1.52 ±0.29	424-426	ore
220	1.87 ±0.41	1.44 ±0.38	433-439	ore
128	0.74	2.21	463-465	basement
137	0.81	0.03	473-475	basement
199	106 ±2.3	7.78 ±4.14	446-452	altered basement
139	1.73 ±0.60	0.65 ±0.16	437	inflow south **
81	9.20 ±2.48	1.77 ±0.63	438	outflow north ***
219	0.83 ±0.15	0.95 ±0.15	414-426	outflow north ****
83	1.27 ±0.41	1.11 ±0.36	18-477	artesian
122	1.00 ±0.19	1.37 ±0.35	0-200	artesian
P3.12	1.75 ±0.08	0.91 ±0.24	4-7	overburden #
P3.8	18.10 ±1.4	13.00 ±4.9	10-22	overburden #
P3.7	20.50 ±3.8	10.30 ±2.7	10-23	overburden #

* Based on hydrologic observations, this piezometer appears to be set near a major fracture zone.

** Located just above the unconformity.

*** Located just above the unconformity, near the clay zone. From the core log, the piezometer is set in altered sandstone, near a fracture.

**** Located just above the unconformity, beyond the quartz cap.

\# Sampled with peristaltic pump.

a The error values are given for boreholes for which more than one sample was taken, and are given by the standard deviation divided by the square root of the number of data points.

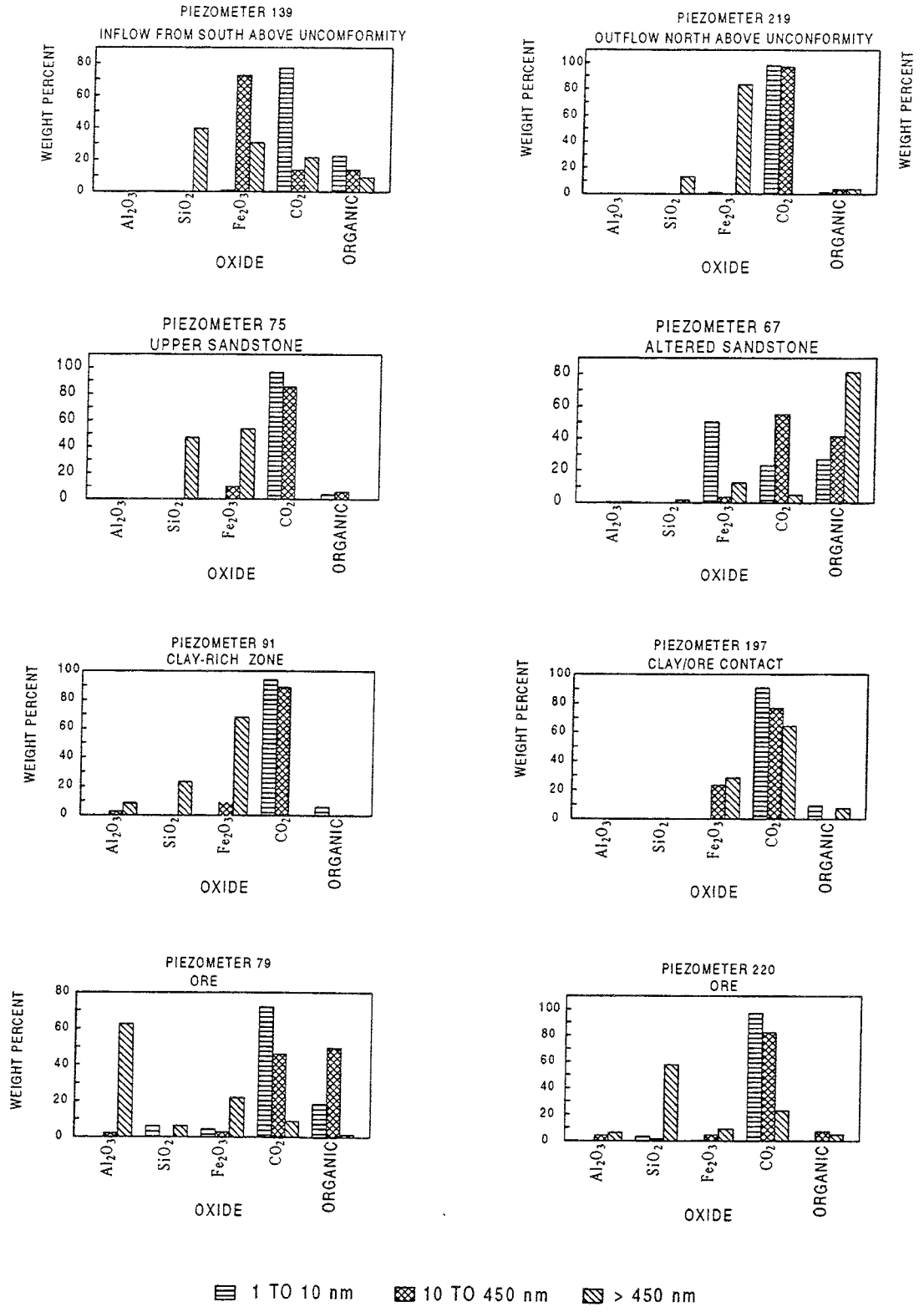

FIGURE 3.87 Compositions of colloids and suspended particles in Cigar Lake selected groundwaters.

In the above equations F3 represents element concentrations filtered through the 450 nm filter, F1 is the filtrate from the 100,000 NMWL membrane, R1 is the retentate from the 100,000 NMWL filtration, and C1 is the colloid concentration factor for the 100,000 NMWL filtration. The concentrations of elements associated with suspended particles is given by the average of equations 5 and 6.

$$\text{particles}(>450\text{ nm}) = (R3-F3)/C3/C1 \quad (5)$$

$$\text{particles}(>450\text{ nm}) = (R1-F3)/C1 \quad (6)$$

Since the fraction of dissolved salts concentrated along with colloids can be between 0 and 4 %, it is necessary to account for salt retention when calculating colloid compositions from particle concentrates. First the percent of a given element's groundwater concentration, which is enriched in the particle concentrate, is calculated. Then the measured percent salt retention, determined by conductivity, is subtracted from this value. The amount of the given element associated with colloids is calculated from the "corrected" percent.

TABLE 3.40
AVERAGE RADIONUCLIDE CONCENTRATIONS
IN GROUNDWATER PARTICLES FROM CIGAR LAKE

Zone	Uranium μg/L	Thorium μg/L	Radium-226 Bq/L
Lower sandstone (LSS)	183 ±120	11	1
Upper sandstone (USS)	120 ± 12		
Altered sandstone (AS)	190 ± 35		
Artesian (USS + LSS)	67 ± 34	9 ± 1	4 ± 1
Inflow from south (LSS)	58 ± 17	0	4
Outflow to north (LSS)	124 ± 98	5 ± 0	15 ± 8
Clay	470 ±121	6 ± 4	20 ± 6
Clay/Ore contact	323 ±138	15 ± 8	57 ± 18
Ore	623 ±126	21 ± 10	62 ± 12
Basement	80 ± 26	11 ± 8	6 ± 4

Figure 3.87 summarizes the major oxide-forming element compositions of colloids and suspended particles for selected samples. Aluminum, which was observed in particles larger than 10 nm and which indicates the presence of clay, is present in higher concentrations in parts of the clay and ore zones. The absence of aluminum in piezometer 197 at the clay/ore contact is consistent with the presence of stable local rock conditions, which generate only low particle concentrations. Silica concentrations are usually higher in the suspended particles and larger colloids, and indicate the presence of quartz, clay or Fe-Si hydroxides.

Iron is more dominant in suspended particles and the larger colloids (10-450 nm), suggesting that precipitated Fe oxyhydroxide colloids are metastable and either recrystallize or form coatings on larger particles. Carbonate is associated with particles in all locations, and constitutes a major fraction of colloids between 1 and 10 nm. Organic carbon is present in all particle size classes and may include humic materials, bacteria and organic coatings on particles. Concentrations of organic carbon appear to be higher in the altered sandstone (not shown in Figure 3.87) and parts of the ore body. This carbon may have been derived from reaction products produced by the hydrothermal degradation of graphite beneath the ore body at the time of ore formation, and it may include bitumens sorbed onto particles.

TABLE 3.41
URANIUM AND THORIUM ISOTOPE RATIOS IN SOLUTION AND IN PARTICLES

Sample #	Dissolved $^{234}U/^{238}U$	Particulate $^{234}U/^{238}U$	Dissolved $^{230}Th/^{234}U$	Particulate $^{230}Th/^{234}U$
198A		1.63 ±6.87		0.014 ±0.023
198B	2.64 ±0.16	1.15 ±0.08	0.004 ±0.003	0.069 ±0.052
198C	1.78 ±0.25	1.14 ±0.17	0.007 ±0.033	0.038 ±0.192
198D	1.67 ±1.94	1.64 ±1.92	0.867 ±0.851	0.154 ±0.154
197A	1.48 ±0.18	1.62 ±0.20	0.023 ±0.023	0.004 ±0.004
197B	1.70 ±0.05	1.26 ±0.07	0.006 ±0.002	0.047 ±0.020
197C	1.87 ±0.08	1.58 ±0.11	0.003 ±0.002	0.021 ±0.016
197D	1.59 ±0.09	5.92 ±0.66	0.001 ±0.003	0.548 ±1.105
81A	2.14 ±0.40	6.43 ±1.70	0.067 ±0.028	0.023 ±0.012
81B	4.00 ±1.33	2.15 ±0.78	0.059 ±0.038	0.031 ±0.025
91A	1.49 ±0.02	1.51 ±0.03	0.001 ±0.000	0.055 ±0.022
91B	1.48 ±0.04	1.67 ±0.05	0.001 ±0.001	0.006 ±0.004
91C	1.56 ±0.13	1.39 ±0.11	0.006 ±0.006	0.003 ±0.003
91D	1.53 ±0.19	1.47 ±0.18	0.011 ±0.011	0.006 ±0.006
91E	1.57 ±0.11	1.51 ±0.11	0.017 ±0.009	0.017 ±0.009
199A	2.04 ±0.13	1.84 ±0.14	0.005 ±0.006	0.095 ±0.127
199B	2.38 ±0.16	1.13 ±0.08	0.006 ±0.006	0.243 ±0.244
199C	1.89 ±0.08	0.87 ±0.05	0.002 ±0.002	0.071 ±0.107
Average	1.93 ±0.15	1.99 ±0.36	-	-

The major-element compositions are not useful for mapping particle dispersions from the ore zone, because the compositions of particles in the ore are not significantly different from those in other parts of the deposit. However, uranium and radium are potential tracers for particle migration because they have above-background concentrations in the ore zone.

From Table 3.40 it is apparent that the average uranium concentrations are significantly higher for particles in the ore and clay zones than in other parts of the deposit. The uranium concentrations for particles in the outflow from the deposit to the north are not significantly higher than in the sandstones surrounding the deposit, indicating that there is no measurable plume of uranium-rich particles migrating beyond the clay. Average ^{226}Ra activities (Bq/g) are also higher in particles found in the ore and clay zones than other parts of the deposit. Although thorium concentrations ($\mu g/g$) are also higher within the clay and ore, the difference is not significant because of the low Th concentration within the ore.

TABLE 3.42
DISSOLVED AND PARTICULATE RADIUM AND THORIUM ACTIVITIES

Sample	Dissolved (Bq/L)		Particulate (Bq/L)	
	^{226}Ra	^{230}Th	^{226}Ra	^{230}Th
198A	0.18	0.0005	0.13	0.00002
198B	3.65	0.0003	1.54	0.001
198C	1.41	0.00007	0.69	0.0001
198D	0.15	0.0009	0.20	0.0002
197A	0.46	0.0003	0.22	0.00005
197B	0.88	0.0009	0.16	0.00005
197C	0.66	0.0002	0.22	0.00006
197D	0.14	0.00007	0.13	0.0001
81A	0.06	0.0003	0.29	0.0002
81B	0.06	0.0005	0.04	0.00003
91A	0.34	0.0003	1.50	0.001
91B	0.30	0.0002	0.82	0.0003
91C	0.00	0.0001	0.40	0.0002
91D	0.40	0.0001	0.75	0.00008
91E	0.21	0.0003	0.42	0.0004
199A	0.20	0.0002	0.25	0.001
199B	0.03	0.0003	0.19	0.002
199C	0.39	0.0001	0.42	0.0004

The $^{234}U/^{238}U$ and $^{230}Th/^{234}U$ activity ratios for uranium and thorium in solution and on particles (>1 nm) are compiled in Table 3.41. While the $^{234}U/^{238}U$ ratios in rock samples vary between about 0.8 and 1.0 (unpublished results), the activity ratios are significantly higher than 1.0 for dissolved uranium (average= 1.93 ± 0.15) and particulate uranium (average= 1.99 ± 0.36). The $^{234}U/^{238}U$ ratios in groundwater are higher than 1.0 because of the preferential leaching of the alpha-recoil daughter ^{234}U from rock surfaces. The uranium

associated with particles was most likely acquired from groundwater because the $^{234}U/^{238}U$ ratios for dissolved and particulate uranium are similar. In boreholes with high particle concentrations (198 and 199) the particulate $^{234}U/^{238}U$ ratios tend to be lower than the dissolved ratios, probably because a larger portion of the uranium may have been inherited from the rock in the form of suspended particles. While ^{230}Th is in secular equilibrium with its parent, ^{234}U, in the rock, the dissolved $^{230}Th/^{234}U$ ratio is significantly below 1.0 (average= 0.06 ± 0.05). The particulate $^{230}Th/^{234}U$ ratio is also well below 1.0, indicating that U has sorbed onto particles and ^{230}Th has not had enough time to come into secular equilibrium with its parent. If it is assumed that ^{230}Th on particles has ingrown from ^{234}U attached to particles, then the oldest age of these particles may be 8000 a. This is based on sample 91A, whose particulate isotopic ratio is significantly higher than the dissolved ratio. The activities of ^{226}Ra and ^{230}Th given in Table 3.42 show that the dissolved $^{226}Ra/^{230}Th$ ratios are also much greater than 1.0, because Ra is more soluble than Th. The particulate $^{226}Ra/^{230}Th$ ratios greatly exceed the ratios for rock, which are less than 2.5, indicating that particles acquire most of their Ra from solution.

Trace-element concentrations associated with colloids and suspended particles in selected parts of the deposit are given in Table 3.43. Most of the trace elements do not show a correlation with location within the deposit, and cannot be used as a tracer for particle migration. Although Mo appears to be higher in the ore and clay zones, its high concentration in hole 71 suggests that Mo may be associated with particles in other parts of the deposit. The source of Mo is probably molybdenite associated with sulfides within the ore. Since Zn concentrations in suspended particles are highest in the ore and clay zones, Zn may have some use as a tracer for particles formed in regions containing sulfides. In many samples the trace-element concentrations in colloids are higher than in suspended particles, suggesting that the higher specific surface area of colloids has been a factor in trace element sorption by colloids and suspended particles.

3.6.3 Behaviour during sampling

During sampling of water from selected piezometers the pumping rate was varied to determine whether higher sampling rates would produce higher concentrations of colloids and suspended particles. Particle concentrations were not affected by pump rates between 4 and 25 L/h. The observed variations in suspended particle concentrations appeared to result from piezometer flushing and not from a change in the pumping rate.

Many piezometers have been sampled periodically during different field campaigns since 1986, providing a record of changes in particle concentrations as a function of borehole flushing (Table 3.44). Two examples of changes in particle concentration with continual sampling are shown in Figure 3.88. In most boreholes (such as 139) the concentrations of suspended particles decreased during the collection of the first 350 L. Although these concentrations varied during subsequent sampling periods, they did not recover to the original values. On the other hand, colloid (10 to 450 nm) concentrations could not be

permanently reduced by continued borehole flushing. During a given sampling period, the colloid concentrations typically decreased with progressive sampling. However, at the beginning of the next sampling period these concentrations had recovered to previous levels. This pattern was not observed in some boreholes, such as the ones collecting water from the ore zone (hole 79), where the hydraulic conductivity is low. In these holes particle concentrations may actually increase during a sampling period. Since the formation permeability is low, the water level in the piezometer may drop by as much as 10 m during sampling. The resulting increase in the pressure differential between the piezometer and the formation may mobilize additional colloids, resulting in higher particle concentrations.

The initial decline in suspended particles could be attributed to the removal of drilling artifacts or easily mobilized particles near the piezometer intake. The variation in particle concentrations during subsequent sampling periods suggests that there is a mechanism for reducing particle concentrations and a mechanism for regenerating these concentrations for the beginning of the next sampling period.

Particle concentrations could be reduced because the water being drawn toward the piezometer from other parts of the formation carries a lower particle concentration, since suspended particles may not travel with the velocity of groundwater. Another cause for the reduction in colloid concentrations may be particle filtration in constricted pore spaces. When groundwater flow is induced by sampling, particles are mobilized, and preferential particle deposition may occur at constrictions in the pore spaces. As particle deposition begins to form "log jams" in pore spaces there is an increase in particle filtration and a possible reduction in formation permeablity.

During periods of no sampling, particle concentrations may be regenerated as the "log jams" are dispersed by double layer repulsions (since the ionic strength is usually less than 0.003) combined with natural groundwater flows. Particle concentrations may also be increased by the precipitation of Fe oxyhydroxides or the formation of new alteration products on mineral surfaces. However, since no systematic changes in the composition of particles has been observed in a given sampling period, it is unlikely that Fe precipitation plays a role in regenerating particles between sampling periods.

Piezometers were usually flushed with pressurized N_2-gas before a given sampling period to draw fresh formation water into the standpipe. The possibility that this process produced higher particle concentrations at the beginning of the sampling period was investigated by carrying out the flushing in the middle of a sampling period instead of at the beginning. As shown in Figure 3.88, the particle concentrations in borehole 139 were not affected by N_2 flushing.

TABLE 3.43
TRACE-ELEMENT CONCENTRATIONS (μg/g) IN
COLLOIDS AND SUSPENDED PARTICLES

ZONE	HOLE	Mn COLL.*	Mn >450 nm	Ba COLL.	Ba >450 nm	Mo COLL.	Mo >450 nm
lower SS	71	5	6371	0	828	1213	376
altered S	67	0	1144	229	0	0	0
	67	14112	1512	359	70	0	0
	67	10043	6053	286	348	0	0
	mean	8052	2903	291	139	0	0
clay	197	1502	0	154	77	0	1617
	197	303	603	13	28	0	885
	197	26	53	0	36	602	0
	mean	610	219	56	47	201	834
ore	79	0	16	0	337	499	0
	79	2060	160	0	320	0	0
	79	0	880	0	1092	0	0
	220	2565	1021	875	254	1555	42
	220	4213	879	756	0	1176	0
	220	1571	990	480	255	2664	301
	mean	1735	658	352	376	982	57
inflow S	139	327	1133	0	0	0	0
	139	11022	3665	3062	604	0	0
	mean	5675	2399	1531	302	0	0
outflow N	219	5330	1323	487	0	0	0
	219	884	1053	115	79	0	0
	mean	3107	1188	301	40	0	0
artesian	83	0	1910	73	0	0	0
	122	670	0	0	113	0	0
	mean	335	955	37	57	0	0

* COLLOID: colloids from 10 to 450 nm
>450 nm: suspended particles >450 nm

TABLE 3.43 (concl.)
TRACE-ELEMENT CONCENTRATIONS (μg/g) IN
COLLOIDS AND SUSPENDED PARTICLES

ZONE	HOLE	Sr COLL.*	Sr >450 nm	Zn COLL.	Zn >450 nm	Li COLL.	Li >450 nm
lower SS	71	0	351	0	0	0	0
altered S	67	608	114	900	52	117	0
	67	1735	179	2124	433	19	0
	67	422	3594	525	174	0	0
	mean	922	1296	1183	220	45	0
clay	197	80	0	1183	5224	111	538
	197	2913	1005	2438	3217	115	281
	197	398	0	15	0	0	21
	mean	1130	335	1212	2814	75	280
ore	79	0	224	0	5339	0	0
	79	0	1602	3197	13293	0	240
	79	0	729	0	17690	0	57
	220	591	163	2768	713	0	6
	220	0	753	48003	8412	239	0
	220	2771	0	901	617	220	49
	mean	560	579	9145	7677	77	59
inflow S	139	42	0	1472	809	552	0
	139	3892	0	11194	582	0	216
	mean	1967	0	6333	696	276	108
outflow N	219	1392	364	292	308	0	0
	219	395	421	170	89	18	0
	mean	894	393	231	199	9	0
artesian	83	364	0	4667	0	16	264
	122	101	0	1764	0	435	0
	mean	233	0	3216	0	226	132

* COLLOID: colloids from 10 to 450 nm
>450 nm: suspended particles >450 nm

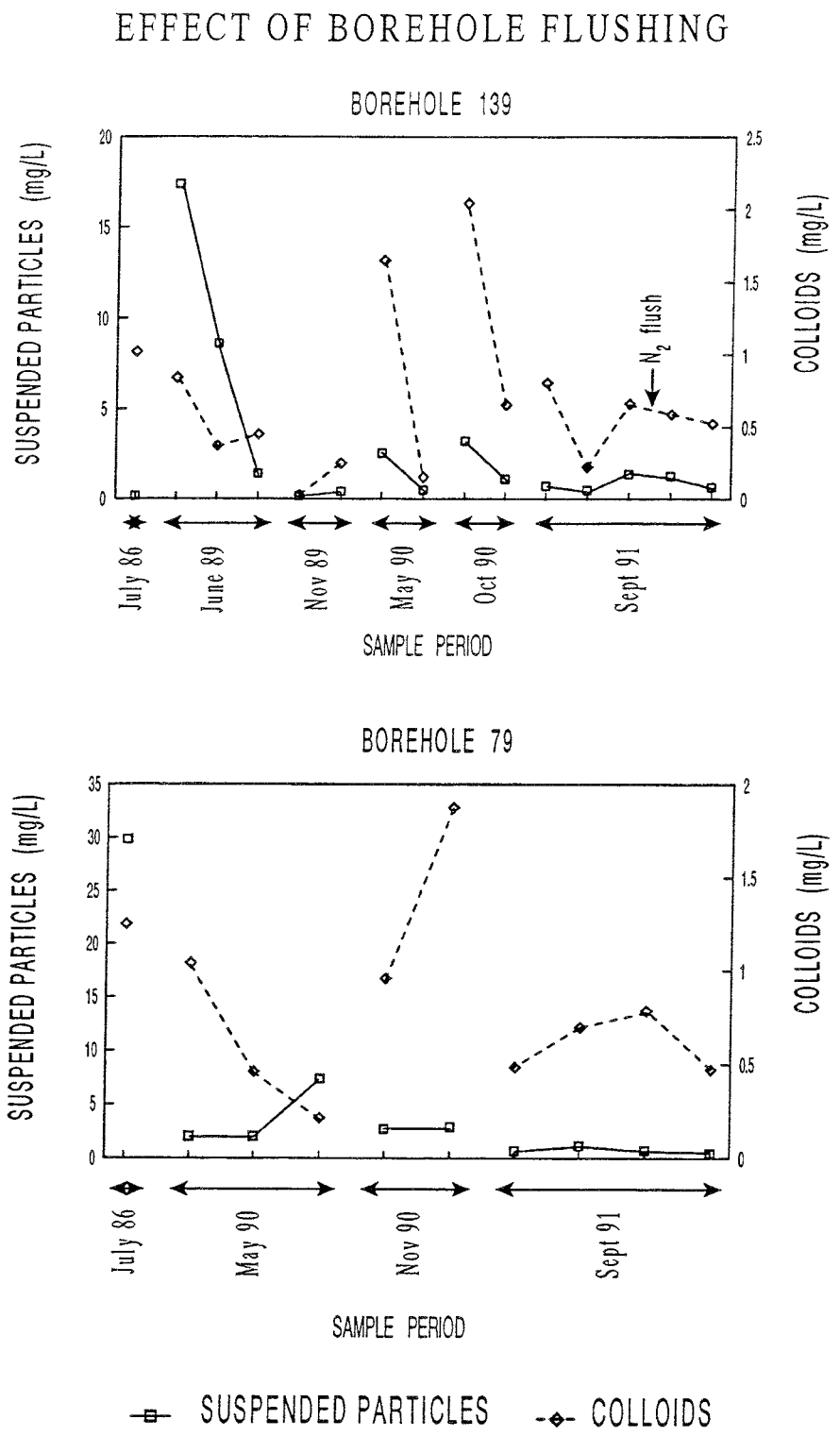

FIGURE 3.88 Two examples of the effects of piezometer flushing on the concentration of colloids and suspended particles.

TABLE 3.44
VARIATION IN SUSPENDED PARTICLE AND
COLLOID CONCENTRATIONS WITH SAMPLING

DATE	PART mg/L	COLL mg/L	DATE	PART mg/L	COLL mg/L	DATE	PART mg/L	COLL mg/L
lower sandstone: 71			lower sandstone: 139			lower sandstone: 219		
Jun-89	2.91	0.73	Jul-86	0.17	1.02	Jun-89	2.40	0.44
Jun-89	3.25	0.44	Jun-89	17.4	0.84	Jun-89	2.51	0.75
Nov-89	0.59	1.40	Jun-89	8.60	0.37	Jun-89	0.27	0.31
Nov-89	0.65	0.44	Jun-89	1.42	0.45	Nov-89	0.47	1.04
Nov-89	1.88	0.32	Nov-89	0.17	0.03	Nov-89	0.16	0.36
May-90	1.30	1.07	Nov-89	0.42	0.25	May-90	0.99	0.80
			May-90	2.56	1.65	May-90	1.24	1.96
			May-90	0.50	0.15	Oct-90	1.85	1.26
			Oct-90	3.22	2.04	Oct-90	0.89	0.74
			Oct-90	1.11	0.65	Sep-91	0.99	0.78
			Sep-91	0.73	0.81	Sep-91	0.80	0.77
			Sep-91	0.50	0.23	Sep-91	0.68	1.51
			Sep-91	1.37	0.66			
			Sep-91	1.29	0.59			
			Sep-91	0.64	0.52			
lower sandstone: 81			altered sandstone: 211			altered sandstone: 67		
Mar-87	4.06	5.07	Jun-89	7.47	1.62	Jun-89	42.9	0.56
Apr-87	0.46	1.00	Jun-89	8.39	0.78	Jun-89	14.9	0.47
Jun-89	15.7	0.47	Jun-89	5.49	0.66	Jun-89	2.23	0.51
Jun-89	17.6	0.68	Nov-89	3.04	0.53	Nov-89	5.25	0.67
Oct-90	10.5	1.70	Nov-89	1.83	0.08	Nov-89	2.44	0.25
Oct-90	6.88	1.68	May-90	2.00	1.68	Oct-90	1.22	2.00
			May-90	2.37	0.98	Oct-90	0.61	0.70
			May-90	0.83	1.01	Sep-91	1.46	0.91
			Oct-90	1.98	2.26	Sep-91	2.00	0.84
			Oct-90	1.00	0.48	Sep-91	1.10	0.52
			Sep-91	2.64	0.86	Sep-91	1.05	0.60
			Sep-91	1.60	1.25			
			Sep-91	2.56	3.81			
			Sep-91	1.11	1.70			

PART: suspended particles (>450 nm); COLL: colloids (10 to 450 nm)

TABLE 3.44 (concl.)

DATE	PART mg/L	COLL mg/L	DATE	PART mg/L	COLL mg/L	DATE	PART mg/L	COLL mg/L
basement: 199			artesian: 83			artesian: 122		
Jul-86	258	3.18	Jul-86	0.54	0.03	Jul-86	1.11	0.02
Mar-87	127	4.05	May-89	0.17	0.73	May-90	0.67	1.53
Mar-87	95	22.1	May-90	0.50	1.56	Oct-90	1.61	1.52
Apr-87	96	1.84	Nov-90	1.19	0.62	Jan-91	0.39	2.44
			Jan-91	2.42	2.78	Sep-91	1.21	1.34
			Sep-91	2.80	0.94			
upper sandstone: 75			clay: 197			clay: 91		
Jun-89	11.82	0.89	Jul-86	2.11	1.07	Mar-87	41.89	3.24
Jun-89	3.47	0.35	Mar-87	2.71	2.93	Mar-87	2.24	0.79
Nov-89	0.49	0.17	Mar-87	2.55	1.97	Mar-87	16.98	0.84
Nov-89	0.50	0.38	Apr-87	0.70	1.26	Apr-87	15.01	0.89
Oct-90	1.13	2.00	Apr-87	1.11	0.29	Jun-89	9.75	0.45
Oct-90	0.41	1.22	May-89	0.52	0.56	Jun-89	7.75	0.76
			May-89	0.31	0.33	Jun-89	2.52	0.46
			May-89	0.40	0.00	Nov-89	3.66	0.14
			Nov-89	0.31	0.50	Nov-89	0.93	0.47
			Nov-89	0.14	0.33			
			May-90	0.85	1.97			
			May-90	1.62	1.88			
			May-90	0.12	0.00			
			Oct-90	1.17	1.26			
			Oct-90	0.41	0.22			
ore: 79			ore: 198			ore: 220		
Jul-86	30	1.25	Mar-87	31	2.05	Jun-89	154	0.28
May-90	2.03	1.04	Mar-87	5.57	2.30	Jun-89	60	0.61
May-90	2.04	0.46	Jul-86	3.86	1.73	Nov-89	31	3.92
May-90	7.38	0.21	Apr-87	1.18	0.84	Nov-89	25	0.18
Nov-90	2.74	0.96	Mar-87	0.84	0.69	Nov-89	17	0.63
Nov-90	2.89	1.88				May-90	5.40	1.68
Sep-91	0.69	0.48				May-90	3.17	1.98
Sep-91	1.14	0.70				May-90	2.00	2.54
Sep-91	0.73	0.78				Nov-90	1.09	0.98
Sep-91	0.44	0.47				Nov-90	1.24	0.39

PART: suspended particles (>450 nm); COLL: colloids (10 to 450 nm)

TABLE 3.45
FIELD-DERIVED DISTRIBUTION COEFFICIENTS FOR RADIONUCLIDE PARTITIONING ON PARTICLES LARGER THAN 10 nm

Sample*	Location	pH	Uranium R_d mL/g	Thorium R_d mL/g	Radium R_d mL/g
79	ore	7.21	6×10^4	5×10^4	7×10^3
198	ore	7.33	5×10^5		6×10^4
198A	ore	7.43	2×10^7	2×10^6	5×10^5
198B	ore	6.93	8×10^4	1×10^4	1×10^4
198C	ore	7.70	2×10^5	7×10^5	6×10^4
198D	ore	7.08	4×10^6	2×10^5	7×10^5
197	clay/ore	7.25	8×10^5		9×10^3
197A	clay/ore	7.04	4×10^5	3×10^5	8×10^4
197B	clay/ore	6.93	2×10^3	2×10^4	4×10^4
197C	clay/ore	6.83	5×10^4	3×10^5	2×10^5
197D	clay/ore	6.69	5×10^4	2×10^5	7×10^5
91A	clay	6.72	6×10^3	9×10^3	1×10^5
91B	clay	7.23	3×10^4		6×10^4
91C	clay	6.96	5×10^4	1×10^3	
91D	clay	6.79	3×10^5	4×10^5	1×10^5
91E	clay	7.01	2×10^5	3×10^3	1×10^5
134	clay	7.07	6×10^4	8×10^4	3×10^4
81A	alter. SS	7.33	7×10^3	7×10^4	7×10^4
81B	alter. SS	8.50	6×10^5	3×10^4	4×10^5
128	basement	6.50	7×10^5		3×10^5
137	basement	7.49	5×10^5	9×10^5	1×10^6
199	basement	7.64	3×10^4	8×10^3	9×10^3
199A	basement	7.93	1×10^4	3×10^4	9×10^3
199B	basement	7.83	3×10^4	3×10^5	5×10^4
199C	basement	7.85	4×10^3	2×10^4	1×10^4

* Letter indicates repeat samples on the same piezometer.

In summary, the observed particle concentrations are likely the result of a dynamic steady state between mechanisms of particle generation and particle capture. These mechanisms are controlled by formation permeability and structure, and by the groundwater flow field, which is induced by sampling. In hole 122, which has had a continuous artesian flow for over six years, particle concentrations have not declined with time and may have reached a steady state.

The overburden piezometer, 3.10, was sampled with both a bailer and a peristaltic pump. A comparison of results from these techniques showed that particle concentrations in waters collected with a bailer can be an order of magnitude too high. Therefore, the particle concentrations reported in the Second Annual Report (Cramer and Smellie 1992), for waters collected with the bailer, should be disregarded. The bailer is a plastic tube, containing a check valve in the bottom, which was used in those piezometers that could not be sampled by pumping. As the bailer is moved up and down the piezometer it probably rubs off particles from the walls of the piezometer stand pipe. Furthermore, the bailer cannot remove enough water to properly flush the piezometer.

3.6.4 Element distributions between particles and groundwater

The concentrations of dissolved ([R], mol/L) and particulate ($[R]_p$, mol/L) uranium, thorium and radium, along with total particle concentrations (C, mg/L), can be used to calculate field-derived distribution coefficients (R_d) between particles and groundwater:

$$R_d = \frac{[R]_p}{[R] \times C} \times 10^6 \ (mL/g)$$

These R_d values provide an estimate of the magnitude of radionuclide partitioning onto particles in a natural system. The actual mechanism(s) responsible for radionuclide association with particles cannot be identified from this approach. On average, the R_d values for uranium and thorium are higher in the ore zone than in other parts of the deposit (Table 3.45). There is no correlation between pH and the R_d values for any of the above radionuclides. If elements can exchange freely between particles and groundwater, the R_d values should be identical for a given groundwater and particle composition. The wide range of field-derived R_d values observed for uranium, thorium and radium in a given borehole indicates that these radionuclides in particulate form may not be in equilibrium with groundwater. For example, in hole 198 the R_d values for uranium varied from 8×10^4 to 2×10^7 mL/g.

The natural distributions of elements between particles and groundwater are controlled by several processes, including sorption, precipitation, and inclusion in mineral structures. To obtain R_d values that can be attributed mainly to sorption, sorption experiments were carried out at Cigar Lake by spiking 50 L volumes of groundwater with selected trace elements (Li, Sr, Cs, Zn, Ni, Co, U, Eu, La). After a 2- to 4-h reaction time, colloids were concentrated for chemical analysis using tangential-flow ultrafiltration. Provided element concentrations are kept below solubility limits, the distribution of trace elements in spiked samples is controlled mainly by sorption.

TABLE 3.46
FIELD DERIVED DISTRIBUTION COEFFICIENTS (mL/G)

This table compares the R_d values obtained by spiking groundwater samples with Sr, Li, and U, with R_d values measured without the addition of any trace elements. The R_d values for the colloid (COLL.) fraction represent elements attached to particles in the 10 to 450 nm size range, while the other values are for suspended particles larger than 450 nm. Note that sample 219 was not spiked with uranium.

Sample	Comment	Sr Coll.	Sr >450 nm	Li Coll.	Li >450 nm	U Coll.	U >450 nm
79-1		1×10^5	6×10^2	6×10^3	-	-	6×10^5
79-2	spike	2×10^4	-	8×10^3	-	-	1×10^4
79-3		7×10^4	-	1×10^3	6×10^3	-	6×10^5
79-4		2×10^5	8×10^3	3×10^3	-	-	1×10^5
139-1		2×10^4	-	-	4×10^3	-	2×10^4
139-2		3×10^5	7×10^3	-	1×10^5	-	2×10^5
139-3	spike	1×10^4	-	-	-	7×10^5	1×10^6
139-4		-	1×10^3	-	2×10^3	8×10^4	2×10^5
139-5		1×10^5	-	-	5×10^4	2×10^4	-
211-1		1×10^4	7×10^3	-	-	5×10^4	8×10^4
211-2	spike	3×10^4	2×10^3	-	2×10^3	4×10^5	3×10^5
211-3		3×10^4	6×10^3	-	-	-	3×10^5
211-4		2×10^5	4×10^3	-	-	4×10^3	2×10^5
219-1		3×10^4	4×10^3	6×10^3	-	5×10^4	-
219-2	spike	5×10^4	5×10^3	-	-	7×10^4	-
219-3		4×10^4	-	1×10^4	-	4×10^4	1×10^5

The R_d values for Sr, Li and U are summarized in Table 3.46 for the spiked sorption experiments and for the other samples with no element additions. The Sr and Li R_d values determined from the spiked experiments were similar to the R_d values obtained without the addition of a trace-element spike. This suggests that, for these elements, the R_d values obtained from regular colloid sampling are representative of sorption reactions on colloids. Compared to samples without a U spike, the R_d values for U in the spiked experiments were lower for hole 79, but higher for holes 139 and 211. The R_d values for the elements that could not be measured without spiking the groundwater sample are summarized in Table 3.47. If sorption is determined mainly by surface area, the R_d values for sorption on colloids should be higher than for suspended particles (>450 nm) because colloids have a higher specific surface area. This was observed for Sr, Cs, Ni, and Co. The R_d values for suspended particles were higher than for colloids for Eu and La, while the R_d values for U

and Zn were similar for both types of particles. In the case of these latter elements compositional differences between colloids and suspended particles may have overcome the difference in specific surface area.

TABLE 3.47
FIELD-DERIVED DISTRIBUTION COEFFICIENTS FROM SPIKED EXPERIMENTS

The distribution coefficients (R_d) are given as mL/g for colloids (COLL.) from 10 to 450 nm and suspended particles larger than 450 nm. The combined R_d values for all particles larger than 10 nm are listed under total. These combined R_d values were calculated using the less than 10 nm fraction (F1) to define dissolved element concentrations, while the dissolved element concentrations for the other R_d values were obtained from the less than 1 nm fraction (F2).

Sample	pH	Cs Coll.	Cs >450 nm	Cs Total	Ni Coll.	Ni >450 nm	Ni Total
79	6.4	1×10^4	-	7×10^3	-	-	2×10^3
139	7.2	2×10^4	-	-	8×10^3	-	-
211	7.2	2×10^4	3×10^3	5×10^3	2×10^4	-	-
219	7.4	3×10^4	8×10^3	1×10^4	3×10^4	9×10^3	1×10^4

Sample	pH	Zn Coll.	Zn >450 nm	Zn Total	Co Coll.	Co >450 nm	Co Total
79	6.4	-	-	7×10^2	-	6×10^3	5×10^3
139	7.2	-	4×10^3	-	6×10^3	-	-
211	7.2	1×10^4	1×10^4	5×10^3	2×10^4	1×10^3	1×10^3
219	7.4	2×10^4	2×10^4	1×10^4	3×10^4	9×10^3	1×10^4

Sample	pH	Eu Coll.	Eu >450 nm	Eu Total	La Coll.	La >450 nm	La Total
79	6.4	-	5×10^4	-	-	5×10^4	-
139	7.2	1×10^6	4×10^6	6×10^5	2×10^5	1×10^6	3×10^5
211	7.2	6×10^5	8×10^5	8×10^5	5×10^5	7×10^5	7×10^5
219	7.4	-	-	-	-	-	-

3.6.5 Colloid migration: status

If colloids are completely mobile in the subsurface, their impact on radionuclide migration will depend on colloid concentration and whether or not radionuclide attachment to particles is reversible. If sorption is reversible, the radionuclides attached to particles can desorb and

interact with the geomatrix. In this case colloids could be treated as a ligand in solution, and their effect on the retardation factor for a given radionuclide could be calculated with an equilibrium model (Vilks et al. 1991). This approach indicates that the average particle concentrations in the deep groundwaters at Cigar Lake are too low to have a significant impact on radionuclide migration.

If radionuclide attachment to colloids is not reversible, and if colloids are stable for long periods of time, radionuclides attached to particles may not interact with the geomatrix, and their transport would be determined by particle migration properties. The wide range in field-derived R_d values for U, Th and Ra in a given borehole indicates that these radionuclides may be irreversibly associated with particles. Isotopic evidence indicates that most of the U and Ra on particles was derived from groundwater, possibly by sorption. Furthermore, some particles may have retained their U for as long as 8000 a. Therefore, since some radionuclides are fixed by particles for thousands of years, a reversible sorption model should not be used to argue that the observed particle concentrations in deep Cigar Lake groundwaters will have a negligible impact on radionuclide transport. In a given volume of rock, radionuclides will sorb onto the rock mass as well as the much smaller mass of particles in groundwater. Although, given the colloid concentrations observed in the deep Cigar Lake groundwaters, less than 0.01% of radionuclides in a given volume of rock are likely to form radiocolloids (Vilks et al. 1991), the transport of these radiocolloids could represent an important radionuclide flux over geological time. Therefore, an understanding of particle migration is necessary to evaluate the importance of radionuclide transport by colloids and suspended particles.

This study has established some boundary conditions for the development of a particle transport model for the Cigar Lake deposit (Vilks et al. 1993). A particle migration model will have to take into account a very broad particle size distribution, which is not dominated by any particular size class. Observed particle compositions indicate that a large portion of natural particles in Cigar Lake groundwaters are generated by the erosion of minerals and alteration products from the host rock. The production of these particles depends very much on the local rock conditions. In comparison with open fractures and zones of friable sandstone, the generation of particles is very low in well-consolidated clay and parts of the basement with low permeability. The average U concentration in particles from the ore zone (0.06 % U) is significantly lower than the average uranium content of the ore (12 % U). This suggests that within the ore, particles originate mainly from clay and not from uranium minerals. Organic colloids may be added from recharge waters, as well as from particle erosion. Iron colloids may precipitate in situ, but are not likely to migrate because of their coagulation and sorption to the rock. After a new flow field is established particle concentrations will decrease until a steady state between particle generation and capture is reached.

Although the particle concentrations in artesian holes and sampled piezometers indicate that colloids and suspended particles are mobile when there is substantial groundwater flow, they do not prove that colloids migrate under natural flow regimes. Geochemical evidence for particle migration is limited because the major-element compositions of particles throughout

the deposit are similar. However, if the organic carbon in the 1- to 10-nm size class originates from humic material in surface waters, then at least the small organic colloids travel long distances through sandstone. The high concentrations of U, Th and Ra in particles from the ore zone, compared with particles in the sandstone, indicate that the transport of particles through the clay zone has been negligible, and the mobilization of clay particles from the clay into the sandstone has not been important. This is consistent with the presence of well-compacted clay, which in sections is plastic and is known to be an effective hydraulic seal between the ore and nearby water-bearing fractures. This suggests that a compacted clay buffer in a disposal vault would be an effective barrier to particle transport and would not likely release significant amounts of clay particles to the geosphere, even in the presence of low ionic-strength groundwater.

3.6.6 References

AIREY, P.L. 1984. Radionuclide migration around uranium ore bodies -- Analogue of radioactive waste repositories. Austral. Atom. Energy Comm., **NUREG/CR-3941**.

CHIU, N.W. and DEAN, J.R. 1984. Analytical Methods Manual, National Uranium Tailings Program, Monenco Consultants Ltd., 47-57.

CRAMER, J.J. and SMELLIE, J.A.T.S. 1992. Second Annual Report of the AECL/SKB Cigar Lake Project. Year 2: 1990-1991. AECL Internal Proj. Rep., **CLR-91-03**.

GASCOYNE, M. and LAROCQUE, J.P.A. 1984. A rapid method of extraction of uranium and thorium from granite for alpha spectrometry. Nucl. Instrum. Meth. Phys. Res., **223**, 250-252.

KIM, J.I., BUCKAU, G., BAUMGARTNER, F., MOON, H.C. and LUX, D. 1984. Colloid generation and the actinide migration in Gorleben groundwaters. In *Proc. 7th Symp Scientific Basis for Nuclear Waste Management.* Mat. Res. Soc. Proc., **26**, 31-40.

MCDOWELL-BOYER, L.M., HUNT, J.R. and SITAR, N. 1986. Particle transport through porous media. Water Resour. Res., **22**, 1901-1921.

MILLS, W.B., LIU, S. and FONG, F.K. 1991. Literature review and model (COMET) for colloid/metals transport in porous media. Ground Water, **29**, 199-208.

NERETNIEKS, I. 1978. Some aspects on colloids as a means for transporting radionuclides. Kärnbränslesäkerhet, Stockholm Rep., **KBS-TR-103**.

VILKS, P. and DREW, D.J. 1986. The effects of colloids on actinide migration. In *Proc. 2nd Int. Conf. Radioactive Waste Management.* Can. Nucl. Soc., 667-673.

VILKS, P., CRAMER, J.J., SHEWCHUK, T.A. and LAROCQUE, J.P.A. 1988. Colloid and particulate matter studies in the Cigar Lake natural-analog program. Radiochim. Acta, **44**, 305-310.

VILKS, P., BACHINSKI, D.B. and VANDERGRAAF, T.T. 1991. The role of particulates in radionuclide transport. In *Proc. 3rd Int. Symp. Advanced Nuclear Energy Research.* Mito City, Japan, March 13-15, 1991.

VILKS, P., CRAMER, J.J., BACHINSKI, D.B., DOERN, D.C. and MILLER H.G. 1993. Studies of colloids and suspended particles, Cigar Lake uranium deposit, Saskatchewan, Canada. Appl. Geochem., **8**, 605-616.

3.7 ORGANICS & MICROBIOLOGY

3.7.1 Introduction

(P. Vilks)

In order to successfully model trace-element and radionuclide geochemistry in Cigar Lake groundwater it is important to understand all the processes affecting element solubility and speciation in solution. If present in high enough concentrations, organic compounds that complex trace elements could increase the concentrations of these elements above the solubility limits predicted by chemical speciation models, which consider only inorganic complexes. Therefore, it is important to evaluate the concentration of organic compounds in groundwater throughout the deposit and to identify natural organic compounds that could form strong complexes with trace elements. The issue of organics was initially addressed with a survey of total organic carbon (TOC) in all groundwaters. The nature of the organic compounds making up the TOC was characterized with gas chromatograph/mass spectrometer analysis of solvent-extractable organics, and by using cellulose resin to extract humic compounds from large volumes of groundwater. Since humic substances are likely to be the most important for trace-element complexation, isolated fulvic acids were characterized for composition, complexing capacity, and ^{14}C ages. The effect of organic contamination from the piezometer was also addressed.

The mobility of trace elements can be affected by micro-organisms in the subsurface through metabolic reactions affecting redox, pH, and complexation. The microbiology of subsurface environments is not well understood and needs to be characterized in greater detail to assess the potential impact of micro-organisms on a hypothetical disposal vault for waste fuel. The Cigar Lake natural analog study has provided an excellent opportunity to study subsurface microbiology in a natural UO_2 deposit that has been well characterized with respect to geology, hydrology and geochemistry. Microbial research has focused on evaluating the potential for microbial growth based on water composition, and for identifying and quantifying the presence of micro-organisms likely to affect redox and uranium chemistry.

3.7.2 Humic substances in groundwaters from the Cigar Lake area

(C. Pettersson, B. Allard, J. Ephraim and P. Vilks)

3.7.2.1 Introduction

The search for natural analogs and the evaluation of relevant processes related to these systems have become important parts of the design and evaluation of concepts for long-term storage of spent nuclear fuel and high-level radioactive waste. Atomic Energy of Canada Limited (AECL) has conducted studies of sandstone-hosted deposits of uranium ore in northern Saskatchewan as analogs for spent fuel disposal vault systems since 1982 (e.g., Cigar Lake: Cramer 1986). The studies at the Cigar Lake area have been conducted as a collaboration between AECL and the Swedish Nuclear Fuel and Waste Management Company (SKB) since 1989.

An important subtask within the programme is to establish the role of natural organic materials, notably humic substances, in the mobilization and transport of radionuclides from the ore zone at Cigar Lake. Since humic substances generally form very strong complexes with highly charged metal ions (like the actinides: see Choppin and Allard (1985)), the complexing and transporting capacity of the humics have to be estimated on the basis of composition and concentrations of organics in the groundwater within or in the vicinity of the ore zone.

This report describes some initial studies of organic substances from groundwater and surface waters in the Cigar Lake area. The objectives of the study are to characterize the aquatic humic substances and to quantify their role in the transport of uranium within and away from the ore body.

3.7.2.2 The Cigar Lake area

The geology and geohydrology of the Cigar Lake area are described in detail in several papers (Cramer 1986; Cramer et al. 1987) and particularly in the progress reports of the project (Cramer and Smellie 1991). Altogether some 20 exploration boreholes have been selected for study from different rock units around the Cigar Lake ore body (Figure 3.89). Some 15 of these holes have been completed for water sampling at various levels. Additional sampling of water has been done in surrounding lakes, Waterbury Lake, Cigar Lake and Aline Lake, as well as in the overburden.

Hydrochemical reference data are compiled in Cramer and Smellie (1991) and discussed in detail by Cramer and Nesbitt (see Section 3.5.3). The lake waters in the area (e.g., Waterbury Lake) has a total salinity of less than 15 mg/L (TDS), with HCO_3^- as the dominating single species (7-8 mg/L). Also, the groundwater in the upper sandstone, and largely also in the lower sandstone, is HCO_3^--dominated with about equal levels of Na^+ ($+K^+$) and Ca^{2+} ($+Mg^{2+}$) among the cations, and has a low TDS-level (< 100 mg/L). The basement water, however, is a Na^+-Cl^--type groundwater with low alkalinity (HCO_3^-: 50-70 mg/L) and TDS of 220-240 mg/L, representative of crystalline granitic bedrock.

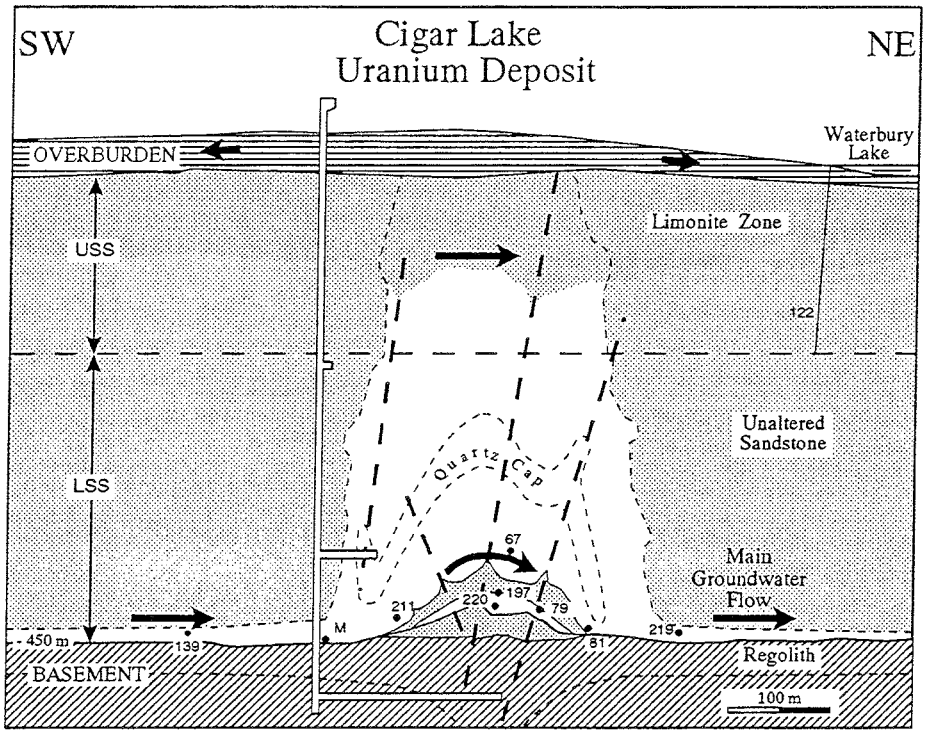

FIGURE 3.89 Section through the Cigar Lake deposit showing the location of piezometers used for groundwater sampling. (USS= upper sandstone; LSS= lower sandstone).

3.7.2.3 Experimental

3.7.2.3.1 Water sampling and isolation of humics

Water was sampled from 17 locations (i.e., from 11 boreholes and from 6 overburden and lake stations) during three campaigns (October 1990, January and September 1991). Rock type, depth and water volumes are summarized in Table 3.48.

The humic fraction was recovered from the water samples by adsorption on a weak anion exchange resin (diethylaminoethyl-cellulose, DEAE). The advantage of this common procedure is that the adsorption can be conducted directly in the field (e.g., on-line in water that is pumped from a deep hole) without any adjustment of pH (Miles et al. 1983; Paxéus 1985; Allard et al. 1990; Pettersson 1992). Moreover, since pH is not altered the original distribution of trace metals may be kept intact, and the amounts of trace cations bound to the humic substances can be determined.

The adsorbed humic fraction (HFA) was eluted with 0.3 M NaOH followed by acidification to pH 2 (with HCl) for precipitation of the humic acid fraction (HA, high molecular weight). The fulvic acid fraction (FA, low molecular weight) remains in solution. Determinations of associated trace elements had to be performed on the adsorbed fraction

after elution from the DEAE resin, but before any acidification steps were pursued. In the cases when a pure (dry) humic substance was prepared, a series of steps (adsorption on XAD-8 at low pH, desalting, elution with 0.1 M NaOH, transformation to the H^+-form when passed through a strong cation exchange resin, freeze-drying) followed (Pettersson, 1992).

Three slightly different procedures for extracting humics were followed for practical reasons (see Table 3.48):

A A batch technique; 50 L of water were shaken with 10 g of the DEAE cellulose. After a contact time of 1-2 h the cellulose was separated from the water by settling/filtration.

B A continuous flow technique; water entered into a flow-through cell from the side and was allowed to flow over onto a large opening covered by a straining cloth supporting the DEAE-cellulose sorbent.

C A batch technique; pH was adjusted to 5.5-6 and the DEAE was added after 20 h (used for one sample only, since it was radioactive from the presence of radon and had to be left for ventilation and decay).

3.7.2.3.2 Characterization of humics

Concentrations of total organics (TOC) were measured in original solutions (Shimadzu TOC-5000-analyzer, catalytic combustion) and concentrations of HFA from the UV-absorbance at 250 nm (calibration by using the dry isolated humics from the area).

The HFA (or purified HA or FA) was characterized with respect to:

- **elemental composition** (purified dry FA-fraction): major elements (C, O, H, N, S) as well as trace elments (by ICP-MS);
- **molecular weight distribution**: gel filtration using an HPLC system. This system comprised a column filled with a silica-based material modified by a vinylic alcohol, TSK2000SW, and a UV-absorbance detector (254 nm), the mobile phase being a 50 mM phosphate buffer with pH 6.8. Sulphonated polystyrenes were used as reference substances for the calibration of retention time versus molecular weight;
- **acid-base properties**: potentiometric titration in 0.001, 0.01 and 0.1 M $NaClO_4$ solution, and calculation of total acidic (carboxylic) capacity; and
- **age from ^{14}C-determination** (accelerator mass spectrometry).

The procedure has previously been applied in studies of humic substances from deep groundwater (Pettersson et al. 1989; Allard et al. 1990)

3.7.2.4 TOC and humics

3.7.2.4.1 Concentrations

The TOC as well as the concentrations of HFA in the various samples are summarized in Table 3.49.

TABLE 3.48
WATER SAMPLES FOR RECOVERY OF DISSOLVED ORGANIC MATERIAL

Sample ID	Rock type*	Depth (m)	Sample volume (L) Oct. 1990	Jan. 1991	Sept. 1991	Isolation technique+
Waterbury L.	-	0[a]		100	100	A
Cigar L.	-	0		100		A
Aline L.	-	0		100		A
P3.7,P3.8,P3.12	OB	4-23		3x100		A
122	US	0-200[b]	90	100	100	A
83	US+LS	18-477[b]	110	100	100	A
139	LS	439-443	410		100	B
219	LS	414-426			100	B
67	AS	345-348	500		64	B
211	AS	416-418			100	B
81	AS	440-444	300			B
197	C/O	416-421	365			B
79	O	430-433	105		100	B
220	O	432-439	50			C
M[c]	B	480	150			A

* OB= overburden; US, LS, AS= upper-, lower-, altered sandstone; C= clay; O= ore; B= basement.
\+ See text.
a Surface water (lake).
b Artesian water.
c From lower level test mine (possible mixed water).

Total organics concentrations range from 0.6 to 1.7 mg/L except for sample 79 (10.6 mg/L; from the ore zone). Previously reported measurements have given similar values, i.e., <2 mg/L in surface waters and in the sandstone groundwater, but up to 13 mg/L in the ore zone.

The HFA fraction of the TOC was generally around 15-25 % in the surface waters and sandstone groundwater but less in the altered zones and probably also in the basement (<10 %). This could indicate a higher progression of decomposition in these layers, either because of the differences in hydrochemical conditions (e.g., higher salinity) or longer residence times. The HFA fraction was only 1-2 % (or below) of the TOC in the ore zone, which also could be an indication of a chemical degradation or even longer residence times.

3.7.2.4.2 Composition of humics

Analysis of the major components was performed on six samples and of trace elements on three samples (Table 3.50); acid capacity (four samples) and ^{14}C-ages (six samples) were also determined. The proportions of the major elements are all within limits that can be expected for groundwater HFA (Pettersson et al. 1992). There are no pronounced

differences in composition or capacity (per gram) between the "modern" and the 15,000-a-old HFA.

TABLE 3.49
TOTAL ORGANIC (TOC) AND HUMIC (HFA) CONTENTS IN CIGAR LAKE WATER

Sample ID	pH	TOC* mg/L	HFA mg/L	HFA/TOC %	HFA** mg
Lakes	5.8-8.1	3.4[a]	0.46, 0.92	7-14	110
Overburden	7.3-8.7	1.4, 1.5	0.14, 0.46	5-9	31
122	6.7-7.2	0.63	0.21, 0.32	17-25	48
83	6.7-7.4	0.76	0.21, 0.26	14-17	49
139	6.5-7.3	1.69 (1.24,0.38)	0.54	14	50
219	6.3-6.8	1.53 (0.72)	-	-	b
67	6.7-7.2	0.90 (0.65,0.22)	0.14	8	22
211	6.7-7.1	(1.39)	>0.09	4	b
81	6.2-6.8	(1.30)	>0.04	>6	13
197	5.6-6.4	(0.89)	>0.09	6	31
79	6.5-7.1	10.6 (13.2,2.9,3.3)	0.16, 0.50	1-2	68
220	7.3-8.0[c]	(3.97)	>0.06	>0.7	3
M	6.8	0.86	>0.06	>4	9

* 1987 and 1989 data (Cramer and Smellie, 1991) in brackets.
** Total amount recovered.
a 2.5-7.5 from measurements in 1983-86.
b Not purified; fluorescing sample.
c pH= 11 measured in October 1990.

There were no striking accumulations of cations associated with the HFA, except possibly for the high Si-levels (possibly colloids of clays and silica that have followed the HFA-fraction in the initial separation).

The sample from borehole 197 evidently represents a modern water, although sampled in the clay/ore zone (possibly an artefact of sampling). The radiation from the ore is being ruled out to explain the observed ^{14}C-levels in the HFA, indicating a modern origin (see Section 3.8.2).

The potentiometric titration curves (Figure 3.90) indicate some qualitative differences, as well as variations in the total capacity (Table 3.50). Still, the differences are minor considering the variation in ages: the ionic strength effects are negligible at the salinities encountered in the natural system. A detailed analysis of the curves (evaluation of pK_a-values for individual acidic functional groups) could possibly explain the observed differences (c.f., discussion below related to molecular weights).

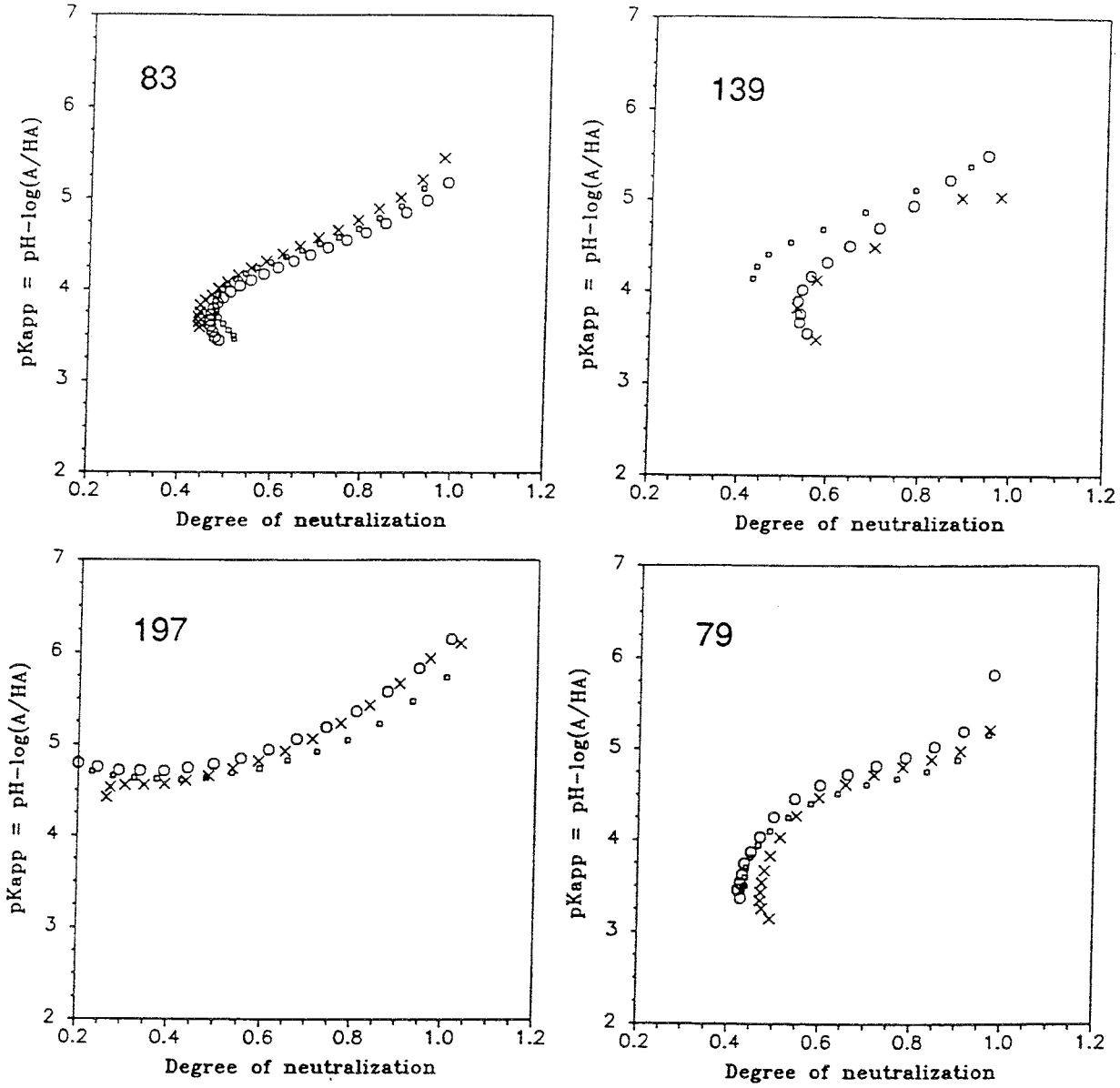

FIGURE 3.90 Titration curves: pK_a versus the degree of neutralization (in $NaClO_4$: 0.001 M, 0.01 M and x 0.1 M). For the theory behind these plots see Ephraim et al. (1986).

3.7.2.4.3 Molecular weight of humics

Molecular weights (number average (M_n) and weight average (M_w)) for all the samples are given in Table 3.51. The ratio M_w/M_n is a good measure of the polydispersity: as expected the HFAs from the lakes generally have higher ratios (and higher individual values, e.g., $M_w > 1000$). In general, the measured ^{14}C-ages agree with the molecular weight ratios:

very low (1.14) for sample 79 (15,330 a) and considerably higher for all other samples, including 197 (denoted as "modern" in Table 3.50).

TABLE 3.50
COMPOSITION OF ISOLATED HUMICS

Sample	83	139	67	211	81	197	79	M
C %	56.1*	53.4	55.6		57.0	55.0	57.1	
H	5.7	5.4	5.9		5.7	5.4	4.1	
N	0.5	1.2	1.4		1.0	0.8	0.2	
O	37.2	39.2	36.2		35.7	38.2	38.5	
S	0.5	0.8	0.9		0.6	0.6	0.1	
Na mg/g			-	-			-	
K			7.7	11.8			5.4	
Mg			0.32	0.37			0.51	
Ca			2.6	5.8			5.0	
Sr			<0.01	0.08			0.02	
Ba			<0.01	0.05			0.01	
Al			1.3	4.9			1.2	
Cr			0.07	0.41			0.07	
Mn			0.06	0.13			0.01	
Fe			2.8	7.2			0.90	
Co			0.01	0.02			<0.01	
Ni			1.4	0.47			0.06	
Cu			0.16	0.86			0.51	
Zn			0.29	1.4			0.13	
Cd			0.03	0.07			0.01	
Pb			0.01	0.06			0.01	
U			0.98	0.66			0.36	
Si			11.9	0.01			11.0	
Acid cap meq/g**	3.78 ±0.18	3.31 ±0.15				5.26 ±0.30	5.44 ±0.20	
^{14}C-age a	Mod+		560 ±90		3905 ±85	Mod++	15330 ±150	4375 ±85
HFA mg/L	0.21 0.26	0.54	0.14	>0.09	>0.04	>0.09	0.16 0.50	>0.06

* Values for C, H, N, O and S normalized to 100 %.
** From potentiometric titrations.
\+ Modern origin.
++ Duplicate samples.

The chromatograms from the gel filtrations can be resolved into several overlapping fractions, as illustrated in Figure 3.91. The fresh HFA (Waterbury L.) has three distinct peaks corresponding to molecular weights below 1000. The somewhat older (mixed) HFA from sample 67 has lost most of the high molecular weight fraction, and the proportion of the lowest molecular weight has increased even further for the old sample 79.

TABLE 3.51
MOLECULAR WEIGHTS (M_n AND M_w) FOR THE HFA FRACTION

Sample ID	M_n* Oct. 1990	M_n* Jan. 1991	M_n* Sep. 1991	M_w Oct. 1990	M_w Jan. 1991	M_w Sep. 1991	M_w/M_n Oct. 1990	M_w/M_n Jan. 1991	M_w/M_n Sep. 1991
Wbry L.		740	910		1010	1320		1.36	1.45
Cigar L.		810			1260			1.56	
Aline L.		830			1180			1.42	
P3.7		580			700			1.21	
P3.8		700			880			1.26	
P3.12		650			870			1.34	
122	820	700	710	1260	840	980	1.54	1.20	1.38
83	700	740	660	900	940	800	1.29	1.27	1.21
139	810		860	1060		1100	1.31		1.28
219			620			750			1.21
67	690		740	1020		1030	1.40		1.39
211			650			770			1.18
81	710			930			1.31		
197	680			860			1.26		
79	470		630	560		720	1.19		1.14
220	920			1190			1.29		
M	640			850			1.33		

* October 1990: fulvic acid fraction.
January and September 1991: HFA fraction after eluation from DEAE.

3.7.2.5 Uranium distribution

The measured uranium concentrations in the humic fraction (Table 3.50) as well as in the waters (Cramer 1991) show that only a small fraction of the total uranium (0.5-2 % and 0.8-1 %) is bound to humics in samples 67 and 79, respectively, and around 2-3 % for sample 211.

Calculations of the distribution between soluble species for Th(IV) as well as U(IV)-U(VI), considering the relevant concentrations of inorganic ligands (OH^-, $CO_3^{=}$tot, $SO_4^{=}$, F^- and $HPO_4^{=}$ concentrations corresponding to pH <7.8, <95 mg/L, <25 mg/L, <0.7 mg/L and <0.05 mg/L, respectively) show that hydrogen phosphate complexes (1,2; 1,3) as well as

the hydroxide (1,4) for uranium would dominate for the tetravalent state, and carbonates (1,1; 1,2; 1,3) as well as hydrogen phosphates (1,1: 1,2) would be the dominating species for a hexavalent system (in the absence of humics).

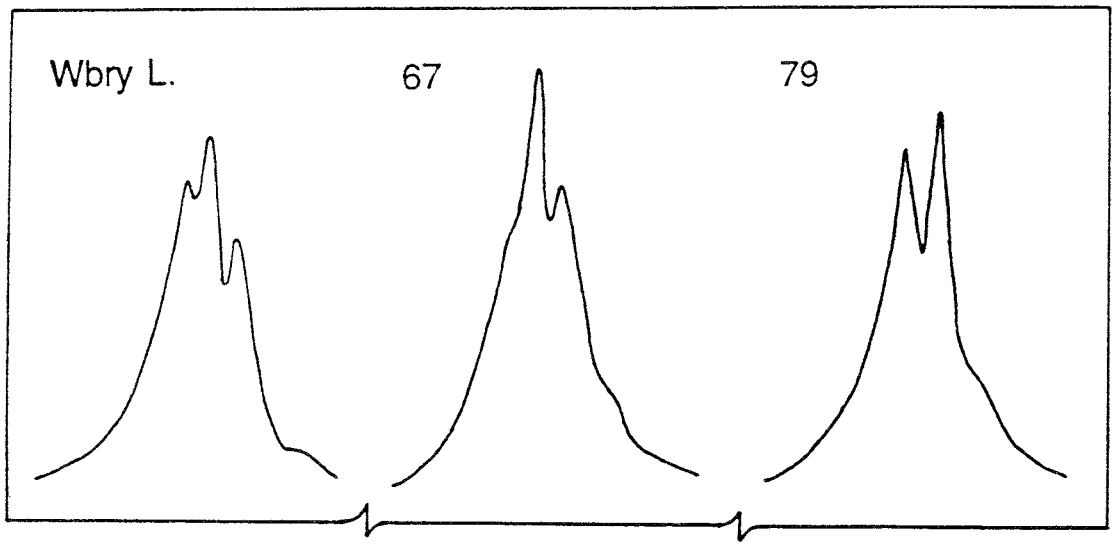

FIGURE 3.91 Gel filtration: Absorbance (at 254 nm) plotted versus retention time.

Contributions from humic substances can be assessed, assuming conditional formation constants defined as

$$\beta_{ov} = \Sigma M_{bound}/(M_{free}\Sigma A^{-}).$$

Recent measurements by ultrafiltration (Nordén et al. 1993) have yielded $\log\beta_{ov}$ values of 5.5 ± 0.5 for U(VI) and 7 ± 1 for Th(IV), respectively (extrapolated to pH 6.5). Calculations based on these data show that the corresponding fraction of Th-HFA complex is expected to be entirely negligible (less than 10^{-6} of the dissolved Th), while for U(VI) the formation of U(VI)-HFA complexes corresponding to a maximum of 10^{-3} of the total dissolved U is feasible (assuming the observed maximum concentration levels of HFA).

There is no correlation between the observed uranium concentrations and the TOC concentrations (or HFA concentrations), and no such correlations would be expected, considering the indications from the calculations of dominating species in the system (see above). It is likely that the system is saturated with respect to various reduced U-oxide species. Some correlation between carbonate (as $CO_3^{=}$) and dissolved uranium (containing a minor fraction of U(VI) as determined by the U(VI)/U(IV) equilibrium at the relevant Eh/pH) would therefore be expected, at least in zones with a uranium source term (i.e., in the ore zone and in zones with precipitated uranium). Some relations between total dissolved uranium and carbonate are, in fact, obtained (Figure 3.92), particularly in the ore zone. Apparently, another relation is obtained in the clay zone as compared with the basement-sandstone-surface water systems, which show less correlation and may represent mixing of waters with different uranium concentrations rather than uranium dissolution.

The qualitative observations in Figure 3.92 can, of course, not give any conclusive answers concerning the mechanism behind mobilization and transport of uranium within the area, but merely illustrate the fact that the carbonate concentration has a larger impact on the uranium concentration than the TOC concentration.

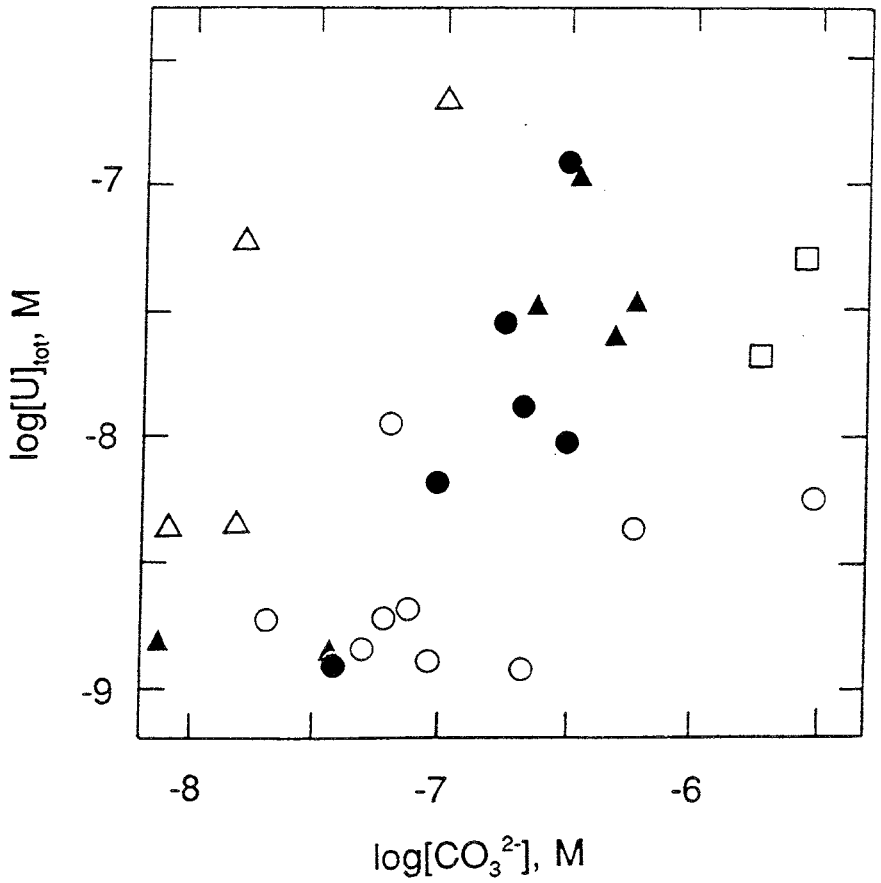

FIGURE 3.92 Total uranium concentrations versus carbonate concentrations (AS; O; LS, US; B; C).

3.7.2.6 Conclusions

The humic fraction, largely of low molecular weight, has a composition typical for a groundwater fulvic acid. The differences between humics from the various sampling places were minor, despite the differences in age (from modern to 15,000 a). The uranium complexing capacity (considering acid capacity and stability constants for the humic complexes with uranium) is not sufficient to significantly influence the speciation of uranium in the system. This assessment is largely confirmed by direct measurements of the distribution of uranium between inorganic and organic species in situ. It is not likely that the humics, under the present conditions, will have any significant mobilizing effect on the uranium. The measured uranium concentrations are at least qualitatively correlated with the carbonate concentrations in the water, but not with the TOC levels.

3.7.2.7 Acknowledgements

Valuable comments and suggestions by the project coordinators J.J. Cramer and J.A.T. Smellie are gratefully acknowledged. The project has been part of the AECL/SKB joint Cigar Lake analog study program.

3.7.2.8 References

ALLARD, B., ARSENIE, I., BORÉN, H., EPHRAIM, J., GÅRDHAMMAR, G. and PETTERSSON, C. 1990. Isolation and characterization of humics from natural waters. SKB Tech. Rep., **TR 90-27**.

CHOPPIN, G.R. and ALLARD, B. 1985. The complexes of actinides with naturally occurring organic compounds. In *Handbook of the Actinides* (ed. C. Keller, A. Freeman and J. Landers). North-Holland Publ. Corp., Amsterdam, 409-429.

CRAMER, J.J. 1986. A natural analog for a fuel waste disposal vault. In *Proc. 2nd Int. Conf. Radioactive Waste Management.* Can. Nuclear Soc. Proc., 697-702.

CRAMER, J.J. 1991. Hydrogeochemistry. In *Second Ann. Rep. AECL/SKB Cigar Lake analog study. Year 2: 1990-1991* (ed. J.J. Cramer and J.A.T. Smellie). AECL Internal Proj. Rep., **CLR-91-3**, 10-30.

CRAMER, J.J. and SMELLIE, J.A.T. 1991. Second Annual Report of the AECL/SKB Cigar Lake analog study. Year 2: 1990-1991. AECL Internal Proj. Rep., **CLR-91-3**.

CRAMER, J.J., VILKS, P. and LAROCQUE, J.P.A. 1987. Near-field analog features from the Cigar Lake uranium deposit. In *Natural analogs in radioactive waste disposal* (ed. B. Côme and N.A. Chapman). Com. Europ. Commun. Publ., **EUR 11035**, 59-72.

EPHRAIM, J., ALEGHET, S., MATHUTHU, A., BECKING, K., MALCOLM, R.L. and MARINSKY, J.A. 1986. A united physicochemical description of the protonation and metal ion complexation equilibria of natural organic acids (humic and fulvic acids). 2: Influence of polyelectrolyte properties and functional group heterogeneity on the protonation equilibria of fulvic acid. Environ. Sci. Technol., **20**, 354-366.

MILES, C.J., TUSCHALL Jr, J.R and BREZONIK, L. 1983. Isolation of aquatic humus with dietylaminoetyl cellulose. Anal. Chem., **55**, 410-411.

NORDÉN, M. EPHRAIM, J. and ALLARD, B. 1993. A comparative study of europium, thorium and uranium binding to an aquatic fulvic acid. Sci. Basis for Nucl. Waste Manag. (in press).

PAXÉUS, N. 1985. Studies on aquatic humic substances. Ph.D. Dissertation, Univ. of Gothenburg, Sweden.

PETTERSSON, C. 1992. Properties of humic substances from groundwater and surface waters. Ph.D. Dissertation, Linköping Univ., Sweden.

PETTERSSON, C., ARSENIE, I., EPHRAIM, J, BORÉN, H. and ALLARD, B. 1989. Properties of fulvic acids from deep groundwaters. Sci. Tot. Environ., **81/82**, 287-296.

PETTERSSON, C., EPHRAIM, J and ALLARD, B. 1992. On the composition and properties of humic substances isolated from deep groundwater and surface waters. (Manuscript submitted to Organic Geochemistry).

3.7.3 Total organic carbon and other organics
(P. Vilks and D. Bachinski)

The total organic carbon (TOC) in groundwater provides a measure of the combined concentration of all organic compounds, and flags waters where organic complexing of contaminants is likely to dominate over inorganic complexing. Although TOC by itself does not indicate the type of organic compounds present, a size fractionation of TOC would give an indication of the physical organic compounds, and may identify the presence of humics. Since a detailed characterization of humics and other organics was carried out on only selected samples, the results of TOC analysis may be used to extrapolate the conclusions obtained from the detailed characterization to other groundwater samples. Therefore, the following section summarizes the results of TOC analysis from 1989 to 1991, and discusses the problems associated with TOC size fractionation by filtration.

The distribution of an element between dissolved species, colloids and suspended particles can be determined from the chemical analyses of filtrates and concentrates produced by tangential-flow filtration of groundwater samples, provided the element's concentration is not affected by some other process such as sorption to the filter membrane. To check for irregularities during filtration (see Figure 3.86), a mass balance is determined between the element's total concentration before filtration (original) and the summed concentration of dissolved and particulate forms of the element. Table 3.52 summarizes TOC concentrations measured in the original groundwater and two filtrates, and TOC values calculated for colloid and suspended particle fractions. A comparison of filtrate (F1 and F2) TOC concentrations with the TOC concentration in untreated water shows that for at least 75 % of Cigar Lake groundwater samples, the filtrates have more TOC than the original groundwater. Although not shown in the table, in some cases colloid concentrates had less TOC than the corresponding filtrate. This problem rarely occurs with other elements.

Sample cross-contamination or contamination from soap used to clean filter membranes could explain higher TOC concentrations in the filtrates and retentates than in the untreated sample. However, an examination of the filtration order of Cigar Lake samples indicates that neither of the above contaminations are responsible for high TOC concentrations in filtered water. High TOC in filtrates and retentates are correlated with higher TOC in untreated water. A random contamination from a degenerating filter membrane is also not likely, because the occurrence of higher TOC in filtrates and retentates is more frequent in some boreholes and rarely occurs for surface water samples. This suggests that the nature of the organic interaction with the filter membrane is influenced by the type of organic compounds in groundwater.

If there was incomplete mixing of TOC in the 50 L carboy at the time the "original" subsample was taken (Figure 3.86), this subsample would not be representative of the organic carbon in the 50 L sample. Some organic compounds may form an immiscible phase that is concentrated in the upper part of the 50 L sample-carboy. Since the untreated sample (original) is collected from the bottom of the carboy, it would not contain any organics concentrated at the top of the carboy. These organics would eventually be filtered and contribute to the TOC in the filtrate and particle concentrate samples.

If the TOC in the retentate samples is lower than in the filtrate, some process must remove organic compounds from the recirculating retentate water, while passing organics on to the filtered water. Organics could be removed from the recirculating water by weak adsorption to the surface of the filter membrane. The water that is forced through the membrane to the filtrate side may desorb these organics, increasing the TOC in filtered water.

Since the behavior of TOC during filtration can be complicated by processes that are controlled by the nature of organic compounds in groundwater, it is difficult to make a universal choice as to which subsample (original, F1, F2) best represents the dissolved organic carbon for a given sample. In light of these uncertainties, the reader is advised to choose the appropriate values for dissolved organic carbon from Table 3.52, with the following recommendations. If the concentration of colloidal or particlulate TOC is not significant, the TOC of the original sample may be the best choice because it has not come into contact with any filter membranes. If it is necessary to use the TOC value from a filtered sample, F1 may be the best choice because it has had the minimum interaction with a filter membrane. Furthermore, the calculated concentration of colloidal TOC in the 1- to 10-nm size range is usually significantly less than the difference between F1 and F2.

An attempt was made to characterize the organic compounds in Cigar Lake groundwaters using a gas chromatograph/mass spectrometer. Water samples from selected boreholes were collected in one-liter glass bottles. Volatile organic compounds were extracted by purging a water sample with helium and trapping the organic compounds on a sorbent column. The sample was transferred to the gas chromatograph/mass spectrometer by heating the sorbent column and backflushing it with helium. Nonvolatile organics were extracted from groundwater with methylene chloride, which was then analyzed by the gas chromatograph/mass spectrometer (GC-MS).

The results of these analysis are summarized in Table 3.53. The samples taken in 1990 were collected with a squeeze pump after extensive borehole flushing. In 1991 samples were collected with the down-hole system after a quick piezometer flush with pressurized nitrogen. A comparison of organic compound concentrations with TOC shows that volatile and solvent extractable organics account for a very small fraction of the TOC in most of the samples collected in 1990. Samples collected with the down-hole system in 1991 contain much higher concentrations of solvent extractable organics, which account for 42 to 84 % of the TOC. Some of these compounds are plasticizers, which may have been leached from the PVC standpipe of the piezometer. Contamination from the down-hole sampler is a possibility, although not very likely because of the short contact time with the water sample. These results demonstrate the importance of adequate piezometer flushing before sampling groundwater for TOC and organic characterization.

TABLE 3.52
ORGANIC CARBON (mg/L) IN CIGAR LAKE GROUNDWATER

SAMPLE	ORIGINAL	F1	F2	COLLOID 1-10 nm	COLLOID 10-450 nm	PARTICLE >450 nm
67-1	2.22	0.55	0.66	0.00	0.16	1.14
67-2	1.85	0.64	0.68	0.03	0.54	0.57
67A1	1.20	0.77	0.43	0.10	0.21	0.17
67A2	1.61	0.82	0.41	0.03	0.83	1.18
67A3	2.28	1.89	1.10	0.03	0.10	0.42
67B1	0.89	0.67	0.65	0.04	0.01	0.00
67B2	0.67	0.56	0.22	0.14	0.16	0.24
67-1	2.66	3.39	3.11	0.00	0.32	0.42
67-2	1.39	1.32	1.47	0.18	0.18	0.23
67-3	1.13	0.61	-	0.00	0.40	0.12
67-4	1.63	0.67	1.13	0.03	0.39	0.15
71-1	1.65	1.60	1.70	0.00	0.00	0.01
71-2	0.63	1.17	0.53	0.01	0.00	0.01
71-3	0.58	1.79	0.56	0.00	0.00	0.01
71A1	0.85	0.71	1.00	0.02	0.17	0.00
75-1	0.44	0.96	0.62	0.00	0.01	0.00
75-2	0.37	0.55	0.17	0.03	0.02	0.00
75B1	0.60	1.11	0.52	0.15	0.00	0.02
75B2	1.16	1.68	0.46	0.34	0.15	0.05
79A1	0.85	0.71	1.00	0.05	0.18	0.00
79A2	5.27	11.5	10.6	0.16	0.09	0.00
79A3	1.85	4.09	3.90	0.10	0.00	0.08
79B1	0.59	2.93	2.88	0.00	0.00	0.00
79B2	0.71	2.89	3.26	0.00	0.00	0.00
79-1	2.18	5.07	4.77	0.00	0.00	0.00
79-2	4.94	5.09	4.54	0.11	0.01	0.00
79-3	2.26	3.61	3.68	0.00	0.00	0.01
79-4	2.48	2.91	3.00	0.00	0.00	0.03
81B1	0.46	1.31	1.09	0.15	0.00	0.09
81B2	0.49	1.80	1.51	0.06	0.00	0.03
83A1	0.59	0.43	0.35	0.09	0.00	0.00
83B1	0.48	0.62	0.26	0.09	0.02	0.00
83-91FW3	0.37	0.52	0.86	0.03	0.06	0.00
91-1	0.55	1.01	0.33	0.06	0.00	0.00
91-2	0.62	1.36	0.94	0.03	0.00	0.00
122-1	1.83	2.19	3.37	0.00	0.00	1.05
122-2			1.91			
122-91FW3	0.40	0.41	0.69	0.02	0.11	0.01
139-1	0.34	0.34	0.70	0.00	0.04	0.00
139-2	0.33	0.38	0.22	0.03	0.04	0.00
139A1	0.81	0.73	0.50	0.10	0.07	0.15
139A2	0.59	0.57	0.39	0.07	0.00	0.02
139B1	0.70	1.12	1.24	0.00	0.00	0.03

TABLE 3.52 (concl.)

SAMPLE	ORIGINAL	F1	F2	COLLOID 1-10 nm	COLLOID 10-450 nm	PARTICLE >450 nm
139B2	0.60	1.07	0.38	0.07	0.00	0.00
139-1	0.93	1.84	0.42	0.07	0.00	0.01
139-2	0.53	1.58	0.46	0.04	0.00	0.02
139-3	1.52	1.85	1.39	0.08	0.00	0.02
139-4	0.55	0.54	2.27	0.00	0.06	0.04
139-5	0.57	1.14	1.12	0.00	0.01	0.00
197-1	0.59	0.74	0.40	0.06	0.00	0.00
197-2	0.48	0.60	0.34	0.05	0.00	0.01
197A1	2.09	1.26	0.51	0.11	0.00	0.00
197A2	1.77	1.78	1.41	0.02	0.00	0.00
197A3	1.75	1.50	0.70	0.06	0.00	0.00
197B1	0.51	0.70	0.89	0.00	0.05	0.01
197B2	0.50	1.03	0.36	0.17	0.04	0.00
211-1	0.14	0.14	0.09	0.02	0.04	0.01
211-2	0.48	0.35	0	0.14	0.00	0.00
211B1	0.22	0.78	2.51	0.00	0.00	0.00
211B2	0.28	0.21	0.26	0.00	0.00	0.00
211-1	1.25	1.23	1.26	0.00	0.00	0.00
211-2	0.51	0.53	1.10	0.00	0.00	0.00
211-3	0.39	0.75	0.89	0.00	0.00	0.00
211-4	0.59	0.71	0.66	0.03	0.01	0.00
219-1	0.18	0.35	0.18	0.00	0.06	0.04
219-2	0.14	0.13	0.39	0.00	0.00	0.16
219A1	1.28	1.56	1.53	0.01	0.03	0.00
219A2	1.18	1.11	0.97	0.00	0.00	0.00
219B1	0.38	1.28	1.57	0.00	0.00	0.00
219B2	0.28	0.82	0.17	0.06	0.00	0.00
219-1	0.99	1.66	1.40	0.03	0.03	0.00
219-2	1.05	1.35	1.41	0.00	0.00	0.00
219-3	1.05	1.05	2.62	0.00	0.00	0.00
220-1	1.86	0.75	0.88	0.00	0.55	1.02
220-2	2.12	1.07	0.80	0.01	0.74	0.80
220-3	1.76	1.30	0.64	0.07	0.41	1.33
220A1	2.53		1.77	0.00	0.30	0.02
220A2	5.10	5.62	4.90	0.00	0.00	0.02
220A3	6.71	4.66	5.20	0.00	0.03	0.03
220B1	2.67	3.75	3.57	0.00	0.00	0.00
220B2	3.12	3.40	4.35	0.00	0.06	0.05
ALINE C	3.80	1.93	1.63	1.16	0.99	0.37
ALINE C	7.79	4.49	2.89	1.33	0.00	2.10
ALINE L	2.55	1.78	1.02	0.69	0.24	0.22
CIGAR L	5.14	13.25	15.1	0.00	0.00	0.40
CIGAR L	2.99	0.99	0.86	0.19	1.06	0.46
W LAKEB1	1.37	1.16	0.61	0.42	0.10	0.18
W LAKE91	2.74	1.77	1.76	0.16	1.03	0.54
W LAKE91	2.96	1.46	1.00	0.29	1.27	0.85

TABLE 3.53
ORGANIC COMPOUNDS IDENTIFIED WITH GC-MASS SPECTROMETRY

Sample	Compound	Approximate Concentration mg/L
67A2	2-ethyl-1-hexanol	0.001
May 90	3-nitro-1,2-benzenedicarboxylic acid	0.003
	TOC	0.82
67A3	N-butyl-benzenesulfonamide	0.020
May 90	dicarboxylic acid	0.001
	TOC	1.89
79A1	N-propyl benzenesulfonamide	0.400
May 90	TOC	0.71
79	Bis(2-ethylhexyl)phthalate	0.002
May 91	2-Chloroethanol,phosphate (3:1)	0.090
down hole	Chloro phenyl sulphone @	2.000
	Caffeine	0.006
	Di-isodecyl phthalate @	0.005
	4-Octanone @	0.006
	2-propanone	0.020
	TOC	5.08
197A1	2-methyl-1-penten-3-ol @	0.010
May 90	bis(2-ethylhexyl)ester 1,2-benzenedicarboxylic acid	0.002
	TOC	1.26
197	N-butyl benzenesulfonamide @	0.090
May 91	Chloro phenyl sulfone @	0.500
down hole	2-Methyl-1-penten-3-ol @	0.260
	2-propanone	0.010
	Benzene	0.007
	TOC	1.03

@: or similar compound
TOC: total organic carbon from F1

TABLE 3.53 (concl.)

Sample	Compound	Approximate Concentration mg/L
220	2-butoxyl-ethanol	0.001
May 90	benzothiazole	0.002
	1,1'-sulfonylbisbenzene	0.002
	bis(2-ethylhexyl)ester 1,2-benzenedicarboxylic acid	0.001
	unidentified peak	0.020
	TOC	5.6
220	Bis(2-ethylhexyl)phthalate	0.009
May 91	N-propyl benzenesulfonamide @	0.200
down hole	Chloro phenyl sulfone @	0.800
	N-butyl benzenesulfonamide @	2.000
	1-Tetradecanol, acetate	0.008
	Di-isodecyl phthalate @	0.007
	Benzene	0.007
	2-propanone	0.030
	Isoxazole	0.005
	5-methoxy-1-AZA-6-oxabicyclo (3.10) hexane	0.003
	2-butanone	0.006
	TOC	3.4
CLU10	2-(1,1-dimethylethyl)-phenol	0.003
May 90	4,4'-(1-methylethylidene)-bis phenol	0.001
	1,2-benzenedicarboxylic acid	0.001
	3-nitro-1,2-benzene-dicarboxylic acid	0.010
	unidentified compound	0.020
	TOC	0.21

@: or similar compound
TOC: total organic carbon from F1

3.7.4 Microbial research

(S. Stroes-Gascoyne, A.J. Francis and P. Vilks)

3.7.4.1 Introduction

The presence of micro-organisms (c.q., bacteria) in (deep) subsurface environments has not been appreciated until fairly recently. It is now generally recognized that micro-organisms through their metabolic reactions could have significant effects on the geochemistry of (deep) subsurface environments (i.e., on the redox processes, migration, concentration levels, etc.). The Canadian Nuclear Fuel Waste Management Program is investigating the concept of geological disposal of nuclear fuel waste, and the safety assessment of this concept calls for a study of all processes that could potentially affect the performance of a nuclear fuel waste disposal facility. It is therefore required to assess the potential effects of microbes on such a facility, and the natural analog site at Cigar Lake provides a unique opportunity to investigate microbial life in a natural UO_2 deposit.

Factors affecting microbial development and growth include the physicochemical environment (e.g., temperature, pH, pressure, radiation, salinity, toxins, etc.) and the availability of water, macro- and micro-nutrients, electron donors and acceptors and usable energy. Specific questions need to be answered with respect to the potential effects of microbes on the stability of a waste disposal vault (J.M. West pers. comm.):

i Do microbes exist in a vault environment?

ii Can they survive in the harsh vault environment?

iii If they exist and can survive, what effects could they have on the performance of the vault?

iv How can the significance of microbial growth and activity be evaluated?

Microbial studies in the Cigar Lake deposit can be used to search for answers to these questions, because it has similarities to a nuclear fuel waste disposal site.

Initial microbial work on Cigar Lake water samples (i.e., microbial enumeration on various agar media and adenosine triphosphate (ATP) analysis (Champ 1987)) tentatively confirmed the presence of certain groups of microbes. Recently, these results were partially corroborated by analyses using BART tubes ("Biological Activity Reaction Tests", a recently developed, commercially available field method for bacterial analysis (Vilks 1991; Stoes-Gascoyne et al. 1991)) and by direct microscopic counting of bacteria using DAPI (4,6-diamidino-2 phenylindole dihydrochloride) stain (Francis et al. 1992).

3.7.4.2 Sampling

The sampling of groundwaters from the Cigar Lake uranium deposit includes the collection of both pressurized and pumped samples from depths of up to ~450 m below surface. These two sampling methods provide important complementary information, resulting in a well-characterized composition of each water sample.

The samples collected for microbial analyses are collected with the down-hole sampling rig and the samples are brought to surface under the ambient pressure at the sampling depth. A string of stainless-steel pressure vessels (~55-110 mL), with a one-way checkvalve at each end of the string, is attached to a pressure hose and lowered down the piezometer to about 15 m above the bottom of the piezometer. The vessels and the pressure hose are charged with a N_2-gas overpressure up to the checkvalve between the bottom of the lowermost vessel and the intake port. Once the sampling string has been lowered into place, the N_2-pressure is bled off at surface, opening the bottom checkvalve and letting water rise up through the string of vessels and inside the pressure hose. When the water levels in- and outside the hose have equilibrated, the checkvalves automatically shut, sealing in the water sample under the ambient pressure at that depth. An N_2-gas overpressure is then applied to the top of the pressure hose and the whole assembly is raised to surface.

The vessel (~55 mL) used for the collection of the microbiology sample is placed at the bottom of the vessel string directly above the intake port. This arrangement allows this vessel to be filled last after it has been thoroughly rinsed with all the formation water filling the other vessels and the pressure hose (over a length of ~150-400 m). The microbiology vessel (including its two valves) is sterilized at 550 °C for ~4-8 h in a muffle furnace before assembly of the vessel string. The non-sterilized components of the sampling rig that are in contact with the water below the microbiology vessel include the checkvalve (brass), intake port and weight (both stainless steel).

Once the microbiology vessel has been isolated from the string at surface, the contents are transferred to a sterile serum bottle (glass) sealed with a sterilized septum and filled with dry N_2-gas. A sterilized stainless-steel connector and needle are attached to one end of the vessel, and a He-gas overpressure is used at the vessel's other end to transfer the water sample through the septum into the bottle. A second sterilized needle is used to bleed the gas overpressure from the bottle during the transfer. The sample bottle is then labelled and stored in the dark at ~4 °C in a refrigerator in the field lab on site at Cigar Lake. Transport of the samples from Cigar Lake to elsewhere for analysis is done in coolers with dry ice added to maintain a cool temperature.

3.7.4.3 Results

Table 3.54 summarizes all microbial analyses performed on Cigar Lake groundwater samples as well as the analyses carried out on lake, drill and overburden waters.

To evaluate whether these numbers are in agreement with the actual amount of nutrients found in the Cigar Lake groundwaters, model calculations were performed (using a method

described by Stroes-Gascoyne, 1989). These calculations established the maximum amount of microbial cells that could be supported in a water sample, based on the limiting nutrient(s) present in that sample and an average composition for microbial cells (assuming that energy availability would not be a limiting factor). The water compositions were taken from the reference groundwater data sets that have been established for Cigar Lake groundwaters.

Table 3.55 shows the results of these calculations. In this table, a comparison between actually measured numbers of bacteria and calculated numbers is made.

3.7.4.4 Discussion

Table 3.54 shows that the numbers and types of microbes in the groundwater samples from the various boreholes in the Cigar Lake system vary considerably. This is particularly obvious in the cases where more than one sample was collected and analyzed at different times in the sampling program. It cannot be concluded what causes these fluctuations. Sample collection was generally done in a consistent fashion, as described above. Contamination from drilling and other human intrusions cannot be ruled out, although most boreholes have been in existence for a considerable time now and should be well flushed with formation water. However, the altered habitat provided by the borehole may also influence microbial composition and growth (Champ 1987). The counting methods used (ATP, BART and DAPI) will influence the analysis, because each is based on different principles. The ATP method measures the bacterial component adenosine-triphosphate, whose concentration depends on the metabolic activity of the microbes, hence the range in Table 3.54. Considering the low nutrient levels in the groundwaters, the lower numbers are probably more indicative of the actual number of cells (Champ 1987). The BART tests actually induce growth of bacteria and derive a number from the colour change in the growth medium, whereas DAPI stains DNA of both living and non-living bacteria but suffers from interference of debris in solution. It is therefore not possible to draw any meaningful conclusions from these numbers, other than that micro-organisms are present in subsurface Cigar Lake samples and seem capable of surviving in this particularly harsh environment.

Analyses were also performed for various physiological groups of micro-organisms. Table 3.54 shows that in approximately 80 % of the samples, the numbers of anaerobes are at least equal to or up to more than an order of magnitude larger than the numbers of aerobes. This could be indicative of the prevailing reducing environments where these samples came from, and may indirectly indicate that contamination has not completely altered the microbiological signature of these deep subsurface samples. Sulphate-reducing bacteria seem to be common in the ore-zone samples (5 out of 7 times). However, recent samples (U15A, U16A) taken underground directly into the orezone do not contain sulphate reducers. Iron bacteria appear to be distributed throughout the whole area, perhaps indicating their diverse nutrient requirements. Also, iron is present in most of the groundwater samples. Methanogens were indicated mainly in basement samples taken early in the microbial sampling program, but this has yet to be confirmed by the analysis of more recent samples.

Table 3.55 indicates that, generally, N is the limiting nutrient in these groundwaters (11 of 15 cases), although P is almost always nearly as limiting. A comparison between maximum microbial populations based on calculations using the limiting nutrient indicates that most of the numbers found in the water samples are lower than the calculated numbers. This could be caused by several factors, including energy constraints and unsuitability or unavailability of nutrients. The lower numbers could also be a result of the counting method used or of sample treatment subsequent to sampling. The possibility also exists that by sampling only the water most microbes are "missed", because they are attached to solid surfaces (Pederson et al. 1991).

Future microbial research at Cigar Lake will include the continuing study of the distribution of microbes in the ore body, the clay halo and the sandstone in order to confirm the presence of microbes and to establish the prevalent physiological groups of organisms. Methanogens, because they require a highly reducing environment and because these organisms are less likely to be introduced into the system, will be studied with particular attention. Experiments to assess UO_2 dissolution and mineralization in the presence and absence of bacteria isolated from core from the ore zone will also be performed. Results from these studies will help evaluate the influence of bacteria on the redox environment and on the UO_2 stability, and, hence, will help us assess the efficiency of a clay barrier in reducing the transport of radionuclides by bacteria.

3.7.4.5 References

CHAMP, D.R. 1987. Cigar Lake internal report 1987.

FRANCIS, A.J., GILLOW, J.B. and ANDERSON, H. 1992. Microbiological study. In *Cigar Lake Analog Study Prog.Rep., Nov 1991-March 1992* (ed. J.J. Cramer). AECL Internal Proj. Rep., **CLR-92-2**, 39-41.

PEDERSON, K., EKENDAHL, S. and ARLINGER, J. 1991. Microbes in crystalline bedrock. Assimilation of CO_2 and introduced organic compounds by bacterial populations in groundwater from deep crystalline bedrock at Laxemar and Stripa. SKB Tech. Rep., **SKB-91-56**.

STROES-GASCOYNE, S. 1989. The potential for microbial life in a Canadian high-level fuel waste disposal vault : a nutrient and energy source analysis. AECL Research Rep., **AECL-9574**.

STROES-GASCOYNE, S., BROWN, A. and VILKS, P. 1991. Microbial research. In *Second Annual Report of the AECL/SKB Cigar Lake Project, Year 2: 1990-1991* (eds. J.J. Cramer and J.A.T. Smellie). AECL Internal Proj. Rep., **CLR-91-3**, 112-115.

VILKS, P. 1991. Organic geochemistry and microbiology. In *Cigar Lake Analog Study Prog. Rep., May-October 1991* (ed. J.J. Cramer) AECL Internal Proj. Rep., **CLR-91-5**, 47-50.

TABLE 3.54
SUMMARY OF RESULTS FOR MICROBIAL CHARACTERIZATION

Location/ Hole #	Data From	Sample Date	Total Cells/mL (+ method)		Aerobes	Anaerobes	Sulphate Reducers	Iron Related	Denitri-fiers	Fermen-ters	Methan-ogens
Surface											
Waterbury Lake	[1]	1/91	1.0×10^5	(b)			nd	nd			
Cigar Lake	[1]	1/91	5.5×10^5	(b)			nd	nd			
Drill Water	[1]	1/91	1.0×10^6	(b)			nd	nd			
Overburden											
P3.8	[1]	1/91	1.0×10^6	(b)			nd	++			
P3.12	[1]	1/91	1.0×10^6	(b)			nd	++			
Upper Sandstone											
75	[3]	8/85	$<5.0 \times 10^4$	(c)	1.7×10^2	7.1×10^2	nd	+			
83	[1]	1/91	5.6×10^5	(b)			+	++			
	[3]	8/85	$<5.0 \times 10^4$	(c)	<1	<1	nd	nd			
Lower Sandstone											
139	[4]	9/91	$2.9 (\pm 0.9) \times 10^3$	(a)	2.7×10^5	2.7×10^5					
	[2]	9/91	1.0×10^4	(b)			+	++			
	[3]	4/87	$7.39 - 888 \times 10^5$	(c)	$4.6 (\pm 0.1) \times 10^3$	$1.1 (\pm 0.2) \times 10^4$	nd				nd
219	[4]	9/91	$2.9 (\pm 0.7) \times 10^3$	(a)	2.3×10^5	1.6×10^5					
	[2]	9/91	1.5×10^5	(b)			+	++			
80	[3]	4/87	$1.9 - 223 \times 10^5$	(c)	$1.9 (\pm 0.9) \times 10^3$	$3.7 (\pm 0.5) \times 10^4$	nd				nd
Altered Sandstone											
67	[4]	9/91	$4.2 (\pm 1.1) \times 10^3$	(a)	9.5×10^3	2.0×10^4	+		++	++	nd
	[2]	9/91	5.3×10^4	(b)			nd	++			
81	[4]	9/91	$7.3 (\pm 2.4) \times 10^3$	(a)	2.0×10^4	4.9×10^4	+		++	+	nd
	[2]	9/91	1.5×10^3	(b)			+	+			
211	[4]	9/91	$2.4 (\pm 0.2) \times 10^4$	(a)	1.4×10^5	2.1×10^5	nd		++	+	nd
	[2]	9/91	6.1×10^4	(b)			+	++			
195	[2]	9/91	5.0×10^4	(b)			nd	nd			
Clay Zone											
91	[3]	8/85	$1.0 - 119 \times 10^5$	(c)	$>2 \times 10^3$	$>2 \times 10^3$	nd	++			
197	[4]	9/91	$6.5 (\pm 1.0) \times 10^3$	(a)	4.0×10^5	3.2×10^5					
	[2]	9/91	1.0×10^5	(b)			+	++			
	[3]	4/87	$5.9 - 705 \times 10^5$	(c)	$7.9 (\pm 0.4) \times 10^2$	$8.0 (\pm 0.4) \times 10^3$	nd				+
134	[3]	4/87	$1.6 - 187 \times 10^5$	(c)	$1.4 (\pm 0.08) \times 10^4$	$3.6 (\pm 0.5) \times 10^4$	nd				
Orezone											
79	[4]	9/91	$2.3 (\pm 0.6) \times 10^3$	(a)	9.1×10^5	1.0×10^5	nd		++	nd	nd
	[3]	8/85	$<5.0 \times 10^4$	(c)	$>10^3$	$>2 \times 10^3$	++				
	[3]	4/87	$2.6 - 314 \times 10^5$	(c)	1.3×10^2	$8.8 (\pm 0.4) \times 10^3$	nd				nd
198	[3]	4/87	$4.5 - 542 \times 10^5$	(c)	$26 (\pm 0.1) \times 10^3$	$2.5 (\pm 0.6) \times 10^4$	++				++
220	[4]	9/91	$5.1 (\pm 1.0) \times 10^2$	(a)	3.2×10^1	2.0×10^2	+		nd	nd	nd
	[2]	9/91	7.9×10^5	(b)			+	++			
	[2]	5/91	1.0×10^4	(b)			+	++			
Ore Underground											
U15A	[1]	1/91	5.6×10^5	(b)			nd	++			
U16A	[1]	1/91	1.0×10^5	(b)			nd	nd			
Basement											
128	[3]	4/87	$5.3 - 642 \times 10^5$	(c)	$1.7 (\pm 0.1) \times 10^4$	$4.1 (\pm 0.8) \times 10^3$	nd				++
199	[3]	4/87	$0.5 - 60 \times 10^5$	(c)	$2.1 (\pm 0.6) \times 10^3$	$1.5 (\pm 0.1) \times 10^4$	nd				++
137	[3]	4/87	$1.1 - 135 \times 10^5$	(c)	$2.5 (\pm 0.04) \times 10^3$	$1.5 (\pm 0.04) \times 10^4$	+				++
480	[2]	9/91	7.8×10^3	(b)			nd	++			

[1] Cigar Lake Annual Report Year 2 (1990-1991)
[2] Cigar Lake Progress Report May-Oct. 1991
[3] Champ: Cigar Lake Internal Report 1987 (Appendix F)
[4] Cigar Lake Progress Report Nov. 1991 - March 1992

(a) direct microscopic counts using DAPI
(b) Biological Activity Reaction Tests (BART tubes)
(c) ATP analysis

nd not detected
\+ present ($<10^2$ cells/mL)
++ present ($\geq 10^2$ cells/mL)

TABLE 3.55
LIMITING NUTRIENTS AND CALCULATED AND OBSERVED MICROBIAL POPULATIONS IN VARIOUS CIGAR LAKE WATER SAMPLES

Location/ Borehole #	Limiting Nutrient *	"Usable" C * mg/L	Calculated * Max. Microbial Population cells/mL	Observed ** Range of Microbes cells/mL
Surface Waterbury Lake	N	<0.16	$<1.6\times10^{6}$ - $<1.6\times10^{8}$	1.0×10^{5}
Upper Ss.				
75	N	<0.05	$<5.4\times10^{5}$ - $<5.4\times10^{7}$	$<5.0\times10^{4}$
Lower Ss.				
139	N	<0.05	$<5.4\times10^{5}$ - $<5.4\times10^{7}$	1.0×10^{4} - 8.9×10^{7}
219	N	<0.05	$<5.4\times10^{5}$ - $<5.4\times10^{7}$	1.5×10^{5} - 3.9×10^{5}
Altered Ss.				
67	N	<0.05	$<5.4\times10^{5}$ - $<5.4\times10^{7}$	3.0×10^{4} - 5.3×10^{4}
81	N	<0.05	$<5.4\times10^{5}$ - $<5.4\times10^{7}$	1.5×10^{3} - 6.9×10^{4}
211	P	<0.27	$<2.7\times10^{6}$ - $<2.7\times10^{8}$	6.1×10^{4} - 3.5×10^{5}
Clay Zone				
91	N	<0.05	$<5.4\times10^{5}$ - $<5.4\times10^{7}$	1.0×10^{5} - 1.2×10^{7}
197	N	<0.05	$<5.4\times10^{5}$ - $<5.4\times10^{7}$	1.0×10^{5} - 7.1×10^{7}
Ore Zone				
79	P	<0.27	$<2.7\times10^{6}$ - $<2.7\times10^{8}$	3.0×10^{3} - 3.1×10^{7}
198	N	<0.05	$<5.4\times10^{5}$ - $<5.4\times10^{7}$	4.5×10^{5} - 5.4×10^{7}
220	P,N	<0.27	$<2.7\times10^{6}$ - $<2.7\times10^{8}$	5.1×10^{2} - 7.9×10^{5}
Basement				
199	N	<0.05	$<5.4\times10^{5}$ - $<5.4\times10^{7}$	5.0×10^{4} - 6.0×10^{6}

* Calculated from reference groundwater compositions at Cigar Lake (see Table 3.30 in Section 3.5.3), an average microbial cell composition ($C_1N_{0.28}S_{0.02}P_{0.06}Fe_{0.004}$) and the assumption that 1 g C produces 10^{13} - 10^{15} cells (Stroes-Gascoyne, 1989).

** Data from Table 3.54 (combination of total cells/mL and (aerobes + anaerobes)/mL).

3.8 NUCLEAR REACTION PRODUCT GEOCHEMISTRY

3.8.1 Introduction
(J. Cramer)

The uranium deposit at Cigar Lake contains some very uranium-rich zones in the high-grade "Main Pod" (the 0.8-km-long eastern part) of the deposit. Some drillcores intersect mineralization with concentrations of >40 % U over several metres, and grades of >50 % U have been observed locally throughout this "Main Pod". The presence of these high concentrations of uranium, and of groundwater within the mineralized zones, led to speculations on the occurrence of nuclear reaction processes within this deposit. The age of formation of the uranium mineralization (1.3 Ga) precludes the occurrence of sustained fission-reactions as have been observed at Oklo in Gabon. The maximum concentration of ^{235}U in the Cigar Lake deposit would have been only ~2 % (at 1.3 Ga ago), producing a neutron density that was too low, with natural water as a moderator, for sustained fission. Also, measurements of the ^{235}U abundance in many Cigar Lake samples show consistent natural $^{235}U/^{238}U$ ratios (e.g., Phillippe et al. 1993), supporting this observation.

However, the occurrence of "natural fission" reactions in natural systems containing radioactive elements has been recognized for some time, and the development of ultra-sensitive analytical techniques now allows the measurement of the reaction products. In fact, elements that used to be labeled "synthetically prepared", such as Tc and Pu, have now been determined to occur naturally, albeit in extremely small quantities. As in the case of the Oklo deposit, data and information on the geochemistry of nuclear reaction products, such as ^{99}Tc, ^{129}I and ^{239}Pu from Cigar Lake, would be very valuable to provide analog information to help in performance assessment. The determination of the content of these isotopes in natural uraninites, their associated minerals and groundwaters at Cigar Lake can provide information on the mass balance and mobility of the isotopes, as well as on other processes such as the dissolution of uraninite (congruent vs. incongruent).

Section 3.8.2 summarizes the results of both the theoretical and analytical studies on Cigar Lake samples conducted by David Curtis and June Fabryka-Martin at the Los Alamos National Laboratory (LANL) in Los Alamos, New Mexico. This section includes model predictions on the concentration of ^{3}H, ^{14}C, ^{36}Cl, ^{99}Tc, ^{129}I, ^{237}Np and ^{239}Pu expected in the Cigar Lake deposit, based on LANL's MCNP code and available analytical data on the ore. Also, a comparison is made with measured concentrations of each isotope where available at this time.

Section 3.8.3 summarizes the modelling on the extent and potential effects of radiolysis in the mineralized zone of the Cigar Lake deposit. This work was carried out by Hilbert Christensen at Studsvik Nuclear in Studsvik, Sweden, and focussed on determining whether radiolysis (α and/or γ) could produce a significant oxidation potential in the groundwater in contact with the uranium minerals.

PHILIPPE, S., LANCELOT, J.R., CLAUER, N. and PACQUET, A. 1993. Formation and evolution of the Cigar Lake uranium deposit based on U-Pb and K-Ar isotope systematics. Can. J. Earth Sci., **30**, 720-730.

3.8.2 Natural nuclear products in the Cigar Lake deposit

(J. Fabryka-Martin, D.B. Curtis, P. Dixon, D. Rokop, F. Roensch, R. Aguilar and M. Attrep)

3.8.2.1 Background philosophy

A common component of performance assessments of geologic repositories for radioactive waste is a scenario of aqueous transport from the repository to the environment accessible by man. In the Sandia Total Safety Performance Assessment (TSPA) (Barnard et al. 1991), scenarios of radionuclide release to the accessible environment are developed by considering "well-defined connected sequences of features, events or processes". *Features* (boundary conditions) are the geologic or hydrologic properties of the site or system that are expected to be durable. *Processes* ("the physics") are phenomena that have gradual continuous interactions with the system. *Events* (initial conditions or forcing terms) are occurrences that have a specific starting time (and usually a duration shorter than the time being simulated). The aqueous transport scenario at Yucca Mountain, Nevada, is simulated by mathematical descriptions of radionuclide release from an engineered barrier system, groundwater flow and radionuclide transport, coupled in computer-based models. Predictions of cumulative releases to the accessible environment, expressed as probability distributions, are the measures of performance resulting from these coupled models.

Source-term models calculate radionuclide releases from the engineered barriers system and near-field environment into the far-field region (Barnard et al. 1991; Cossik et al. 1991). Models are developed from conceptual processes that simulate failures of the engineered barriers system, radionuclide exposure by waste-form degradation and transport of radionuclides through the near-field environment. After failure has occurred, release rates depend upon 1) waste-form degradation rates, 2) mass transport rates from the waste package, and 3) rates of radionuclide sequestering processes such as precipitation and sorption. Oxidative dissolution of UO_2 is assumed to be the degradation process controlling rates of radionuclide transfer from the solid immobile phase to the mobile groundwater. In the TSPA, matrix alteration rates are entered as a log-normal distribution with values based upon results of leaching experiments of spent fuel. In localized regions where there is moisture, but no flowing water, radionuclide transport is exclusively controlled by diffusion. In locally saturated areas where there is flowing water, release may be by both advection and diffusion. To encompass extremes of groundwater flow at Yucca Mountain, the TSPA considers two alternative models: "The composite-porosity model, a model based on Darcy's law ... allows unrestricted water movement between fractures and the tuff matrix; the weeps model ... depicts essentially all of the percolating water travelling down fractures". The TSPA model inventory is comprised of nine radionuclides. The aqueous concentrations of four of them, including ^{99}Tc and ^{129}I, are characterized as alteration-limited. In other words, these elements are considered to be infinitely soluble and are, thus, upon contact with groundwater, contained exclusively in the aqueous phase. Aqueous concentrations are dependent exclusively upon their rate of transfer from the host phase to the water and the length of time water stays in contact with the radionuclide host. Five radionuclides, including those of plutonium and uranium, form insoluble phases under many natural conditions and thus, upon exposure to groundwater, aqueous concentrations are

limited by mineral solubility. Parameters for solubility controls on these elements are bounded by results from laboratory measurements and geochemical models. The other critical process for radionuclide sequestering is sorption, which is modelled using ranges, means and variables of sorption coefficients. The use of sorption assumes that the process is instantaneous and reversible. For purposes of modelling sorption effects, radionuclides were placed in one of three categories: 1) the ^{99}Tc and ^{129}I were assumed to have little or no tendency to adsorb, and were given singular sorption coefficients of zero; 2) four radionuclides, including ^{234}U, were assumed to have small but variable sorptive tendencies and were assigned sorption coefficients parameterized by distributions as a function of rock type; and 3) ^{239}Pu and two others with large but variable sorptive properties were assigned constant minimum sorption coefficients (Meijer 1990).

The development and utilization of models as predictive tools was recently discussed by Bredehoeft and Konikow (1993):

> "Models are adjusted until an *adequate* match ... to historical data is achieved. Once ... achieved, the model is commonly used to predict the response of the system into the future ... Usually care is taken to predict only for a time comparable to the period that was matched ... In making longer predictions, one can expect that the cumulative errors arising from mistakes in the conceptual model, model structure and parameter estimates could become significantly large ... The difficulty in the nuclear waste problem ... is the fact that we are attempting to analyze the fate of wastes which are very long-lived in a geologic environment, an environment where there is uncertainty. We are asked to make predictions for times of 10,000 years or more. History matching followed by predictions of more or less equal duration is out of the question. It will be important to get the best possible conceptual model of the system."

Natural systems contain information about processes analogous to those that are being modelled, over times considered in safety assessments of high-level nuclear waste repositories. Because information from studies of natural systems is often ambiguous, and such a system is never a perfect analog of the actual repository, it can not be used in isolation. Such information must be part of an effort that includes models and laboratory experiments. When used in such an integrated program, the results of natural analog studies provide information that will assist in developing and evaluating effective safety assessments for geologic repositories of high-level radioactive waste.

Our studies are observational: we have no control over conditions, the *features*, that are boundary conditions for processes that we observe. Consequently we do not necessarily seek to duplicate the *features* of a particular repository site. For instance, the environment of a particular uranium deposit is very different from that of the potential repository site at Yucca Mountain, Nevada. Instead, we are providing information that can be used to evaluate the conceptual model, model structure and parameter estimates used to do a safety assessment of a specific site. In other words: *Under conditions represented in the uranium deposit* is the concept of alteration- vs. solubility-controlled aqueous concentrations of radionuclides consistent with observations? Are values used to parameterize mineral

alteration rates reasonable for describing radionuclide releases from uranium host minerals? Is there evidence of radionuclide mobility consistent with the understanding of local hydrology? Are the geochemical properties of a radionuclide compatible with assumptions regarding sorptive properties in the TSPA models?

3.8.2.2 Research objectives and approach

Radioactive nuclides are produced in the earth by nuclear reactions. In some geologic settings, abundances of these nuclides can be measured by modern analytical methods, and the results can be used to further our understanding of nuclear and non-nucler processes in the geologic environment. Rocks containing abundant uranium have the highest concentrations of natural nuclear products. Uranium is the primary source of neutrons that induce many of the nuclear reactions and it is the parent of many of the reaction products. Among these are ^{99}Tc and ^{129}I, fission products produced by both spontaneous and neutron-induced fission of uranium, and ^{239}Pu, ^{237}Np, ^{36}Cl, ^{14}C and ^{3}H representing products of neutron capture reactions on isotopes of a variety of elements. Materials containing radionuclides produced exclusively in situ by nuclear reactions will achieve a state of nuclear equilibrium in which abundances are a function of rates of production and decay. Such a condition will be referred to as secular equilibrium, to emphasize the analogy with the more familiar conditions established by decay of long-lived parents to their shorter-lived progeny. Systematics of nuclear processes are understood, and in principal can be used to predict radionuclide concentrations at secular equilibrium. We are measuring abundances of radioactive nuclear products in samples from the Cigar Lake uranium deposit, and comparing them with abundances predicted at secular equilibrium to characterize the timing, rates and chemical effects of non-nuclear processes in this deposit. If samples contain secular equilibrium abundances one can draw the following conclusions regarding non-nuclear processes in the system: 1) no process has impacted the system from the present to a time in the past equivalent to several daughter half-lives, *or* 2) the process rate was significantly slower than the radionuclide production rate, *or* 3) the process did not selectively add or remove the parent relative to the daughter.

If abundances of radioactive natural nuclear products are not at secular equilibrium, it indicates that 1) the system has been disturbed within the time domain of the nuclear process, *and* 2) the process rate was faster than or comparable to the radionuclide production rate, *and* 3) the process selectively added or removed daughter relative to parent. We characterize the state of secular equilibrium in a sample by determining a disequilibrium factor (α) obtained by normalizing the measured daughter/parent ratio to the daughter/parent ratio at secular equilibrium. The disequilibrium factor is exactly analogous to the daughter/parent ratio used in characterizing disequilibrium between radionuclides in the uranium and thorium decay chains. An α value of unity indicates a condition of secular equilibrium. Values greater than or less than unity represent systems in which the daughter has been, respectively, enriched or depleted relative to the parent. As with uranium/thorium decay series, interpretations regarding non-nuclear processes from disequilibrium of natural

nuclear products are often ambiguous. We seek to minimize ambiguity by working in well-characterized hydrogeological, mineralogical and geochemical systems where knowledge of conditions constrains the interpretations of chemical and temporal effects associated with release, transport and retention of radionuclides.

Our participation in the Cigar Lake analog study up to this time has largely involved developing techniques to measure the extremely small radionuclide concentrations in materials from the Cigar Lake uranium deposit, developing and evaluating procedures to define secular equilibrium concentrations of radionuclides in these materials, and to model production rates for a number of radionuclides based on measured properties of these materials.

3.8.2.3 Radionuclides in ore samples

3.8.2.3.1 Plutonium-239

Abundances of ^{239}Pu have been determined in three samples of Cigar Lake ore by isotope dilution mass spectrometry (Perrin et al. 1985; Attrep et al. 1992). Masses of indigenous plutonium in the analyzed samples are extremely small, and thus the results are vulnerable to inaccuracies from contamination introduced during storage, sampling or preparation for analysis. Consequently, numerous blanks, samples containing no indigenous plutonium, were periodically analyzed in conjunction with the samples. The results of the analyses of blanks show that measurable plutonium is introduced randomly during analyses. The average quantity of contaminant ^{239}Pu is $8\pm6 \times 10^7$ atoms. All samples were corrected for this quantity. The detection limit for ^{239}Pu, defined as three standard deviations above the average measured blank, is 2.4×10^8 atoms. Blank corrected abundances in Cigar Lake samples are given in Table 3.56.

TABLE 3.56
RADIONUCLIDE ABUNDANCES IN CIGAR LAKE ORE SAMPLES

Sample #	U wt.%	$^{239}Pu/U$ $\times 10^{12}$	$^{129}I/U$ $\times 10^{12}$	$^{99}Tc/U$ $\times 10^{12}$	$^{36}Cl/Cl^*$ $\times 10^{11}$
CS-235L	55.6	1.9±0.1	4.85±0.48 2.35±0.20 1.72±0.13 2.10±0.17		2.0
W83A	39.0	3.2±0.2	3.49±0.36 2.05±0.19	<1.8	4.6
W83C	46.8	2.8±0.2	4.52±0.44 2.75±0.25		

* Unpublished data from Jack Cornett. These analyses were done on a different aliquot than that used for the U, ^{99}Tc, ^{129}I and ^{239}Pu analyses.

3.8.2.3.2 Iodine-129

Iodine-129 measurements were made by accelerator mass spectrometry. For this purpose iodine was extracted from the rock samples and chemically purified. Initially the element was extracted from a solution produced by sodium peroxide fusion and acid dissolution. However, blank samples analyzed by this method indicated that variable, and often significant, quantities of ^{129}I were introduced during analysis. A procedure using high-pressure + high-temperature acid dissolution in a microwave oven produced insignificant blanks. However, the procedure did not completely dissolve the samples, resulting in uncertainties as to whether the ^{129}I had been quantitatively released from the solid phase. Measured ^{129}I abundances in the Cigar Lake samples are presented in Table 3.56. These results have not been corrected for blanks. Until the constraints on the analysis for this nuclide are better understood, these results should be viewed as limiting the actual concentration of indigenous ^{129}I in the sample.

3.8.2.3.3 Technetium-99

One of the samples was analyzed to measure the concentration of ^{99}Tc. Blank samples showed that spurious large quantities of contaminant ^{99}Tc were introduced into samples during the analyses. Consequently, this single result was not corrected for blank and is reported as an upper limit in Table 3.56.

3.8.2.3.4 Uranium

Abundances of uranium in the samples was measured by alpha-spectrometry at the AECL Whiteshell Laboratory. The results are included in Table 3.56.

3.8.2.3.5 Whole rock analyses

Abundances of major and selected minor and trace elements were made on samples from drillcore of Hole 220 by the X-Ray Analysis Laboratory (XRAL) in Don Mills, Ontario. Results of the analyses are given in Table 3.57.

3.8.2.4 In-situ production of nuclides

3.8.2.4.1 Background

Calculations of nuclide production rates in the Cigar Lake ore body are necessary for several reasons. First, these calculations provide a baseline against which to compare measured concentrations of plutonium, technetium and iodine-129 in the ore in order to assess the mobility of these species. Secondly, the calculations provide a basis for evaluating the extent to which correlations should be expected among the various in-situ-produced nuclides, under the assumption of closed-system behavior. Knowledge of such correlations may allow constraints to be put on interpretations of measured nuclide concentrations, even if the model predictions of absolute concentrations are highly uncertain. Finally, unexpectedly high tritium concentrations ranging up to 280 TU in waters extracted from the

TABLE 3.57

WHOLE ROCK ANALYSES ON LANL CORE-PROFILE FROM HOLE 220 AT CIGAR LAKE.
Results from XRAL, Don Mills, Ontario, 1992 October+November

	CS-604	CS-605	CS-609	CS-610	CS-615	CS-619	CS-620B	CS-625	CS-627	CS-228	CS-230	BL-5
SiO2 wt.%	10.10	16.50	33.10	35.70	10.60	30.30	14.10	25.80	20.80	97.20	91.30	48.10
TiO2	0.33	0.56	4.95	2.05	0.59	14.70	1.22	2.45	5.77	0.13	0.57	0.60
Al2O3	4.44	8.26	19.70	30.30	3.77	27.90	7.33	17.90	15.80	1.17	5.04	12.10
Fe2O3	8.29	18.14	13.12	11.34	2.90	2.40	1.28	9.20	6.45	0.14	0.08	3.26
FeO	0.50	0.50	0.70	0.50	1.30	2.10	1.10	2.70	0.60	<0.10	<0.10	4.70
MnO	0.09	0.04	0.04	0.03	0.12	0.01	0.04	0.01	0.03	0.01	0.02	0.06
MgO	0.30	0.53	1.18	1.38	1.43	2.79	0.37	4.72	1.06	0.07	0.19	2.21
CaO	1.15	0.39	0.46	0.38	2.00	0.41	0.99	12.70	0.81	0.23	0.25	5.53
Na2O	0.06	0.05	0.11	0.12	0.14	0.07	0.06	0.07	0.05	0.03	<0.01	3.93
K2O	1.02	1.48	4.50	5.12	0.70	1.90	0.62	1.92	1.42	0.29	1.29	0.41
P2O5	0.25	0.33	0.47	0.67	0.17	0.41	0.37	9.36	0.75	0.05	0.13	0.16
S	1.10	2.84	0.46	0.13	0.57	1.73	1.31	6.61	3.71	0.11	0.05	0.29
LOI										0.50	1.20	
Cl ppm	850	700	1300	1900	1100	1000	920	2100	570	520	540	1100
F	1300	860	1200	1500	960	1700	1900	6500	1400	23	130	380
B	421	527	1140	1370	576	1140	476	1220	592	60	121	43
Li	<100	<100	200	200	<100	800	300	600	500	<100	<100	<100
Cr	300	100	300	200	300	400	300	300	600	11	16	200
Pb	56100	11400	5400	1600	72300	9200	64000	1500	24500	<100	<100	15500
Sm	323	240	69	83.1	172	19.3	111	43.6	404	3.4	6.9	12
Gd	682	417	80.3	56.3	392	38.9	307	65.5	535	1.8	4.6	15
Zr	445	1040	3460	2680	278	3770	608	44	2260	160	811	399
U	440960	126352	61056	38160	487600	51050	427392	23744	221328	466	237	64109
U BL +	393749	139465	66995	38927	442265	50345	379741	26598	236888			
U LL +			69789		529310		470714					
U Other +										17	126	79000

+ Uranium assay data: BL= Becquerel Laboratories; LL= Loring Laboratories; Other= INAA (AECL) for CS-228 and -230, reference value for BL-5.

ore zone of the Cigar Lake deposit raised the question of whether such levels could possibly result from in-situ production of ^{3}H by neutron capture by ^{6}Li. Elevated levels of ^{36}Cl, which is also commonly assumed to be atmospheric in origin, have also been measured in waters from the ore zone. In these cases, comparison of measured isotopic compositions in the water against calculated accumulation rates for those isotopes may permit limits to be established either on transfer rates or on groundwater residence times in the orebody.

This report summarizes the underlying assumptions and results of calculations to provide estimates of in-situ production rates for neutron-capture products ^{237}Np and ^{239}Pu, and for fission products ^{129}I and ^{99}Tc. Where possible, calculations are compared with the limited number of analyses that are available for concentrations of these species in Cigar Lake or other uranium ores. These comparisons indicate the general validity of the approach. The same estimation procedures are applied to the calculation of production rates for ^{3}H, ^{14}C and ^{36}Cl. The results indicate that in-situ-produced concentrations of these radionuclides should be detectable in Cigar Lake ore, and may even be in excess of bomb-pulse concentrations in Cigar Lake groundwaters.

The calculations require assumptions to be made about the composition of the ore, the geometry of the ore body, and the rate of neutron production. These assumptions then provide the basis for the data input into a Monte Carlo neutron transport code, which tracks the fate of the neutrons in the ore body and provides estimates of nuclear reaction rates for the bulk rock. More detail on this approach is provided in Fabryka-Martin and Curtis et al. (1992). From these production rates in the bulk ore, one can set limits on the concentrations in the groundwater by making assumptions about rates of escape from the rock to the water. Each of these steps is outlined below.

3.8.2.4.2 Modelled case studies

Three cases were modelled:

Case 1: Ore with the elemental composition measured for Cigar Lake sample CS235L (54.6 % U);

Case 2: Ore with an elemental composition considered to be representative of the bulk average (15-20 % U) for the primary ore; and

Case 3: A profile of hole 220, which provides a section 6.3 m in length through the primary ore zone. This case was added because of the expectation that, in a heterogeneous system such as that typical of uranium ore bodies, the relevant elemental composition for modelling purposes is that of the surrounding matrix rather than that of the analyzed sample. On the basis of visual examination of the mineralogy and γ-counting data to obtain relative U contents, J. Cramer (AECL) subdivided the section into 31 unevenly spaced intervals for which uranium analyses are available (Figure 3.93). A mockup profile was devised as described below in order to assess the magnitude of variations expected in nuclide production rates in these 31 intervals. The modelled profile contains several abrupt boundaries between high-grade and low-grade ores as well as

variable thicknesses of individual strata. This characteristic provides a means to examine how production rates of neutron-capture products are affected under a number of different geometries.

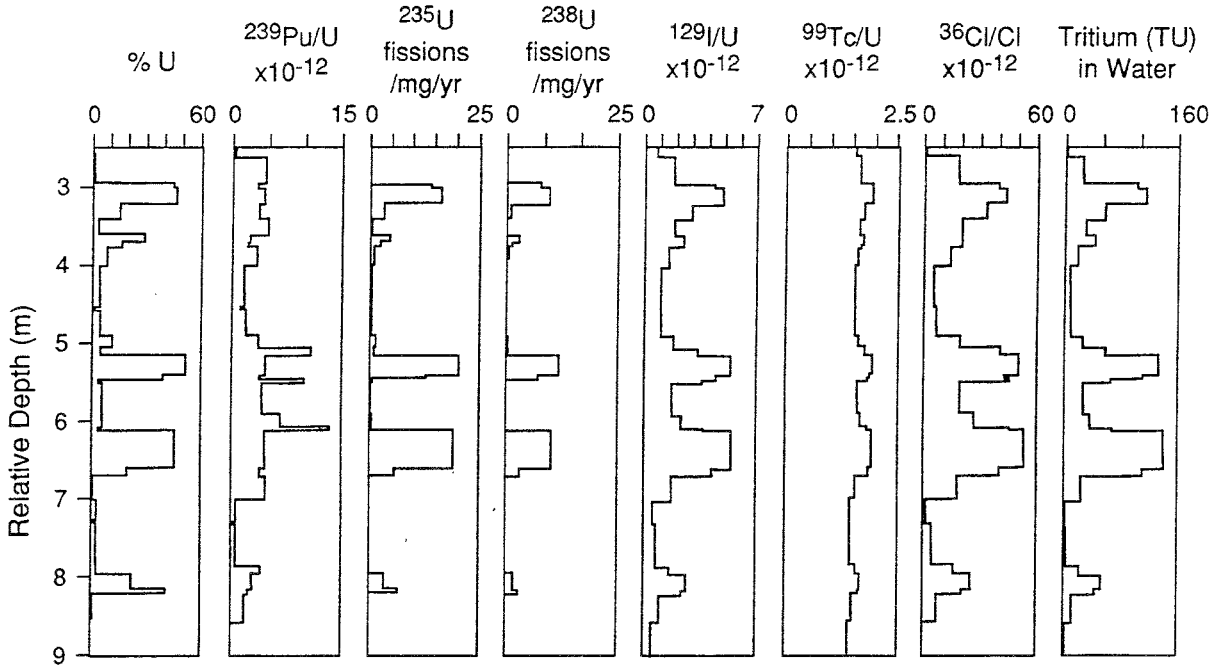

FIGURE 3.93 Predicted distribution of ^{235}U and ^{238}U induced fission rates, $^{239}Pu/U$, $^{129}I/U$, $^{99}Tc/U$ and $^{36}Cl/Cl$ ratios, and an upper limit for the Tritium content of groundwater in a profile through the ore zone in Hole 220.

3.8.2.4.3 Ore composition

Elemental compositions adopted for the three cases were obtained in the following manner.

Case 1: Sample CS235L

An elemental analysis was obtained for CS235L from X-Ray Assay Laboratories, Ltd. (XRAL), Don Mills, Ontario. Uranium concentration was measured by α-spectrometry (J. Cramer pers. commun. 1989). Minerals identified in XRD scans include uraninite, chlorite, illite and kaolinite (J. Cramer pers. commun. 1989). For convenience in the estimation of H contents (see below), U was assumed to be present as UO_2 and Pb as PbO_2; in reality, these elements are also probably present as U_3O_7, $USiO_4$ and PbS_2.

Because of its effectiveness as a neutron moderator, hydrogen is a key parameter in neutron transport calculations. Unfortunately, concentrations of this element are not generally measured and hence must be estimated by indirect means. The total hydrogen content of CS235L is assumed to include a contribution of 0.14 % by weight for the uraninite (UO_2) phase (Frondel 1958, pp 16-17), plus 0.75 % by weight of the silicate fraction of this ore (i.e., that portion excluding UO_2 and PbO_2); this proportion is an average value measured

for muscovite, chlorite, and illite (Deer et al. 1966; Weaver and Pollard 1973). By this approach, the estimated H content of the mineral phases in CS235L is:

$(1.4 \times 10^{-3} \times 619{,}000 \text{ ppm } UO_2) + (7.5 \times 10^{-3} \times 301{,}000 \text{ ppm silicates}) + (0 \times 80{,}000 \text{ ppm } PbO_2) = 3124 \text{ ppm H.}$

An average grain density of 6.00 g/cm^3 is estimated by assuming a density of 7.5 g/cm^3 for UO_2 and associated PbO_2, and 2.5 g/cm^3 for the remaining minerals.

TABLE 3.58
ELEMENTAL COMPOSITIONS (PPM) AND OTHER PROPERTIES
OF ORE ASSUMED FOR NEUTRON TRANSPORT MODELLING CALCULATIONS
(INCLUDES. 2 VOL.% H_2O)

COMPOSITION	**Case 1** CS235L 56 % U	**Case 2** Bulk average ores 15 % U	20 % U
H	3500	6965	6521
B	498	1184	1091
C	4584	10892	10036
O	205325	403939	381599
F	1096	2605	2400
Na	149	355	327
Mg	57205	135916	125236
Al	13654	32440	29891
Si	31094	73878	68073
P	867	2060	1898
S	3388	8051	7418
Cl	1894	4499	4145
K	1694	4025	3709
Ca	21028	49962	46036
Ti	2292	5446	5018
Mn	1096	2605	2400
Fe	36875	87611	80727
Sm	59	16	21
Gd	246	67	89
Pb	69165	18636	24849
U	544119	149092	198789
Neutron production rate	5.16×10^5 (measured)	1.63×10^5 (estimated)	2.10×10^5 (estimated)
Bulk density (assumed)	5.90 g/cm^3	3.25 g/cm^3	3.55 g/cm^3
Porosity (assumed)	2 % by vol.	2 % by vol.	2 % by vol.

Case 2: Bulk average ore

The composition of the mineral fraction of bulk average ore was estimated from that of sample CS235L in the following manner:

a- Assume 15 or 20 % U for the bulk average ore, present as UO_2. Assume a H content of 0.14 % for this mineral phase.

b- Assume the weight ratios Pb/U, Sm/U, and Gd/U are the same in the bulk average ores as those measured for CS235L.

c- Assume that the remainder of the bulk average ores (i.e., the portion excluding UO_2, PbO_2, Sm, Gd) contains 47 % O, based on the average O content of silicate rocks (Fabryka-Martin 1988, Appendix A), and 0.75 % H. Assume the remaining elements are present in the same relative proportions as measured or estimated for the portion of CS235L excluding UO_2, PbO_2, Sm and Gd.

d- Estimate the grain density for the bulk average ores in the same way as was done for CS235L.

After estimating the grain compositions for Cases 1 and 2 as described above, a total water content of 2 % by volume was assumed. The bulk composition and bulk density of each ore was adjusted correspondingly to account for the addition of water (Table 3.58).

Case 3: Hole 220 profile

Elemental compositions for the hole 220 core section were obtained in a manner similar to that described above. At the time that the modelling was conducted, no elemental analyses were available for any of the hole 220 samples. Hence, each of the 31 intervals in the hole 220 profile was assigned one of 4 artificial elemental compositions: 2, 15, 25, or 40 % U ore. These were estimated by making the following assumptions:

a- As in the case of the bulk average ore (Case 2 above), assume that each sample can be described by 2-component mixing between uraninite (with associated Sm, Gd, and Pb) and a homogeneous non-UO_2, non-PbO_2 (i.e., silicate) phase. The composition of CS235L is assumed to be explained by this model.

b- Assume that, for the purpose of neutron-transport calculations, the U content of each sample can be classified as one of four types of average ore: 2, 15, 20 or 40 % U, with an associated H content of 0.14 %.

c- Assume that the weight ratios Pb/U, Sm/U, and Gd/U in each of the 4 types of average ore are the same as those measured for CS235L (Table 3.58).

d- Assume that the remaining fraction of each type of average ore (i.e., excluding UO_2, PbO_2, Sm or Gd) contains 47 % O, based on the average

O content of silicate rocks, and 0.75 % H. Assume the remaining elements (i.e., excluding U, Pb, Sm, Gd) are present in the same relative proportions as measured or estimated for CS235L.

e- Estimate the average grain density of each type of average ore by assuming a density of 7.5 g/cm^3 for UO_2 and PbO_2, and 2.5 g/cm^3 for all other minerals.

The above procedure produced the solid-phase compositions shown in Table 3.59. A total water content of 2 % by volume was then assumed for each ore type, and the bulk composition and bulk density of the ores were adjusted correspondingly to account for the addition of water.

TABLE 3.59
ELEMENTAL COMPOSITIONS (PPM) AND OTHER PROPERTIES
OF DRY BULK ORE ASSUMED FOR NEUTRON-TRANSPORT MODELLING
CALCULATIONS FOR THE PROFILE IN HOLE 220

COMPOSITION	2 % U	15 % U	25 % U	40 % U
Dry bulk density g/cm^3	2.61	3.35	3.92	4.77
H	7311	6088	5136	3719
Li	100	100	100	100
B	1431	1191	1005	728
C	13161	10959	9246	6694
O	460856	400985	355634	287026
F	3147	2621	2211	1601
Na	429	357	302	218
Mg	164227	136744	115380	83529
Al	39197	32638	27538	19936
Si	89266	74328	62715	45402
P	2489	2073	1749	1266
S	9728	8100	6834	4948
Cl	5436	4526	3819	2765
K	4864	4050	3417	2474
Ca	60369	50267	42413	30705
Ti	6581	5479	4623	3347
Mn	3147	2621	2211	1601
Fe	105861	88145	74374	53843
Sm	2	16	26	42
Gd	9	67	112	180
Pb	2500	18750	31250	50000
U	20000	150000	250000	400000

3.8.2.4.4 Neutron production rate

The neutron production rate was measured for CS235L and for nine samples from hole 220 using a neutron coincidence counter at Los Alamos National Laboratory. Linear regression of the neutron production rate P_n as a function of U content produced the relationship,

$$P_n = (2.13 \times 10^4) + (9.42 \times 10^3)\ (\%\ U) \quad \text{neutrons/g-ore/a,}$$

with a correlation coefficient of 0.991. This relationship was used to estimate the neutron source strength for the bulk average ores (Table 3.58) and for each of the 31 intervals within the hole 220 profile.

3.8.2.4.5 Modelling nuclear reaction rates

3.8.2.4.5.1 *General description of MCNP*

MCNP is a continuous-energy neutron/photon transport code based on the Monte Carlo method (Briesmeister 1986). The current version of the code and its documentation represents an approximate 300 person-years of subsequent improvement and is continually updated and maintained by the Radiation Transport Group of the Applied Theoretical Physics Division at Los Alamos National Laboratory. The user specifies the geometry of the problem, descriptions of the materials, the cross-section evaluations that are to be used, characteristics of the neutron sources, and the type of answers desired. The neutron energy regime ranges from 10^{-11} to 20 MeV.

The model output consists of tallies of events per target nucleus per starting neutron. Estimates of uncertainties are provided for each tally and are a function of the number of neutron histories followed, i.e., one can reduce the numerical uncertainty by increasing the number of starting neutrons. In our case studies, each MCNP prediction of events/target nucleus/starting neutron (e.g., ^{235}U fissions/^{235}U atom/starting neutron) is multiplied by the measured or estimated neutron production rate in the modelled geometry (n/a) and by the target isotope composition in the spatial interval of interest (e.g., ^{235}U concentration) in order to convert the results to events/a.

3.8.2.4.5.2 *Assumptions and data sources for uranium ore calculations*

For the CS235L and bulk average ore calculations (Cases 1 and 2), each ore sample was assumed to be infinite in extent, i.e., no neutron leakage was allowed from the modelled region. This approximation may be reasonable for the case of the bulk average ore. However, it is likely to be unrealistic for high-grade ores such as sample CS235L, such that the neutron flux and hence radionuclide production rates would both tend to be overestimated for this sample. For the hole 220 profile (Case 3), each of the 31 ore intervals was assumed to be infinite in lateral extent, with neutron leakage allowed only from the top and bottom of the profile.

3.8.2.4.5.3 *Predicted radionuclide concentrations*

The MCNP program reports reaction rates in units of events per target nucleus per starting neutron. The events included in the model output are:

- production of tritium	$^{6}Li + n \rightarrow \alpha + {}^{3}H$
- production of ^{14}C	$^{14}N + n \rightarrow p + {}^{14}C$
	$^{17}O + n \rightarrow \alpha + {}^{14}C$
	$^{13}C + n \rightarrow \gamma + {}^{14}C$
- production of ^{36}Cl	$^{35}Cl + n \rightarrow \gamma + {}^{36}Cl$
- production of ^{237}Np	$^{238}U + n \rightarrow 2n + {}^{237}Np$
- production of ^{239}Pu	$^{238}U + n \rightarrow \gamma + {}^{239}Pu$
- neutron-induced fission of ^{235}U.	

Calculated tritium production rates are tabulated for the three cases in Table 3.60. Carbon-14 production rates are summarized only for cases 1 and 2 in Table 3.61; this calculation was not done for the Case 3. Production rates for other neutron-capture products and fission products are shown for all three cases in Table 3.62. Profiles for fission rates and reaction products are shown for hole 220 in Figure 3.93.

3.8.2.5 Discussion of results and comparisons with measured concentrations

3.8.2.5.1 Tritium (Table 3.60)

The only production reaction that need be considered for ^{3}H is neutron capture by ^{6}Li. Assuming that Li concentrations are at least on the order of 100 ppm in the bulk ore, then production of ^{3}H by ternary fission of uranium isotopes (fractional yield = 1.25×10^{-4} (Hyde 1964, p. 131)) contributes ≤ 1 % to the total in-situ production of this nuclide. Direct production of tritium in the groundwater is far below detectable levels, resulting in concentrations $< 10^{-3}$ TU. However, the model predicts that a maximum tritium content of 354 TU could be attained in groundwater associated with sample CS235L. For groundwater in average ore (Case 2), an upper limit of 54-75 TU is predicted; and a range of 29-149 TU is predicted for pore waters associated with selected intervals in hole 220 (Figure 3.93).

Two assumptions inherent in these upper limits are that all tritium produced in the rock matrix escapes to the groundwater before decaying, and that this occurs without the ^{3}H activity being diluted by isotopic exchange with stable H in the mineral grains. Lower limits can be established under the assumption that the in-situ-produced tritium is diluted by mixing with the total H content of the ore (i.e., pore water + H in the mineral structures). This lower limit ranges from 3 to 39 TU for the three cases.

Measured tritium contents exceed 100 TU for holes 198 and 220 in the ore zone, attaining a maximum of 280 TU in an early sampling of hole 220. These high contents are probably due to in-situ production. In particular, the preceding production calculations assume 100 ppm Li in the ore. Elemental analyses of nine intervals in hole 220 came available after these model calculations had been completed, and indicate that Li contents usually exceed

TABLE 3.60
EQUILIBRIUM CONCENTRATIONS OF TRITIUM PRODUCED BY NEUTRON CAPTURE IN THE CIGAR LAKE ORE DEPOSIT AND LIMITS FOR ITS CONCENTRATION IN THE GROUNDWATER

PRODUCTION MECHANISM	**Case 1** CS235L U 54.6 %	**Case 2** Bulk average U 15 %	U 20 %	**Case 3** Range for profile Hole 220 (intervals containing ≥10 % U) Lower Limit	Upper Limit
SECULAR EQUILIBRIUM CONCENTRATIONS, FOR CLOSED SYSTEM Assumes 100 ppm Li in bulk rock, 50 ppb Li in water					
In bulk ore (atoms/g) due to neutron capture by ^{6}Li	80,300	221,000	284,000	15,000	42,600
In bulk ore (atoms/g) due to ternary fission	420	81	113	54	330
In water (atoms/mL) due to neutron capture by ^{6}Li	40	11	14	7.5	21
CONCENTRATIONS IN GROUNDWATER Unless otherwise indicated, results are in Tritium Units (TU) (1 TU= $^{3}H/H$ atom ratio of $1x10^{-18}$)					
Production in water only	0.0006	0.0002	0.0002	0.0001	0.0003
Complete mixing with H in bulk ore	39	5.3	7.3	3.1	17
100 % escape from rock to water without isotopic exchange with H in rock	354	54	75	29	149
^{3}He accumulation rate, 10^{6} atoms/mL/a, 100 % escape (see Note below)	1.3	0.20	0.28	0.14	0.56

Note: For comparison, the ^{3}He concentration of groundwater in equilibrium with the atmosphere at 10 °C is $1.8x10^{6}$ atoms/mL.

TABLE 3.61
EQUILIBRIUM CONCENTRATIONS OF CARBON-14 PRODUCED BY NEUTRON CAPTURE AND ALPHA CAPTURE IN THE CIGAR LAKE ORE AND LIMITS FOR ITS CONCENTRATION IN THE GROUNDWATER

PRODUCTION MECHANISM (units)	**Case 1** CS235L 54.6 % U	**Case 2** Bulk Average Ore 15 % U	20 % U
In bulk ore (atoms/g)			
- n-capture by ^{14}N (20 ppm N)	$1.2x10^5$	$3.1x10^4$	$4.0x10^4$
- n-capture by ^{17}O	$2.7x10^5$	$9.0x10^4$	$1.2x10^5$
- n-capture by ^{13}C	--	$2.6x10^2$	$3.5x10^2$
Total produced by n-capture	$3.9x10^5$	$1.2x10^5$	$1.6x10^5$
In bulk ore (atoms/g)			
- α-capture by ^{11}B (100 ppm B)	$2.2x10^7$	$4.3x10^6$	$5.8x10^6$
In water (atoms/mL)			
- Capture by ^{14}N (20 ppm N)	$1.2x10^5$	$3.1x10^4$	$4.0x10^4$
- Capture by ^{17}O	$1.1x10^6$	$2.0x10^5$	$2.7x10^5$
- Capture by ^{13}C	--	0.3	0.3
Total	$1.2x10^6$	$2.3x10^5$	$3.1x10^5$
In calcite (atoms/g calcite)			
- Capture by ^{17}O	$6.2x10^5$	$8.8x10^4$	$1.2x10^5$
- Capture by ^{13}C	--	$2.9x10^3$	$1.3x10^4$
Total	$6.2x10^5$	$9.1x10^4$	$1.3x10^5$
In organics[1] (atoms/g organic)			
- Capture by ^{14}N	--	--	$1.8x10^7$
- Capture by ^{17}O	--	--	$1.0x10^5$
- Capture by ^{13}C	--	--	$1.9x10^4$
Total	--	--	$1.8x10^7$
Carbon-14 in groundwater[2] (pmC)			
- Production in water only (excludes contribution from α-capture by ^{11}B)	230 pmC	29 pmC	48 pmC
- Complete mixing with C in bulk rock	7.9 pmC	0.7 pmC	0.7 pmC
- 100 % escape from rock to water without isotopic exchange with C in rock	$1x10^6$ pmC	$1x10^5$ pmC	$2x10^5$ pmC
- Equilibrium content of calcite	0.01 pmC	0.001 pmC	0.002 pmC
- Equilibrium content of organics	--	--	0.06 pmC
Nitrogen accumulation in groundwater[3] assuming 100 % escape (10^5 atoms/mL/a)	79	0.9	1.3

1 Assume weight proportions of 0.55 C, 0.01 N, and 0.39 O (B. Allard pers. commun. 1991).
2 Assuming 10 mg/l total inorganic carbon in water, and total carbon in bulk rock as shown in TABLE 3.58. (100 pmC= 100 % modern C= $^{14}C/C$ atom ratio of $1.116x10^{-12}$)
3 For comparison, the N_2 concentration of groundwater in equilibrium with the atmosphere at 10 °C is $3.9x10^{17}$ atoms/mL.

this level. A maximum of 800 ppm Li was reported. Tritium production rates scale proportionally to Li concentrations, and hence the bounding concentrations estimated above may be several times too low.

3.8.2.5.2 Carbon-14 (Table 3.61)

Predicted ^{14}C concentrations due to neutron-capture reactions are 4 x 10^5 atoms/g for CS235L and 1 x 10^5 atoms/g for bulk average ore (Table 3.61). (Neutron-capture reactions producing ^{14}C were not evaluated for Case 3, the hole 220 profile). A much more significant source of ^{14}C, however, is probably its production by α-capture by ^{11}B. Contributions from this reaction mechanism were evaluated following the approach of Perry and Wilson (1981), as detailed in Fabryka-Martin (1988, pp. 71-76). Assuming 100 ppm B in the bulk ore, predicted equilibrium concentrations range from 4 x 10^6 atoms/g for 15 % U ore, to 2 x 10^7 atoms/g for CS235L (Table 3.61).

Boron concentrations measured in 12 Cigar Lake ore samples ranged from 300 to 1400 ppm, and thus one might expect that the above predicted production rates may be too low. Aside from this source of bias in the results, the magnitude of the uncertainty in the α-capture calculation is difficult to assess on theoretical grounds because the production rate is controlled by the micro-distribution of B relative to members of the U decay series. Nonetheless, the general validity of the approach is supported by published measurements of ^{14}C contents in several uranium ores (Jull et al. 1987). These authors reported ^{14}C levels of 1-6 x 10^6 atoms/g in five ores with uranium concentrations of 33-70 % and boron concentrations ranging from 9 to 99 ppm. The measured ^{14}C contents are nearly an order of magnitude above that predicted for CS235L as attributable to neutron capture alone, and thus support the contention that α-capture by ^{11}B is the major production mechanism for ^{14}C in uranium ores.

Because of dilution by dead carbon in the mineral phase, the specific activity of ^{14}C in the bulk rock is expected to be near detection limits (predicted range, 1 to 8 pmC, Table 3.61). However, because a considerable proportion of the total ^{14}C production occurs in the water itself, which has a very low dissolved inorganic carbon content, ^{14}C activities should be readily detectable with a lower limit on the order of 29-48 pmC or more, depending upon the significance of the $^{11}B(\alpha,p)^{14}C$ reaction in the water (not evaluated). Upper limits are calculated by assuming that 100 % of the ^{14}C produced in the mineral phases by neutron- and α-capture escapes to the water before decaying and without being diluted by dead carbon in the solid phase. This upper limit is on the order of 100,000 pmC for bulk average ore (Table 3.61). Despite these high production rates, it is improbable that production and decay of ^{14}C in the ore could result in any measurable buildup of its decay product, ^{14}N, in the ore and groundwater. An upper limit for the rate of buildup is obtained by assuming complete escape of the nitrogen. For sample CS235L (Case 1), this accumulation rate would be only 2 x 10^{-11} ppm N/a in the presence of background concentrations on the order of 10 ppm N_2.

In-situ production of ^{14}C was also calculated for calcite and for organics. In both cases, atomic concentrations are large but ^{14}C activities would be below detection ($<<1$ pmC) due to dilution by dead carbon in these phases (Table 3.61).

TABLE 3.62
PREDICTED FISSION RATES AND EQUILIBRIUM CONCENTRATIONS
OF FISSION PRODUCTS AND OTHER NEUTRON-CAPTURE PRODUCTS *

PRODUCTION REACTION	Case 1 CS235L U 54.6 %	Case 2 Bulk average U 15 %	Case 2 Bulk average U 20 %	Case 3 Hole 220 profile (intervals with ≥10 % U) Lower Limit	Case 3 Hole 220 profile (intervals with ≥10 % U) Upper Limit
Fission rates (fiss/g/a)				10.5 % U	52.9 % U
- ^{238}U spont. fission	117400	32200	43000	22600	113700
- ^{235}U induced fission	46200	3270	5630	1500	22300
- ^{238}U induced fission	26000	1150	2110	330	12800
^{129}I content (atoms/g)					
- ^{238}U spont. fission	9.2×10^{8}	2.5×10^{8}	3.4×10^{8}	1.8×10^{8}	9.0×10^{8}
- ^{235}U induced fission	7.8×10^{9}	5.6×10^{8}	9.6×10^{8}	2.5×10^{8}	3.8×10^{9}
- ^{238}U induced fission	5.7×10^{9}	2.5×10^{8}	4.6×10^{8}	7.3×10^{7}	2.8×10^{9}
Total	1.4×10^{10}	1.1×10^{9}	1.8×10^{9}	5.0×10^{8}	7.5×10^{9}
^{129}I/U atom ratio ($\times10^{-12}$)	10	2.8	3.5	1.9	5.6
^{99}Tc content (atoms/g)					
- ^{238}U spont. fission	2.2×10^{9}	6.0×10^{8}	8.0×10^{8}	4.2×10^{8}	2.1×10^{9}
- ^{235}U induced fission	8.7×10^{8}	6.1×10^{7}	1.1×10^{8}	2.8×10^{7}	4.2×10^{8}
- ^{238}U induced fission	4.9×10^{8}	2.2×10^{7}	4.0×10^{7}	6.1×10^{6}	2.4×10^{8}
Total	3.5×10^{9}	6.9×10^{8}	9.4×10^{8}	4.5×10^{8}	2.7×10^{9}
^{99}Tc/U atom ratio ($\times10^{-12}$)	2.6	1.8	1.9	1.7	1.7
^{36}Cl/Cl atom ratio ** ($\times10^{-11}$)	11	3.0	3.8	2.0	5.2
^{237}Np/U atom ratio ($\times10^{-13}$)	not calc.	3.3	4.6	1.0	10
^{239}Pu/U atom ratio ($\times10^{-12}$)	8.2	3.0	3.6	1.9	4.8

* Fission product calculations assume the following constants:

-^{238}U spontaneous fission half-life	= 8.16×10^{15} a
-Mass 129 yield for ^{238}U spontaneous fission	= 0.035 % (Hebeda et al. 1987)
-Mass 129 yield for ^{235}U fission	= 0.75 %
-Mass 129 yield for ^{238}U fission	= 0.97 %
-Mass 99 yield for ^{238}U spontaneous fission	= 6.1 %
-Mass 99 yield for ^{238}U and ^{235}U induced fission	= 6.2 %

** ^{36}Cl results are independent of the total Cl content or its distribution in the ore.

3.8.2.5.3 Chlorine-36 (Table 3.62)

Unlike the other radionuclides examined here, the equilibrium $^{36}Cl/Cl$ ratio is independent of total chloride concentration or the chloride distribution. The model predicts the same equilibrium value for the solid phase as for the water. The range of values predicted for Cigar Lake ore for Cases 2 and 3, 2-5 x 10^{-11}, match those measured by J. Cornett (Chalk River Laboratory) (also 2-5 x 10^{-11}) for five high-grade samples (including CS235 and three samples from hole 220) containing 14-55 % U. As expected, the ^{36}Cl production rate is greatly overpredicted under the assumptions used for Case 1 (CS235L), the predicted $^{36}Cl/Cl$ ratio of 1 x 10^{-10} exceeding the measured ratio of 2 x 10^{-11} for this sample several fold.

3.8.2.5.4 Plutonium (Table 3.62)

Predicted $^{239}Pu/U$ atom ratios are generally 2-5 x 10^{-12} for the cases 2 and 3 (Table 3.62). In the hole 220 profile, three peak values of 1 x 10^{-11} are predicted for narrow (3-10 cm thick) intervals of low-grade ore where these are immediately adjacent to massive intervals of high-grade ore (Figure 3.93). Such enhancement of ^{239}Pu production might be a result of a shift in the neutron energy spectra to lower energies, where reaction cross-sections are higher, at such locations; or this effect may merely be an artifact of the large numerical uncertainty in the MCNP tally result for these narrow intervals.

Three high-grade (39-56 % U) Cigar Lake samples (CS235L, W83A, W83C) had measured $^{239}Pu/U$ atom ratios ranging from 1.9 to 3.2 x 10^{-12}, in excellent agreement with the predicted range (Curtis et al. 1992). Again, as in the case for ^{36}Cl, the ^{239}Pu production rate is greatly overpredicted under the assumptions used for Case 1. This disparity would be expected to the extent that these ores may be relatively small pockets of high-grade material which experience a neutron flux that is determined by as much by the characteristics of the surrounding lower-grade ore as by their own characteristics.

3.8.2.5.5 Neptunium (Table 3.62)

Predicted $^{237}Np/U$ atom ratios are 3-4 x 10^{-13} for bulk average ore and 1-10 x 10^{-13} for the hole 220 samples; generally, predicted ^{237}Np equilibrium concentrations are about 5-20 % of those for ^{239}Pu (Table 3.62). No measurements of natural ^{237}Np are available against which to compare these predictions.

3.8.2.5.6 Iodine-129 (Table 3.62)

Predicted ^{129}I concentrations range from 5 x 10^{8} up to 1 x 10^{10} atoms/g for the three modelled cases (Table 3.62). Predicted $^{129}I/U$ atom ratios range from 2 x 10^{-12} to 1 x 10^{-11}. Measurements of this fission product in three Cigar Lake ores (CS235L, W83A, W83C) toward the lower end of these ranges, at 2-3 x 10^{9} atoms/g with associated $^{129}I/U$ ratios of 2-3 x 10^{-12}.

3.8.2.5.7 Technetium (Table 3.62)

Predicted ^{99}Tc concentrations are 5 x 10^{8} to 4 x 10^{9} atoms/g for the three modelled cases, corresponding to $^{99}Tc/U$ ratios of 1.7-2.6 x 10^{-12} (Table 3.62). An upper limit for this fission product was measured in Cigar Lake ore W83A (39 % U), as 1.8 x 10^{9} atoms/g with a $^{99}Tc/U$ ratio of 1.8 x 10^{-12}.

3.8.2.6 Implications and applications of model results

3.8.2.6.1 Bounding concentrations for nuclear reaction products in Cigar Lake ores

Modelling results for Case 1 (CS235L) provide upper limits for the production rates of the various neutron-capture products and neutron-induced fission rates. However, a comparison of measured with calculated concentrations of three products (^{36}Cl, ^{129}I, and ^{239}Pu) suggests that the underlying assumptions for this case consistently lead to an overestimation of production rates by factors of 4 to 5. This disparity is to be expected to the extent that a sample such as CS235L probably occurs as a relatively small pocket of high-grade material (i.e., small compared to the average neutron path length), which experiences a neutron flux that is determined as much by the characteristics of the surrounding lower-grade ore as by its own characteristics. Production rates predicted by Case 3 (hole 220 profile) for samples with the same U content as CS235L are about half those for Case 1, and hence appear to provide more reasonable estimates of the upper limits.

The modelled hole 220 profile also establishes a realistic range of production rates for the various processes in high-grade ore. In all cases where comparisons were possible, measured radionuclide concentrations for high-grade Cigar Lake ores fell within the ranges predicted from the hole 220 profile.

The major sources of uncertainties in the model predictions arise from lack of detailed knowledge about:

a- the elemental composition of the ore to be used for neutron-transport calculations, particularly the critical elements H, Sm and Gd;

b- spatial variability in the elemental composition; and

c- spatial variability in concentrations of B and Li, the dominant target elements for ^{3}H and ^{14}C production.

3.8.2.6.2 Predicted correlations among radionuclide abundances

This modelling study shows the extent to which various nuclear reaction products are correlated, such that one provides a constraint on the production rates of others. For example, under most conditions, the ratio $^{36}Cl/Cl$ is shown to be an ideal in-situ monitor of the ^{235}U fission rate (Figure 3.94), the dominant source term for ^{129}I. The $^{36}Cl/Cl$ ratio also serves as a precise monitor of the ^{3}H production rate, provided the latter is expressed in terms of its product/target ratio $^{3}H/Li$. The constant of proportionality between the

modelled ^{36}Cl production rates and ^{235}U fission rates is the ratio of their effective cross sections, about 13. This value is the same as the ratio of the thermal cross sections for the two reactions, although considerably less than the ratio of their resonance integrals (16), suggesting that most of the modelled production is caused by low-energy neutrons. The predictive relationship between the two radionuclide production rates is:

$$^{235}U \text{ fissions/a}/^{235}U \text{ atom} = (^{36}Cl/Cl)\ (13)\ \lambda_{36} / 0.7577.$$

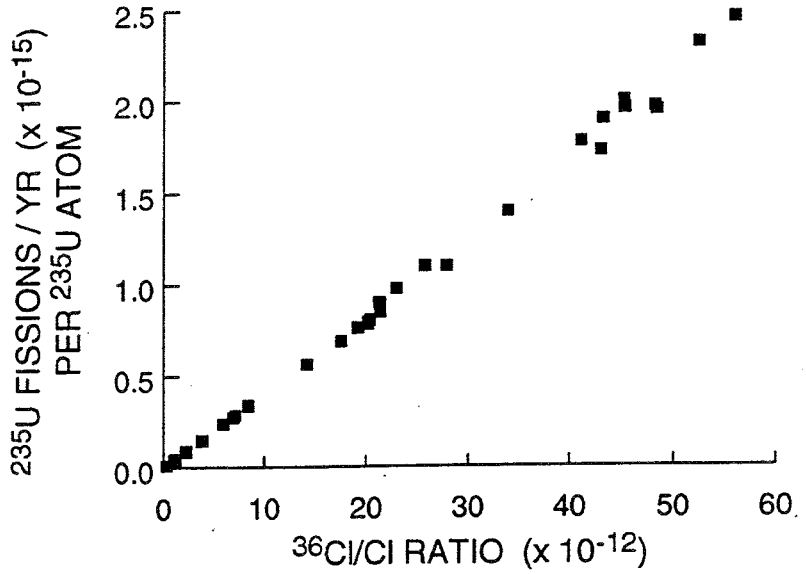

FIGURE 3.94 Predicted correlation between ^{235}U fission rate and $^{36}Cl/Cl$ in samples from Hole 220, showing that measured $^{36}Cl/Cl$ ratios may be used as an in-situ monitor of the ^{235}U fission rate.

Modelling results also suggest that measured $^{239}Pu/U$ ratios can be used to establish limits on the ^{238}U neutron-induced fission rate (Figure 3.95). For $^{239}Pu/U$ ratios $<4 \times 10^{-12}$, the upper limit for measured $^{239}Pu/U$ ratios in uranium ore samples thus far, the model results indicate that ^{238}U-induced fission should be no more than 10 % of the ^{238}U spontaneous fission rate. Because ^{99}Tc fission yields are essentially the same for each of the three fission processes (6 %), this conclusion means that in-situ ^{99}Tc production will always be dominated by spontaneous fission of ^{238}U, which can thus be assumed to contribute ≥ 80 % of the ^{99}Tc inventory. The production of ^{99}Tc by induced fission of ^{235}U is 5-20 % of the total for cases 2 and 3, and that by neutron-induced fission of ^{238}U is generally negligible and probably always less than 10 %. The dominance of the spontaneous fission component should simplify interpretation of measured ^{99}Tc concentrations in uranium minerals.

In contrast, although spontaneous fissions of ^{238}U constitute at least 75 % of the total number of fissions in any given sample, ^{235}U fissions typically account for about half of the in-situ ^{129}I production in uranium ores because the ^{129}I yield from ^{238}U spontaneous fission is <5 % that from either of the induced fission processes. Production from the two ^{238}U

processes account for the remainder of the ^{129}I inventory in highly variable relative proportions, with ^{238}U-induced fission possibly accounting for as much as 30 % of the total ^{129}I production rate. This distribution gives rise to much larger uncertainties in the predictions than is the case for ^{99}Tc.

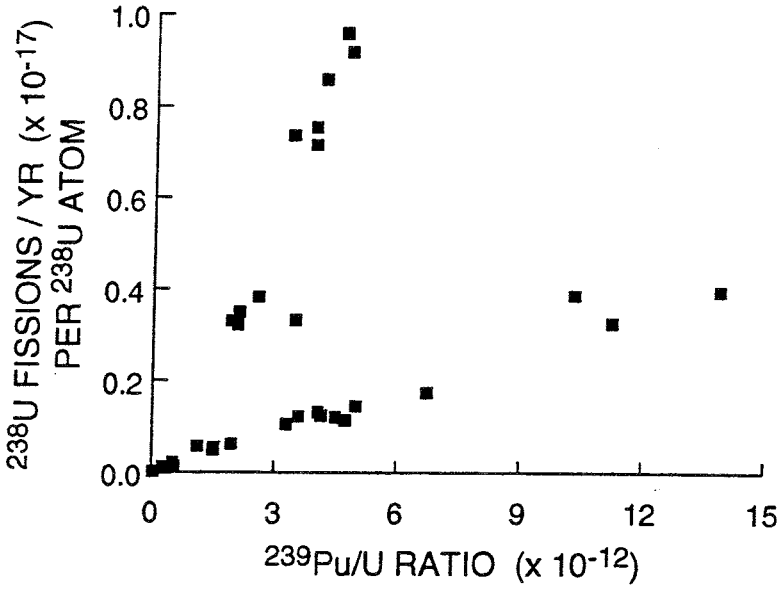

FIGURE 3.95 Predicted correlation between $^{239}Pu/U$ ratios and ^{238}U-induced fission rates, suggesting that measured $^{239}Pu/U$ ratios may be used to establish constraints on the contribution of ^{238}U-induced fission to the production of fission products ^{99}Tc and ^{129}I. For comparison, the ^{238}U spontaneous fission rate is $8.5x10^{-17}$ fissions/a/^{238}U atom.

3.8.2.6.3 Bounding concentrations for nuclear reaction products in groundwaters

The model results can be used to establish bounding concentrations of ^{239}Pu, ^{237}Np and ^{99}Tc to be used by geochemical modellers in speciation and solubility calculations. By assuming complete escape of in-situ-produced ^{239}Pu, ^{237}Np and ^{99}Tc to the water, at 2 % total volumetric porosity, one calculates maximum concentrations in the water of 10^{12} atoms/mL (10^{-9} M) for ^{239}Pu and ^{99}Tc, and 10^{11} atoms/mL (10^{-10} M) for ^{237}Np.

In-situ production of ^{3}H, ^{14}C, and ^{36}Cl within the ore zone is expected to result in levels in excess of those in the surrounding sandstone aquifer; this expectation has been borne out by several measurements showing elevated ^{3}H and ^{36}Cl in the ore zone. However, interpretation of the measured concentrations in terms of groundwater residence time has not been possible because of large uncertainties in the predicted groundwater concentrations due to uncertainties about target concentrations, emanation rates, and extent of dilution by mixing with stable H and C in the solid phases of the ore. This problem is most severe for ^{3}H and ^{14}C, for which predictions of groundwater concentrations range over five orders of

magnitude. An additional severe constraint on the interpretation is the uncertainty concerning the extent to which these radionuclides may be released from the mineral phase into the groundwater as a result of disturbance during the drilling process.

3.8.2.6.4 Predicted production of ^{14}C in carbonates and organics

The model indicates that in-situ-produced ^{14}C activity should be negligible in calcite and in organic matter but measurable in groundwater from the ore zone. Consequently, measurements of ^{14}C activity in fracture-filling calcite, if such calcite could be found, could provide an indication of flow paths for groundwater leaving the ore zone. However, this fracture-fill mineral has not been observed to occur at Cigar Lake. To the extent that colloids containing carbonate can be found, in-situ-produced ^{14}C activity may be a useful indicator of colloid stability or a tracer of colloid migration outside of the ore zone. Similarly, based upon the extent to which the ^{14}C contents of dissolved organic carbon (DOC) fractions are found to be in isotopic equilibrium with dissolved inorganic carbon (DIC) in the groundwater, such measurements may be a useful indicator of the stability of the various types of organics in the ore zone.

3.8.2.7 Future work

It is important to emphasize that these calculations are based upon mocked-up elemental compositions for the modelled cases. Additional analyses of nine samples from hole 220 are now available, allowing more realistic estimates to be made of elemental compositions throughout this profile and making it feasible to directly compare measured radionuclide concentrations with those predicted for a specific interval. Because of the sensitivity of the model results to assumptions about H and Gd contents, sensitivity analyses need to be conducted to evaluate the magnitude of uncertainty in predictions as these parameters are varied. Model predictions could also be extended to include other nuclear reaction products, chiefly noble-gas isotopes, which could serve as independent qualitative indicators of groundwater residence time. Finally, the modelling approach should be applied to the estimate of in-situ production rates of these radionuclides in major lithological units surrounding the primary ore body, particularly the massive clay zone, in order to assess the potential for this unit to act as a source term releasing radionuclides into the sandstone aquifer.

3.8.2.8 Acknowledgements

The work contained in this report was supported by the United States Department of Energy, Office of Civilian Radioactive Waste Management, Office of International Programs and Strategic Planning, United States Department of Energy, Office of Basic Energy Sciences, Division of Engineering and Geosciences, and the Alligator Rivers Analogue Project.

3.8.2.9 References

ATTREP, M., ROENSCH, F.R., AGUILAR, R. and FABRYKA-MARTIN, J. 1992. Separation and purification of plutonium in uranium ores for mass spectrometric measurement. Radiochim. Acta, **57**, 15-20.

BARNARD, R.W., WILSON, M.L., DOCKERY, H.A., GAUTHIER, J.H., KAPLAN, P.G., EATON, R.R., BINGHAM, F.W. and ROBEY, T.H. 1991. TSPA 1991: An initial total-system performance assessment for Yucca Mountain. Sandia Lab. Rep., **SAND91-2795-UC-814.**

BREDEHOEFT, J.D. and KONIKOW, L.F. 1993. Groundwater models: validate or invalidate. Ground Water, **31/2**, 178-179.

BRIESMEISTER, J. (ed.) 1986. MCNP -- A General Monte Carlo Code for Neutron and Photon Transport, Version 3A. Los Alamos National Laboratory, LA-7396-M, Rev. 2 (manual), 583 p.

COSSICK, R., MILLER, I. and CUNNANE, M. 1992. Integrated performance assessment model for waste package release and radionuclide release. In *Proc. Int. High Level Radioactive Waste Management Conf., Las Vegas, NV, April 12-16, 1992.* Vol. **2**, 1786-1791.

CURTIS, D.B., FABRYKA-MARTIN, J., AGUILAR, R., ATTREP, M. and ROENSCH, F.R. 1992. Plutonium in uranium deposits: natural analogues of geologic repositories for plutonium-bearing nuclear wastes. In *Proc. Int. High Level Radioactive Waste Management Conf., Las Vegas, NV, April 12-16, 1992.* Vol. **1**, 338-344.

DEER, W.A., HOWIE, R.A., and ZUSSMAN, J. 1966. *An Introduction to the Rock-Forming Minerals* Longmans, Green and Co., Ltd., London.

FABRYKA-MARTIN, J. 1988. Production of radionuclides in the earth and their hydrogeologic significance, with emphasis on chlorine-36 and iodine-129. Unpublished PhD dissertation, Dept. of Hydrology and Water Resources, University of Arizona, Tucson AZ.

FABRYKA-MARTIN, J.T. and CURTIS, D.B. 1993. Alligator Rivers Analogue Project, Final Report, Volume 15, Geochemistry of ^{239}Pu, ^{129}I, ^{99}Tc and ^{36}Cl. Report **DOE/HMIP/RR/92/085** and **SKI TR 92:20-15.** An OECD/NEA International Project managed by the Australian Nuclear Science and Technology Organisation.

FRONDEL, C. 1958. Systematic Mineralogy of Uranium and Thorium. U.S. Geol. Survey Bull., **1064**, U.S. Govt. Printing Office, Washington D.C..

HEBEDA, E.H., SCHULTZ, L. and FREUNDEL, M. 1987. Radiogenic, fissiogenic and nucleogenic noble gases in zircons. Earth Planet. Sci. Lett., **85**, 79-90.

HYDE, E.K. 1964. *The Nuclear Properties of the Heavy Elements, Vol. III, Fission Phenomena* Prentice-Hall, Inc., Englewood Cliffs, New Jersey, 519 p.

JULL, A.J.T., BARKER, D.L. and DONAHUE, D.J. 1987. On the ^{14}C content in radioactive ores. Chem. Geol. (Isot. Geos. Sect.), **66**, 35-40.

MEIJER, A. 1990. A strategy for the derivation and use of sorption coefficients in performance assessment calculations for the Yucca Mountain site. In *Proc. Workshop on radionuclide adsorption, Los Alamos, NM, September 11-12, 1990.* Los Alamos Nat. Lab. Rep., **LA-UR-91-3747**.

PERRIN, R.E., KNOBELOCH, G.W., ARMIJO, V.M. and EFURD, D.W. 1985. Isotopic analysis of nanogram quantities of plutonium by using a SID ionization source. Int. J. Mass Spect. Ion Proc., **64**, 17-24.

PERRY, R.T. and WILSON, W.B. 1981. Neutron production from (α,n) reactions and spontaneous fission in ThO_2, UO_2, and $(U,Pu)O_2$ fuels. Los Alamos National Laboratory (Los Alamos, New Mexico) Rep. **LA-8869-MS**, 34 p.

WEAVER, C.E. and POLLARD, L.D. 1973. *The Chemistry of Clay Minerals* Elsevier Scientific Publishing Co., New York.

3.8.3 Oxidation by water radiolysis products
(H. Christensen)

3.8.3.1 Introduction

The high-level spent fuel resulting from the Canadian and Swedish nuclear industry comprises a crystalline UO_2 matrix that incorporates most of the fission and activation products from the nuclear reaction chain. The long-term stability of the UO_2 matrix under disposal conditions is therefore seen as being central to the ultimate safety of the repository system. Naturally occurring uraninite, consisting predominantly of UO_2 and considered analogous to spent fuel, provides an excellent opportunity to study the long-term behaviour of the spent fuel matrix and the geochemical constraints for its stability. The presence of ancient ($\sim$1.3 Ga) uraninite phases at Cigar Lake, which contain both natural-decay and fission products, should therefore be an ideal testing ground for uraninite/spent fuel stability under natural geological conditions.

At Cigar Lake the uraninite is assumed to undergo oxidation as a result of reaction with normal oxidizing groundwater and/or radiolysis. In the safety assessment of the Canadian disposal concept, the UO_2 dissolution model is based on congruent dissolution of the UO_2 matrix through limited oxidation of UO_2 to U_4O_9-U_3O_7 (Johnson et al. 1994). In contrast, the Swedish concept is based on radiolysis-induced oxidation of UO_2 proceeding beyond the U_3O_7 stage (SKB-91). When this occurs the corresponding change in the crystal structure strongly influences the release of radionuclides from the UO_2-U_3O_7 matrix.

One of the main objectives of the modelling calculations carried out in this report has therefore been to determine whether water radiolysis products do in fact contribute to oxidation and dissolution of uraninite in the Cigar Lake deposit. In addition, radiolysis was also studied as to its role in explaining the presence of amorphous ferrihydrites and hematite concentrations (by oxidation of Fe^{2+}) within the clay halo (at the ore/clay contact) that surrounds the ore deposit. If proven, this would provide evidence that radiolysis is occurring and therefore lend support to potential uraninite dissolution mechanisms.

3.8.3.2 Calculation procedure and initial conditions

3.8.3.2.1 General

It has been shown in experiments both at Whiteshell and Studsvik that water radiolysis products (mainly OH, O_2^- and H_2O_2) oxidize UO_2 to higher oxidation states and thus make the uranium oxide more soluble (Sunder at al. 1989; Christensen et al. 1990a,b; Christensen 1991). Corrosion experiments at Whiteshell were followed by measuring the corrosion potential of an irradiated UO_2 electrode immersed in water. In separate electrochemical experiments a relationship was established between potential and corrosion current (Shoesmith et al. 1988). At Studsvik a UO_2 disc immersed in water was irradiated; this was followed by analysing the surface of the solid phase. The composition and layer thickness of the oxidized UO_2 surface was determined using electron spectroscopy for chemical analysis

(ESCA) and secondary ion mass spectrometry (SIMS). The amount of uranium that had dissolved, or was deposited elsewhere other than the sample surface, was measured. By adding these two fractions a corrosion rate was determined. Some of the results are shown in Tables 3.63 and 3.64.

3.8.3.2.2 The model

The model (Christensen et al. 1990a,b; Christensen and Bjergbakke 1987) is based on three assumptions:

- oxidation of UO_2 is caused by water radiolysis products produced within one diffusion length from the surface,

- water radiolysis products react with the solid UO_2 phase as if initially a mono-molecular UO_2 layer was dissolved within the range of the radicals, and

- rate constants for the heterogeneous oxidation reactions are deduced from similar rate constants in a homogeneous aqueous phase.

The computer program Macksima-Chemist (Carver et al. 1979) has been used for these calculations. The reaction mechanism, excluding and including reactions with UO_2, is shown in Tables 3.65 and 3.66, respectively.

3.8.3.2.3 Irradiation conditions

G-values for various types of irradiation (α and γ-β) have been presented previously (Christensen, 1990a). The calculated dose rates, based on measurements, are 2.7×10^{-5} Gy/s for α-radiation and 6.3×10^{-9} Gy/s for γ-radiation, in both cases assuming an average ore with 10 % uranium. In the calculations an irradiation time of 30 a has been assumed, based on typical dimensions of a fracture and a typical groundwater flow-rate. The dimensions used were a fracture opening of 10^{-4} m, a length of 1 m and a flow rate of 3.3×10^{-2} m/a (Christensen 1990a). However, according to more recent information (J.J. Cramer pers. comm. 1992), the flow rate may be considerably lower than that assumed in the calculations.

In Table 3.67 the dose rate in thin fractures in the Cigar Lake case is compared with expected dose rates during the long-term storage of high-level waste. It can be seen that the dose rate at Cigar Lake is less than that which would occur during storage of spent fuel, even after a storage time of 1 Ma based on the Swedish repository concept.

The dose rate at Cigar Lake has remained relatively stable with time during the existence of the deposit, as evidenced by the half-lives of ^{238}U and ^{235}U, which are 4.5×10^{9} and 7.1×10^{8} a respectively. If equilibrium is assumed, the dose rate will be determined by the longest living isotope in the decay scheme.

3.8.3.2.4 Chemical conditions

The initial chemical conditions used in the calculation are shown in Table 3.68.

3.8.3.3 Calculations disregarding reactions with UO_2

3.8.3.3.1 General

Radiolysis has also been studied in respect its role in explaining the presence of red-coloured amorphous ferrihydrites and hematite concentrations within the clay halo (at the ore/clay contact). Assuming that radiolysis is occurring at the ore/clay contact, oxidants (e.g., OH^- radicals, H_2O_2 and O_2^-) and hydrogen will be generated. As hydrogen is not very reactive at ambient temperatures, it is expected to escape from the ore zone by diffusion through the water-filled matrices of the ore and the surrounding clay halo. The net chemical effect will be the oxidation of components in the groundwater, contact rock and ore minerals.

In principle, the following reductants present at Cigar Lake can react with the oxidants produced by radiolytically generated reactions:

- in the groundwater Fe^{2+}, HS^- and DOC (Dissolved Organic Compounds); and

- in minerals other than UO_2, Fe(II) (e.g., siderite), sulphide (e.g., Fe_2S, PbS) and SOC (Solid Organic Content).

The question posed is whether radiolysis can result in the oxidation of Fe^{2+}, thus producing an outward "redox front" movement of Fe(III) into the surrounding clay layer whereupon it precipitates to form hematite and ferrihydrite.

3.8.3.3.2 Reaction mechanism

The radiolysis reaction mechanism, shown in Table 3.65, includes reactions with carbonate species; hydrogen and oxygen are produced in near-stoichiometric amounts with G-values that decrease with irradiation time (Figure 3.96). The Fe^{3+} concentration increases to $9x10^{-6}$ M until $3.15x10^7$ s = 1 a, when it starts to decrease. At 1 a, hydrogen is produced with a G-value of 0.78, and at 100 a with a G-value of $8.7x10^{-3}$; oxygen is produced in near-stoichiometric quantities. Thus, radiolysis decreases with time, and at 1000 a, a near-steady state has been obtained with G (H_2) = $2x10^{-5}$.

It is likely that Fe^{3+} is precipitated at some concentration above 10^{-6} M, depending on pH and the presence of complexing agents. Oxidation of Fe^{2+} to Fe^{3+} results in an increase in pH; see reactions 45, 46, 48, 50 and 52 in Table 3.65. Precipitation of Fe^{3+} can be simulated by the reactions:

$$Fe^{3+} + OH^- \rightarrow Fe(OH)^{2+} \quad \text{(A)}$$
$$Fe(OH)^{2+} \rightarrow Fe^{3+} + OH^- \quad \text{(B)}$$

in combination with a buffer of $Fe(OH)^{2+}$.

At steady state, equations A and B lead to:

$$[Fe^{3+}] = \frac{k_B \cdot [Fe(OH)^{2+}]}{k_A \cdot [OH^-]}$$

which is the maximum Fe^{3+} concentration obtainable, i.e., above this value "precipitation" occurs.

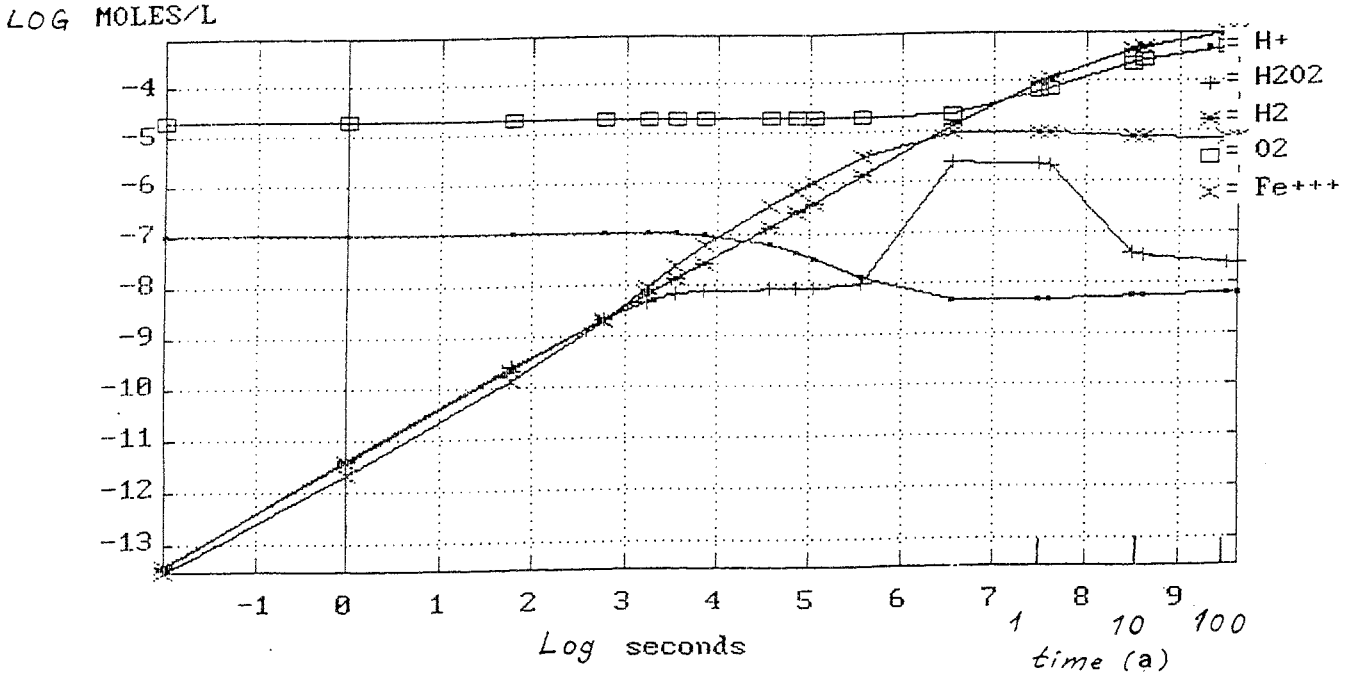

FIGURE 3.96 Concentrations as a function of time; UO_2 reactions excluded. ($Fe^{2+} = 9x10^{-6}$ M; Cigar 50 = reaction 50 in Table 3.65).

In practical terms, assuming a typical fracture with an opening of 10^{-4} m (= 100 μm), most of the water in the gap will be irradiated (the α-particle range is estimated to be about 30 μm), which is not the case for the wider fractures. Calculations have therefore been carried out to simulate a situation in which Fe^{2+} is added continuously from a buffer A to the irradiated solution using the equations:

$$A \rightarrow Fe^{2+} \quad (C)$$
$$Fe^{2+} \rightarrow A \quad (D)$$

In this way the concentration of Fe^{2+} may be kept constant at a value of:

$$\frac{[A] \cdot k_C}{k_D}$$

It is also assumed that oxygen is diffused into the reaction zone and allowed to react with e^-_{aq} to form O_2^-. Thus, the overall result of the combined diffusion of Fe^{2+} and precipitation of Fe^{3+} is a production of precipitated iron, Fe↓, with a G-value of 1.4 after an irradiation time of 10 a (Table 3.69).

3.8.3.4 Calculations including reactions with UO_2

3.8.3.4.1 General

The surface oxidation of uranium ore (UO_2) to higher mixed oxides is of interest from a performance assessment viewpoint. If oxidation proceeds beyond U_3O_7 to U_3O it will alter the crystal lattice structure. If the crystal structure is changed by oxidation, radionuclides that are contained within the UO_2 matrix of spent fuel will become available for dissolution through release. A further mechanism for release would be the oxidation of U(IV) to U(VI) and thereby the dissolution of uranium as uranyl ions. The following calculations were carried out to establish the potential impact of radiolysis on UO_2 oxidation.

3.8.3.4.2 Reaction mechanism

In these calculations the UO_2 oxidation model has been combined with the iron oxidation model described above (Section 3.8.3.3). The reaction mechanism is shown in Table 3.66. Reactions with HCO_3^- have been disregarded; as the rates for the reaction of carbonate radicals with UO_2 are unknown it would be necessary to use assumed rate constants. Thus, the inclusion of carbonate reactions would not make the calculations more reliable. The effect of Fe^{2+} on the oxidation of UO_2 by radiolysis products has not been studied experimentally. In the present calculations the possible cross reactions between iron ions and U (IV, V or VI) have also been disregarded.

In the initial calculations (Table 3.69), Cigar 36 and 37 (i.e., reactions 36 and 37 in Table 3.66), the iron concentration was set at zero, i.e., the radiolytic oxidation of UO_2 was calculated in the absence of iron ions. This resulted in the production of hydrogen and U(VI) (= UO_3D where D is the dummy variable used to model the transport of UO_3 away from the system) in stoichiometric amounts, G= 1.16 at 30 a and G= 1.04 at 100 a. In the presence of an initial concentration of 9×10^{-6} M Fe^{2+} the G-values of hydrogen and UO_3D were slightly lower (see Cigar 38 and 39). Fe^{3+} increased to a maximum of 7.4×10^{-5} M after about 1 a. At this concentration Fe^{3+} may be expected to precipitate.

Calculations (Table 3.66; reactions 16, 24, 58, 59, 61, 63, 65) were therefore carried out in which it was assumed that iron and oxygen diffused continuously into the reaction zone in such a way that both concentrations were kept constant. The results can be seen in Table 3.69 (calculation numbers 41 and 59). Precipitated Fe(III), Fe↓, was produced with a G-value of 0.9 and U(VI) with a G-value of 1.4.

One of the results of these calculations is that the G-value for oxidation of UO_2, G(U(VI)), is higher in the presence of Fe(II) than in its absence. Initially it was expected that Fe(II) might protect UO_2 against oxidation. The reason for the higher yield is not clear, but it may be caused by the substitution of reaction E with reaction F and G.

$$UO_2 + 2H_2O_2 \rightarrow UO_2 + H_2O + \tfrac{1}{2}O_2 \quad (E)$$
$$Fe^{2+} + H_2O_2 \rightarrow Fe^{3+} + OH \quad (F)$$
$$UO_2 + OH \rightarrow UO_3H \quad (G)$$

The consequence is that H_2O_2, which in the absence of Fe^{2+} may decompose catalytically, in the presence of Fe^{2+} may react to form OH, which may oxidize UO_2. It is well known that the presence of Fe^{2+} ions increases the oxidation of organic compounds by H_2O_2, i.e., the "Fenton's" reagent, due to the formation of OH radicals (Haber and Weiss 1934; Millero et al. 1991).

However, as the Fe^{2+}/UO_2 system has not been studied experimentally, the mechanism, as pointed out above, is not known. The calculated results may therefore be erroneous.

In conclusion, these calculations have shown that as a result of radiolysis of water, Fe^{2+} ions are oxidized to Fe(III), which will probably precipitate because of its low solubility. The production of precipitated Fe(III), Fe↓, has been calculated under various conditions, both including and excluding reactions between water radiolysis products and UO_2.

If the supply of Fe^{2+} is unlimited, Fe↓ is produced with G-values of 0.9 or 1.4 for conditions including or excluding reactions with UO_2 respectively. A G-value of 1.4 in a 10^{-3}-m-wide fracture corresponds to a production of Fe↓ at a rate of 10^{-8} g/a for the first 30 a (Christensen 1990a). The time of 30 a corresponds to the irradiation time in a typical fracture (vide supra).

If the supply of Fe^{2+} is restricted to the amount dissolved in the flowing water, the limit for the production of Fe↓ will be this amount of Fe^{2+}. Thus a production of Fe(III) in the groundwater flowing up through the uranium deposit can be explained by radiolysis. However, the deposition of Fe↓ in the hematite-containing clay layer just above the ore has not been elucidated in the present calculations. This would require information about deposition rates under the local conditions. Such information is presently not available.

3.8.3.5 Further developments of the model

3.8.3.5.1 General

In previous calculations (Christensen et al. 1990a,b; Christensen and Sunder 1989) a fair agreement was obtained between the modelled results and data resulting from γ-radiolysis experiments carried out at Whiteshell and Studsvik (Table 3.64). However, it was found that the model overestimated the oxidation caused by α-radiolysis products (Christensen 1990b). Consequently, a number of adjustments to the model have been tested in the hope of improving the agreement with the α-radiolysis experiments (Christensen et al. 1992).

3.8.3.5.2 Approach

Decreases in the yield of U(VI) were obtained by introducing a mechanism for catalytic decomposition of H_2O_2 on a UO_2 surface containing UO_3 sites. Experimentally, it has been shown that H_2O_2 decomposition can occur on UO_2 surfaces at around pH= 8.3 (Christensen et al. 1990a,b). This reaction appears to be catalyzed by a combination of U(IV)/U(V) or U(V)/U(VI) sites present in the UO_2 surface (Shoesmith and Sunder 1990). An attempt to simulate catalytic decomposition of H_2O_2 on a UO_2 surface, when the UO_2 surface contains both oxidized and reduced sites, was made. The mechanism used to simulate this effect is represented by reactions 54-57 (Table 3.70):

		Reaction #	k
$UO_2 + H_2O_2$	$\Leftrightarrow UO_2 + H_2O_2X$	54	100
H_2O_2X	$\Leftrightarrow H_2O + O$	55	10^4
$UO_3 + H_2O_2X$	$\Leftrightarrow UO_3 + H_2O_2$	56	10^8
$O + O$	$\Leftrightarrow O_2$	57	10^9

In the above reactions the dummy intermediate H_2O_2X may be either decomposed to O_2 (reactions 55 and 57), or, when the surface is mainly coated by UO_3, revert to H_2O_2, i.e., in that case when catalytic decomposition is eliminated or decreased.

The introduction of reactions 54-57 served to reduced the yield of U(VI) by about 30 %. A decrease in the yield was also obtained by increasing the rate for reduction reaction of O_2^- and decreasing its oxidation reaction (by using similar rate constants as those found in the Fe(II)/Fe(III) system). Further decreases were obtained by decreasing the diffusion of the dummy variable UO_3D (i.e., modelled escape of UO_3 from the reaction system) and by decreasing the steady-state concentration of UO_2.

One of the objectives of the present calculations was to obtain a more than linear decrease in the yield of U(VI) with decreasing dose rate as found in the experiments. This effect could be obtained by introducing pseudo third-order reactions in combination with effectively competing pseudo first-order removal reactions of OH and O_2^- (reactions H to K):

$UO_2 + OH + OH$	$\rightarrow UO_3 + H_2O$	(H)
$UO_2 + O_2^- + OH$	$\rightarrow UO_3 + HO_2^-$	(I)
$UO_2 + O_2^- + O_2^-$	$\xrightarrow{H_2O} UO_3 + HO_2^- + HO_2^-$	(J)
$B + OH$	$\rightarrow BOH$ (large rate)	(K)

It can be shown (Christensen et al. 1992) that, by a suitable choice of constants (dummy constant B= 100 mol/dm^3, k_K= 200 and 600 dm^3/mol/s (reaction K) of dummy B with OH and O_2^-, respectively), the rate of UO_3 production is proportional to $(DR)^2$ (DR = dose rate).

The introduction of this mechanism thus resulted in:

1. decreasing the yield of U(VI), and

2. establishing the desired effect at least for the dose rates 280 and 28 Gy/h (the yield of U(VI) decreased by a larger factor than the factor for decrease in dose rate).

An alternative explanation for the non-linear effect of dose rate on dissolution rate could be a change in relative importance of dissolution compared with reactions such as H_2O_2 decomposition and radical recombination. Both of these last two reactions appear to involve U(IV)/U(V) or U(IV)/U(VI) sites on the UO_2 surface (Shoesmith and Sunder 1990). Such sites will be present at the lower steady-state corrosion potentials achieved for lower dose rates. At higher dose rates, the greater positive potentials associated with more highly oxidized surfaces (i.e., higher in U(VI)) may block the H_2O_2 decomposition and radical recombination reactions, and the dissolution rate will appear to have a higher than expected dose rate dependence. At present, the accuracy of the corrosion potential measurements in the presence of α-radiolysis, from which corrosion rates are determined, is insufficient to determine whether this latter explanation is appropriate.

The mechanism shown in Table 3.70 was used for calculations simulating Cigar Lake conditions. Diffusion of O_2, H_2 and H_2O_2 is probably very low in the Cigar Lake case, assuming that diffusion takes place only longitudinally. All diffusion reactions except that for UO_3 were therefore removed. $G(UO_3D)$ was 0.97 in the presence of, and 0.94 in the absence of, 9×10^{-6} M Fe^{2+}. This is only slightly lower than in the previous calculations (Christensen 1990a).

The mechanism including pseudo third-order reactions and the presence of an impurity B (reaction K) was also tested under Cigar Lake conditions. The calculations resulted in $G(UO_3D)$ values of 3.7×10^{-2} and 3.6×10^{-2}, which, as expected, were considerably lower than in previous calculations (Christensen 1990a; Christensen et al. 1992). The lower $G(UO_3D)$ values are consistent with the oxidation state studies of uranium in this deposit (Sunder et al. 1993). X-ray photoelectron spectroscopic studies show that the oxidation state of uranium in this deposit is less than U_3O_7.

The results presented above are uncertain for the following reasons:

1. Literature data on possible reactions between iron and uranium species have not been found and have, therefore, not been included in the mechanism.

2. The mechanism involving the impact of impurities is rather speculative and needs experimental verification.

3. A threshold dose rate may exist, below which oxidation of UO_2 to dissolvable states does not take place.

3.8.3.5.3 Discussion

The original model used in the calculations has been experimentally tested by γ-radiolysis. However, as the model has been shown to overestimate the effect of α-radiolysis, which is the dominating source of radiation in the Cigar Lake deposit, the calculated oxidation of UO_2 has probably been overestimated by more than an order of magnitude.

The introduction of a mechanism for the catalytic decomposition of H_2O_2 served to reduce the corrosion rate (i.e., UO_2 oxidation) by about 30 %. Introduction of third-order reactions resulted in a further decrease and also produced the effect of a more than linear decrease in corrosion rate with decreasing dose rate.

Alpha-radiolysis experiments indicate a threshold corrosion potential, below which no oxidation takes place (Shoesmith and Sunder 1992). This has indicated a threshold dose rate of about 0.01 Gy/s or about 36 Gy/h corresponding to the lowest α-source in the experimental series (Christensen 1990b). As the α-dose rate in the Cigar Lake deposit has been estimated at 0.1 Gy/h, the conclusion is that α-radiation in this case should not cause oxidation of UO_2 to exceed those oxidation states which lead to dissolution. However, if the corrosion potential, for reasons other than radiolysis (e.g., see Section 3.9.3), is greater than -100 mV (SCE= standard calomel electrodrode), dissolution may still be possible (Shoesmith and Sunder 1990).

3.8.3.6 Summary and Conclusions

Mineralogical and geochemical observations at Cigar Lake note that Fe(III), present as amorphous ferrihydrites and hematite, has been precipitated in the clay near the ore/massive clay contact. Furthermore, the uranium ore shows signs of surface alterations to mixed oxides (albeit only in minor quantities) of stoichiometries in the range of U_4O_9 to U_3O_7. Hydrogen has also been analyzed in groundwaters sampled from the ore/clay zone. The presence of these oxidation and other products can, in principle, be generated by radiolysis.

The surface oxidation of uranium ore (UO_2) to higher mixed oxides is of interest from a performance assessment viewpoint. If oxidation proceeds beyond U_3O_7 to U_3O_8 it will alter the crystal lattice structure. Spent nuclear fuel consists of UO_2 with radionuclides contained in the crystal matrix. If the matrix is changed by oxidation these radionuclides can become available for dissolution through release. A further mechanism for release would be the oxidation of U(IV) to U(VI) and thereby the dissolution of uranium as uranyl ions.

The model calculations presented here confirm that the radiolysis products of water oxidize Fe(II) to Fe(III), which may then precipitate due to low solubility. Oxidation may even take place under deaerated conditions. This model supports the red colouration at the ore/massive clay contact (from precipitation of ferrihydrite and hematite) through scavenging of radiolysis-produced oxidants by dissolved Fe^{2+} in the ore zone groundwaters (Cramer 1986). Although the calculations confirm that products from α-radiolysis of water can oxidize dissolved Fe^{2+} to Fe^{3+}, it is uncertain as to whether all the Fe(III) minerals can be accounted for by this process.

The laboratory experiments described indicate that no radiolytic oxidation occurs beyond the $UO_{2.33}$ stage at the UO_2 surface below a certain corrosion potential. This may explain the lack of significant quantities of higher-valency uranium oxides at the uraninite mineral surfaces. In fact, calculations using SKB's current radiolysis models using a corrosion redox potential value of +120 mV (SHE= standard hydrogen electrode) for UO_2 dissolution show that the Cigar Lake ore should have been totally oxidized within 18 to 170 Ma. As this is not the case, the radiolytic model originally proposed for the oxidation of UO_2 by α-radiolysis was consequently modified, showing that the oxidation of UO_2 had been overestimated by an order of magnitude in the earlier calculations and a threshold value of +120 mV appears to be unreasonably low.

The overall conclusion is that the effects of α- and γ-radiolysis are insufficient to cause significant oxidation of the UO_2 at Cigar Lake, even when integrated over the lifetime of the deposit. Recent experimental work (Sunder et al. 1993) indicates that oxidative dissolution of UO_2 does not become important until the redox potential reaches values above -100 mV (SCE) or +140 mV (SHE). This is supported by spent fuel stability calculations based on pyrite/siderite stabilities (i.e., the Fe(II)/Fe(III) redox couple). These suggest that a redox potential of $> +200$ mV (SHE) is required for oxidative dissolution of UO_2 (Bruno and Casas, see Section 3.9.2).

3.8.3.7 References

CARVER, M. B., HANLEY, D.V. and CHAPLIN, K.R. 1979. Maksima-Chemist. AECL Res. Rep., **AECL-6413**.

CHRISTENSEN, H. 1990a. Calculation of radiolysis at the Cigar Lake uranium deposit. Studsvik AB Rep., **NS-90/136**.

CHRISTENSEN, H. 1990b. Calculation of the effect of α-radiolysis of UO_2 oxidation. Studsvik AB Rep., **NS-90/72**.

CHRISTENSEN, H. 1991. Radiation induced dissolution of UO_2. In *Proc. 14th Symp. Sci. Basis Nucl. Waste Manag.* Mat. Res. Soc. Proc., **212**, 213-220.

CHRISTENSEN, H. and BJERGBAKKE, E. 1987. Radiation induced dissolution of UO_2. In *Proc. 10th Symp. Sci. Basis Nucl. Waste Manag.* Mat. Res. Soc. Proc., **84**, 115-122.

CHRISTENSEN, H. and SUNDER, S. 1989. Calculations of radiolysis in connection with UO_2 oxidation studies. Studsvik AB Rep., **NS-89/117**.

CHRISTENSEN, H., FORSYTH, R., LUNDQWIST, R. and WERME, L.O. 1990a. Radiation-induced dissolution of UO_2. Studsvik AB Rep., **NS-90/85**.

CHRISTENSEN, H., SUNDER, S. and SHOESMITH, D.W. 1990b. Calculations of radiolysis in connection with UO_2 oxidation studies. III: Adjustment of the final stage of oxidation. Studsvik AB Rep., **NS-90/99**.

CHRISTENSEN, H., SUNDER, S. and SHOESMITH, D.W. 1992. Calculation of radiation induced dissolution of UO_2. Adjustment of the model based on α-radiolysis experiments. Studsvik AB Rep., **M-92/20**.

CRAMER, J.J. 1986. A natural analog for a fuel waste disposal vault. In *2nd Int. Conf. on Radioactive Waste Manag.* Can. Nucl. Soc. Proc., 697-702.

HABER, F. and WEISS, J. 1934. Catalytic decomposition of hydrogen peroxide by iron salts. Proc. R. Soc. Lond., Series **A147**, 332.

JOHNSON, L.H., SHOESMITH, D.W., LENEVEU, D.M., GARISTO, N.C., OSCARSON, D.W., GRAY, M.N. and LEMIRE, R.J. 1994. The disposal of Canada's nuclear fuel waste: The vault model for postclosure assessment. AECL Res. Rep., **AECL-10714, COG-93-4**.

MILLERO, F. J., SOTOLONGO, S., STADE, D.J. and VEGA, C.A. 1991. Effect of ionic interactions on the oxidation of Fe_{II} with H_2O_2 in aqueous solutions. J. Soln. Chem., **20**, 1079-1092.

SHOESMITH, D.W. and SUNDER, S. 1990. An electrochemistry-based model for the dissolution of UO_2. AECL Res. Rep., **AECL-10488**.

SHOESMITH, D.W. and SUNDER, S. 1992. The prediction of nuclear fuel (UO_2) dissolution rates under waste disposal conditions. J. Nucl. Mat., **190**, 20-35.

SHOESMITH, D.W., SUNDER, S., BAILEY, M.G. and WALLACE, G.J. 1988. Corrosion of nuclear fuel (UO_2) in oxygenated solutions. Corros. Sci., **29**, 1115-1128.

SKB-91, 1992. Final disposal of spent nuclear fuel. Importance of the bedrock for safety. (May, 1992). SKB Tech. Rep., **TR 92-20**.

SUNDER, S., SHOESMITH, D.W., CHRISTENSEN, H., BAILEY, M.G. and MILLER, N.H. 1989. Electrochemical and X-ray photoelectron spectroscopic studies of UO_2 fuel oxidation by specific radicals formed during radiolysis of groundwater. In *Proc. 12th Symp. Sci. Basis Nucl. Waste Manag.* Mat. Res. Soc. Proc., **127**, 317-324.

SUNDER, S., CRAMER, J.J. and MILLER, N.H. 1993. X-ray photoelectron spectroscopic study of Cigar Lake uranium ore: a natural analog for used fuel. In *Proc. 15th Symp. Sci. Basis Nucl. Waste Manag.* Mat. Res. Soc. Proc., **257**, 449-457.

TABLE 3.63
CALCULATED AND MEASURED CORROSION RATES
AFTER OXIDATION OF UO_2 BY O_2 OR H_2O_2*

Dose Rate Gy/h	Solution	Purge gas	Oxidizing species	Corrosion Rate $\mu g/cm^2.d$ Calculated	Experimental
600	t-bu	O_2	O_2^-	5.5	3
600	DDW	N_2O	OH	1.4	3
0	0.05 M H_2O_2	Ar	H_2O_2	13	5

* Christensen (1991)

TABLE 3.64
COMPARISON OF CALCULATED AND EXPERIMENTAL CORROSION RATES

Solution	Dose rate Gy/h	Corrosion potential mV	ΔU6 M	G-value	Corrosion rate Calculated $\mu g/cm^2.d$	Experimental+ $\mu g/cm^2.d$
Ar	5	-140	1.06E-6	0.20	0.003	n.a*
	120	12				4.7E-3
	280	~90	1.24E-4	0.42	0.12	0.10
N_2O	5	-100	1.34E-5	2.6	0.04	n.a
	110	73				4.4E-2
	260	135	8.1E-4	2.8	0.84	0.36
	600					3
O_2	0	5	3.5E-6		2.3E-2	3.8E-3
	5	≥100	2.1E-5	4.0	0.06	0.13
	100	110				0.17
	280	150	8.1E-4	2.8	0.84	0.75
	600					3
H_2O_2**	E-6 M	-40	1.23E-7		8.0E-4	2.1E-4
	2E-4 M	100	2.1E-4		1.4	0.13
	3E-4 M	111				0.18

\+ Derived from the corrosion potential according to CR=78E (-4.4 + 0.016xpotential(mV)) (Christensen et al. (1990a)

** Unirradiated solutions with initial concentrations given in next column.

TABLE 3.65
REACTION MECHANISM EXCLUDING REACTIONS WITH UO_2

	Reaction						Rate constant, $M^{-1} \cdot S^{-1}$	
1	OH	+OH	= H2O2				K(1)=	5.500E+09 *
2	OH	+E-	= OH-				K(2)=	3.000E+10 *
3	OH	+H	= H2O				K(3)=	2.000E+10 *
4	OH	+HO2	= H2O	+O2			K(4)=	7.900E+09 *
5	OH	+O2-	= O2	+OH-			K(5)=	9.000E+09 *
6	OH	+H2O2	= HO2	+H2O			K(6)=	2.700E+07 *
7	OH	+H2	= H	+H2O			K(7)=	3.400E+07 *
8	OH	+OH-	= H2O	+O-			K(8)=	1.200E+10 *
9	OH	+HO2-	= HO2	+OH-			K(9)=	5.000E+09 *
10	O-	+H2O	= OH	+OH-			K(10)=	9.300E+07 *
11	E-	+E-	= H2	+OH-	+OH-		K(11)=	5.500E+09 *
12	E-	+H	= H2	+OH-	-H2O		K(12)=	2.500E+10 *
13	E-	+O2-	= HO2-	+OH-	-H2O		K(13)=	1.300E+10 *
14	E-	+HO2	= HO2-				K(14)=	2.000E+10 *
15	E-	+H2O2	= OH	+OH-			K(15)=	1.200E+10 *
16	E-	+O2	= O2-				K(16)=	1.900E+10 *
17	E-	+H+	= H				K(17)=	2.200E+10 *
18	E-	+H2O	= H	+OH-			K(18)=	2.000E+01 *
19	E-	+HO2-	= O-	+OH-			K(19)=	3.500E+09 *
20	H	+H	= H2				K(20)=	1.000E+10 *
21	H	+O2-	= HO2-				K(21)=	2.000E+10 *
22	H	+HO2	= H2O2				K(22)=	2.000E+10 *
23	H	+H2O2	= H2O	+OH			K(23)=	6.000E+07 *
24	H	+O2	= HO2				K(24)=	1.800E+10 *
25	H	+OH-	= E-	+H2O			K(25)=	1.500E+07 *
26	HO2	+HO2	= H2O2	+O2			K(26)=	8.400E+05 *
27	HO2	+O2-	= O2	+HO2-			K(27)=	9.600E+07 *
28	HO2		= H+	+O2-			K(28)=	8.000E+05 *
29	H+	+O2-	= HO2				K(29)=	4.500E+10 *
30	O2-	+O2-	= HO2-	+O2	-H+		K(30)=	1.000E+06 *
31	H2O2		= H+	+HO2-			K(31)=	3.560E-02 *
32	H+	+HO2-	= H2O2				K(32)=	2.000E+10 *
33	H2O		= H+	+OH-			K(33)=	2.574E-05 *
34	H+	+OH-	= H2O				K(34)=	1.430E+11 *
35	OH	+CO3--	= CO3-	+OH-			K(35)=	4.000E+08 *
36	OH	+HCO3-	= CO3-	+H2O			K(36)=	1.000E+06 *
37	O2-	+CO3-	= CO3--	+O2			K(37)=	3.200E+08 *
38	H2O2	+CO3-	= CO3--	+HO2	+H+		K(38)=	4.300E+05 *
39	CO3-	+CO3-	= CO4--	+CO2			K(39)=	7.000E+07 *
40	H2O	+CO4--	= CO3--	+H2O2			K(40)=	1.000E+02 *
41	CO2	+OH-	= CO3--	+H+			K(41)=	1.000E+06 *
42	CO3--	+H2O	= HCO3-	+OH-			K(42)=	3.600E+03 *
43	HCO3-	+OH-	= CO3--	+H2O			K(43)=	1.000E+09 *
44	CO3-	+Fe++	= CO3--	+Fe+++			K(44)=	1.000E+08 *
45	Fe++	+OH	= Fe+++	+OH-			K(45)=	3.400E+08 *
46	Fe++	+E-	= Fe+++	+OH-	+H-		K(46)=	1.200E+08 *
47	Fe+++	+E-	= Fe++				K(47)=	2.000E+10 *
48	Fe++	+H	= Fe+++	+H-			K(48)=	1.300E+07 *
49	Fe+++	+H	= Fe++	+H+			K(49)=	1.000E+08 *
50	Fe++	+O2-	= Fe+++	+O2--			K(50)=	2.000E+08 *
51	Fe+++	+O2-	= Fe++	+O2			K(51)=	5.000E+08 *
52	Fe++	+H2O2	= Fe+++	+OH	+OH-		K(52)=	6.000E+01 *
53	H-	+H2O	= H2	+OH-			K(53)=	1.000E+00 *
54	O2--	+H2O	= HO2-	+OH-			K(54)=	1.000E+00 *
55	A		= Fe++				K(55)=	1.000E-07 *
56	Fe++		= A				K(56)=	1.000E-02 *
57	Fe+++	+OH-	= FOH++				K(57)=	1.000E+04 *
58	FOH++		= Fe+++	+OH-			K(58)=	1.000E-06 *

TABLE 3.66

REACTION MECHANISM INCLUDING REACTIONS WITH UO_2

	Reaction						Rate constant $M^{-1} \cdot S^{-1}$
1	OH	+OH	= H2O2				K(1)= 5.500E+09 *
2	OH	+E-	= OH-				K(2)= 3.000E+10 *
3	OH	+H	= H2O				K(3)= 2.000E+10 *
4	OH	+HO2	= H2O	+O2			K(4)= 7.900E+09 *
5	OH	+O2-	= O2	+OH-			K(5)= 9.000E+09 *
6	OH	+H2O2	= HO2	+H2O			K(6)= 2.700E+07 *
7	OH	+H2	= H	+H2O			K(7)= 3.400E+07 *
8	OH	+OH-	= H2O	+O-			K(8)= 1.200E+10 *
9	OH	+HO2-	= HO2	+OH-			K(9)= 5.000E+09 *
10	O-	+H2O	= OH	+OH-			K(10)= 9.300E+07 *
11	E-	+E-	= H2	+OH-	+OH-		K(11)= 5.500E+09 *
12	E-	+H	= H2	+OH-	-H2O		K(12)= 2.500E+10 *
13	E-	+O2-	= HO2-	+OH-	-H2O		K(13)= 1.300E+10 *
14	E-	+HO2	= HO2-				K(14)= 2.000E+10 *
15	E-	+H2O2	= OH	+OH-			K(15)= 1.200E+10 *
16	E-	+O2	= O2-				K(16)= 1.900E+10 *
17	E-	+H+	= H				K(17)= 2.200E+10 *
18	E-	+H2O	= H	+OH-			K(18)= 2.000E+01 *
19	E-	+HO2-	= O-	+OH-			K(19)= 3.500E+09 *
20	H	+H	= H2				K(20)= 1.000E+10 *
21	H	+O2-	= HO2-				K(21)= 2.000E+10 *
22	H	+HO2	= H2O2				K(22)= 2.000E+10 *
23	H	+H2O2	= H2O	+OH			K(23)= 6.000E+07 *
24	H	+O2	= HO2				K(24)= 1.800E+10 *
25	H	+OH-	= E-	+H2O			K(25)= 1.500E+07 *
26	HO2	+HO2	= H2O2	+O2			K(26)= 8.400E+05 *
27	HO2	+O2-	= O2	+HO2-			K(27)= 9.600E+07 *
28	HO2		= H+	+O2-			K(28)= 8.000E+05 *
29	H+	+O2-	= HO2				K(29)= 4.500E+10 *
30	O2-	+O2-	= HO2-	+O2	-H+		K(30)= 1.000E+06 *
31	H2O2		= H+	+HO2-			K(31)= 3.560E-02 *
32	H+	+HO2-	= H2O2				K(32)= 2.000E+10 *
33	H2O		= H+	+OH-			K(33)= 2.574E-05 *
34	H+	+OH-	= H2O				K(34)= 1.430E+11 *
35	UO2	+OH	= UO3H				K(35)= 4.000E+08 *
36	UO2	+H2O2	= UO3H	+OH			K(36)= 2.000E-01 *
37	UO2	+HO2	= UO3H	+H2O2	-H2O		K(37)= 2.000E+08 *
38	UO2	+O2-	= UO3H	+HO2-	-H2O		K(38)= 2.000E+08 *
39	UO3H	+UO3H	= UO3	+UO2	+H2O		K(39)= 1.000E-01 *
40	UO3H	+OH	= UO3	+H2O			K(40)= 8.000E+08 *
41	UO3H	+E-	= UO2	+OH-			K(41)= 5.000E+08 *
42	UO3H	+H2O2	= UO3	+H2O	+OH		K(42)= 2.000E-01 *
43	UO3H	+O2-	= UO3	+HO2-			K(43)= 4.000E+08 *
44	UO3H	+HO2	= UO3	+H2O2			K(44)= 4.000E+08 *
45	UO3H	+H	= UO2	+H2O			K(45)= 4.500E+06 *
46	UO3	+E-	= UO3H	+OH-	-H2O		K(46)= 5.000E+08 *
47	UO3	+O2-	= UO3-	+O2			K(47)= 4.000E+07 *
48	UO3	+H	= UO3H				K(48)= 4.500E+06 *
49	UO3	+HO2	= UO3H	+O2			K(49)= 4.000E+07 *
50	UO3-	+H2O	= UO3H	+OH-			K(50)= 1.000E+01 *
51	H2O2		= H2O	+O			K(51)= 1.000E-03 *
52	O	+O	= O2				K(52)= 1.000E+09 *
53	UO3		= UO3D				K(53)= 4.000E-04 *
54	UO2	+O2	= UO3H	+HO2	-H2O		K(54)= 1.000E-03 *
55	UO3H	+O2	= UO3	+HO2			K(55)= 1.000E-03 *
56	UO2		= UO2D				K(56)= 7.000E-04 *
57	UO2D		= UO2				K(57)= 3.500E-07 *
58	Fe++	+OH	= Fe+++	+OH-			K(58)= 3.400E+08 *
59	Fe++	+E-	= Fe+++	+OH-	+H-		K(59)= 1.200E+08 *
60	Fe+++	+E-	= Fe++				K(60)= 2.000E+10 *
61	Fe++	+H	= Fe+++	+H-			K(61)= 1.300E+07 *
62	Fe+++	+H	= Fe++	+H+			K(62)= 1.000E+08 *
63	Fe++	+O2-	= Fe+++	+O2—			K(63)= 2.000E+08 *
64	Fe+++	+O2-	= Fe++	+O2			K(64)= 5.000E+08 *
65	Fe++	+H2O2	= Fe+++	+OH	+OH-		K(65)= 6.000E+01 *
66	H-	+H2O	= H2	+OH-			K(66)= 1.000E+00 *

TABLE 3.67
COMPARISON OF DOSE RATES IN THIN FRACTURES

Source		Dose rate Gy/h α	β	Total
Cigar Lake ore		0.1		
Spent fuel (PWR, 45 MWd/kg)				
Storage time:	10^2 a	1560	910	2500
	10^3 a	350	0.2	350
	10^4 a	66	0.2	66
	10^6 a	2.8	0.01	2.8
CANDU fuel				
	500 a			80

TABLE 3.68
INITIAL CONCENTRATIONS OF SPECIES USED FOR CALCULATIONS

	Concentration range mg/L	Value used mg/L	M
Fe^{2+}	0.01-0.9	0.5	9.0E-6
HCO_3^-	10-65	40	6.6E-4
Mn	0.01-0.07	n.a	
O_2	0.05-1	0.6	1.9E-5
H^+	E-9 - E-6 (M)		3.16E-8
pH		7.5	

TABLE 3.69
CALCULATED G-VALUES OF SELECTED SPECIES AFTER 10 a OF IRRADIATION

Conditions Fe(II)*	UO_2*	H_2	O_2	Fe↓ prec Fe_{III}	U(VI)	Calculation number **
var	-	0.22	0.11	n.a	n.a	50, 52
const	-	0.11	0	1.4	n.a	53
-	+	1.2	0	n.a	1.2	36, 37
var	+	1.1	0	n.a	1.1	38, 39
const	+	0.8	0	0.9	1.4	41, 59

* $[Fe^{2+}]_i = 9 \times 10^{-6}$; $[UO_2]_i = 5 \times 10^{-4}$ (i= initial)
** see Tables 4 and 5 in Christensen et al. (1990a) for additional details

TABLE 3.70
MODIFIED REACTION MECHANISM FOR THE OXIDATION OF UO_2

NO	REACTION					RATE CONSTANT	CATALYST
1	OH	+OH	= H2O2			K(1)= 5.500E+09	*
2	OH	+E-	= OH-			K(2)= 3.000E+10	*
3	OH	+H	= H2O			K(3)= 7.000E+09	*
4	OH	+HO2	= H2O	+O2		K(4)= 6.600E+09	*
5	OH	+O2-	= O2	+OH-		K(5)= 1.000E+10	*
6	OH	+H2O2	= HO2	+H2O		K(6)= 2.700E+07	*
7	OH	+H2	= H	+H2O		K(7)= 3.400E+07	*
8	OH	+OH-	= H2O	+O-		K(8)= 1.200E+10	*
9	OH	+HO2-	= HO2	+OH-		K(9)= 7.500E+09	*
10	O-	+H2O	= OH	+OH-		K(10)= 1.700E+06	*
11	E-	+E-	= H2	+OH-	+OH-	K(11)= 5.500E+09	*
12	E-	+H	= H2	+OH-	-H2O	K(12)= 2.500E+10	*
13	E-	+O2-	= HO2-	+OH-	-H2O	K(13)= 1.300E+10	*
14	E-	+HO2	= HO2-			K(14)= 2.000E+10	*
15	E-	+H2O2	= OH	+OH-		K(15)= 1.100E+10	*
16	E-	+O2	= O2-			K(16)= 1.900E+10	*
17	E-	+H+	= H			K(17)= 2.300E+10	*
18	E-	+H2O	= H	+OH-		K(18)= 1.900E+01	*
19	E-	+HO2-	= O-	+OH-		K(19)= 3.500E+09	*
20	H	+H	= H2			K(20)= 7.800E+09	*
21	H	+O2-	= HO2-			K(21)= 2.000E+10	*
22	H	+HO2	= H2O2			K(22)= 2.000E+10	*
23	H	+H2O2	= H2O	+OH		K(23)= 9.000E+07	*
24	H	+O2	= HO2			K(24)= 2.100E+10	*
25	H	+OH-	= E-	+H2O		K(25)= 2.200E+07	*
26	HO2	+HO2	= H2O2	+O2		K(26)= 8.400E+05	*
27	HO2	+O2-	= O2	+HO2-		K(27)= 9.600E+07	*
28	HO2		= H+	+O2-		K(28)= 8.000E+05	*
29	H+	+O2-	= HO2			K(29)= 5.000E+10	*
30	H2O2		= H+	+HO2-		K(30)= 3.560E-02	*
31	H+	+HO2-	= H2O2			K(31)= 2.000E+10	*
32	H2O		= H+	+OH-		K(32)= 2.599E-05	*
33	H+	+OH-	= H2O			K(33)= 1.430E+11	*

TABLE 3.70 (Concluded)

34	O2-	+O2-	= HO2-	+O2	-H+	K(34)=	1.000E+06 * H+
35	O2		= O2D			K(35)=	4.200E-05 *
36	H2		= H2D			K(36)=	1.000E-04 *
37	UO2	+OH	= UO3H			K(37)=	4.000E+08 *
38	UO2	+H2O2	= UO3H	+OH		K(38)=	2.000E-01 *
39	UO2	+HO2	= UO3H	+H2O2	-H2O	K(39)=	2.000E+08 *
40	UO2	+O2-	= UO3H	+HO2-	-H2O	K(40)=	2.000E+08 *
41	UO3H	+UO3H	= UO3	+UO2	+H2O	K(41)=	1.000E-01 *
42	UO3H	+OH	= UO3	+H2O		K(42)=	8.000E+08 *
43	UO3H	+E-	= UO2	+OH-		K(43)=	5.000E+08 *
44	UO3H	+H2O2	= UO3	+H2O	+OH	K(44)=	2.000E-01 *
45	UO3H	+O2-	= UO2	+OH-	+O2	K(45)=	4.000E+08 *
46	UO3H	+O2-	= UO3	+HO2-		K(46)=	2.000E+08 *
47	UO3H	+HO2	= UO3	+H2O2		K(47)=	4.000E+08 *
48	UO3H	+H	= UO2	+H2O		K(48)=	4.500E+06 *
49	UO3	+E-	= UO3H	+OH-	-H2O	K(49)=	5.000E+08 *
50	UO3	+O2-	= UO3-	+O2		K(50)=	4.000E+08 *
51	UO3	+H	= UO3H		21	K(51)=	4.500E+06 *
52	UO3	+HO2	= UO3H	+O2		K(52)=	4.000E+07 *
53	UO3-	+H2O	= UO3H	+OH-		K(53)=	1.000E+01 *
54	UO2	+H2O2	= UO2	+H2O2X		K(54)=	1.000E+02 *
55	H2O2X		= H2O	+O		K(55)=	1.000E+04 *
56	UO3	+H2O2X	= UO3	+H2O2		K(56)=	1.000E+08 *
57	O	+O	= O2			K(57)=	1.000E+09 *
58	UO3		= UO3D			K(58)=	4.000E-05 *
59	UO2	+O2	= UO3H	+HO2	-H2O	K(59)=	1.000E-03 *
60	UO3H	+O2	= UO3	+HO2		K(60)=	1.000E-03 *
61	UO2		= UO2D			K(61)=	7.000E-04 *
62	UO2D		= UO2			K(62)=	3.500E-09 *
63	H2O2		= H2O2D			K(63)=	3.200E-05 *

3.9 PERFORMANCE ASSESSMENT-RELATED MODELLING

3.9.1 Introduction
(J. Cramer)

The prediction of the long-term safety of a disposal concept for nuclear waste is based on both "expert opinion" and the use of computer-based assessment models. Studies of analogous natural processes and systems are needed to provide input to the assessment models and to build confidence in the long-term predictions. Because analog systems are by nature complex, the results and conclusions from such studies are seldom unambiguous. For this reason, analogs cannot be used to directly validate computer codes developed for performance assessment of the overall safety of a disposal concept. However, analog information can be used to provide feedback to the conceptual models and laboratory data used to construct the assessment models, to test specific submodels, and to provide illustrative support for the performance assessment.

In the Cigar Lake analog study, a number of modelling activities were carried out to address the following four objectives related to performance assessment:

1- The evaluation of the role of colloids, organics and microbes in transport processes for radionuclides.

2- The evaluation of equilibrium thermodynamic codes and databases for predicting radionuclide solubility and speciation in groundwaters.

3- The evaluation of UO_2 stability and the influence of radiolysis on UO_2 dissolution and radionuclide migration.

4- The evaluation of generic mass-transport models for potential radionuclide migration through clay-based sealants.

The role of colloids, organics and microbes in radionuclide transport and their relative importance in performance assessment has been presented in Sections 3.6 and 3.7. The evaluation of solubility and speciation codes (Sections 3.9.2 and 3.9.3) did not include truly blind-predictions, but rather an evaluation of the validity and accuracy of such codes. The evaluations provided important information on the stability of UO_2-based phases and radionuclide speciation in the naturally reduced system of the Cigar Lake deposit.

In the Cigar Lake deposit no evidence has been found in the ore-clay-altered sandstone sequence of significant radionuclide migration taking place, neither currently nor during the recent $\sim$1-Ma history of the deposit. Therefore, in the area of mass-transport modelling, the focus was on calculating hypothetical release rates using simplified models, similar to those used in performance assessment, and for a range of assumed conditions. These models were used to yield bounding estimates of the total amounts of material that could possibly be released from the deposit.

Section 3.9.5 reviews the results of the modelling carried out for the four objectives, and summarizes the conclusions from a performance assessment perspective.

3.9.2 Testing of solubility and speciation codes
(I. Casas and J. Bruno)

3.9.2.1 Introduction

Chemical thermodynamic models provide two main types of data for repository performance assessment purposes (Bruno et al. 1990):

1- Solubilities of particular elements or radionuclides, which constrain their maximum concentration in solution and, if solute transport is limited, their maximum rate of release from a solid phase.

2- Speciation of such elements in solution, which determines the extent to which the dissolved element will interact with solid phases along a transport path.

Application of these models is widespread, and a number of different codes are available that perform the required calculations. However, there are two main uncertainties in their use in performance assessment:

1- The databases of thermodynamic constants needed for such calculations are rather poorly defined. Uncertainties of many orders of magnitude in the equilibrium constants are quite common and, what is more important, key thermodynamic data may be missing from these databases. Thus, the solubilities will be overestimated in the case where an important solubility-limiting solid phase is missing, and underestimated if a predominant aqueous complex is absent. In any case, the predicted aqueous speciation will be incorrect.

2- The models assume that the entire groundwater chemical system is at equilibrium. This is, however, not commonly the case in natural water systems, primarily because of the slow kinetics of the water-rock and redox reactions at low temperature. This can normally be handled either by incorporating kinetics into the model or by "switching off" particular reactions.

It requires expertise to both determine the critical uncertainties in the thermodynamic databases and to apply geochemical knowledge to a particular system in order to decide which reactions are possible.

The Cigar Lake analog study provided an ideal opportunity to test the thermodynamic models (and their associated databases) used for performance assessment. The predicted solubilities could be compared with the measured trace-element concentrations in the selected groundwaters. The aqueous speciation was also calculated even though in this case no analytical measurements were available for comparison.

In this approach, however, there is no guarantee that the water has had the time (or the opportunity) to reach saturation. Thus, if predicted solubilities are above or equal to observed concentrations, we still cannot be sure that the model is correct (or that it conservatively predicts). Nevertheless, if the predicted solubilities are lower than observed concentrations, then the model is certainly incorrect.

3.9.2.2 Methodology

Major and trace element and parameter data from the set of reference groundwater compositions (Table 3.30 in Section 3.5.2) were used for this exercise. The trace elements (TE) chosen for these calculations included those of relevance for high-level nuclear waste management and those for which analytical data exist and which reflect the geochemistry of the site. The complete set of modelled TE include U (see Section 3.9.3 for results and discussion), Pu, Th, Tc, Cu, Ni, Ba, Pb, Sr, Zn, Mo, Cr and As. The model-testing exercise proceeded as follows:

1- Establish the individual-solubility limiting phases for each trace element in the different groundwaters selected,

2- Calculate the total concentration of the TE in equilibrium with the selected individual solid phases, and

3- Determine the aqueous speciation of the TE in equilibrium with the solubility-limiting phase.

Generally, the exercise was run as a "blind" prediction modelling, followed by comparing the results with the actual field measurements where available.

The PHREEQE program was used as a geochemical code, together with the ZZ-Hatches v.3.0 database (Harwell Laboratory, Oxfordshire); Pu was calculated using the SKBPU database (Puigdomènech and Bruno 1991).

3.9.2.3 Results and discussion

Plutonium

Because of the lack of analytical data for this element, the calculated predictions were compared with the upper limit calculated for Pu (J. Fabryka-Martin pers. comm. 1991). An average value of $1x10^{-12}$ for the Pu/U ratio in rock was selected, assuming secular equilibrium. Also, a fractional release rate of "one" was assumed to result in an upper limit of Pu concentration.

Good agreement is obtained between the predicted and calculated solubilities (Figure 3.97) when an amorphous plutonium (IV) phase is considered, although, as stated above, this constitutes a conservative upper limit value. If a more crystalline phase is used, a much lower Pu concentration should be found in the aqueous phase. Nevertheless, the solubility-limiting phase, according to the Oswald rule, should be considered to be $Pu(OH)_4$.

The speciation varies considerably depending on the groundwater conditions, i.e., redox potential, pH and phosphate concentration. For reducing, low phosphate waters (pe <1.2, total PO_4^{3-} <0.05), the predominant species in solution is found to be $PuCO^{3+}$, although the $Pu(OH)_4$ contribution increases as pH increases (see Figure 3.98).

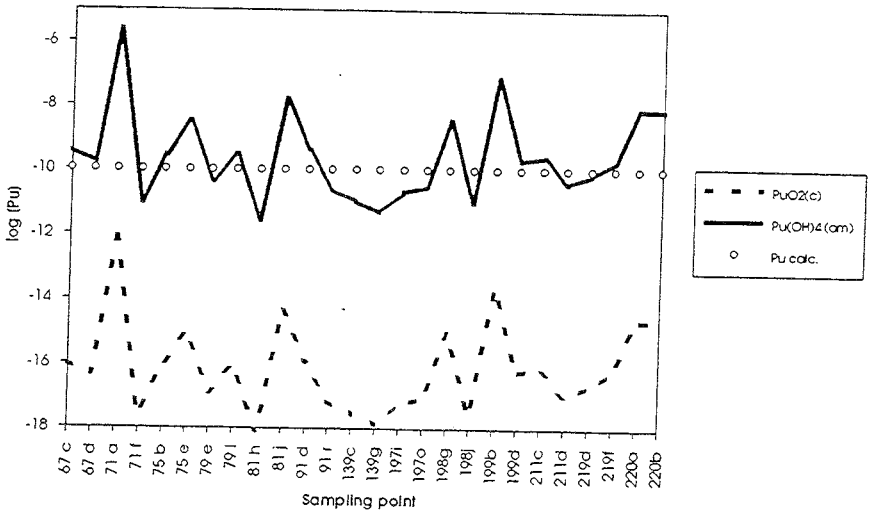

FIGURE 3.97 Predicted and calculated solubilities for plutonium.

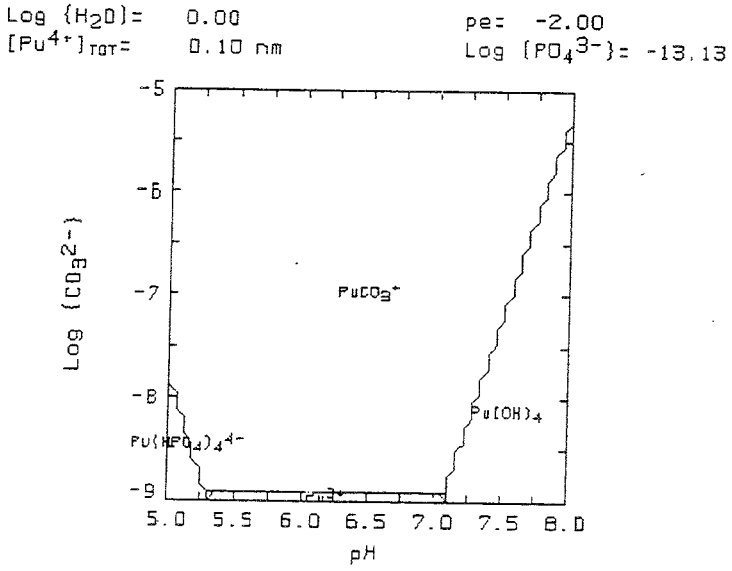

FIGURE 3.98 Predicted aqueous speciation for plutonium (reducing conditions).

For more oxidizing conditions (Figure 3.99) $Pu(OH)_4$ becomes the predominant species; for relatively high phosphate concentrations (samples 91d, 199b and 199d) $Pu(HPO_4)_4^{4-}$ becomes the predominant calculated aqueous species.

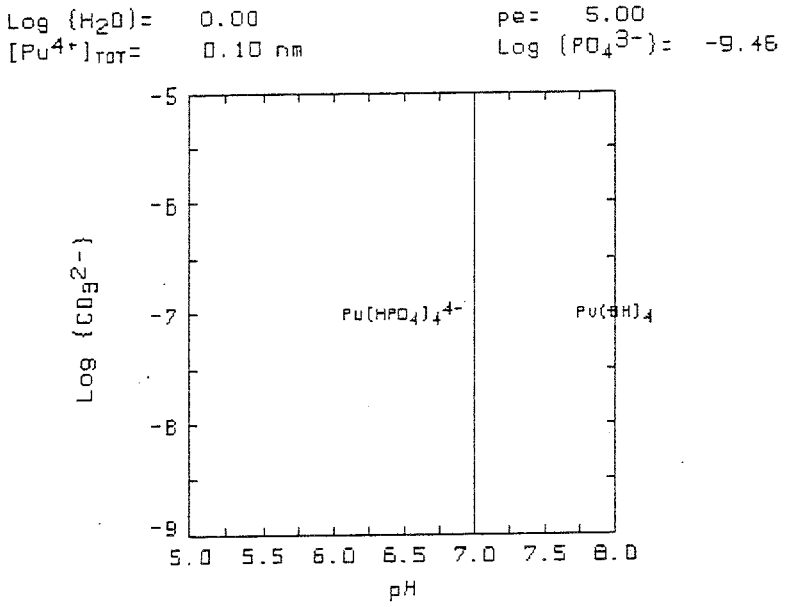

FIGURE 3.99 Predicted aqueous speciation for plutonium (oxidising conditions).

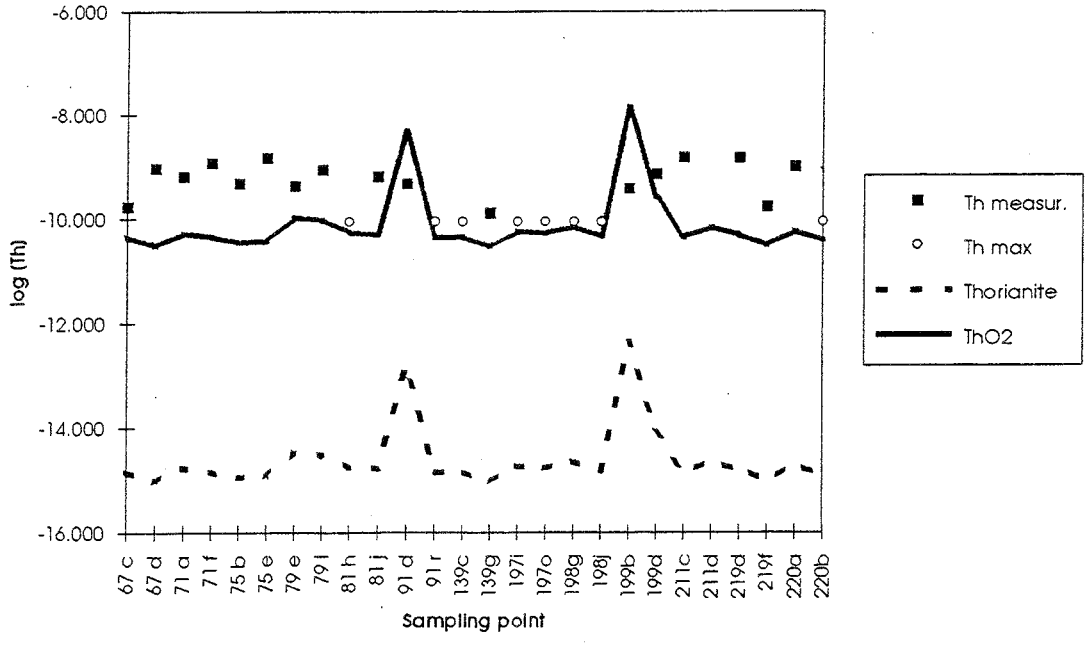

FIGURE 3.100 Predicted aqueous speciation for thorium.

Thorium

There is fairly good agreement (within one order of magnitude) between the analytical data, where available, and the predicted concentrations for an amorphous ThO_2 phase (Figure 3.100). According to the Oswald rule this amorphous phase should precipitate first instead of the more crystalline thorianite with identical stoichiometry. The mineralogical reference data from Cigar Lake (Smellie et al. 1991) does not include this solid phase; instead, monazite ($(Ce,La,Th)PO_4$) and brannerite ($(U,Th,Ca)(Ti,Fe)_2O_6$) tend to be the phases found in accessory amounts in the unaltered sandstone and the ore zone.

In almost all cases the predominant aqueous species is found to be $Th(OH)_4(aq)$. Only for the three samples specified above with higher phosphate concentrations, is the predominant aqeous complex $Th(HPO_4)_3^{2-}$. The increase in solubility due to the presence of this phosphate complex is not apparent from the analytical results, thus leading to some doubt as to its existence. Speciation measurements could have distinguished its presence from its negative charge compared with the neutral thorium hydroxide complex. However, since such a determination was not performed, the suggestion that such a species may exist should be considered a request for a reevaluation of its formation constant.

Technetium

The solubility obtained for a Tc_3O_4 solid phase, which is found to be the most saturated one in all cases, is compared in Figure 3.101 with values calculated in a similar fashion as for Pu.

FIGURE 3.101 Predicted and measured solubilities for technetium.

The predicted results are most dependent on the redox potential and, to a lesser extent, on the pH, which accounts for the broad scattering of values obtained. The lowest solubility corresponds to the lowest redox potentials. When we consider the given Tc concentrations as upper limits, it is clear that predicted values range from conservative to non-conservative, depending, as stated above, on the redox potentials used in the calculations.

The most predominant species under reducing conditions is $TcO(OH)_2$ and under oxidizing conditions TcO_4^-.

Copper

On the basis of the chemical character of the groundwaters, two solubility-limiting phases are indicated: cuprite (CuO) and native copper. Although the mineralogical database gives only chalcopyrite ($(Cu,Fe)S_2$) as the major copper component in the ore zone, native copper is also present there, which is consistent with the predictions (see samples 220A and B in Figure 3.102). Unfortunately, because of the low groundwater concentrations of copper (below the detection limit) in the ore zone, there is no possibility of comparing the predicted values in that zone to measured values. For the rest of the samples either cuprite or native copper are the predicted solubility-limiting phases. In general, the concentrations calculated for cuprite show a better agreement with the analytical data; exceptions are samples 199B and 199D located in the basement.

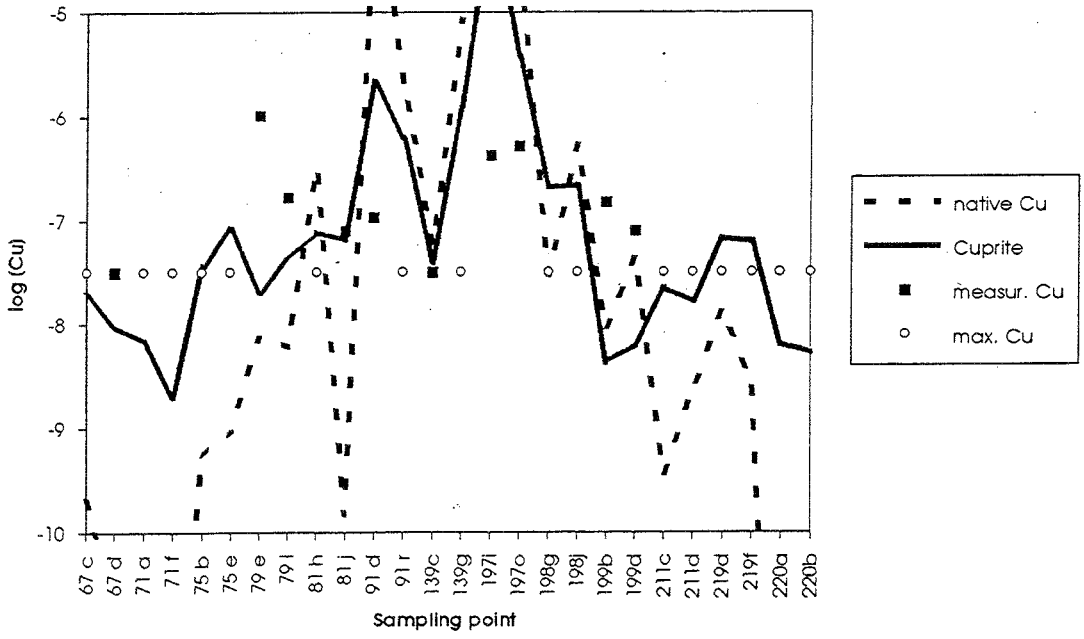

FIGURE 3.102 Predicted and measured solubilities for copper.

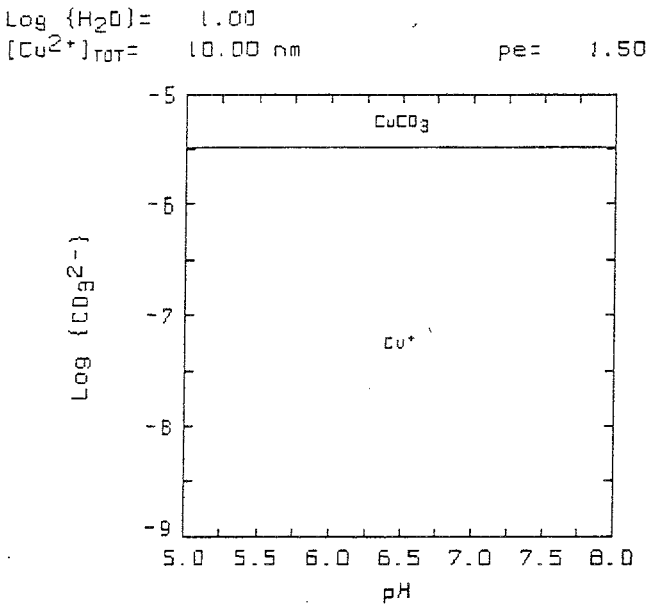

FIGURE 3.103 Predicted aqueous speciation for copper (reducing conditions).

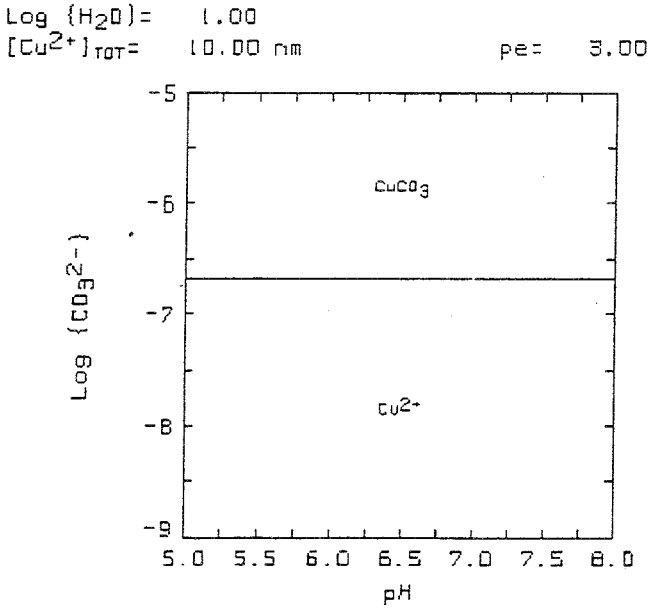

FIGURE 3.104 Predicted aqueous speciation for copper (oxidising conditions).

The predominant aqueous species under reducing conditions is Cu^+, although $CuCO_3$ shows increasing predominance as the carbonate concentration increases (see Figure 3.103).

Under oxidizing conditions (Figure 3.104) Cu^{2+} is the predominant aqueous species although, as before, $CuCO_3$ becomes more predominant at high carbonate concentrations.

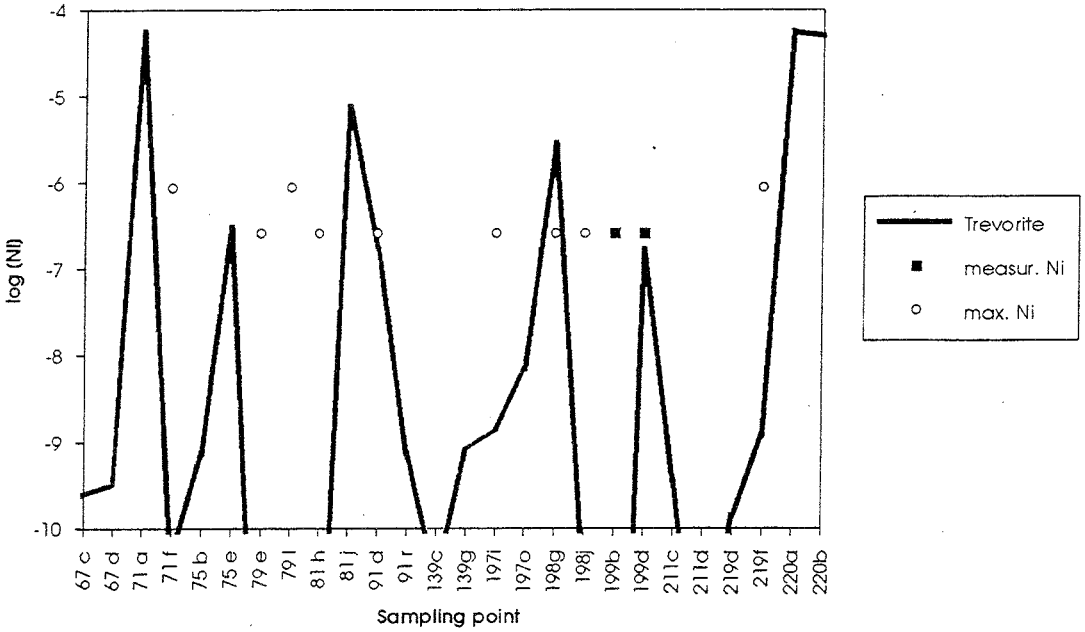

FIGURE 3.105 Predicted and measured solubilities for nickel.

Nickel

Only two samples contained sufficient Ni concentrations for analysis (Figure 3.105). The predicted solubility-limiting phase, trevorite ($NiFe_2O_4$), shows very good agreement with one of the measurements; the other is highly non-conservative. This phase can be questioned since its formation occurs only at high temperatures and, furthermore, the presence of iron supports this degree of uncertainty.

Under strongly reducing conditions (i.e., borehole 220) the predicted solubility-limiting solid phase is bravoite (NiS_2), which results in very low Ni concentrations. This solid phase has been positively identified as a minor component in the ore zone. The only predominant species in the aqueous phase is found to be the free Ni^{2+} cation.

Barium

This trace element is above the detection limit for the complete set of selected groundwaters. The analytical measurements are plotted together with the predicted values in Figure 3.106.

Two different solid phases are illustrated; in most cases witherite ($BaCO_3$) is found to be the most saturated phase, although in a few cases the solubility-limiting phase is found to be barite ($BaSO_4$). Nevertheless the values predicted for the barium carbonate phase are in very good agreement with the field measurements. The free Ba^{2+} ion is the predominant aqueous species in all cases.

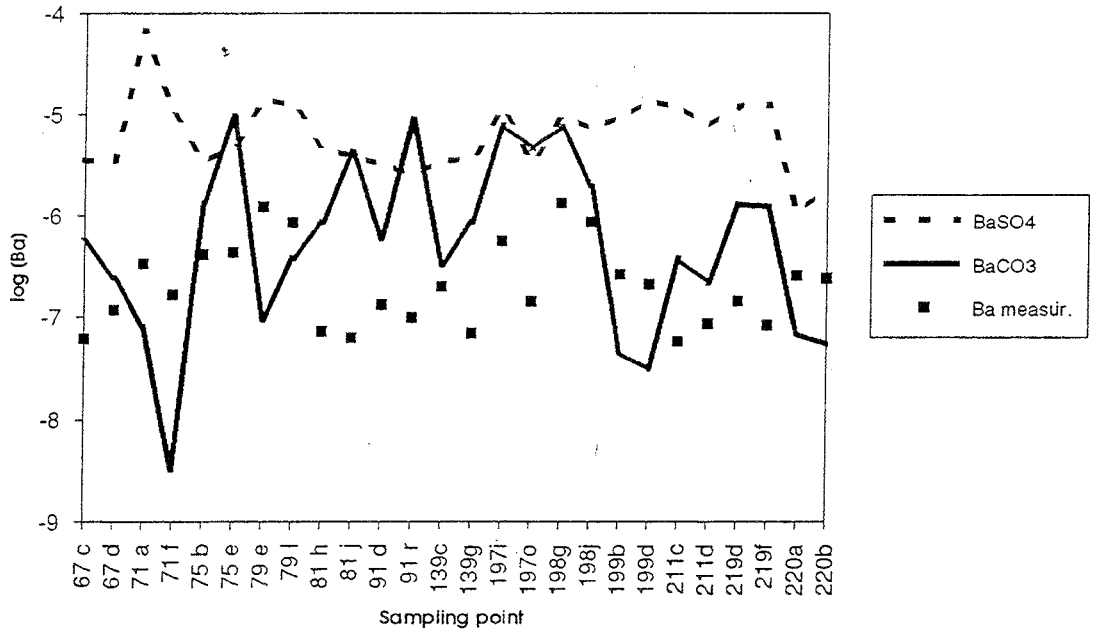

FIGURE 3.106 Predicted and measured solubilities for barium.

Lead

In common with nickel only two actual groundwater measurements exist, the remainder of the samples being below the level of detection (Figure 3.107).

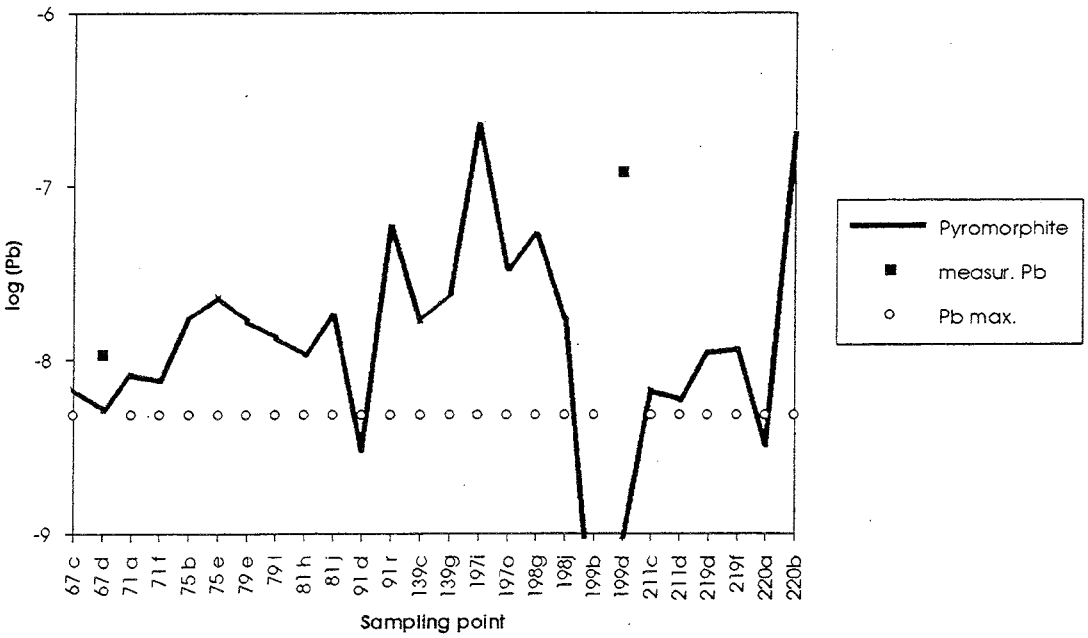

FIGURE 3.107 Predicted and measured solubilities for lead.

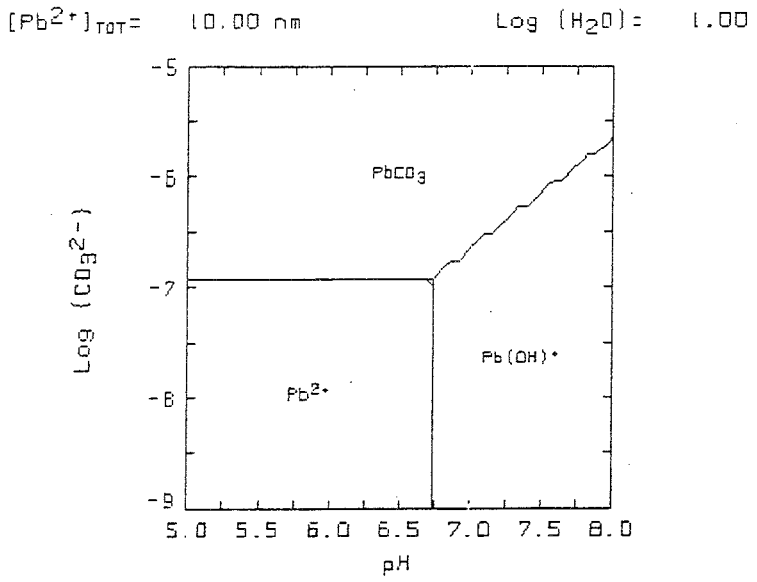

FIGURE 3.108 Predicted aqueous speciation for lead.

The predicted solubility-limiting solid phase for lead is $Pb_5(PO_4)_3Cl$, which is in good agreement with one of the measurements; the other measurement is non-conservative. In those samples with strongly reducing conditions (i.e., samples 71A, 220A and 220B), galena is found as the limiting phase, giving very low solubility values (about 10^{-15} mol/L). This prediction agrees with the mineralogy, where galena was identified as a minor component in the ore zone.

The predominant aqueous species are Pb^{2+}, $Pb(OH)^+$ and $PbCO_3$, depending on the pH and carbonate concentration (Figure 3.108).

Strontium

The solubility-limiting phases of strontium are predicted to be either celestite ($SrSO_4$) or strontianite ($SrCO_3$) depending on the groundwater chemistry (Figure 3.109). In any case the predictions are about three orders of magnitude higher than the actual measurements; these conservative results may reflect the lack of key minerals in the database used. It has been proposed that a solid solution of Sr^{2+} in calcite might control the solubility of Sr^{2+} in the ocean (Schindler 1967). As calculated by Stumm and Morgan (1981), the solubility of Sr^{2+} in solid solution with calcite ($1x10^{-4}$ mol/L) would be more than six times lower than when the equilibrium with strontianite would be considered (about $6.3x10^{-4}$ mol/L, as calculated for the reference groundwaters in Cigar Lake). The substitution of Ca^{2+} by Sr^{2+} is even more favoured for aragonite. In this case the Sr^{2+} solubility would be reduced about 55 times (to about $1.2x10^{-5}$ mol/L), which is much closer to the mean strontium concentration actually measured in the reference Cigar Lake groundwaters (about $1x10^{-6}$ mol/L). However, as calcite is the stable phase after prolonged periods of time, it is important to know in this case the nature of the calcium carbonate in the original sediment before a more definite conclusion can be drawn.

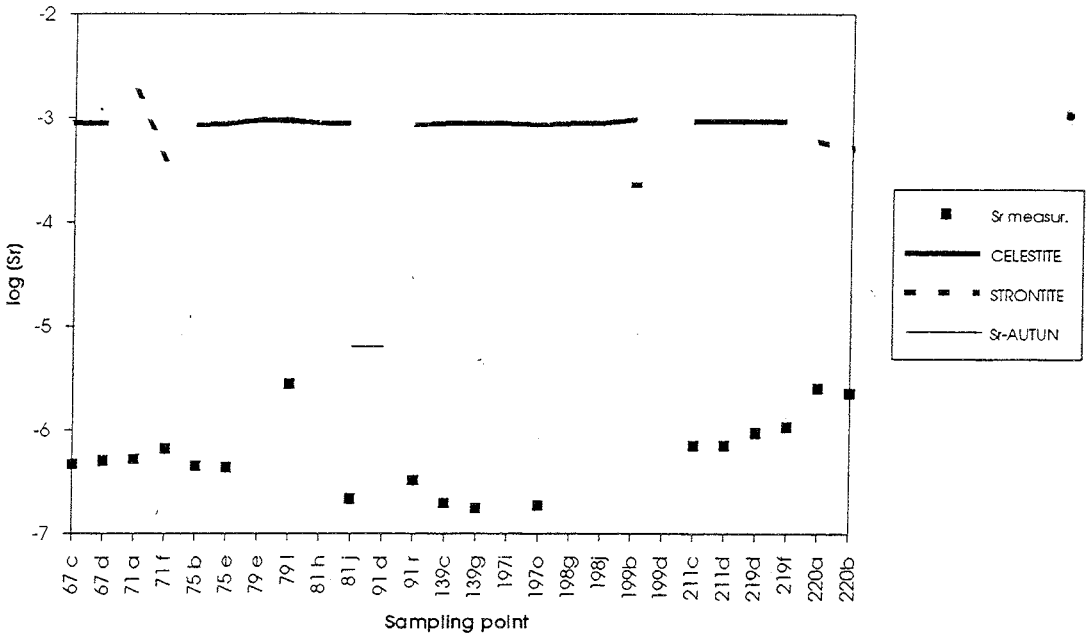

FIGURE 3.109 Predicted and measured solubilities for strontium.

The predominant aqueous species is Sr^{2+} and to a lesser extent $SrSO_4$ except for strongly reducing conditions.

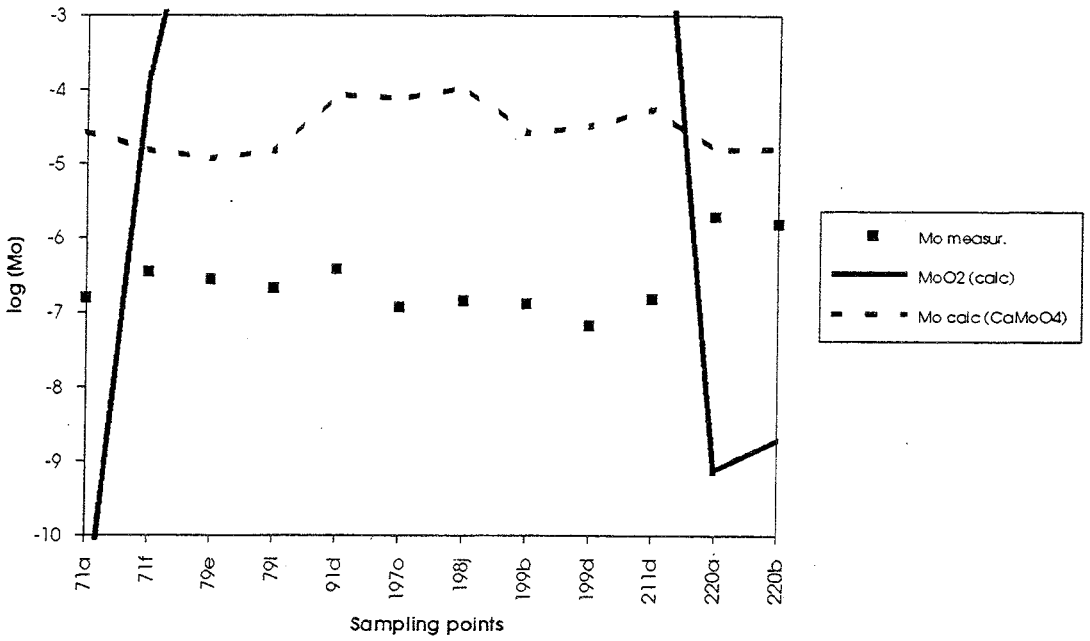

FIGURE 3.110 Predicted and measured solubilities for molybdenum.

Molybdenum

Figure 3.110 presents the predicted and measured solubilities for molybdenum; as no thermodynamic data for this element were found in the ZZ-Hatches version tested, other sources were used (Högfeldt 1982).

The only non-conservative predictions corresponded to the strongly reducing conditions characterizing samples 71A, 220A and 220B, where the solubility-limiting phase (MoO_2) predicted solubilities a few orders of magnitude lower. For the remaining samples the limiting phase was found to be $CaMoO_4$, which results in conservative predictions (about 2-3 orders of magnitude higher concentrations than measured).

In the ore zone jordisite (MoS_2) has been identified as a minor component, but no thermodynamic data exists for this solid phase. The predominant aqueous species is found to be MoO^{4-}.

Zinc

In almost all cases the solubility-limiting phase for zinc was found to be a ferrite-related mineral (Fe_2ZnO_4), which gave solubility values in fair agreement with the analytical data. Exceptions were samples 79E, 81H, 199B and 211D, for which predictions were about two orders of magnitude lower than the measured values (Figure 3.111). For strongly reducing conditions, sphalerite (ZnS) was found to be the limiting phase, resulting in much lower solubilities than indicated by the corresponding analytical data.

In the aqueous phase Zn^{2+} is the predominant species, although at high pH values there is some predominance of the hydroxo complexes $ZnOH^+$ and $Zn(OH)_2$.

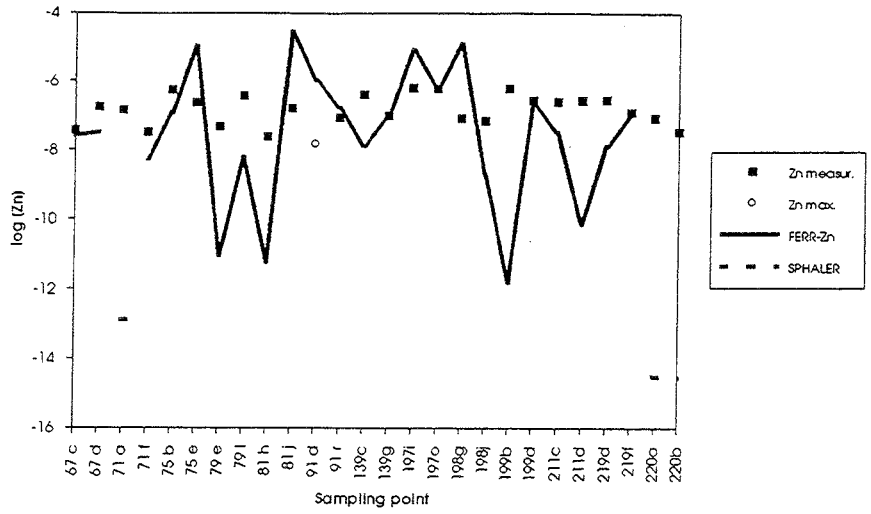

FIGURE 3.111 Predicted and measured solubilities for zinc.

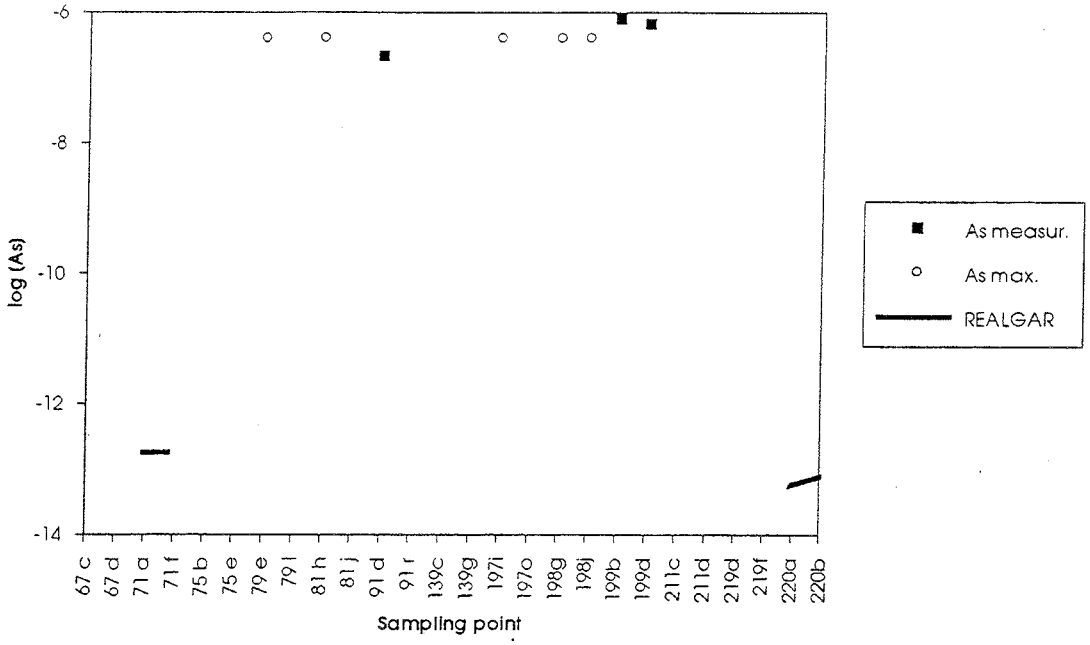

FIGURE 3.112 Predicted and measured solubilities for arsenic.

Arsenic

For most of the groundwaters claudeti (As_2O_3) was the limiting phase for arsenic, although this gave very high solubilities (about 10^{-1} mol/L or higher). As these are highly conservative compared to the actual measurements available, they are not presented in Figure 3.112. Only in strongly reducing environments were very low solubility values obtained, using realgar (AsS) as the solubility-limiting phase. The mineralogy of the ore zone shows minor amounts of As present either as arsenides or sulfur-arsenides of Ni, Co or Fe. Realgar constitutes in this case the best approximation to the system, considering the inherent limitation of the database used.

$As(OH)_3$, and for higher pH values some minor amounts of $As(OH)_4^-$, is the predominant aqueous species.

Chromium

It should be pointed out here that, in the database used, Cr is present only in its trivalent state. This has obvious implications for the results presented here. In this case the predicted values (Figure 3.113) show highly non-conservative results for the two groundwaters where actual data are available. The two solubility-limiting phases are chromium oxides, in some cases with iron also included in the mineral phase. These results would imply that there is no solubility limit for this element, although the scarcity of reference groundwater data must be a consideration. Furthermore, there is no mineralogical identification of any chromium solid phases present in Cigar Lake.

The most predominant aqueous species is the second hydroxo complex, with small contributions from the rest of the hydroxo complexes depending on pH conditions.

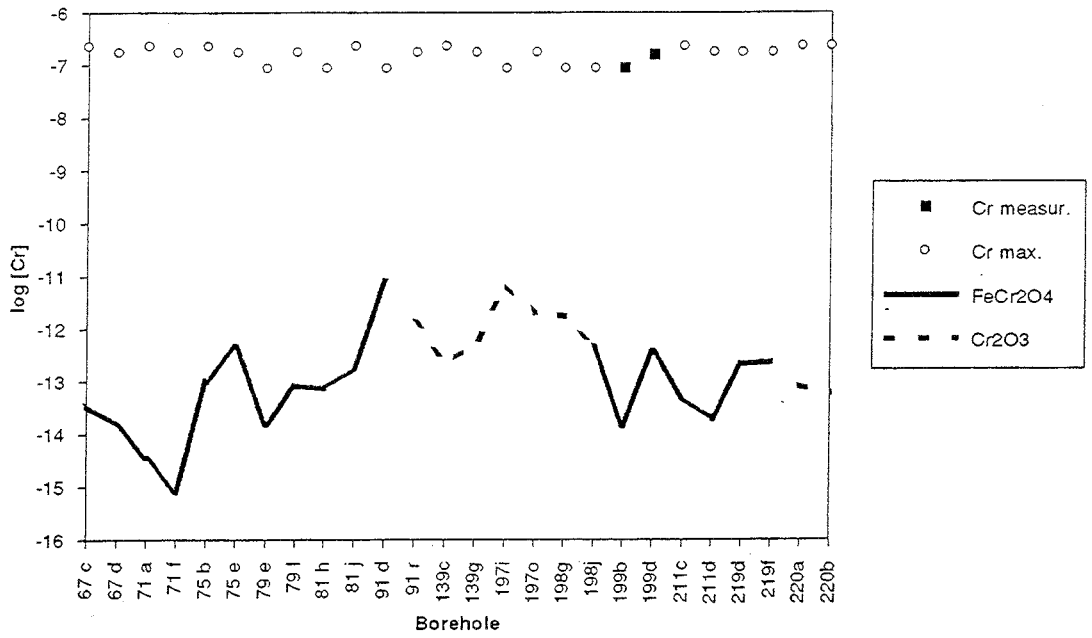

FIGURE 3.113 Predicted and measured solubilities for chromium.

3.9.2.4 Conclusions and recommendations

In summary, the general predictions of the trace-element solubility limits for which there are good thermodynamic data, are reasonably comparable to the field measurements (i.e., barium, copper, thorium, and, to a lesser extent, zinc). This indicates that the natural system can be adequately described by the chemical equilibrium approach. For some of the trace elements there is a lack of analytical data because of very low concentrations, and hence comparisons are not reliable. These include nickel and lead where only two groundwater determinations are above the level of detection. In both cases one actual value is in very good agreement with the predictions, whereas the other is several orders of magnitude greater, resulting, in these specific cases, in a highly non-conservative prediction. For the ore zone the calculations predict the formation of NiS_2 and PbS, which corresponds to the mineralogy; here the predicted solubilities are too low to be actually measured.

Plutonium and technetium predictions were compared with the calculated upper limit concentrations. For plutonium these calculated values are in good agreement with the solubility of an amorphous $Pu(OH)_4$, so they are considered to be reasonably conservative. The comparison is not so straightforward for technetium, since the predicted values fall within a broad range, as a result of their dependency on both Eh and pH. The calculated values are bracketed by the predicted ones, some of them being in good agreement and the rest shifting from conservative to non-conservative.

The trace elements that were not successfully modelled can be separated into two different groups. In one group there is strontium, arsenic and molybdenum, for which the predictions are conservative. In all three cases the discrepancies could be due to the lack of key

minerals in the database used. The lower than predicted strontium concentrations could be attributed to the possibility of this element substituting for Ca^{2+} in the $CaCO_3$ structure, which would lower its solubility. For arsenic and molybdenum the mineralogy of the Cigar Lake system indicates that the solid phases in which these two elements are found are not included in the thermodynamic database, possibly because of a lack of thermodynamic characterization.

In the other group where predictions are non-conservative, the case of chromium is interesting. It indicates that this element has no solubility limit, although, it has to be taken into account that only two reference groundwaters contained chromium concentrations above the detection limit.

With regard to speciation, unfortunately, there is no possibility of comparing the predicted results to the field determinations, since these were not carried out. In the event that future studies could provide field speciation data, then the predictions presented above should be checked against actual measurements.

Overall, the solubility and speciation tests carried in the Cigar Lake analog study project have strengthened confidence in the thermodynamic modelling of radionuclide solubilities. They have also helped to identify potential shortcomings in the currently used thermodynamic databases and, in some cases, to correct them, particularly in the case of uranium described in Section 3.9.3.

Important data still required from future exercises of this kind include:

- a positive identification, in the natural systems studied, of the solid phases that actually control the trace metal solubility; and

- an effort to perform "in situ" speciation analysis to enable a comparison with the aqueous speciation predictions.

This would strengthen our confidence in chemical equilibrium models to predict the long-term solubility and speciation of radionuclides in a repository environment.

3.9.2.5 References

BRUNO, J., CROSS, J.E., McKINLEY, I.G., READ, D., SANDINO, A. and SELLIN, P. 1990. Testing of geochemical models in the Poços de Caldas analogue study. Nagra Tech. Rep., **NTB 90-29** / SKB Tech. Rep., **TR 90-20** / UK DOE Tech. Rep., **WR 90-051**.

HÖGFELDT, E. 1982. Stability constants of metal-ion complexes. IUPAC Chemical Data Series, **21**, Pergamon Press.

PUIGDOMÈNECH, I. and BRUNO, J. 1991. Plutonium solubilities. SKB Tech. Rep., **TR 91-04**.

SCHINDLER, P. 1967. Equilibrium concepts in natural waters. In *Advances in Chemistry Series, No. 67.* Amer. Chem. Soc., p196.

SMELLIE, J.A.T., PERCIVAL, J.B. and CRAMER, J.J. 1991. Mineralogical and geochemical database for the major lithological and hydrothermal subdivisions of the Cigar Lake uranium deposit. AECL/SKB Cigar Lake analog study. AECL Internal Proj. Rep., **CLR-91-4**.

STUMM, W. and MORGAN, J.J. 1981. *Aquatic Chemistry.* Wiley-Intersci. Publ., John Wiley & Sons, p291.

3.9.3 Spent fuel dissolution modelling
(J. Bruno and I. Casas)

3.9.3.1 Introduction

The Cigar Lake uranium deposit is located entirely under the surface at an average depth of 430 m, without any direct physico-chemical expression at the surface as to its presence at depth. It therefore constitutes an excellent analog site to study the long-term behaviour of the uranium ore (analogous to the spent-fuel matrix) and the geochemical constraints for its stability.

According to Goodwin et al. (1989) the following analogies may be drawn between a spent-fuel repository and the Cigar Lake uranium ore deposit:

- Spent nuclear fuel, either from the CANDU™ or the Swedish PWR and BWR reactors, consists of uranium(IV) dioxide with less than 2 % fission product content mainly located at the outer rim. The chemical composition of the uraninite at the Cigar Lake deposit is close to that of the spent-fuel matrix.

- The hydrogeochemical stability of the waste form in the repository is provided by bentonite clay buffer material. The Cigar Lake uranium ore deposit is surrounded by an illite clay barrier with very low hydraulic conductivity.

Furthermore, an additional specific feature of the Cigar Lake deposit of potential analog interest is the existence of a red halo (Fe(III)-rich) at the clay/ore boundary where there is currently a reducing groundwater environment. This feature might suggest the existence of a local perturbation of the reducing conditions by radiolytic oxidation from the uranium ore. This potential analogy to radiolysis from spent fuel makes the Cigar Lake deposit especially interesting.

It is therefore obvious that an understanding of the hydrogeochemical parameters, which have resulted in the natural stability of the uranium ore, should highlight those critical factors contributing to the long-term stability of the spent-fuel matrix under repository conditions. Furthermore, the paradigms used in the current models for spent fuel dissolution could be tested. Consequently, in this study the models for spent-fuel matrix stability used in performance assessment are contrasted with the observations from the Cigar Lake deposit.

Accordingly, this part of the integrated modelling had the following objectives:

- To determine the solubility-limiting phase for uranium in the Cigar Lake deposit, as well as the predominant uranium speciation. This information is compared with field observations of both the mineralogy and the uranium content in the water samples.

- To derive a simplified model for the redox condition in the Cigar Lake deposit, since the redox condition is one of the key parameters determining the chemical stability of the ore. This is a natural extension of the conceptual hydrogeochemical model derived by Cramer and Nesbitt (Section 3.5.3).

- To compare the findings at Cigar Lake with the current spent-fuel dissolution models, in particular, the radiolytic oxidation of UO_2 and the threshold model for the oxidative dissolution of UO_2 (Shoesmith and Sunder 1991).

- To discuss the implications of these studies for the safety assessment of spent-fuel repositories.

3.9.3.2 Uranium solubility and speciation

3.9.3.2.1 Methodology

Using the reference groundwater database (Table 3.30, Section 3.5.2), uranium solubilities have been calculated for all the Cigar Lake groundwaters. Equilibrium with the following phases has been successively assumed: UO_2, U_3O_7, U_4O_9, coffinite and another $USiO_4$ polymorph. The PHREEQE program (Parkhust et al. 1980) together with the SKBU1 uranium database (Bruno and Puigdomènech 1989) have been used in the calculations. The derived solubilites have been systematically compared with the measured uranium concentrations in the reference groundwaters.

3.9.3.2.2 Results

Uranium solubility

From graphical comparisons between measured and predicted solubilities (Figures 3.114-3.118) it is not possible to distinguish which phase correlates best, although when equilibrium with UO_2, U_3O_7 and U_4O_9 is assumed, the agreement is better for these three phases than for the case of the U(IV) silicate polymorphs. To perform a qualified evaluation of the results, a multivariate statistical approach was used. Here the observed uranium concentrations and the measured geochemical parameters were systematically compared with the calculated values by using the SYSTAT statistical code package (version 5.0). The results are presented as a Pearson correlation matrix (Table 3.71).

A good correlation between two parameters is obtained if the Pearson coefficient is greater than 0.3. Among the several uranium phases tested, only in the case of U_3O_7 did the correlation between the measured and calculated concentrations fulfil this condition (0.345). The measured uranium concentrations show a good correlation with the following geochemical parameters: chloride, fluoride and bicarbonate concentrations, as well as pH. This indicates a clear geochemical control of the measured uranium concentrations.

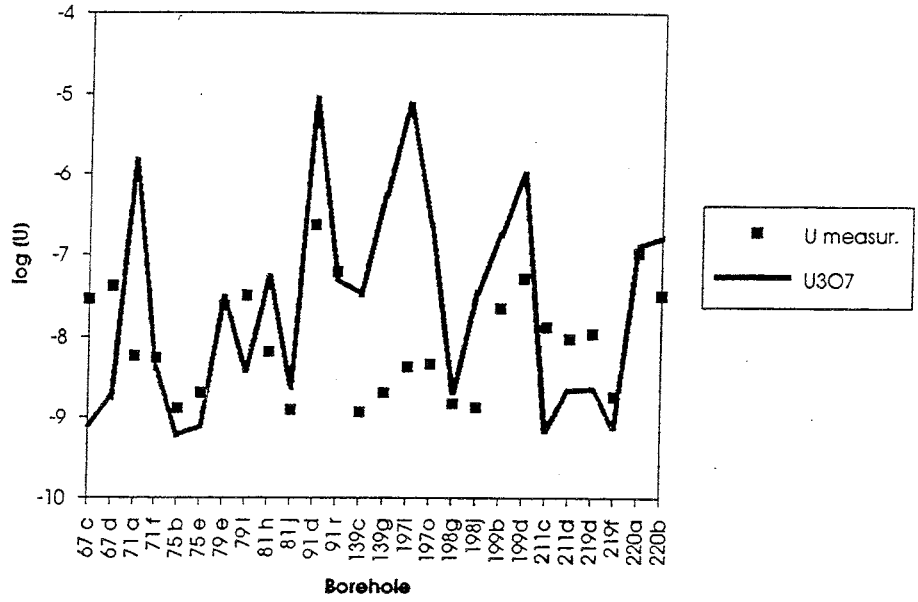

FIGURE 3.114 Predicted vs. measured uranium concentrations for U_3O_7.

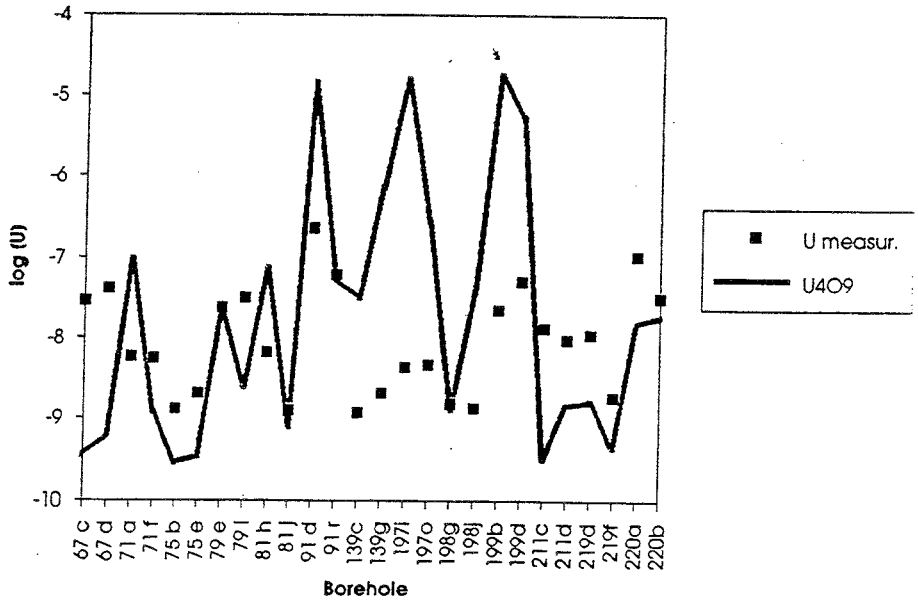

FIGURE 3.115 Predicted vs. measured uranium concentrations for U_4O_9.

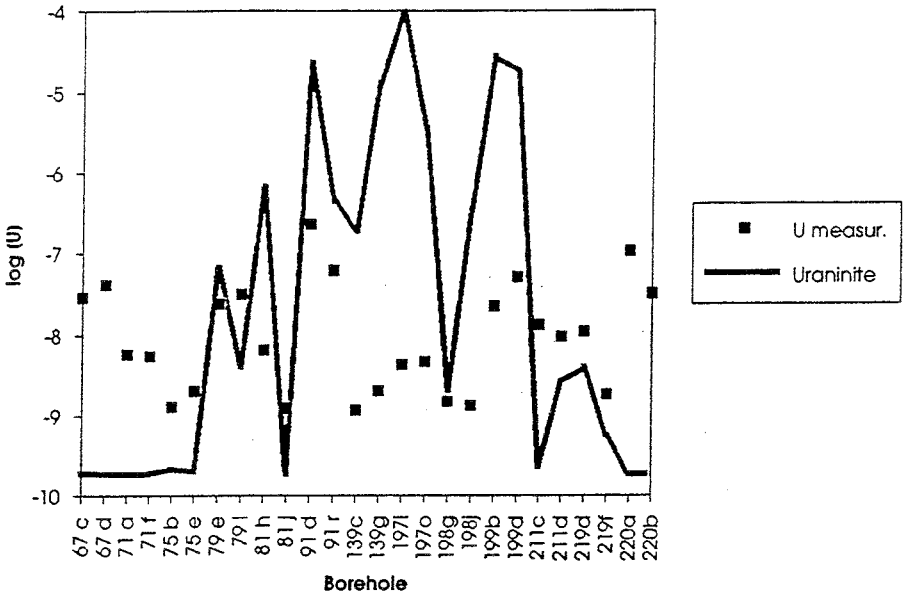

FIGURE 3.116 Predicted vs. measured uranium concentrations for uraninite.

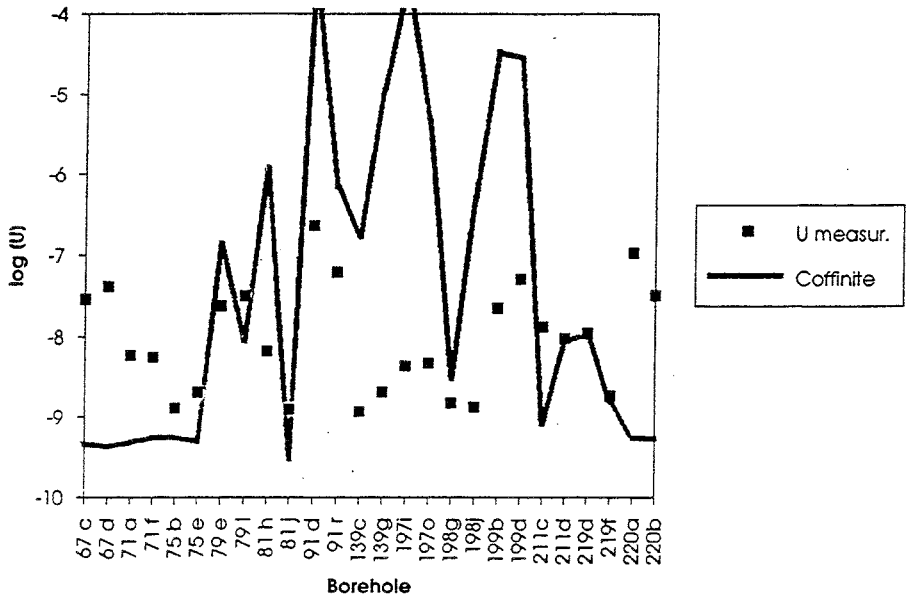

FIGURE 3.117 Predicted vs. measured uranium concentrations for coffinite.

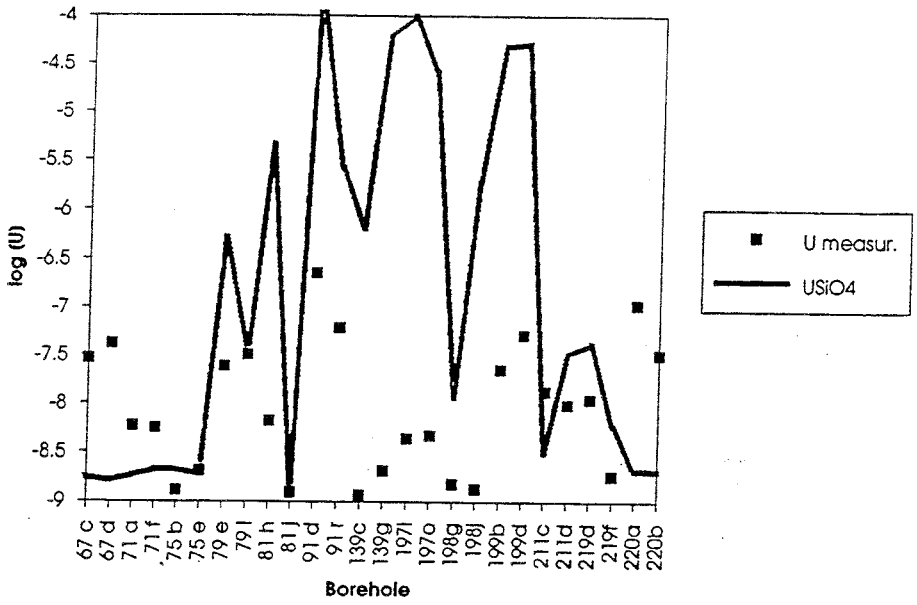

FIGURE 3.118 Predicted vs. measured uranium concentrates for $USiO_4$.

TABLE 3.71
PEARSON CORRELATION MATRIX COMPARING MEASURED AND CALCULATED URANIUM SOLUBILITY VALUES

	MEAS	COFFI	U3O7	U4O9	URAN	USIO4	CL	F	HCO3	PE	PH	SO4
MEASURED	1,000											
COFFINITE	0,184	1,000										
U3O7	0,345	0,780	1,000									
U4O9	0,297	0,899	0,975	1,000								
URANINITE	0,124	0,993	0,768	0,889	1,000							
USIO4	0,154	0,994	0,756	0,879	0,996	1,000						
CL	0,653	-0,088	0,141	0,061	-0,126	-0,113	1,000					
F	0,501	-0,105	0,030	-0,023	-0,122	-0,103	0,635	1,000				
HCO3	0,327	0,003	0,061	0,039	-0,020	-0,007	0,454	0,238	1,000			
PE	-0,185	0,713	0,147	0,358	0,720	0,723	-0,406	-0,330	-0,210	1,000		
PH	0,419	-0,188	0,215	0,079	-0,200	-0,195	0,543	0,487	0,516	-0,698	1,000	
SO4	0,138	-0,203	0,018	-0,063	-0,201	-0,182	-0,280	-0,114	-0,304	-0,319	0,187	1,000

NUMBER OF OBSERVATIONS: 26

Figure 3.119 represents a Pourbaix diagram plotting measured pe and pH data from all the Cigar Lake reference groundwaters. It shows the predominance of the several uranium oxide phases as a function of pH and pe. The measured data plot in the narrow U_3O_7 field, which is an additional indication that a mixed oxide with this composition is controlling the uranium concentrations in Cigar Lake. The mineralogical characterization of the samples from the Cigar Lake ore zone (Janeczek and Ewing 1992) gives, depending on the CaO content, the following composition of uraninite: $(U^{4+}_{0.59}U^{6+}_{0.36}Zr_{0.02}Pb_{0.02}Ca_{0.03}Ce_{0.01})O_{2.265}$ and $(U^{4+}_{0.59}U^{6+}_{0.36}Zr_{0.02}Pb_{0.02}Ce_{0.01})O_{2.33}$. This suggests stoichiometries that are between the U_4O_9 and the U_3O_7 phases.

By plotting the logarithm of the saturation index of U_3O_7 as a function of the position of the sample in the conceptual groundwater flow model, it is possible to observe quite an interesting trend (Figure 3.120). The samples taken at the basement and in the recharge zone (to the south of the deposit) appear to be unsaturated with respect to the uranium phase. They become saturated and close to equilibrium in the ore zone as well as in the discharge area (to the north of the deposit). However, in the clay halo zone they seem to be highly unsaturated. This could indicate either source-term control or that another more insoluble phase is controlling the concentrations of uranium. The presence of iron(III) (oxy)hydroxides in the clay could suggest that either sorption or coprecipitation of uranium with these iron phases is occurring. Similar observations have been reported at Poços de Caldas in Brazil (Bruno et al. 1990). However, there is no mineralogical support for this statement.

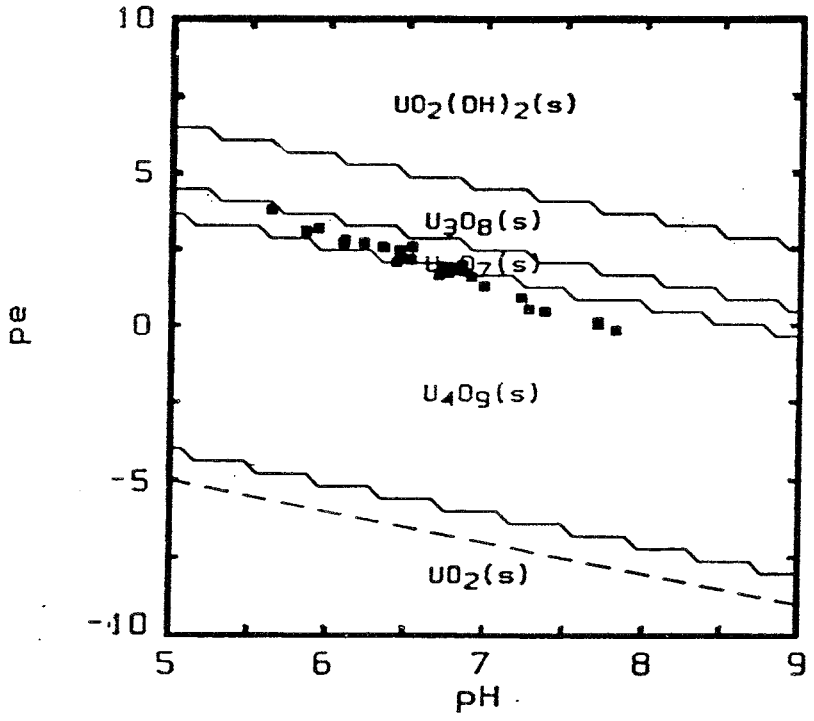

FIGURE 3.119 Pourbaix diagram showing measured pe vs. pH for the Cigar Lake reference groundwaters.

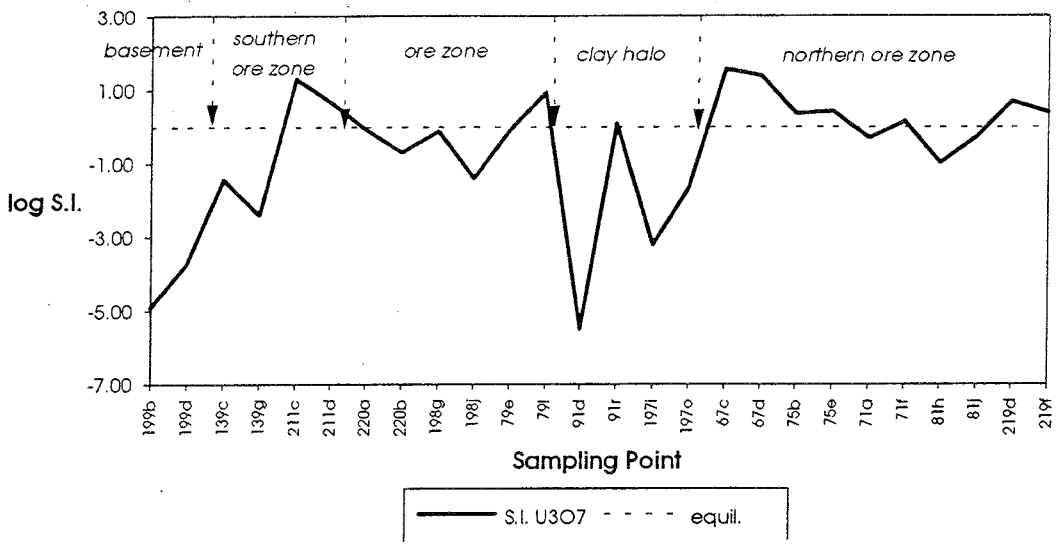

FIGURE 3.120 Plot of saturation indices vs. sample location related to the lithological units of the uranium deposit.

Uranium speciation

The predominant uranium speciation has been calculated for all the reference groundwaters. Figure 3.121 shows the predominant aqueous speciation by plotting the experimental data on a Pourbaix diagram calculated by using the SKBU1 thermodynamic database (Bruno and Puigdomènech 1989), which reflects the uranium database selected by the NEA (Grenthe et al. 1992).

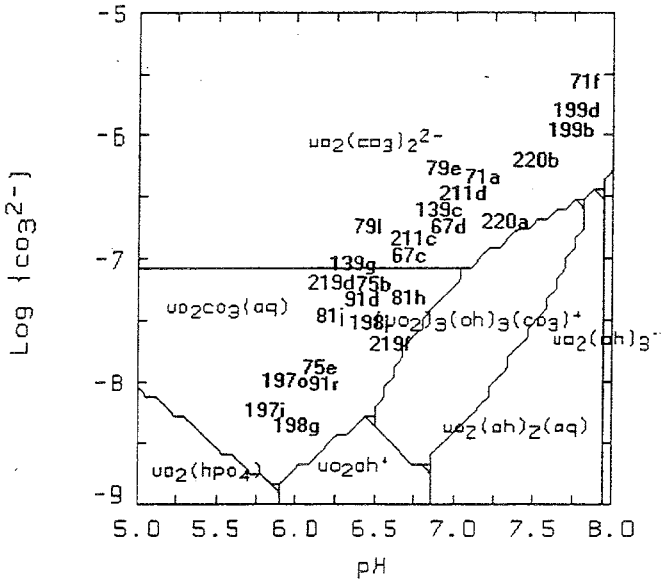

FIGURE 3.121 Pourbaix diagram showing the dominant uranium speciation phases (SKBU1/NEA database).

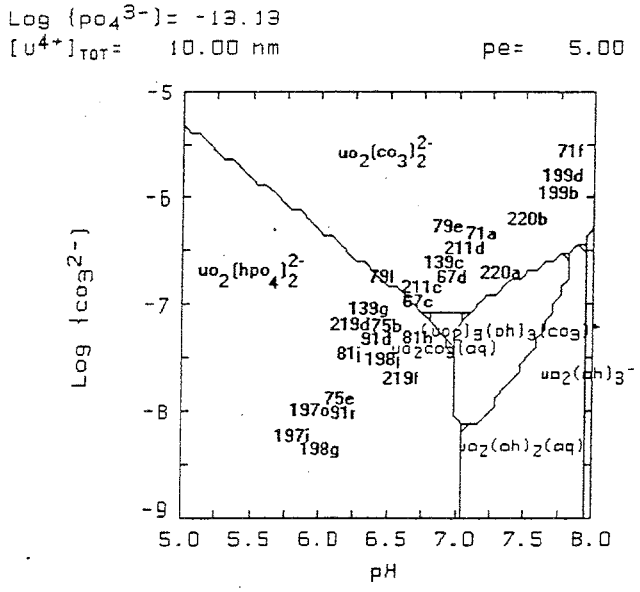

FIGURE 3.122 Pourbaix diagram showing the dominant uranium speciation phases (database of Langmuir, 1978).

In Figure 3.122 the measured data have been plotted on a similar diagram calculated by using the uranium database proposed by Langmuir (1978). The major difference is that in using the Grenthe et al. (1992) database the aqueous U(VI) speciation is dominated by the U(VI) carbonate complexation. By using the Langmuir (1978) database, the $UO_2(HPO_4)_2^{2-}$ complex is the dominant one. However, recent experimental work by Sandino and Bruno (1992) has shown the non-existence of this hydrogenphosphate complex. Puigdomènech (1992) clearly showed that the inclusion of this complex would give non-realistic uranium solubilities at Cigar Lake. Hence, the uranium speciation calculated by using the NEA database has been preferred.

3.9.3.2.3 Influence of redox conditions on uraninite stability

It is well known that the stability of natural uranium deposits is affected by the redox conditions during interaction with groundwater. Consequently, Eh is one of the most critical parameters in these systems. Defining the redox condition at Cigar Lake is a complex task, since the cycling of Fe, S and U may possibly be mediated by bacteria (Stroes-Gascoyne et al. 1993).

The hydrogeochemical model proposed by Cramer and Nesbitt (Section 3.5.4) shows that meteoric waters percolate down through the upper part of the host sandstones. As they reach the mineralized sandstones surrounding the deposit, the initial oxygen content of these waters is reduced, for example, by the presence of siderite. Therefore, in this zone close to the deposit, the redox character of the groundwaters may be partly represented by the following kinetic equilibrium:

$$FeCO_3(s) + 3H_2O \Leftrightarrow Fe(OH)_3(s) + e^- + HCO_3^- 2H^+ \quad (1)$$

with an equilibrium constant defined as:

$$K = \{e\}[HCO_3^-][H^+]^2 \quad (2)$$

where $K_1 = -18.5 \pm 0.1$ (Bruno et al. 1992 a,b).

By rearranging the equilibrium reaction (2), a simple operational definition of the theoretical redox potential is obtained for the sandstone groundwaters by using the following equation:

$$pe = 18.5 - 2pH + \log[HCO_3^-] \quad (3)$$

In this way the pe of the system can be calculated by using two highly reliable field parameters.

In a similar way the groundwater redox conditions from the ore zone can be theoretically calculated. The presence of pyrite coexisting with uraninite (Bruneton 1987; Janeczek and Ewing 1993) indicates a far more reducing environment. Under certain conditions siderite is considered to be the intermediate product of the oxidation of pyrite (Stumm and Morgan 1981). Therefore, the following equilibrium reaction is proposed as the one controlling redox conditions in the ore zone:

$$FeS_2(s) + HCO_3^- + 8H_2O \Leftrightarrow FeCO_3(s) + 2SO_4^{2-} + 17H^+ + 14e^- \quad (4)$$

with

$$K_2 = [SO_4^{2-}]^2 [H^+]^{17} \{e\}^{14}/[HCO_3^-] \quad (5)$$

By combining the thermodynamic data from the ZZ-Hatches database with selected iron data, Nordstrom and Puigdomènech (1986) and more recently Bruno et al. (1992b) have obtained a value of $\log K_2 = -85.8$.

By rearranging equation (5) the following equation is obtained, relating the redox potential to the measured concentrations in the ore groundwaters:

$$pe = -\log K_2/14 + \log[SO_4^{2-}]/7 - 17/14pH - \log[HCO_3^-]/14 \quad (6)$$

Figure 3.123 shows the comparison between the measured and calculated redox potentials in the different zones of Cigar Lake. The agreement between the measured and the calculated redox potentials is reasonably good, indicating that the system can be described as being close to redox equilibrium.

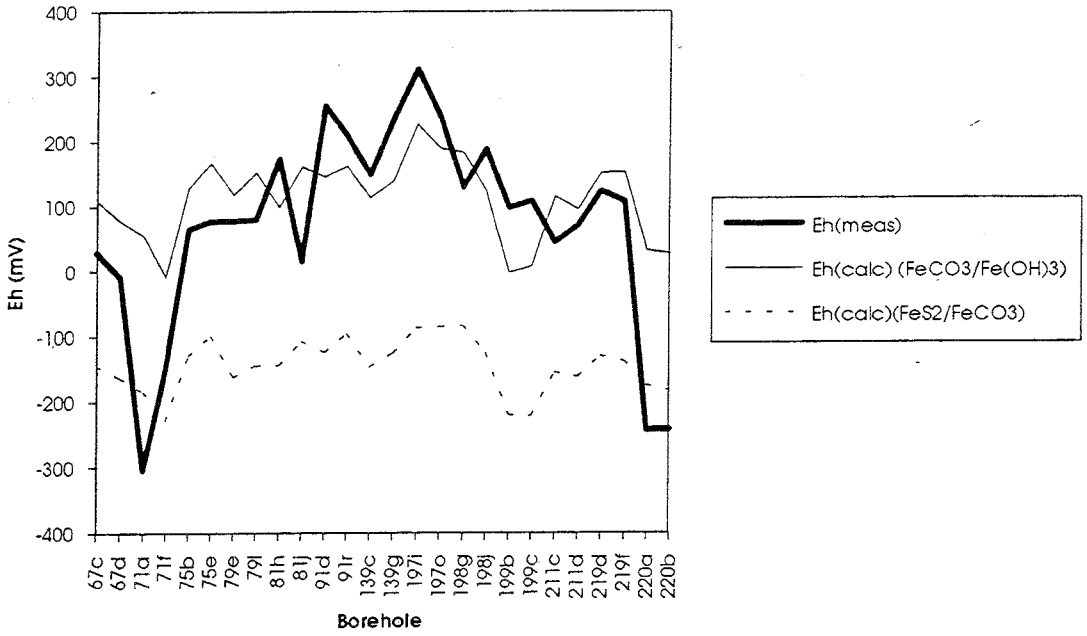

FIGURE 3.123 Comparison between measured and calculated redox potentials for the Cigar Lake reference groundwaters.

3.9.3.3 Comparison with current spent-fuel dissolution models

The current paradigm concerning the stability of spent fuel indicates that under reducing conditions the dissolution of the waste matrix (UO_2) is controlled by the low solubility of UO_2 under reducing conditions. The local oxidation of UO_2 by radiolysis may alter these conditions, and in this case the radiolytic oxidative dissolution model of spent fuel should be applied. A threshold potential value for the switch between reductive and oxidative dissolution of UO_2 has been set around 320 mV from a careful study of the surface oxidation of UO_2 as a function of the corrosion potential (Shoesmith and Sunder 1991).

Figure 3.124 illustrates an attempt to integrate the mineralogical and geochemical information relevant for the stability of uraninite at Cigar Lake, based on the oxidative dissolution model proposed by Shoesmith and Sunder (1991). Furthermore, some comparative information from the Poços de Caldas analog study in Brazil has been included where the oxidative dissolution of uraninite is observed to have taken place.

At Cigar Lake there is no mineralogical data regarding the presence of secondary U(VI) phases, even in the clay halo zone where redox potentials as high as 200 mV have been measured. Furthermore, the measured uranium concentrations are in the range 10^{-7} to 10^{-9} mol/L which clearly correspond to the expected uranium concentrations under reducing conditions. The measured uranium concentrations under an oxidative dissolution regime are in the range 10^{-4} to 10^{-5} mol/L (Forsyth and Werme 1991). On the other hand, oxidative dissolution of uraninite was observed at Poços de Caldas, but at significantly higher redox

potentials ranging from 300-400 mV. Extensive oxidation dissolution at similar redox ranges have been reported from the Peña Blanca (Ildefonse et al. 1990) and Shimkolobwe (Finch and Ewing 1991) sites. In the Alligator Rivers (Duerden 1992) and El Berrocal (J. Astudillo pers. comm. 1992) sites the oxidation of uraninite is observed at redox potentials around 200-250 mV.

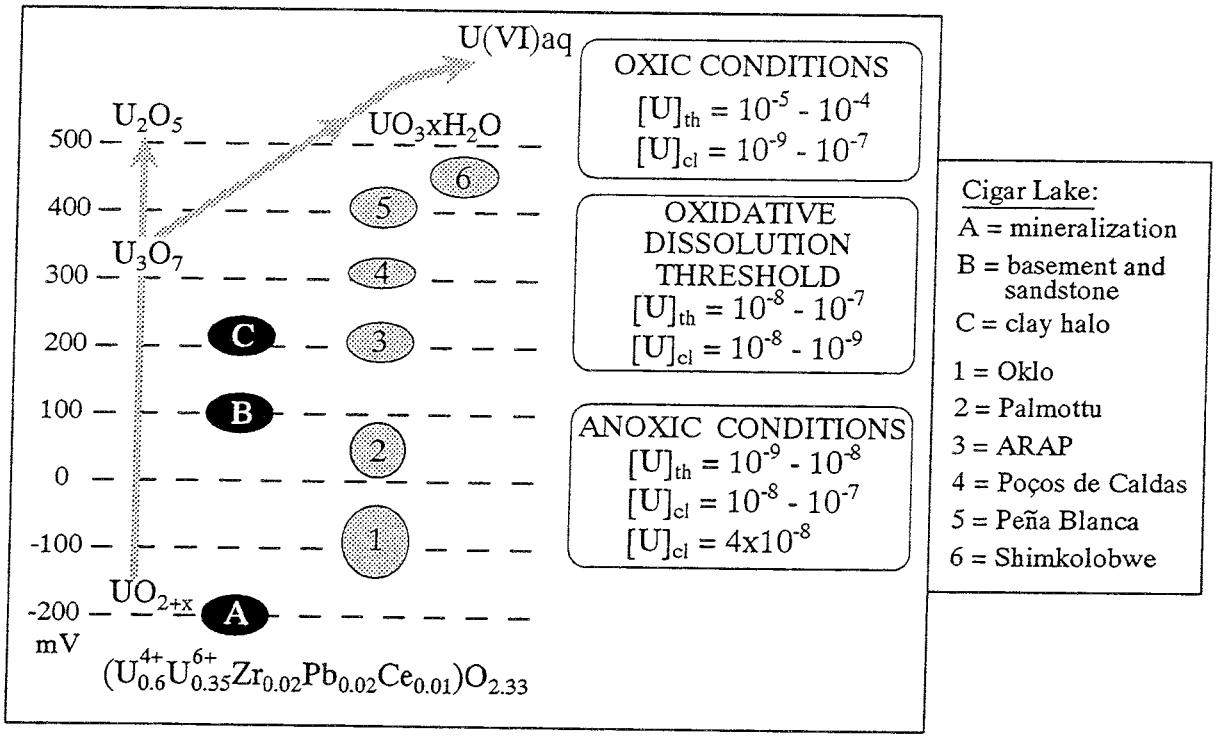

FIGURE 3.124 Schematic integration of uraninite stability for different analog study sites. The redox scale on the left side indicates the various transitions between uranium-oxide phases up to 320 mV where the oxidative dissolution threshold is set, according to Shoesmith and Sunder (1991). The various zones at Cigar Lake, together with other analog sites, are plotted on this diagram according to the measured redox potential. On the right-hand side are shown the theoretical (th) and measured (cl) uranium concentrations in the different zones at Cigar Lake.

All this information would indicate that the oxidative dissolution threshold at Eh= 120 mV proposed by Shoesmith and Sunder (1991) is a conservative value. The observations from the uranium deposits at Cigar Lake and at Poços de Caldas would indicate that the transition to the oxidative dissolution of uraninite occurs in the redox potential range of 200 to 300 mV. If this is the case, the higher oxidative dissolution threshold would allow a more realistic treatment of the radiolytic effects on the stability of spent fuel.

3.9.3.4 Implications for safety assessment

The calculated dose rates generated by the uraninite of the Cigar Lake deposit appear to be quite low in comparison with dose rates expected from spent fuel during the post-disposal period (100 to 10,000 a; Section 3.8.3). The dose rate from Cigar Lake has been calculated to be 0.01 Gy/s. This is much lower than the experimentally determined threshold for radiolytic oxidation of UO_2, which has been established at 2.8 Gy/s. This is in agreement with the observations from the ore composition (Janeczek and Ewing 1992) and the surface oxidation state (Sunder et al. 1988, 1991; see also Section 3.3.3), which indicate that uraninite oxidation has not proceeded further than $UO_{2.33}$ (U_3O_7).

Eriksen (pers. comm. 1992) has calculated rates of oxidant production from α, β and γ radiolysis from the Cigar Lake ore assuming a 10 % U content and a regular geometry. From these data Liu et al. (Section 3.9.4) have estimated that, assuming 100 % efficiency on the oxidation/dissolution process, the ore would have disappeared in 1.68×10^5 a.

A lower limit for the uraninite oxidation and dissolution by oxygen infiltration at Cigar Lake can be calculated by using known paleo-geochemical data. The Cigar Lake deposit was formed about 1.3 Ga ago, corresponding to the transition period between the Precambrian and the Phanerozoic (1,500 to 600 Ma). Observations, for example from the mid-Proterozoic paleosols in the Athabasca Basin, indicate that the oxygen partial pressure was in the range $pO_2 = 0.001$ to 0.01 atm., i.e., 200 to 20 times lower than present atmospheric levels (PAL) or 0.005 to 0.05 PAL. This is also confirmed by studies made on detrital uraninite deposits such as at Elliot Lake in Canada.

In the Phanerozoic period (600 to 300 Ma) the atmospheric oxygen was gradually changing to modern-day levels; the more accepted pO_2 levels for this period are 0.1 PAL. In order to assess the implications of the lower partial pressure of oxygen during these initial geological times, use has been made of the Grandstaff (1980) model for the kinetics of oxidative weathering of uraninite to calculate the amount of uraninite dissolved during the first 1000 Ma (from 1300 to 300 Ma). This model has an advantage in that it has been developed to explain field observations of oxidative weathering of many uraninite deposits in Canada. Furthermore, it has been used to infer oxygen levels in the Precambrian period using detrital uraninite deposits. By applying this model the amount of uraninite dissolved from Cigar Lake would be roughly 1 % of the estimated actual total mass, i.e., hardly detectable from geological observations.

3.9.3.5 Conclusions and recommendations

The Cigar Lake analog study allowed us to check some of the main assumptions used in the evaluation of the performance of a spent nuclear fuel repository.

1- The hydrogeochemical stability of the uranium ore at Cigar Lake is an illustrative example of the overall long-term stability of the presently accepted disposal concepts for spent nuclear fuel. The main aspects to highlight are the stability of uraninite under reducing environments, in

spite of potential oxidative pulses, and the role of the clay halo as a hydrological barrier.

2- This analog study has provided a good opportunity to test current models and their assumptions for the stability of spent fuel under repository conditions.

3- The dissolution behaviour of uranium in the Cigar Lake deposit corresponds to the thermodynamic solubilities of the ideal U_3O_7 phase. The mineralogical observations indicate that the U(VI)/U(IV) ratio in the uraninite samples from Cigar Lake are close to the ideal U_3O_7 ratio.

4- The predominant aqueous speciation of uranium in Cigar Lake is dominated by the carbonate complexes $UO_2CO_3(aq)$ and $UO_2(CO_3)_2^{2-}$. The assumption of a dominating $UO_2(HPO_4)_2^{2-}$ complex would give rise to unrealistically large uranium concentrations.

5- No oxidative dissolution of uraninite is observed in the Cigar Lake site, even in the clay halo zone where relatively high redox potentials (100 to 200 mV) are measured. The determined concentrations of uranium in the ore zone are in the range of 10^{-7} to 10^{-8} mol/L. Laboratory measurements of the solubility of uraninite samples from Cigar Lake, using a granitic groundwater under reducing conditions, give a value of $4 \pm 1 \times 10^{-8}$ mol/L. The oxidative dissolution of the same samples give non-equilibrium concentrations of 10^{-5} mol/L after 4,000 h of contact (Casas et al. 1993).

6- The mineralogical and geochemical information collected at Cigar Lake suggests that the oxidative dissolution threshold of uraninite occurs at redox potentials larger than 200 mV. Comparison with data collected from other analog sites, particularly Poços de Caldas and Alligator Rivers, indicate that the oxidative dissolution of uraninite also occurs at redox potentials higher than 200 mV.

3.9.3.6 References

BRUNETON, P. 1987. Geology of the Cigar Lake uranium deposit (Saskatchewan, Canada). In *Economic Minerals of Saskatchewan* (ed. C.F. Gilboy and L.W. Vigrass). Sask. Geol. Soc. Spec. Publ., **8**, 99-119.

BRUNO, J. and PUIGDOMÈNECH, I. 1989. Validation of the SKBU1 uranium thermodynamic database for its use in geochemical calculations with EQ3/6. In *Proc. 12th Symp. Sci. Basis for Nuclear Waste Management.* Mater. Res. Soc. Proc., **127**, 887-896.

BRUNO, J., CROSS, J.E., EIKENBERG, J., McKINLEY, I.G., READ, D., SANDINO, A. and SELLIN, P. 1990. Testing of geochemical models in the Poços de Caldas analogue study. Nagra Tech. Rep., **NTB 90-29** / SKB Tech. Rep., **TR 90-20** / UK DOE Tech. Rep., **WR 90-051**.

BRUNO, J., WERSIN, P, STUMM, W. and BRANDBERG, F. 1992a. On the influence of carbonate in mineral dissolution: I. The thermodynamics and kinetics of hematite dissolution in bicarbonate solutions at T= 25 °C. Geochim. Cosmochim. Acta, **56**, 1139-1147.

BRUNO, J., WERSIN, P, and STUMM, W. 1992b. On the influence of carbonate in mineral dissolution: II. The solubility of FeCO3(s) at 25oC and 1 atm total pressure. Geochim. Cosmochim. Acta, **56**, 1147-1155.

CASAS, I. CERA, E. and BRUNO, J. 1993. Kinetic studies of natural uranium minerals for the long term evolution of spent nuclear fuel under oxidising conditions. In *Proc. 15th Symp. Sci. Basis for Nuclear Waste Management.* Mater. Res. Soc. Proc., **294**, 521-526.

DUERDEN, P. 1992. (Editor). Hydrogeochemistry of the Alligator Rivers site. In *The International Intraval Project: Phase 1, Case 8.* NEA/OECD, Paris.

FINCH, R. and EWING, R., 1991. Uraninite alteration in an oxidising environment and its relevance to the disposal of spent nuclear fuel. SKB Tech. Rep., **TR 91-15**.

FORSYTH, R.S. and WERME, L.O. 1991. Spent fuel corrosion and dissolution. SKB Tech. Rep., **TR 91-60**.

GOODWIN, B.W., CRAMER, J.J. and McCONNELL, D.B. 1989. The Cigar Lake uranium deposit: An analogue for nuclear fuel waste disposal. In *Natural Analogues in Performance Assessment for the Disposal of Long Lived Radioactive Wastes.* Int. Atom. Ener. Agency Tech. Rep., **304**, App. B, 37-45.

GRANDSTAFF, D.E. 1980. Origin of uraniferous conglomerates at Elliot Lake, Canada and Witwatersrand, South Africa: Implications for oxygen in the Precambrian atmosphere. Precamb. Res., **13**, 1-26.

GRENTHE, I, FUGER, J., KONINGS, R.J.M., LEMIRE, R.J., MULLER, A.B., NGUYEN-TRUNG, C. and WANNER, H. 1992. Chemical thermodynamics of uranium. In *Chemical thermodynamics 1* (eds. H. Wanner and I. Forest). Nucl. Energy Agency of Org. Econ. Coop. Develop. North-Holland, Amsterdam.

ILDEFONSE, P., MULLER, J-P., CLOZEL, B. and CALAS, G. 1990. Study of two alteration systems as natural analogues for radionuclide release and migration. Engin. Geol., **29**, 413-439.

JANECZEK, J and EWING, R.C. 1992. Chemistry and alteration of uraninite at Cigar Lake, Canada. In *AECL/SKB/USDOE Cigar Lake Analog study - Forsmark Meeting (Nov. 1991).* (ed. J.J. Cramer and J.A.T. Smellie). AECL Research Internal Proj. Rep, **CLR-92-1**, Appendix.

LANGMUIR, D. 1978. Uranium solution-mineral equilibria at low temperatures with application to sedimentary ore deposits. Geochim. Cosmochim. Acta, **42**, 547-569.

NORDSTROM, D.K. and PUIGDOMÈNECH, I. 1986. Redox chemistry of deep groundwaters in Sweden. SKB Tech. Rep., **TR 86-03**.

PARKHURST, D.L., THORSTENSON, D.C. and PLUMMER, L.N. 1980. PHREEQE - a computer program for geochemical calculations. USGS Water Resour. Invest. Rep., **80-96**.

PUIGDOMÈNECH, I. 1992. Complex formation in the UO_2^{2+}-PO_4^{3-} system. In *AECL/SKB/USDOE Cigar Lake Analog study. Prog. Rep. (Nov 91-March 92)* (ed. J.J. Cramer). AECL Research Internal Proj. Rep., **CLR-92-2**, 43-47.

SANDINO, A. and BRUNO. J. 1992. The solubility of $(UO_2)_3(PO_4)_2.4H_2O$(s) and the formation of U(VI) phosphate complexes: Their influence in uranium speciation in natural waters. Geochim. Cosmochim. Acta., **56**, 4135-4145.

SHOESMITH, D.W and SUNDER, S. 1991. An electrochemistry-based model for the dissolution of UO_2. SKB Tech. Rep., **TR 91-63**.

STROES-GASCOYNE, S. and FRANCIS, A.J. 1993. Microbiological studies. In *Final report of the AECL/SKB Cigar Lake Analog study* (ed. J.J. Cramer and J.A.T. Smellie). AECL Research Rep., **AECL-10851**, Section 3.7.4.

STUMM, W and MORGAN, J.J. 1981. *Aquatic Chemistry* John Wiley, NY.

SUNDER, S., TAYLOR, P. and CRAMER, J.J. 1988. XPS and XRD studies of uranium rich minerals from Cigar Lake, Saskatchewan. In *Proc. 11th Symp. Sci. Basis for Nuclear Waste Management.* Mater. Res. Soc. Proc., **112**, 465-472.

SUNDER, S., CRAMER, J.J. and MILLER, N.H. 1991. X-Ray Photo-electron Spectroscopic study of uranium minerals from the Cigar Lake uranium deposit. In *Proc. 15th Symp. Sci. Basis for Nuclear Waste Management.* Mater. Res. Soc. Proc., **257**, 449-457.

3.9.4 Mass transport modelling

(J. Liu, I. Neretnieks and J.-W. Yu)

3.9.4.1 Introduction

Understanding mass transport of dissolved radionuclides through the engineered barriers and the host rock surrounding a nuclear fuel waste vault is of paramount importance in assessing the long-term impact of the waste on the biosphere in a disposal repository. In the near field, the following mechanisms govern the possible release and transport of radionuclides after penetration of the metal canister: a) solubility of the solid phases of the spent fuel, b) decay of radionuclides, c) flow of and molecular diffusion in the groundwater, d) near-field groundwater chemistry, e) radiolysis of groundwater, and f) chemical reactions of radionuclides, such as precipitation/dissolution, reduction/oxidation, complexation by other aqueous species, and sorption and desorption onto the fracture and micropore surfaces. Factors such as porosity and fracturing of the engineered barrier and rock matrices will also affect mass transport. Various models have been proposed to describe the mass transport of radionuclides in the near field of a final repository (KBS 1983; Neretnieks 1980, 1985). The validity of the spatial prediction of these models may be verified by field tests, but to test the long-term validity one has to rely on natural analog studies.

In some natural analog studies, naturally occurring uranium deposit systems have been investigated, for example, at Poços de Caldas in Brazil (Chapman et al. 1992). An essential prerequisite is that the system studied has features analogous to those of the final repository. In this respect, the Cigar Lake uranium ore deposit has many features that make it extremely valuable for the development and testing of models that may be used in performance assessment.

In assessing the performance of a disposal concept for nuclear fuel waste, various scenarios are used to study the sequence of events that might influence the system over a long period of time. These scenarios are typically characterized by various parameters which, in turn, can be integrated in models. In order to model such scenarios, it is necessary to both simplify the system and make certain assumptions. As the central values chosen for the various parameters become more realistic, the models are progressively refined such that the simplifications and assumptions made are significantly reduced.

One of the important features of the Cigar Lake uranium deposit is that there is no significant surface expression of the underlying ore deposit. This indicates that the mineralization has been stabilized in the geosphere over time scales of millions of years, probably since its formation some 1.3 Ga ago. One of the major objectives of the Cigar Lake analog study has therefore been to understand the mechanisms that have contributed to the preservation of the uranium mineralization. The possible release and migration of related aqueous species, uranium and other radionuclides have been studied by means of mass transport.

Modelling of the hydrogeology (Section 3.4 in this report), both on a regional and local scale, shows that there is no direct hydraulic connection between the permeable zone,

represented by the altered sandstone, and the low-permeability zones of the altered basement and the clay-rich mineralization. In the latter case, the clay-rich halo is expected to be the least permeable medium of all, forming a tight barrier to the outward release and transport of uranium from the ore (Cramer and Smellie 1990).

Hydrogeochemical investigations (Section 3.5) show that the groundwaters throughout the deposit are reducing, with Eh values ranging between -0.25 and 0.25 V. Dissolved-uranium concentrations are consequently very low, varying between $10^{-9.5}$ and 10^{-7} mol/L. Stable isotope data (δD and δ^{18}O) of the groundwaters plot close to the meteoric water line.

A key question is whether the measured whole-rock trace-element variations in the sandstone reflect primary hydrothermal patterns associated with the ore formation, or whether these variations are the result of low-temperature mobilization and redistribution processes of more recent origin. Most evidence points to a "closed" chemical system and to a hydrothermal origin of, for example, the variations in U-concentration surrounding the ore. This is supported by the study of the uranium and thorium decay-series (Section 3.2.2), which shows that most of the analysed samples are close to secular equilibrium. However, there are also cases of disequilibria (caused by the deposition and removal of either ^{234}U or ^{226}Ra), indicating a recent but slight ($< 10^5$ a) remobilization of uranium and its decay products on a local scale.

Even though radionuclide mobilization and transport away from the mineralization has not been observed at Cigar Lake, the geometry and composition of the deposit make it suitable for the development and testing of mass transport models that could eventually be applied to a repository situation. Mass transport modelling can directly address the issues of trace-element migration. The migration of trace elements, including radionuclides, in the host rocks depends on a number of parameters, such as their content and speciation in the ore and groundwaters, the dissolution and transport mechanisms in the groundwater and the fixation mechanism on the host rocks. In the models presented below, the pathways and fate of reductants and oxidants, which can possibly be generated by radiolysis of water adjacent to uranium ore, are explored; some hypothetical radionuclide release situations are addressed; and the observed hematization of the bleached clay to hematized clay is simulated by means of coupled mass-transport reaction modelling.

The deposit, here considered to include the mineralization proper and the near-field environment, forms a complicated geochemical system. The on-going geochemical processes are complex and their detailed modelling would be rather difficult. Consequently, reaction kinetics and fixation mechanisms are not considered here. The results reported in this study can therefore only be interpreted as the upper boundary of possible radionuclide release from the mineralization to the near field (including the mineralization, the clay-rich halo and the very lower part of the altered sandstone).

The model approach used here relies on simplifying the system to a manageable level of detail. In the following discussions the geometry of the mineralization is considered as a regular lens 800 m long, 50 m wide and 10 m high which is totally enclosed by a clay-rich halo 3 m thick. Outside the mineralization, the altered sandstone host rock is assumed to

extend to infinity. The validity of this infinity assumption is justified in that any escaping plume, for example, of dissolved uranium, is not expected to extend very far from the mineralization.

Furthermore, the data on hydraulic conductivities, groundwater velocities, water compositions, porosities, fracture frequency, etc., vary considerably and it may not even be possible to assign one single representative value to each of these entities. One approach in our models is, therefore, to try to assign some representative values to entities when possible, but to allow for the eventuality of different values being used in other exploratory calculations.

This Section presents the results from the development and testing of three models. In **Model 1** a steady-state near-field release model is developed. The source terms are the dissolved species in the mineralization where solubility-limited dissolution of minerals is assumed. This means that mass transfer of the various species between the aqueous phase and the mineral phases is assumed to be fast and is not the limiting step. Only molecular diffusion and advection flow of the total aqueous species concentration are considered; geochemical reactions are therefore not incorporated. The model is tested against theoretically known helium release and then used to predict the upper boundary of possible uranium release within the near field. The pathways and fate of reductants and oxidants, which can possibly be generated by radiolysis of water adjacent to uranium ore, are explored by means of this model.

In **Model 2** the observed hematization of the bleached clay to hematized clay is simulated by using the available coupled transport/reaction model. Mass transport is coupled with possible geochemical reactions in a one-dimensional pathway within the clay zone; sorption/desorption, however, is not considered. The source term is assumed to be a slightly oxidizing groundwater in the ore zone.

In **Model 3** the concept of mass transport in Model 1 is extended to also include the generation and decay of radionuclides with short half-lives. Mass transport of in-situ nuclear reaction products of neutron capture are studied. The neutron flux within the mineralization has been shown to be intense enough for some of these reactions to take place (Section 3.8.2 in this report). Of the three radionuclides selected, ^{3}H, ^{14}C and ^{36}Cl, elevated concentrations of ^{3}H and ^{36}Cl have been observed by field measurements in the mineralized zones. In the source term of Model 3, 100 % escape of these radionuclides from the massive rock to the pore water is assumed. Therefore, the results of this model should also be interpreted as representing a conservative upper boundary.

3.9.4.2 Model 1: A steady-state near-field mass transport model

3.9.4.2.1 Introduction

The model is conceptualized according to Garisto et al. (1991). The measured solubility concentration of dissolved species in the mineralization is assigned to be the source term of mass transport. The groundwater in the mineralization is relatively stagnant and a constant

concentration (C_o) of the aqueous species is assumed. The clay-rich halo is the least permeable medium, and groundwater flow in it is negligible. The sole mechanism of aqueous species release through the clay will be molecular diffusion. In the altered sandstone, groundwater flows in the direction perpendicular to the axis of the mineralization and parallel to the contour of the clay-sandstone interface. Mass transport in the altered sandstone therefore includes both diffusion, in the direction perpendicular to the clay-sandstone interface, and advection, in the direction of groundwater flow. The release and transport of aqueous species underneath the mineralization are not taken into account because field observations and other studies do not support such a release. A constant concentration (C_i) is assigned to represent the concentration of the aqueous species already existing in the approaching groundwater up-gradient from the deposit. As the mineralization is a relatively closed system, the concentration distributions in the modelled near-field are assumed to be at steady state.

The rock/ore matrices are quite heterogeneous in respect to hydrogeological, geochemical and mineralogical properties. However, it is assumed here that one "central value" can be assigned to represent one mass transport parameter for every rock/ore matrix, i.e., each rock/ore matrix is assumed to be homogeneous in mass transport properties. Being aware of the variations and uncertainties of the transport parameter values, we do not restrict ourselves to using only one set of Representative Central Values (see Table 3.72), even though some of the sets of values are more extensively used than others to conveniently facilitate the mathematical calculations.

The simplified geometry of the whole system with groundwater flow and aqueous species diffusion is shown in Figure 3.125. For the sake of mathematical simplicity, the conceptual model is described in Cartesian co-ordinates as shown in Figure 3.126. Here L is the equivalent length of the outer perimeter of clay measured perpendicular to the mineralization axis (see also Figure 3.125). The total length of the ore is represented by W and the thickness of clay by δ.

3.9.4.2.2 Mathematical analysis

The foregoing discussion can be represented mathematically by the following set of governing mass transport equations and boundary conditions.

a) In the clay zone without advection and only diffusion:

$$
\begin{aligned}
& D_p^c \frac{d^2 C_c}{dx^2} = 0 && \text{at } 0 < z < \infty,\ -\delta < x < 0, \\
& C_c = C^* && \text{at } x = 0, \\
& C_c = C_o && \text{at } x = -\delta.
\end{aligned}
\qquad (1)
$$

b) In the altered sandstone with advection in the z direction and diffusion in the x direction:

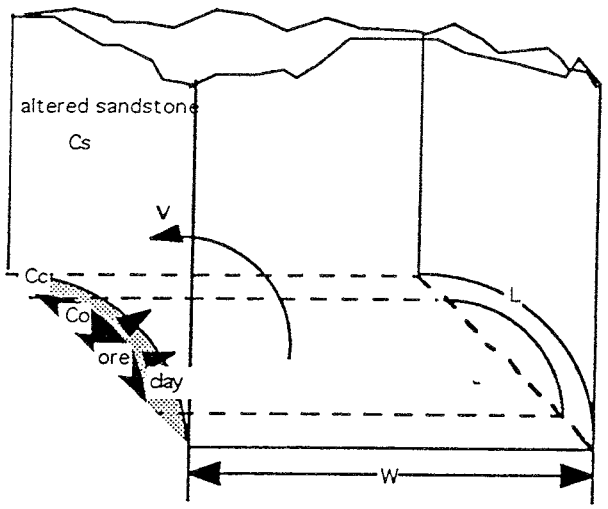

FIGURE 3.125 The simplified geometry of the Cigar Lake deposit with advective groundwater flow in the altered sandstone and diffusion of aqueous-species in the clay zone.

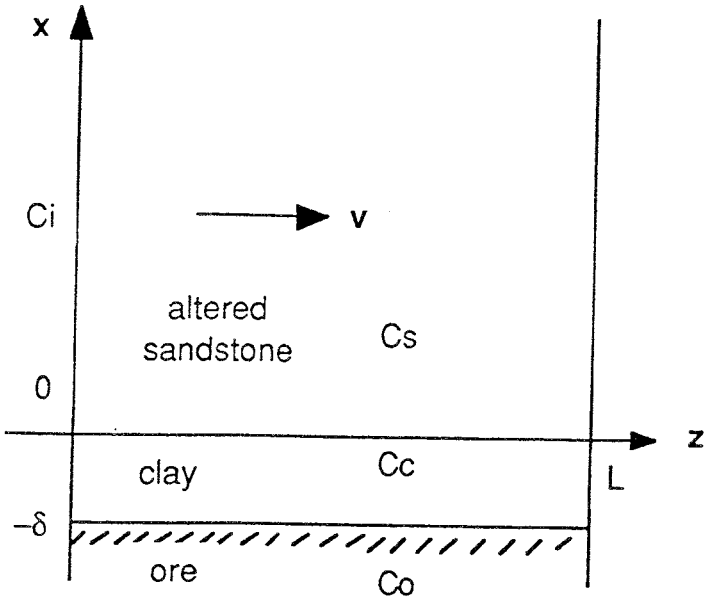

FIGURE 3.126 Conceptual modelling of mass transport in Cartesian coordinates.

$$
\begin{aligned}
& v\frac{\partial C_s}{\partial z} = D_p^s \frac{\partial^2 C_s}{\partial x^2} && \text{at } 0 < z < \infty,\ 0 < x < \infty, \\
& C_s = C_i && \text{at } z = 0, \\
& -D_e^c \frac{dC_c}{dx} = -D_e^s \frac{\partial C_s}{\partial x} && \text{at } x = 0,
\end{aligned} \qquad (2)
$$

where C_c and C_s represent aqueous species concentrations in the clay and in the altered sandstone respectively, $D_e^c = \varepsilon_c D_p^c$ and $D_e^s = \varepsilon_s D_p^s$ with ε_c and ε_s representing porosities of the clay and the altered sandstone and D_p^c and D_p^s being the pore diffusivities of aqueous species in the clay and the altered sandstone, v is the groundwater velocity in the z direction in the altered sandstone, and C^* is the concentration at the clay-sandstone interface. We assume that ε_c, ε_s, D_p^c, D_p^s, v and δ are all constant.

Equations (1) and (2) allow the following solution (Carslaw and Jeager, 1959):

$$
C_c = \frac{C^* - C_o}{\delta}\, x + C^* \qquad (3)
$$

where C^* is the concentration at the clay-sandstone interface ($x = 0$) which is a function of z.

$$
\frac{C^* - C_o}{C_i - C_o} = \exp\left(h^2 D_p^s z/v\right) \operatorname{erfc}\left(h\sqrt{D_p^s z/v}\right) \qquad (4)
$$

The two dimensional concentration distribution in the altered sandstone (C_s) is a function of x and z.

$$
\begin{aligned}
& \frac{C_s - C_o}{C_i - C_o} \\
& = \operatorname{erf}\left(\frac{x}{2\sqrt{D_p^s z/v}}\right) + \exp\left(hx + h^2 D_p^s z/v\right) \operatorname{erfc}\left(\frac{x}{2\sqrt{D_p^s z/v}} + h\sqrt{D_p^s z/v}\right)
\end{aligned} \qquad (5)
$$

where $h = (D_e^c/D_e^s)(1/\delta)$.

Equation (5) shows that when z is fixed, the concentration in the altered sandstone (C_s) decreases as x increases (i.e., the further away from the mineralization the lower the concentration), eventually approaching a value equal to the concentration borne in the incoming groundwater (C_i). When x is fixed, the concentration increases as z increases (i.e., the farther down stream the higher the concentration). But the solution is only valid till $z = L$. No information is given farther downstream.

The total release rate of dissolved species outward from the mineralization through the clay/sandstone interface can be expressed as

$$N|_{x=0} = - D_e^s W \int_0^L \frac{\partial C_s}{\partial x}|_{x=0} \, dz$$

$$= \frac{D_p^c \varepsilon_c WL (C_o - C_i)}{\delta} \frac{1}{H} \{ \exp(H) \, \mathrm{erfc}(\sqrt{H}) - 1 + \frac{2}{\sqrt{\pi}} \sqrt{H} \} \qquad (6)$$

where $H = h^2 D_p^s L/v$.

The various parameters involved in the sets of equations governing mass transport can be categorized into two groups, one pertinent to the clay zone and the other related to the altered sandstone. The former includes the porosity of the clay (ε_c), the pore diffusivity in clay (D_p^c) and the thickness of the clay layer (δ), while the latter consists of the porosity of the altered sandstone (ε_s), the pore diffusivity (D_p^s) and the groundwater velocity in the altered sandstone (v). Such a classification enables us to further analyze their influence on the total release rate.

With the other parameters fixed, the total release rate increases when either v, D_p^s, or ε_s (characteristics of the altered sandstone) increases, but is bounded by a finite value $N_{m,c}$ which is expressed as

$$N_{m,c} = \frac{D_e^c WL (C_o - C_i)}{\delta} \qquad (7)$$

$N_{m,c}$ is just the total release rate when the resistance of the altered sandstone to mass transport is entirely removed and their exists only the resistance of the clay.

The total release rate also increases as the effective diffusivity of the clay (D_p^c) increases or the thickness of the clay (δ) decreases. With whatever changes one makes in either of these two parameters, the total release rate will also be bounded between zero and a maximum value $N_{m,s}$.

$$N_{m,s} = \varepsilon_s WL (C_o - C_i) \sqrt{\frac{4 D_p^s v}{\pi L}} \qquad (8)$$

which is the release rate if all the resistance to mass transport is in the altered sandstone.

3.9.4.2.3 Mass transport parameters

Most values of the various parameters are not well known at present such that any attempt at scoping calculations has to rely on some assigned central values in addition to those obtained directly from field and laboratory tests. Three sets of Representative Central Values were chosen:

1) a porosity of 0.01 and a geometric factor (δ_D/τ^2) of 0.5 for the clay (J. Cramer pers. comm. 1992),
2) a porosity of 0.18 and a geometric factor of 0.11 for the clay as measured by the author, and
3) a porosity of 0.1 and a geometric factor of 0.5 for the clay.

Only one value was used for each of the remaining parameters in all three cases, as shown in Table 3.72.

TABLE 3.72
VARIOUS VALUES ASSIGNED TO MASS TRANSPORT PARAMETERS

Entity	Value(s) 1	2	3	Units
ε	0.01	0.18	0.1	-
δ_D/τ^2 (of the clay)	0.5	0.11	0.5	-
δ_D/τ^2 (of the sandstone)		0.5		-
ε_s		0.16		-
δ		3.0		m
v		3.17×10^{-6}		m/s
L		63.7		m
W		800		m

In the steady-state release modelling the first set of data is used; the other two sets of data are used for comparison where appropriate. In the modelling of the release of *in situ* generated radionuclides and the modelling of coupled transport/reaction, only the third set of data is used to facilitate the calculation.

3.9.4.2.4 Model validation using rate of ^{4}He release

Helium should be a good species for testing the validity of the steady-state release model as it is continuously generated by spontaneous decay in the uranium and thorium series and other nuclear reactions. It is also geochemically inert. Generation is by means of nuclear decay and is independent of its release. The test of helium release should thus provide an independent verification of the release model.

Helium is generated by various nuclear reactions when an alpha particle is emitted during reaction. Possible nuclear decay reactions in the near-field of Cigar Lake include the ^{238}U, ^{235}U and ^{232}Th series and some in situ neutron-capture reactions. In the uranium-rich mineralization, the helium generation by ^{232}Th decay is negligible. In situ neutron-capture reactions are also considered to be occurring within the mineralization and some also emit alpha particles, e.g., ^{7}Li (n,α) ^{3}H.

At steady state, the release rate equals the generation rate. The helium generation rate by nuclear reactions gives an independently determined release rate that can then be compared with the release rate predicted by the near-field release model in order to test the validity of the model.

If the average grade of uranium in the ore is taken to be 12%, and 0.71% of the uranium in the ore zone occurs naturally as ^{235}U, and the calculated neutron production rate (see Section 3.3.8.2) is used, the helium generation rate by nuclear reactions can be calculated by using the nuclear decay equation (independent of our release model). The results are shown in Table 3.73. At steady state, the release rate is the same as the generation rate.

TABLE 3.73
HELIUM GENERATION RATES IN VARIOUS NUCLEAR REACTIONS

	Helium generation rate in entire mineralization (mol/a)
From the ^{238}U decay series	0.442
From the ^{235}U decay series	0.0176
In situ neutron-capture reactions	Negligible
Total	0.46

TABLE 3.74
HELIUM RELEASE RATE CALCULATED BY TWO INDEPENDENT APPROACHES

Calculation method using:	Values used (in Table 3.72)	Calc. release rate (mol/a)
known helium generation		0.46
near-field release model	First set	0.14
	Second set	0.56
	Third set	1.37

The helium gas in groundwater from piezometers 79 and 220 in the mineralization are 0.18 and 0.19 cm^3/L, respectively. Helium gas in the upstream groundwater (piezometer 139) is below the detection limit of 0.01 cm^3/L. When this concentration gradient is used, the helium release rate can also be calculated by our model. The results of the two independent approaches (one by nuclear decay and the other by our model) are listed in Table 3.74 for comparison.

The results of the two different approaches agree surprisingly well if the uncertainties in estimating the representative values of the various mass transport parameters are also considered.

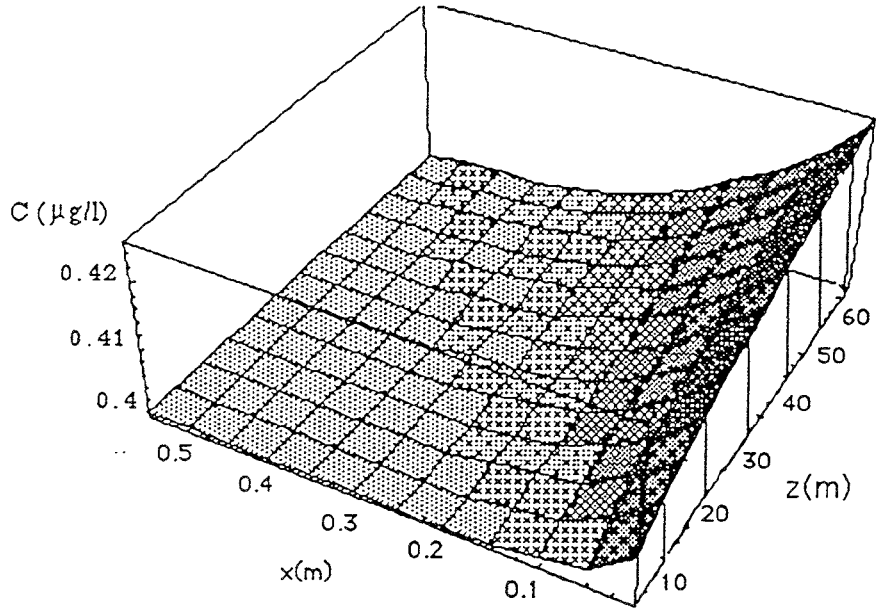

FIGURE 3.127 The two dimensional uranium concentration distribution.

3.9.4.2.5 Uranium release and sensitivity test

The interaction of reducing groundwaters with uranium-bearing minerals within the hydrothermal dispersion-halo in the sandstone host rocks overlying the mineralization produces dissolved-uranium concentrations similar to those measured inside the mineralization. The field data show no evidence for any concentration gradients for dissolved uranium between the mineralization and the sandstone host rocks. In this modelling a hypothetical concentration gradient, between the measured concentration in piezometer 79 in the mineralization and that in the upstream piezometer 139 in the sandstone, is chosen to test the model. Uranium release could even be much lower than that predicted by the model. This is supported by the lack of any surface expression (geophysical or geochemical) of the existence of the underlying ore.

TABLE 3.75
TOTAL RELEASE RATE OF URANIUM AND ITS POSSIBLE MAXIMUM VALUES

N (g/a)	$N_{m,c}$ (g/a)	$N_{m,s}$ (g/a)	$N/N_{m,c}$ (%)	$N/N_{m,s}$ (%)
0.0489	0.0490	15.29	99.90	0.32

When the diffusivity of uranium in the bulk water is assumed to be 3.0×10^{-9} m^2/s, a two-dimensional distribution of concentration is obtained using the first set of assigned values as shown in Figure 3.127. The total release rate N and the other two possible maximum release rates $N_{m,c}$ and $N_{m,s}$ are calculated and tabulated in Table 3.75.

Table 3.75 shows that if there is only the resistance of clay, the total-release rate will be 0.049 g/a ($N_{m,c}$), whereas the total-release rate could be as large as 15.29 g/a ($N_{m,s}$) if only the resistance of the sandstone is considered. In other words, the total-release rate from the clay is only 0.32 % of the value calculated for the sandstone-only case. This means that the clay layer is acting as an effective natural barrier and substantially suppresses the outward release of uranium.

In the sensitivity analyses the following equations have been used, based on a logarithmic sensitivity definition because the parameter values may vary widely.

$$\frac{d(N/N_{m,c})|_{x=0}}{d(\log v)} = \frac{d(N/N_{m,c})|_{x=0}}{d(\log D_p^s)} = \frac{1}{2}\frac{d(N/N_{m,c})|_{x=0}}{d(\log \varepsilon_s)}$$

$$= -\frac{\ln 10}{H}\{(H-1)\exp(H)\,\mathrm{erfc}(\sqrt{H}) + 1 - \frac{2}{\sqrt{\pi}}\sqrt{H}\} \qquad (9)$$

$$\frac{d(N/N_{m,s})|_{x=0}}{d(\log D_p^c)} = \frac{d(N/N_{m,s})|_{x=0}}{d(\log \varepsilon_c)}$$

$$= \frac{2\ln 10}{\sqrt{H}}\sqrt{\pi}\,\{(2H-1)\exp(H)\,\mathrm{erfc}(\sqrt{H}) + 1 - 2\sqrt{\frac{H}{\pi}} \qquad (10)$$

$$\frac{d(N/N_{m,s})|_{x=0}}{d(\log_2 \delta)}$$

$$= \frac{2\ln 2}{\sqrt{H}}\sqrt{\pi}\,\{(2H-1)\exp(H)\,\mathrm{erfc}(\sqrt{H}) + 1 - 2\sqrt{\frac{H}{\pi}}\} \qquad (11)$$

where "log" denotes the common logarithm, "ln" represents the natural logarithm and "$\log_2$" stands for a logarithm with a base of 2. A base of 2 is chosen in Equation (11), but a base of 10 is used in the rest of the equations because the assumption of an error of an order of magnitude will not be practically reasonable for the thickness of clay; a factor of two has been used instead.

The sensitivities of the total release rate to changes of the various parameters at their assigned central values (the scale of the change is one order of magnitude except for the thickness of clay, which is a factor of two instead) are shown in Table 3.76.

Table 3.76 shows that for the assigned central values, changes in the release rate (ΔN) are small for parameters v, D_p^s, and ε_s (each ≤ 0.0004 g/a). For parameters δ, D_p^c and ε_c, however, the change in the release rate is by no means small (could be as large as 0.45 g/a).

It is therefore concluded that the total release rate is sensitive to parameters of the clay but not sensitive to those of the altered sandstone. This is because the clay layer plays such a dominant role in suppressing the outward release of uranium in the Cigar Lake system.

TABLE 3.76
SENSITIVITY OF THE TOTAL RELEASE RATE

	Central value	ΔN (g/a)
v (m/s)	1.0×10^{-6}	0.0003
D_p^s (m^2/s)	1.0×10^{-9}	0.0004
ε_s	1.0×10^{-1}	0.0002
δ (m)	1.0	0.4015
D_p^c (m^2/s)	1.0×10^{-9}	0.3045
ε_c	1.0×10^{-9}	0.3045

3.9.4.2.6 Pathways and fate of radiolytically generated species

Uranium minerals are much more soluble when oxidized from tetravalent to hexavalent forms. Atmospheric oxygen is unlikely to penetrate to the deep bedrock formation so that the only possible source of oxidants is the radiolysis of water in the mineralization. However, despite the possible effects of radiolysis, the uranium ore has remained preserved since its formation 1.3 Ga ago. It may therefore be worthwhile to study the pathways and fate of the radiolytically-generated oxidants and -reductants using the steady-state release model.

The radiolytically-generated reductants are primarily hydrogen molecules, whereas the oxidants may include oxygen molecules, hydrogen peroxide and some oxidizing radicals (Section 3.8.3 in this report). Because dissolved hydrogen is more readily mobile and chemically less reactive, most of the radiolytically-generated hydrogen may be lost relatively quickly from the mineralization. According to mass conservation, an amount of oxidant equivalent to that of the lost hydrogen will be left within the system. These oxidized species will also be released out of the system if no effective fixation mechanisms exist, such as the oxidation of reduced mineral or aqueous species.

Measured concentrations of $SO_4^=$ in groundwater, assumed to be produced by oxidation of sulphide minerals in the mineralization, show a distinct gradient for samples collected from the mineralization and the altered sandstone host rock (Section 3.5 in this report). A similar gradient may exist for other species including dissolved-hydrogen, but the values for this gas phase listed in Table 3.30 are unlikely to represent the water composition of the ambient undisturbed system in all piezometers. However, the steady-state release model may be applied to evaluate the release rates of both dissolved sulphate and hydrogen, and the results (Table 3.77) show that their release rates are comparable. On the other hand, similarly

calculated release rates for tetravalent uranium and ferrous iron are significantly different.

TABLE 3.77
RATE OF RELEASE FROM MINERALIZATION FOR SOME DISSOLVED SPECIES

Species	Release rate, N (eqv/s.m^3)
Sulphate	1.72×10^{-12}
Dissolved H_2	2.34×10^{-12}
Total uranium	4.74×10^{-17}
Oxidant consumption rate by oxidation of reducing iron	3.90×10^{-15} *

* See Table 3.79.

Note that the release rate in Table 3.77 is expressed in terms of equivalent per second per cubic metre of the mineralization. The theoretical maximum values for the rate of oxidant production by radiolysis have also been calculated, without considering the recombination of reductant and oxidant, and the results are given in Table 3.78. Conversion of the values for the release rate in Table 3.77 allows direct comparison with the production rates in Table 3.78, showing that the rate of radiolysis predicted with the mass transport calculation is some hundred times less than the theoretical maximum values.

3.9.4.2.7 Discussion and conclusions

The steady-state release model developed here treats the release and transport in the near-field as a whole entity. Previous modelling efforts either concentrated on the dissolution of the spent fuel itself, or on the release and transport in the engineered barriers. In addition, the steady-state release model is a relatively simple model.

Good agreement has been obtained between the model prediction of helium release from the mineralization and an independent approach using alpha-particle generation. This agreement indicates that the basic approaches in constructing the model are reasonable. Other results predicted by the model, such as those for sulphate, do not contradict actual field observations.

Limitations of this mass-transport model can also be expected. The analyses and calculations are carried out using various assumptions and simplifications. For instance, there are two essential assumptions with regard to transport in the aqueous phase: 1) the various rocks act as porous media, and 2) the groundwater flow within the mineralization is neglected. If the various rock matrices were sparsely fractured, the porous medium assumption may not be valid and the real scenario would be very different. Field observations showed that the major fractures are approximately one metre apart, but information on the geometry of minor and small fractures is not available. However, it is

expected that the results will not change significantly if we include fracture flow, because bulk movement of groundwater in the clay-rich mineralization appears to be very slow (e.g., Sections 3.4 and 3.5.5 in this report).

Additional assumptions and simplifications include, for instance, the omission of any fixation mechanism for the dissolved species and the implied boundaries of the model. As would be expected, the clay may significantly absorb dissolved uranium and other radionuclides. The release rates were always calculated for the clay-to-altered sandstone interface, and mass transport in the lower sandstone and beyond was not considered. Thus, the calculated release rates can only be considered as an upper bounding value of the near-field mass transport and do not necessarily point to any evidence for actual uranium release from the mineralization or the existence of a dispersion-plume for uranium in the sandstone host rocks.

Bearing in mind these limitations, the following conclusions can be drawn:

1- The two dimensional concentration profile of dissolved uranium decreases outward from the mineralization surface through the clay-rich halo and eventually drops to background values in the altered sandstone. In the absence of the clay-rich halo, the concentration profile would show an increase in the direction of groundwater flow.

2- The total release rate will always be bounded between zero and a maximum value accompanied by whatever errors one may introduce in estimating the values of the various parameters.

3- The results, calculated with the set of assigned central values for the various parameters, show that the uranium plume will not extend into the altered sandstone beyond 0.5 m from the clay-sandstone interface if the uranium source-term is restricted only to the main mineralization (i.e., not in the clay-rich halo; Figure 3.127).

4- The steady-state model predicts an upper bounding value of 0.05 g U/a for the total release rate of uranium from the whole mineralization, when using the assigned central values for the various parameters.

5- The clay layer plays an exceedingly dominant role in retaining any dissolved uranium. Sensitivity analyses show that the total release rate of uranium would reach 15 g U/a in the absence of the clay, but the value would be only slightly different in the absence of the sandstone.

6- In the vicinity of the assigned central values the total release rate is much more sensitive to the clay parameters than those of the altered sandstone.

3.9.4.3 Model 2: Mass transport coupled with geochemical reactions in the clay zone

3.9.4.3.1 Introduction

Model 1 describes the possible migration of dissolved uranium and other species from the mineralization through the clay-rich halo into the altered sandstone. This model assumes that the release of the dissolved species from the source term is controlled by solubility-limited dissolution. This approach is valid if the rock matrix can be modelled as a homogeneous medium and the groundwaters are in equilibrium with the identified minerals in the various rock matrices.

However, field observations show that the rock matrices are by no means homogeneous, not even on a metre scale, as exemplified by the hematized layer at the contact of the clay-rich halo with the main mineralization. Model 2 incorporates a redox mechanism to accommodate the oxidation of ferrous iron in the clay halo by some oxidizing species emanating from the main mineralization. In this model the mass transport is coupled with chemical equilibra involving geochemical reactions, such as acid/base reactions, dissolution/precipitation and oxidation/reduction. However, sorption/desorption is not included. This is a natural extension of the previous analytical approach to mass transport where geochemical reactions were excluded.

3.9.4.3.2 Oxidation rate by radiolysis

It is believed that the oxidation of the ~1-m-thick clay at the contact results from the reaction between some oxidizing species emanating from the main mineralization and a ferrous phase. Because it is not clear whether the oxidizing species are of radiolytic origin, the potential consequences of possible radiolysis in the mineralization are here explored.

TABLE 3.78
THEORETICAL MAXIMUM RATE OF OXIDATION

Radiation	Production rate (eqv/s.m^3)
α	2.7×10^{-10}
β, γ	4.6×10^{-11}

The production rate of oxidant, in equivalent of oxidant per unit time per unit volume of the mineralization, has been calculated (T. Eriksen written comm. 1992). The calculated results are listed in Table 3.78; they are based on the following assumptions:

1- an average uranium content in the mineralization of 10 %,
2- an average density for the mineralization of 2000 kg/m^3,

3- an average porosity for the mineralization of 10 %, and
4- the system is completely dispersed, i.e., the radiation energy is absorbed in uranium, clay and water in proportion to the content (by weight) of these fractions.

It can be calculated that the entire mineralization at Cigar Lake would have been oxidized in about 1.68×10^5 a, assuming that the radiolytically-produced oxidant would oxidize only uranium in the uranium ore minerals. Because the field observations do not support this prediction, it may be concluded that the oxidation of uranium by the radiolytic oxidants is, at least partly, inhibited by kinetic and/or geometric constraints.

3.9.4.3.3 Redox reaction predicted by the shrinking core model

In this section we calculate the amount of oxidants needed to oxidize a 1-m-thick clay zone containing ferrous phases, and compare this value with the calculated production rate of radiolytic oxidants.

(1) Assuming a constant flux of oxidants

The calculation is simplified by assuming that the average content of total iron in the bleached-clay zone is equal to that occurring in the ferrous minerals only. Pyrite and siderite, both occurring in trace amounts (Section 3.1 in this report), are assumed to be oxidized completely in the 1-m-thick red-clay zone, producing ferric phases such as ferrihydrite and hematite, which have been identified in minor amounts in this zone (Section 3.2.4 in this report).

The oxidant flux is assumed to be constant,

$$N = \frac{Eqv}{tA} \tag{12}$$

where N is the oxidant flux in equivalent per unit time per unit area of the ore/clay interface, Eqv is the total equivalent of oxidant needed, t is time and A is the area of the ore/clay interface.

TABLE 3.79
CALCULATED RESULT BY ASSUMING CONSTANT FLUX OF OXIDANT

Volume of hematized clay	(m^3)	4.46×10^4
Amount of ferrous iron oxidized in hematized zone	(mole)	1.75×10^7
Oxidant flux	(eqv/s.m^2)	9.70×10^{-15}
Source intensity of oxidant	(eqv/s.m^3)	1.56×10^{-15}

The calculated results, using the simplified geometry of the mineralization and clay, and assuming a porosity of 10 % and a density of 2300 kg/m^3 for the bleached clay (Smellie et al., 1991), are listed in Table 3.79.

In the calculation the conservative assumption is made that the mineral transformation started immediately following the formation of the mineralization. It should be noted that the oxidant flux in Table 3.79 is given with respect to the unit area of the ore/clay interface, whereas the source intensity has been converted with respect to the unit volume of the mineralization.

The calculated total rate of oxidant production by radiolysis since ore formation is 3.16×10^{-10} eqv/s.m^3. The source term to oxidize a 1-m-thick clay zone containing ferrous phases accounts only for about 0.3 millionth of this radiolytic production rate. Oxidation of sulphides could be a competing process to the oxidation of ferrous iron as shown in Model 1. Even though the oxidation of sulphides is accounted for, the theoretical maximum value for the rate of oxidant production is still two orders of magnitude higher. Either the radiolysis production rate was overestimated to be meaningful or other mechanisms are inhibiting oxidation by the radiolytic oxidants. The latter is believed to be the case. Bacterial mediation and oxidant-reductant recombination are only two of potential alternative mechanisms.

(2) Assuming constant oxidant concentration in the mineralization

If the reaction kinetics of mineral dissolution and oxidation are much slower than the rate of mass transport in the aqueous phase, the shrinking-core model applies. The standard shrinking-core model describes diffusion-controlled mass transport by the irreversible dissolution of minerals from a solid matrix. As the mineral is dissolved irreversibly and the dissolved species removed, the mineral front within the solid matrix recedes slowly compared with the relaxation time of the aqueous species concentration profile. The solid-liquid interface that separates the solid matrix and the flowing water will, however, remain stationary. When the standard shrinking-core model is applied, the movement of a redox front will be given by the following equation (Zhu 1988):

$$Z_r = \sqrt{2 \frac{C_o}{f\, q_o} D_e\, t} \qquad (13)$$

where t is time, Z_r is the distance in metres of the redox front movement at time t (in seconds), D_e is the effective diffusivity in m^2/s, C_o is the incoming aqueous concentration of the oxidant in moles per litre water at the inlet boundary of the mineral array, q_o is the mineral concentration in terms of moles of mineral per litre of pore water, and f is the reaction coefficient of the oxidant when the coefficient of the reductant is chosen as 1.

Using the reference mineralogical/geochemical data set (Smellie et al. 1991) and assuming that the mineral contents of pyrite and siderite in the original bleached clay are equal in moles, it can be calculated that an oxidant concentration of 19.25 μg/L is required to

account for a redox front movement of 1 m. The measured concentrations of dissolved oxygen in groundwater collected from the mineralization range from a few micrograms to hundreds of micrograms per litre (Table 3.30), reflecting the difficulty in obtaining representative samples rather than a true range of values for the ambient undisturbed system. The predicted value falls within the range of the observed values. Assuming that similar values for dissolved oxygen occurred in the mineralization since it was formed ~1.3 Ga ago, the oxidation of the bleached-clay contact over a thickness of 1 m appears quite reasonable. The oxidant source for this oxidation process could thus have been the dissolved oxygen from the mineralization.

3.9.4.3.4 Geochemical equilibrium in the mineralized zones

Geochemical equilibration is implicitly assumed in the shrinking-core model and is explicitly used in calculating the coupled mass transport using chemical equilibria codes such as CHEQMATE used in this study. In a complicated natural system such as the Cigar Lake uranium deposit, the geochemical equilibrium approach is only an approximation of reality. The mineral saturation status indicates that for most minerals the saturation indices are rather different from the equilibration value 1. On the other hand, the geochemical equilibrium approach can be justified by the fact that the groundwater compositions in the various rock matrices are essentially buffered by the solubility of some of the abundant and minor minerals identified (Section 3.5 in this report). It is also noted that the measured values for dissolved-oxygen concentration and Eh do not agree if the dissolved oxygen is assumed to be in equilibrium with the aqueous phase.

Measured groundwater compositions from two piezometers (198 and 197) (Table 3.30) were used. Groundwater 198 is equilibrated with the minerals coffinite, illite, pyrite, siderite and uraninite by using PHREEQE (David et al. 1980). The saturation index for a number of minerals is plotted in Figure 3.128.

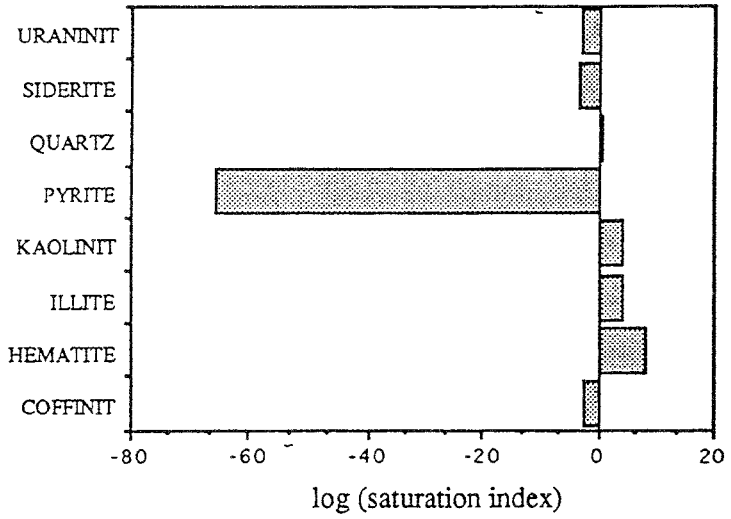

FIGURE 3.128 Calculated saturation index for selected minerals for groundwater 198J from the mineralization.

Following equilibration with the minerals, the Eh value is buffered even lower (-168 mV). The concentrations of Mg, K, Si, C and S are approximately the same before and after equilibration, suggesting that they are solubility-controlled. After equilibration, total-Fe becomes two orders of magnitude higher, total-Al two orders of magnitude lower, and U one order of magnitude lower. The speciation shows that the dominating iron species is Fe^{2+}, which is in agreement with measurements carried out on groundwater from another piezometer (79) in the mineralization (Table 3.30).

The composition of groundwater from piezometer 197 in the clay zone is also equilibrated with the selected minerals, giving results similar to those obtained for groundwater 198J.

3.9.4.3.5 Coupled mass-transport/chemical-equilibrium modelling

The objective of this coupled transport/equilibrium modelling is to simulate the consequences of various geochemical reactions and mass transport, especially the oxidation of reduced phases in the bleached clay.

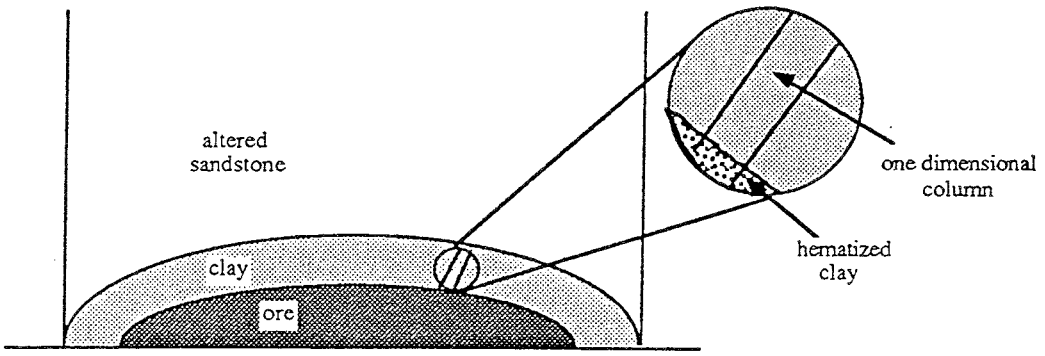

FIGURE 3.129 The rock matrices and the location of the one dimensional column.

The modelling is one-dimensional and the mass transport and geochemical reactions (especially the oxidation and dissolution of minerals) in the clay zone is highlighted. A column extending from the ore to the clay/sandstone interface is selected; it is perpendicular to both the ore/clay and the clay/sandstone interfaces (See Figure 3.129).

It is assumed that the minerals described as abundant to minor in content in the bleached clay initially occurred as solid phases in the column. Seven minerals are included: illite, kaolinite, quartz, pyrite and siderite, and uraninite and hematite, which are allowed to precipitate during the simulation. The water from borehole 197 within the clay is equilibrated with these minerals and used as the initial aqueous phase. The mass transport of 90 complexing species made up of 10 elements (H, O, Mg, K, Fe, Al, Si, C, S and U) are included in the model. The HATCHES thermodynamic database is used for all the species and minerals. The approach used simulates only diffusion of the aqueous species along the column, as groundwater flow in the clay zone is negligible with the probable exception of some discrete fractures (Section 3.4 in this report).

The equilibrated groundwater 198J from the ore zone is the inlet boundary of the column. Aqueous species from the mineralized zone diffuse into the column and react with both the minerals and the aqueous species there. Dissolved oxygen is assumed to be the incoming oxidizing species; when it diffuses into the clay column it is expected to react with the reduced aqueous constituents and the ferrous minerals. The ferric minerals will precipitate behind the redox front when the front propagates. In reality there is an abundant amount of reduced uranium in minerals such as uraninite in the mineralized zone. This is modelled by assuming an "infinite" amount of uraninite at the very beginning of the column.

At the other end of the column (the clay/sandstone interface), a constant concentration boundary is applied; during the simulation the equilibrated water composition in the clay is kept constant. This is justified since water flow in the altered sandstone is large compared with that in the clay. The simulation covers a time span in the order of hundreds to thousands to millions of years.

Representative, present-day groundwater compositions 197 and 198J from the ore have been selected, and the CHEQMATE (Haworth et al. 1988) program was used in this simulation. A version of this program was successfully applied in the redox front movement study in the Poços de Caldas uranium mine in Brazil (Cross et al. 1990). The program uses a two-step approach: geochemical equilibration followed by mass transport. The equilibration part is essentially PHREEQE, which can simulate aqueous speciation and equilibration with minerals. The mass transport part uses the explicit forward finite-difference method to discretize the following mass-transport equation for each aqueous species j:

$$\frac{\partial C_j}{\partial t} = D_L \frac{\partial^2 C_j}{\partial x^2} + v \frac{\partial C_j}{\partial x} \qquad (14)$$

where C_j is the aqueous concentration of species j in mol/L water, $D_L = D_e + \alpha v$ is the dispersivity in m^2/s, D_e is the effective diffusivity of the aqueous species in m^2/s, α is the dispersion length in metres, v is the groundwater velocity in m/s, t is time in seconds and x is the spatial co-ordinate in metres.

At each time step the water in every cell is equilibrated with minerals in the same cell. Discretized mass transport equations are then used to calculate the fluxes of each species between every pair of adjacent cells. The resultant changes in concentration in each cell for every species are added to the old ones of the previous time step in each cell and re-equilibrated again. Minerals are allowed to precipitate when they are over-saturated or to dissolve when they are under-saturated and not yet depleted.

There is a numerical stability limitation on the length of each time step for the explicit forward finite-difference technique to solve parabolic partial-differential equations (Lapidus and Pinder, 1982). The procedure is stable only when the following criterion holds,

$$\Delta t \leq \frac{0.5\,(\Delta x)^2}{D_L} \qquad (15)$$

where Δt is the length of time step in seconds, Δx is the length of each cell in metres and D_L is the dispersivity in m^2/s. Because of restrictions on computing time, calculation up to only around 2000 time steps have been considered, resulting in a total time span covering about 800 a. The hematization of the 1-m-thick clay is believed to happen over a much longer time span, probably commencing shortly after ore formation.

One way to increase the time span to be considered is by scaling the minerals. With an equilibration approach it is only the absence or presence of minerals that matters. The equilibrated water composition will not change as long as none of the minerals are depleted. If the content of a mineral is scaled down one order of magnitude, then the time needed to deplete that mineral (by dissolution and oxidation, for example) will be approximately 10 times less.

However, the scaling of minerals will not always be successful. In practice problems occur when the content of some minerals (expressed in mol/L water) is scaled down to lower than the concentrations of any of the dominating species of its elements. In the case of Cigar Lake, siderite is one such mineral. The problem may be circumvented by excluding the very sensitive mineral siderite in the clay and assigning its reducing power to pyrite. This will not significantly influence the final result.

The output results of the simulation are shown in Figures 3.130 and 3.131 where sharp redox fronts are clearly shown for the elements and minerals relevant to oxidation/reduction reactions. It should be noted that in the figures the first steep changes between cells 1 and 2 are not reaction fronts, they represent only the discontinuity of material properties between the mineralization and clay.

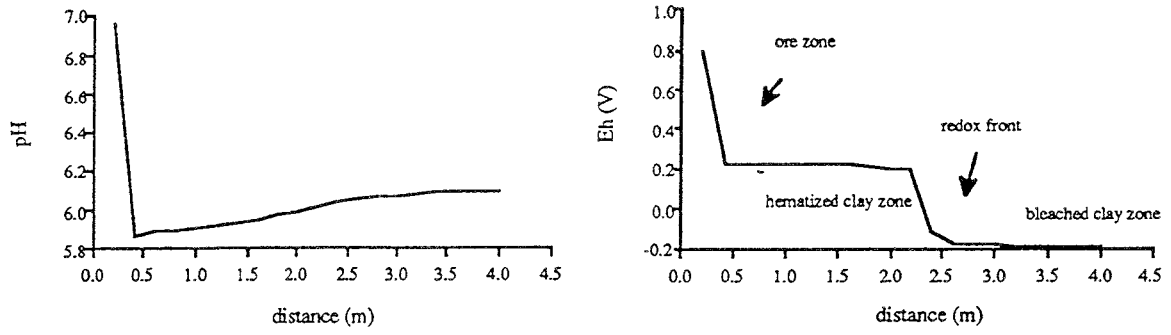

FIGURE 3.130 Profiles for pH and Eh in the ore and clay column at 80 Ma.

Changes in the aqueous concentrations of total K, Al, Si and C, and weight percentages of minerals illite, kaolinite and quartz, are small and not shown.

The pH value in the entire clay zone is about one unit lower than that in the mineralization, i.e., the measured data of 6.43 for piezometer 198J in the mineralization and 5.78 for piezometer 197 in the clay zone. The predicted values are very close to the measured values (Table 3.30).

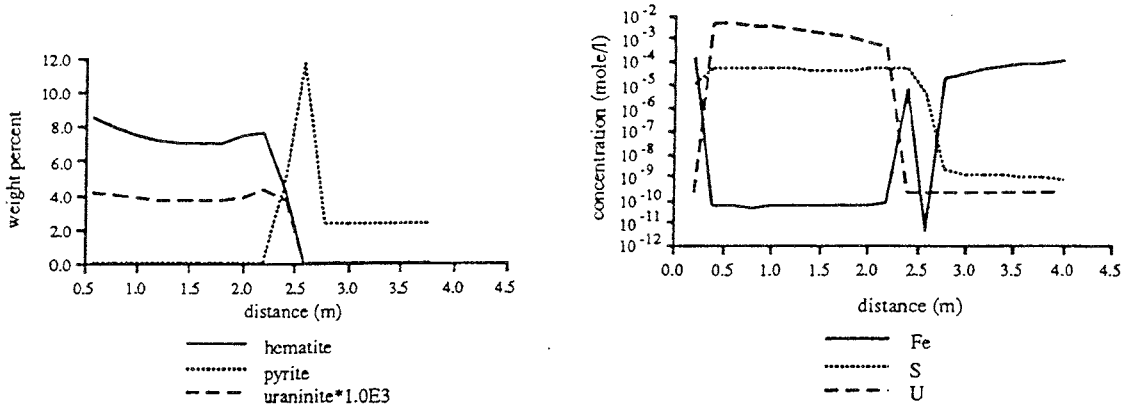

FIGURE 3.131 Profiles showing mineral abundance (left) and total concentration of dissolved-elements (right) at 80 Ma.

The predicted Eh value in the hematized clay zone is about 0.2 V and in the bleached clay about -0.2 V. This compares favourably with the measured values of 0.23 V in piezometer 91 and 0.27 V in piezometer 197 (both are in the clay zone). The more reducing water in the bleached clay zone may not have been detected because of the limited sampling distance achievable from a piezometer-equipped borehole.

Total concentrations of iron and uranium predicted for the hematized zone agree with both the measured value and the equilibrated value. Total concentration of sulphur in the bleached zone agrees with the equilibrated value, whereas that in the hematized zone agrees with the measured value. The very high concentration of uranium predicted in the hematized zone is neither detected in the groundwater sampled from the clay nor predicted by the equilibration calculation. The reason for this is the conservative assumption in the simulation that the ferrous minerals in the hematized clay zone have been completely depleted. In reality ferrous minerals will remain present in addition to ferric minerals because of various inhibitions.

Dissolved-uranium concentrations in the clay zone were predicted by the early analytical approach as ranging from 1.79×10^{-9} to 2.70×10^{-8} mol/L. The predicted value of total uranium in the aqueous phase in the bleached clay is close to the analytical prediction, thus leading to the conclusion that as long as the redox fronts have not broken through the 3-m-thick clay zone, the analytical approach will be valid even though it was less informative than the coupled modelling.

The content of minerals not involved in the redox reactions barely change during the simulation time. The ferrous mineral pyrite is converted to hematite behind the redox front. The predicted hematite content is about 7.0 to 8.0 wt%, compared with the observed value which varies between 1.40 and 30.86 wt%. Again the predicted value falls within the observed range.

Another very interesting aspect is co-precipitation of hematite with uraninite in the hematized clay as predicted by the model. This has long been suspected to be the case at Cigar Lake (J. Cramer pers. comm. 1991).

The predicted redox-front movement is about 2 m in 80 Ma, which is approximately 35 times faster than the assumption made in the shrinking core model. This underlines the fact that the redox-front movement prediction is relatively poor when applying the technique of mineral scaling to a diffusion-dominated system (diffusion only is considered in this present case). In a system with a large Peclet number, where mass transport is dominated by advection, the mineral scaling technique should give a better prediction of redox front movement. In a diffusion-dominated system with small Peclet number, however, the rate of redox-front movement is very complicated and is not just inversely proportional to the mineral contents. This is especially so when mineral contents are scaled down to very low levels. Further study is needed to explore techniques that will predict more accurately the rate of redox-front propagation.

3.9.4.3.6 Discussion and conclusions

The rate of redox-front propagation predicted by the model requires further investigation because mass transport in the clay zone is dominated by diffusion processes. The following conclusions can be drawn from the coupled transport/equilibria modelling:

1- For most of the aspects considered, the one-dimensional modelling gives results in good agreement with the measured data. For some aspects it is difficult to compare the results because of the complexities in the real system.

2- The modelling approach using coupled transport/equilibrium appears suitable for mass transport and geochemical reactions in the near field of a uranium deposit such as Cigar Lake. It is expected to be equally suitable for studies of near-field migration and reactions used in the assessment of disposal concepts.

3- The shrinking-core model predicts that if the present-day level of dissolved oxygen in the ore was held constant during the geological time span since ore formation, it is quite reasonable that it could have oxidized the bleached clay to hematized clay over a thickness of ~ 1 m. The numerical simulation predicts that the time needed might be tens of times less.

4- The uranium concentration could be as high as 1.0×10^{-3} mol/L (0.238 g/L) if all the ferrous minerals had been depleted. But as long as the extent of oxidation by the predicted radiolytic oxidants is contained within the clay-rich halo, the release of uranium is predicted to be very small (tens of milligrams per year in the entire mineralization).

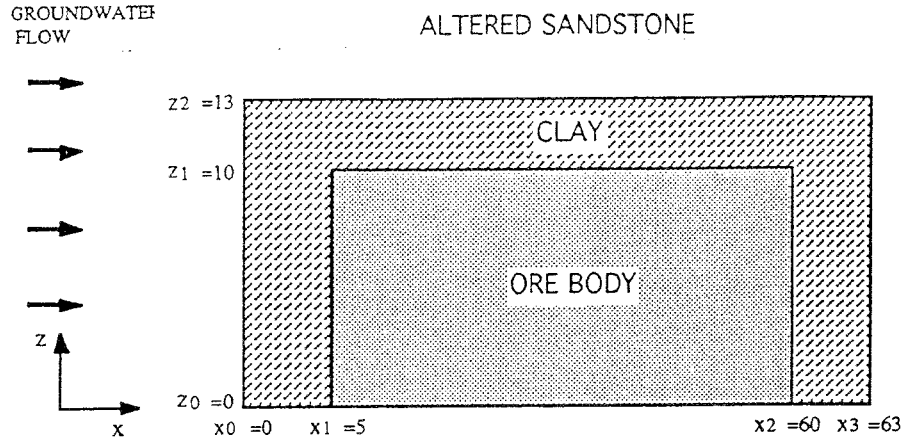

FIGURE 3.132 Schematic illustration of the mineralization, clay and altered sandstone.

3.9.4.4 MODEL 3: Radionuclide migration

3.9.4.4.1 The mathematical model

The model describes the advection, diffusion and decay of a radionuclide in the mineralized and clay zones and altered sandstone, as well as radionuclide generation in the mineralization. A section through the 2D-model, showing the three main lithologies (mineralization, clay, and altered sandstone), is given Figure 3.132. The Cartesian co-ordinate is used where the x axis represents the direction of groundwater flow and the z axis represents the vertical extension of the deposit system. The axis of the mineralization in this simplified geometry is perpendicular to the plane of the other two axes and is not shown in Figure 3.132.

The equation for conservation of mass for a radionuclide in the mineralization can be expressed as

$$\frac{\partial c}{\partial t} = D\left(\frac{\partial^2 c}{\partial x^2} + \frac{\partial^2 c}{\partial z^2}\right) - v_x \frac{\partial c}{\partial x} - v_z \frac{\partial c}{\partial z} + q - \lambda c \qquad (16)$$

It is assumed that no nuclear reactions occur in the clay and altered sandstone and therefore the radionuclide generation term q drops out, and the equation becomes

$$\frac{\partial c}{\partial t} = D\left(\frac{\partial^2 c}{\partial x^2} + \frac{\partial^2 c}{\partial z^2}\right) - v_x \frac{\partial c}{\partial x} - v_z \frac{\partial c}{\partial z} - \lambda c \qquad (17)$$

The boundary conditions used in these equations are: a) zero concentrations far away from the mineralization and, b) continuity of fluxes through the various interfaces.

As the hydraulic conductivity of the mineralized zone and clay halo are much lower than that of altered sandstone, the groundwater changes its flow pattern in and near the mineralization

and clay. To calculate the groundwater flow velocity field, Darcy's Law is used:

$$v_x = -\frac{K}{\varepsilon}\frac{\partial H}{\partial x} \tag{18}$$

For the z co-ordinate the relation is similar.

The following equation is used to calculate hydraulic head distribution, assuming the flow velocity field is at steady state:

$$K\left(\frac{\partial^2 H}{\partial x^2}+\frac{\partial^2 H}{\partial z^2}\right)=0 \tag{19}$$

The velocity thus calculated is a function of x and z and will be used in Equations (16) and (17).

3.9.4.4.2 Scoping calculation using the analytical model

The radionuclide concentration profiles will be influenced by the groundwater flow. In the limiting case when groundwater is stagnant, the radionuclide will reach its maximum concentration at the bottom of the mineralized zone. At steady state, the equations for mass conservation reduce to ordinary differential equations and the concentration profile can be obtained by an analytical model.

The following assumptions are made: radionuclides in the ore zone form, decay and diffuse only in the z direction, whereas they only decay and diffuse in the clay and altered sandstone. The concentration profiles are shown below.

$$c_o = \frac{c_1 - q/\lambda}{\cosh(\sqrt{\lambda/D_o}\, z_1)}\cosh(\sqrt{\lambda/D_o}\, z) + \frac{q}{\lambda} \qquad 0 \le z \le z_1 \tag{20}$$

$$c_c = \frac{c_1 \sinh\left[\sqrt{\lambda/D_c}\,(z_2-z)\right] + c_2 \sinh\left[\sqrt{\lambda/D_c}\,(z-z_1)\right]}{\sinh\left[\sqrt{\lambda/D_c}\,(z_2-z_1)\right]} \qquad z_1 \le z \le z_2 \tag{21}$$

$$c_s = c_2 \exp\left(\sqrt{\lambda/D_s}\,(z_2-z)\right) \qquad z_0 \le z \le z_2 \tag{22}$$

where c_1 and c_2 are two constants depending on the mass transport parameters.

3.9.4.4.3 Influence of fractures

In the above calculation, the mineralization is regarded as a uniform porous medium; if the mineralization is fractured, the conditions will be different. To investigate the influence of fractures it is assumed that the mineralization has vertical fractures parallel to the approaching direction of groundwater, the interval between adjacent fractures is 1 m, the

aperture of the fractures is 1 mm, and the groundwater flows only through the fractures. Figure 3.133 gives a plan view of the fractures.

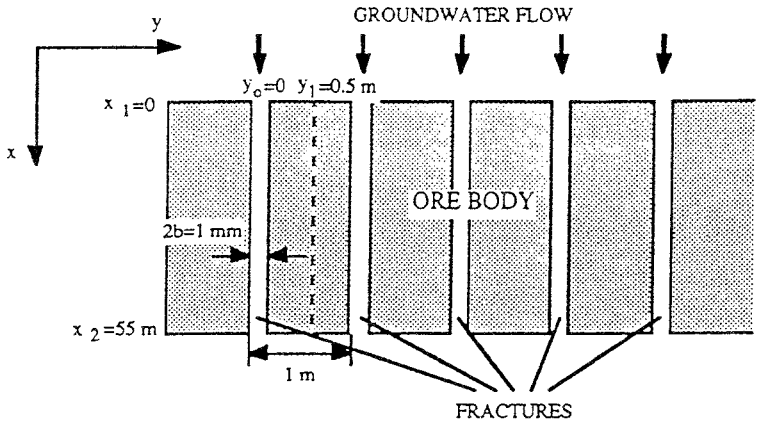

FIGURE 3.133 Plan view of fractures in the mineralization.

At steady state, the diffusion in the pores of the mineralization from the fracture surface is described by

$$D_o \frac{\partial^2 c_o}{\partial y^2} + q - \lambda c_o = 0 \tag{23}$$

The equation for conservation of mass in the fracture is:

$$v_f \frac{\partial c_f}{\partial x} = \frac{D_o \varepsilon_o}{b} \left(\frac{\partial c_o}{\partial y} \right)_{y=0} - \lambda c_f \tag{24}$$

The boundary conditions for these two equations are:

$$\frac{\partial c_o}{\partial y} = 0 \qquad \text{at } y_1 \tag{25}$$

$$c_o = c_f \qquad \text{at } y_0 \tag{26}$$

$$c_o = c_f = c_{in} \qquad \text{at } x_1 \tag{27}$$

The following solution gives the concentration profile along the fracture:

$$c_f = A + (c_{in} - A) \exp (-Bx/v_f) \tag{28}$$

where A and B are two constants depending only on the various parameters.

3.9.4.4.4 Calculated results

The PDE's are solved by the numerical code TRUCHN, a development of TRUMP (Lawrence Livermore Laboratory, the University of California) based on an Integrated Finite Difference Method (IFDM). Three nuclides of nuclear reaction production, i.e., ^{3}H, ^{14}C and ^{36}Cl are included in the calculations. Tables 3.80 and 3.81 list the data used in the calculations.

TABLE 3.80
TRANSPORT DATA USED IN THE CALCULATIONS

	Mineral-zation	Clay	Altered sandstone
Hydraulic conductivity (m/s)	$1.0x10^{-8}$	$1.0x10^{-8}$	$1.0x10^{-5}$
Hydraulic gradient (mH_2O/m)		0.01	
Porosity	0.1	0.1	0.15
Diffusivity (m^2/s)	$1.5x10^{-9}$	$1.5x10^{-9}$	$1.5x10^{-9}$

The hydraulic-head distribution in the mineralization, clay and altered sandstone is illustrated in Figure 3.134. Figure 3.135 shows the 3D diagrams of the concentration distribution of ^{3}H and ^{14}C.

TABLE 3.81
GENERATION RATES AND DECAY CONSTANTS

	^{3}H	^{14}C	^{36}Cl
Generation rate (based on water volume in the pores)	$1.52x10^{-6}$ (TU/s)	$1.73x10^{-8}$ (pmC/s)	$5.07x10^{-20}$ ($mol/m^3.s$)
Decay constant (1/s)	$1.79x10^{-9}$	$3.84x10^{-12}$	$7.09x10^{-14}$

The surface contour of ^{36}Cl is similar to that of ^{14}C. The concentration profiles of ^{3}H, ^{14}C and ^{36}Cl at the middle and at the end of the mineralization (x=36.8 m and x=59.8 m, respectively) are shown in Figure 3.136. The downstream concentration profiles near the bottom of the mineralization are shown in Figure 3.137.

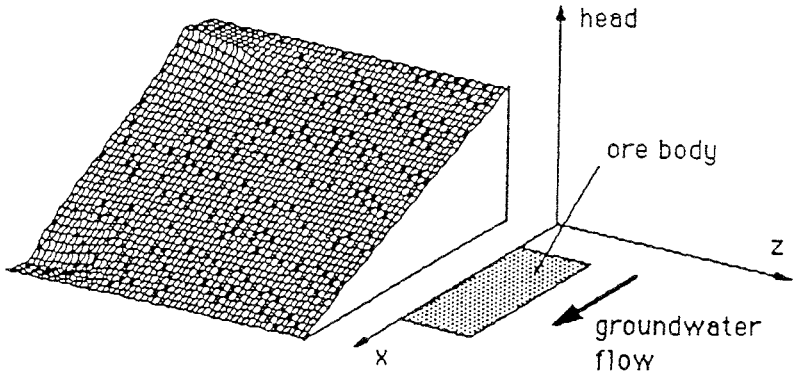

FIGURE 3.134 Groundwater hydraulic head distribution.

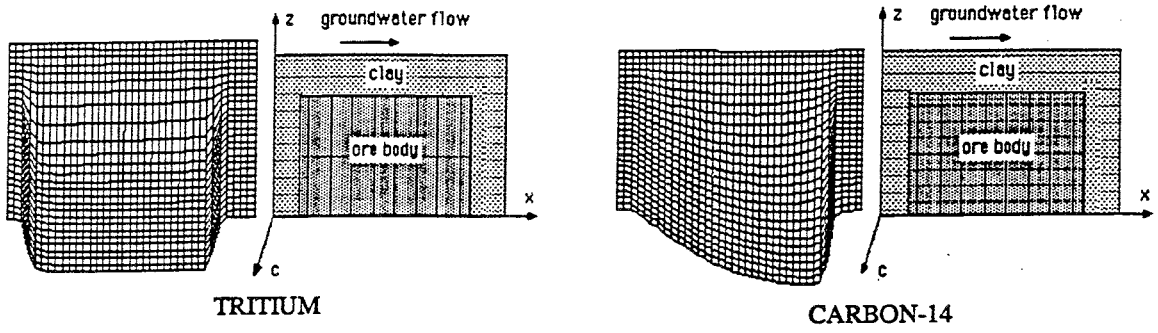

FIGURE 3.135 Three dimensional distributions of ^{3}H and ^{14}C concentrations.

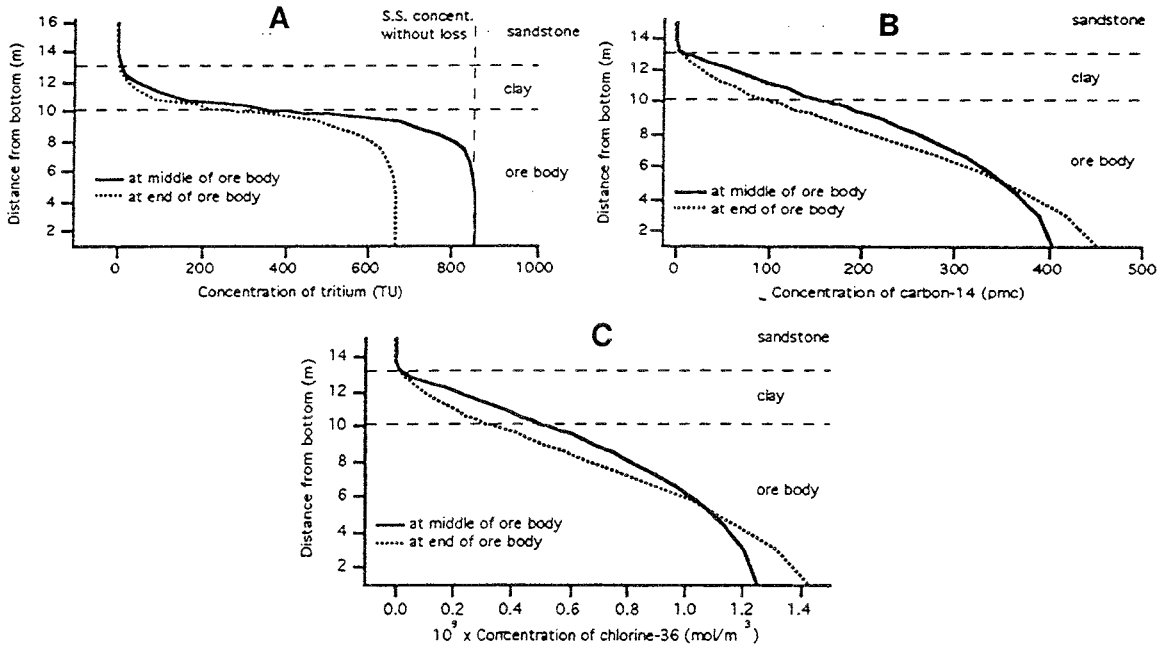

FIGURE 3.136 Concentration profiles in the middle (at x=36.8 m) and at the end (at x=59.8 m) of the mineralization. **A**: ^{3}H. **B**: ^{14}C. **C**: ^{36}Cl.

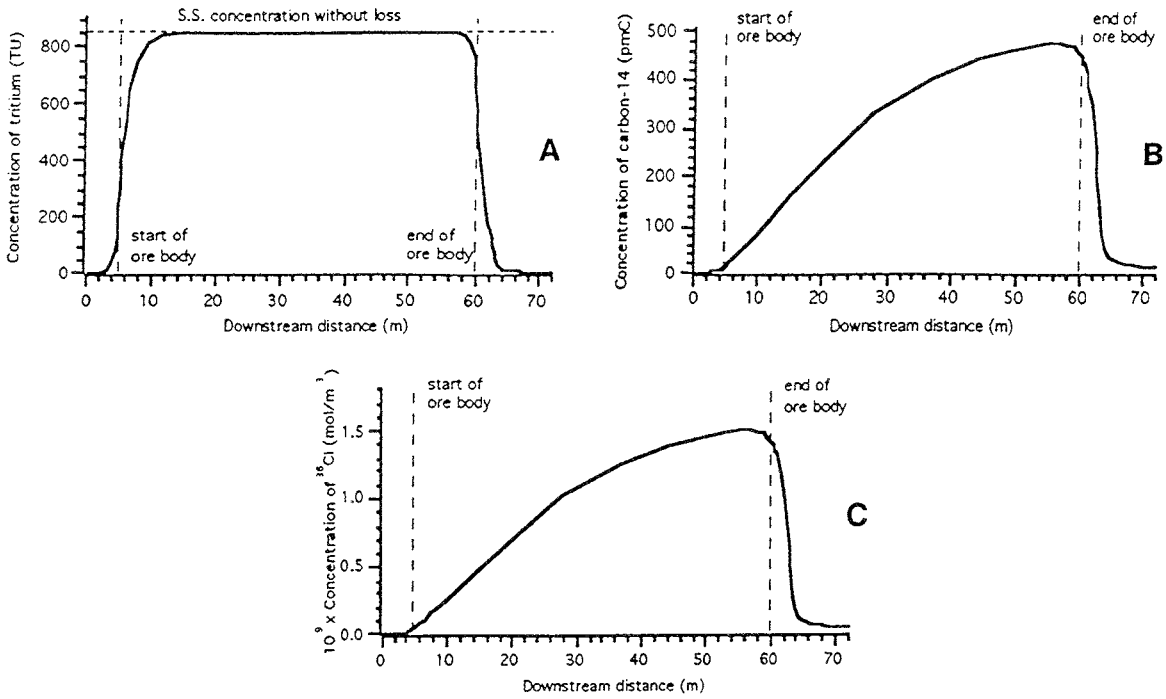

FIGURE 3.137 Downstream concentration profiles near bottom of model system (at z=1.05 m). **A**: ^{3}H. **B**: ^{14}C. **C**: ^{36}Cl.

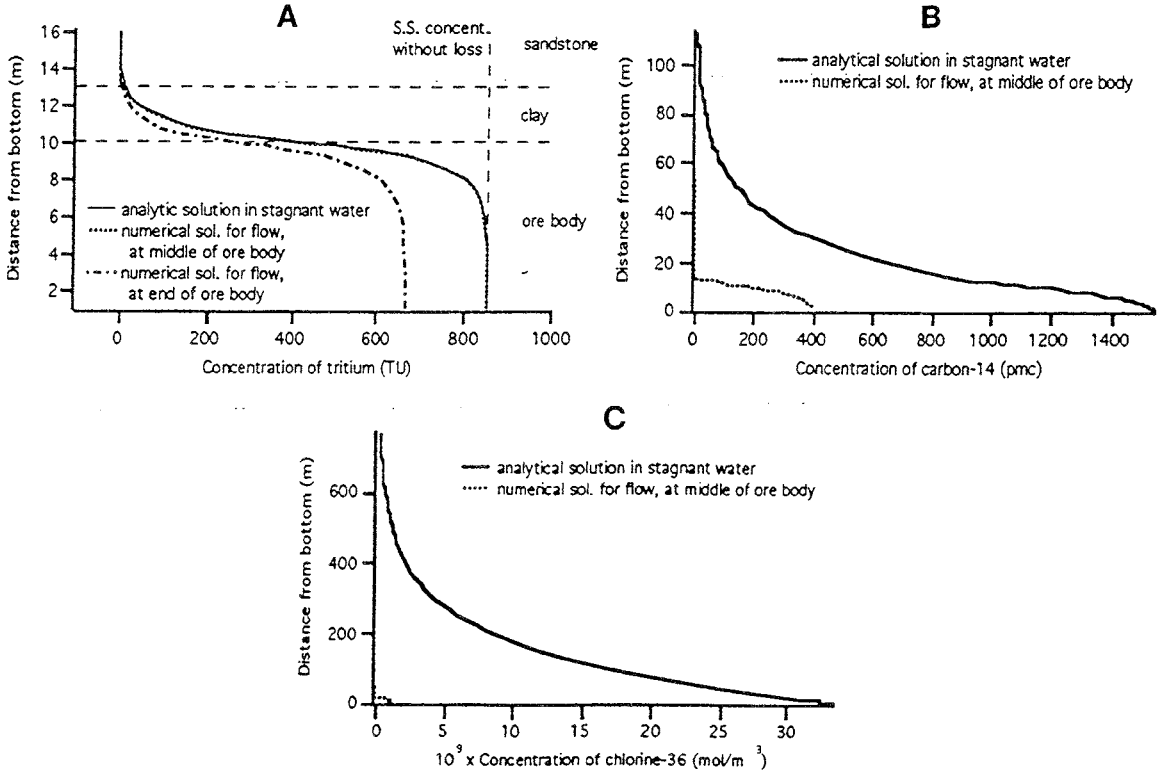

FIGURE 3.138 Results of scoping calculation (diffusion in stagnant water). **A**: ^{3}H. **B**: ^{14}C. **C**: ^{36}Cl.

The results of the scoping calculation from Equations (20) and (21) are shown in Figure 3.138, in which the concentration profiles from the numerical solution of Equations (16) and (17) are also shown for comparison. The calculated amounts of radionuclides carried out of the mineralization by groundwater are compared for both the fractured and unfractured scenarios in Table 3.82.

TABLE 3.82
RADIONUCLIDE LOSS BY FLOW (PERCENT OF GENERATED)

	^{3}H	^{14}C	^{36}Cl
Fractured mineralization	1.0	90.0	99.8
Homogeneous mineralization	1.5	91.0	97.3

3.9.4.4.5 Discussion

The calculation for ore comprizing 20 % U shows that the concentration of ^{3}H is high in the middle of the mineralization (850 TU) and equal to the steady-state concentration without any advection or diffusion loss, assuming a 100 % radionuclide escape from rock to water. This value is higher than the highest measured data, i.e., 105 TU and 281 TU in groundwater from piezometers 198 and 220, respectively. One explanation is that the samples were diluted when they were collected; another explanation is that the assumed 100 % escape of the radionuclide from the rock to the water might not take place. This high concentration, however, is only confined in the mineralization and clay. The concentration of ^{3}H is reduced to a very low level outside the clay. About 98.5 % of the generated ^{3}H is depleted by decay within the mineralization.

The decay rates for ^{14}C and ^{36}Cl are relatively slow. Most of the generated amount is released outside the mineralization by groundwater flow and diffusion before complete decay in the mineralization. The concentrations of ^{14}C and ^{36}Cl are thus much lower than the steady-state concentrations without any advection and diffusion loss. Although the release percentage is high, concentration profiles of ^{14}C and ^{36}Cl are still mainly bound within the clay.

As the hydraulic conductivities of the mineralization and clay are much lower than that of the altered sandstone, the groundwater flow is deflected up and over the mineralized and clay zones flowing through the altered sandstone. On the other side of the mineralized and clay zones, the downward flow of groundwater in the altered sandstone confines the radionuclides to a narrow downstream layer adjacent to the bottom. Even in this narrow layer the predicted concentrations of the radionuclides are very low. The calculated results predict a 2.1-m-thick layer 12 m downstream from the mineralization containing average concentrations of 5.55 TU for ^{3}H, 14.2 pmC for ^{14}C, and 4.48×10^{-11} mol/m^3 for ^{36}Cl, respectively. The concentrations drop off rapidly above this layer. Detection of the radionuclides at such low levels would be very difficult.

3.9.4.4.6 Notations used in Model 3

The notations used in the formulation and equations for Model 3 are listed in Table 3.83.

TABLE 3.136
NOTATIONS FOR MODEL 3

Symbol	Description	Unit
b	Half aperture of fractures	m
c	Concentration of radionuclide	mol/m^3
D	Pore diffusivity of radionuclide	m^2/s
H	Ground water flow head	m
K	Hydraulic conductivity	m/s
q	Radionuclide generation rate	$mol/m^3.s$
t	Time	s
v	Groundwater flow velocity	m/s
x	Horizontal co-ordinate parallel to groundwater flow	m
y	Horizontal co-ordinate perpendicular to groundwater flow	m
z	Vertical co-ordinate	m
ε	Porosity	
λ	Radionuclide decay rate	1/s

Subscript	Description
c	in clay
f	in fractures
in	start of mineralization
o	in mineralization
s	in altered sandstone
ss	steady state without advection and diffusion

3.9.4.5 References

CARSLAW, H.S. and JEAGER, J.C. 1959. Conduction of Heat in Solids. Oxford University Press, 2nd edition.

CHAPMAN, N.A., McKINLEY, I.G., PENNA FRANCA, E., SHEA, M.E. and SMELLIE, J.A.T. 1992. The Poços de Caldas Project: an introduction and a summary of its implications for radioactive waste disposal. J. Geochem. Explor., **45**, 1-24.

CRAMER, J.J. and SMELLIE, J.A.T. 1990. Proceeding of the first workshop. In *Annual Report of the AECL/SKB Cigar Lake Project - Phase I: 1989-1990.* Atomic Energy of Canada Limited Internal Report, **CLR-90-02**.

CROSS, J.E., HAWORTH, A., LICHTNER, P.C., MacKNENZIE, A.B., MORENO, L., NERETNIEKS, I., NORSTROM, D.K., READ, D., ROMERO, L., SCOTT, R.D., SHARLAND, S.M. and TWEED, C.J. (ed. I.G. McKinley). 1990. Testing models of redox front migration and geochemistry at the Osamu Utsumi mine and Morro do Ferro analog sites, Poços de Caldas, Brazil. Poços de Caldas Report **12**; NAGRA Tech. Rep., **NTB 90-30**, Wettingen, Switzerland; SKB Tech. Rep., **TR 90-21**, Stockholm, Sweden; UK-DOE Tech. Rep., **WR 90-052**, London, U.K..

DAVID, L.P., DONALD, C.T. and PLUMMER, L.N. 1980. PHREEQE - A computer programme for geochemical calculations. U.S. Geological Survey Rep., **PB81 167801**.

GARISTO, N.C., CRAMER, J.J., LIU, J. and CASAS, I. 1991. Modelling of uranium-ore dissolution and uranium migration in the Cigar Lake deposit. In *A\ECL/SKB/USDOE Cigar Lake Project, Progress Report for the period May - October 1991* (eds. J.J. Cramer and J.A.T. Smellie). Atomic Energy of Canada Limited Internal Report, **CLR-91-05**.

HAWORTH, A., SHARLAND, S.M., TASKER, P.W. and TWEED, C.J. 1988. A guide to the coupled chemical equilibria and migration code CHEQMATE. Harwell Laboratory, UK-Atomic Energy Agency Report, **NSS-R 113**.

KBS, 1983. Final storage of spent nuclear fuel KBS-3. Swedish Nuclear Fuel Supply Co/Division KBS, May, 1983.

LAPIDUS, L. and PINDER, G.F. 1982. Numerical Solution of Partial Differential Equations in Science and Engineering. John Wiley & Sons, New York.

NERETNIEKS, I. 1980. Diffusion in the rock matrix: an important factor in radionuclide retardation? J. Geophys. Res., **85/B8**, 4379.

NERETNIEKS, I. 1985. Diffusivities of some constituents in compacted wet bentonite clay and the impact on radionuclide migration in the buffer. Nucl. Technol., **71**, 458.

SMELLIE, J.A.T., PERCIVAL, J.B. and CRAMER, J.J. 1991. Mineralogical and geochemical database for the major lithological and hydrothermal subdivisions of the Cigar Lake uranium deposit. Atomic Energy of Canada Limited Internal Report, **CLR-91-04**.

ZHU, M. 1988. Some aspects of modelling of the migration of chemical species in groundwater systems. Licentiate Thesis, Dept. of Chem. Engin., Royal Institute of Technology, Stockholm, Sweden.

3.9.5 Conclusions
(N. Chapman)

3.9.5.1 Role of colloids, microbes and organic species in radionuclide migration

The significance of colloids, organic species and microbes has been suggested, with varying degrees of conviction, to contribute to the uncertainties in performance assessment studies, which have generally modelled radionuclide mobilization and transport as processes involving only inorganic solution geochemistry. Whilst clearly an important feature of near-surface processes, most safety assessments in the last decade have suggested that all three factors are likely to be of only limited consequence in a deep groundwater system, unless the repository itself contributes significantly to the populations of these materials in the deep environment. These assumptions are often based on laboratory data, and are not very conservative in safety terms. Observations from natural systems such as Cigar Lake are helping to put the role of these materials in a more quantitative framework.

- All three materials are present in all the groundwaters studied at the site, regardless of depth or geochemical environment. As noted in Sections 3.6 and 3.7, however, none appear to contribute significantly to radionuclide transport. As far as colloids are concerned, the issue of their overall potential to short-circuit solute transport calculations cannot, however, be said to have been resolved unequivocally. The presence of colloids exhibiting irreversibly fixed radionuclide contents, even though the time scale of fixation is relatively short (in the order of thousands of years), continues to tease the safety assessor. The fact remains that Cigar Lake, in common with all analog studies to date, has found no real evidence for substantial deep transport of radionuclides by colloids. The weight of evidence against such transport thus continues to grow, but such is the potential significance of the issue that it will require a larger body of information from similarly well-characterized systems, in particular providing clear, case-by-case explanations as to why transport has been prevented, before colloid transport can be excluded with confidence from a performance assessment.

- The importance of microbes in repository behaviour has been a contentious issue since it was first raised more than a decade ago. The results from Cigar Lake support the now more-or-less accepted view that, although microbial activity is unlikely to have any additional deliterious effect on the performance of materials in a deep spent-fuel repository, the ubiquitous presence of microbes does need to be taken into account when interpreting deep hydrogeochemistry and when modelling near-field geochemical processes, since they can take part in mediating redox reactions in particular.

- Similarly, the presence of organic species (fulvic acids), even in deep groundwaters, needs to be recognized and accounted for. Although they

have not contributed to uranium transport at Cigar Lake, the organic content of all groundwaters from a repository site needs to be characterized equally thoroughly so that their impact can be quantified and included in or excluded from an assessment.

3.9.5.2 Testing solubility and speciation codes

Blind testing of the thermodynamic modelling approach to predicting solution concentrations of trace elements has now been used several times at natural analog sites. The degree of success depends very much on the amount of field characterization data available. Each exercise reveals, and enables the resolution of, new issues, with the result that the approach is being progressively refined. Cigar Lake is the latest in this sequence, and has shed particular light on uranium behaviour (see Section 3.9.2), as well as on efforts to equate different methods of estimating Pu and Tc concentrations.

- Pu and Tc are, of course, of considerable interest in performance assessment because of their long half-lives and radiotoxicity. However, as no concentration data were available from the Cigar Lake site it is possible only to compare the predictions of one model with those of another; the thermodynamic model predictions of solubility are in reasonable agreement with concentrations predicted by nuclear production models (see Section 3.8.2). It has not been possible to measure concentrations of these elements to make a direct comparison. While the thermodynamic predictions for Pu concentrations can be argued, with reasonable conviction, to be generally conservative, it is debateable whether a performance assessment would actually use this approach to estimate solubilities. In the far field the concept of the existence of a solubility-limiting solid phase for Pu and Tc is clearly inappropriate. Also, whilst this concept may be a reasonable assumption in the matrix of spent fuel, it is probably equally unlikely in other parts of the near field. Overshadowing even these limitations is the question of whether the assumptions of classical thermodynamic equilibrium laws are, in any case, applicable at such exceptionally low concentrations in solution. The drawbacks to the approach are very evident for Tc, where no real agreement of the two models was found for this highly redox-sensitive element. The conclusion on applying the thermodynamic solubility approach to these two elements is, essentially, that it would be unsatisfactory in a performance assessment, apart from helping to establish the source term for spent fuel.

- As noted in Section 3.9.2, results for the other elements were variable in terms of the proximity of predicted to measured concentrations, and the best agreement was found for elements having the best thermodynamic data. From an overview perspective it must be said that the totality of these results does not give confidence in the unsupported use of thermodynamic predictions of radionuclide concentrations for performance assessment purposes. If similar-quality hydrogeochemical and

mineralogical data from a real prepository site had been combined with the existing thermodynamic databases, then the trace-element concentrations predicted would have produced substantial errors if used in a safety assessment. Moreover, these errors are of widely varying magnitude and significance, some being highly unconservative in safety terms. Now, it might be countered that such predictions would not be used, as the supporting field or thermodynamic data are inadequate. However, it is only with hindsight, when there are actual concentrations available with which to compare, that it is possible to pinpoint the poor predictions, and the reasons for them. This, of course, is where analog studies such as the one at Cigar Lake are of great value, as they allow progressive refinement of our understanding of trace metal hydrochemistry. Nonetheless, it is tempting to ask precisely how much data, and of what quality, would be considered acceptable before we would be reasonably confident in a truly "blind" prediction for actual safety assessment use at a real site. The quantitative incorporation of uncertainties of this kind into the geochemical aspects of performance assessment is at a very early stage of development.

- One of the reasons for the patchy performance of the blind predictions was the availability of geochemical data at the site. Three issues are highlighted which should be borne in mind both for future analog studies and for repository site characterization. First, the presence and nature of mineral and amorphous phases controlling trace-element solubilities is difficult to characterize and perhaps requires special study. There are frequent mismatches between phases observed and those indicated by the thermodynamic calculations or selected by the modeller. Second, the development or application of analytical techiques with lower detection limits would help considerably in constraining the thermodynamic predictions. Finally, few analog studies have so far been able to provide more than token data on the speciation of trace elements in groundwaters. Again, there is a problem with the availability of comprehensive analytical techniques, but advances in this area would help the modelling of radionuclide transport considerably.

3.9.5.3 Evaluating spent-fuel dissolution models

Cigar Lake is one of the few analog sites where it is possible to test spent-fuel dissolution models under representative conditions of sustained low groundwater flow rate and reducing chemical conditions. It is particularly interesting as there is evidence suggesting the existence of radiolytic oxidation, as predicted to occur in a waste repository.

- The thermodynamic database as well as the understanding of the aqueous geochemistry of uranium are better developed than for many of the other elements studied in the solubility-speciation project discussed in Section

3.9.5.2 above. For example, it was easier to confirm the nature of the likely solubility-controlling phase (U_3O_7) for uranium. Consequently, predictions of uranium solubility were more generally successful, and usually erred on the side of conservatism in safety assessment terms. As with the other elements, limitations on our ability to determine *in situ* aqueous speciation prevented the resolution of questions arising from the use of alternative databases, which indicate different species dominating solution chemistry. Further advances in this area, using natural analogs as test beds, would be valuable.

- Perhaps the most useful finding for performance assessment concerns the raising of the threshold Eh value above which the dissolution behavior of uraninite (and, consequently, spent fuel) switches from simple dissolution under reducing conditions to surface oxidation and concurrent dissolution (*oxidative dissolution*, which proceeds much more swiftly). This effectively extends the area of redox space in which spent fuel will remain very stable and predictable in behaviour or, conversely, makes current models of fuel dissolution more conservative than had been appreciated. In the Cigar Lake mineralized zone, it was insufficient to reach the threshold Eh value at which the uraninite itself would be attacked, although radiolysis of water in contact with the uraninite may have occurred to an extent sufficient to oxidize iron in the contact zone between the ore and the surrounding clay. The ore has thus remained very stable for an exceptional period of time. Had the threshold Eh value been that currently used in spent-fuel dissolution models, then the ore would have been dissolved and dispersed soon (in geological terms) after its formation. The quantitative significance of these findings on the calculated dissolution rates of spent fuel in a performance assessment depends on the radiation flux and the extent of radiolysis, but it appears that calculations to date are likely to have overestimated releases, both of uranium and of other radionuclides whose dissolution rate would be enhanced in a spent-fuel matrix that had been structurally modified by oxidative dissolution.

3.9.5.4 Evaluation of mass transport models

The very nature of the Cigar Lake site, with little evidence for uranium migration from the mineralization, has made it impossible to carry out any realistic modelling of radionuclide transport as would be performed in the far-field component of a repository safety assessment. However, the close schematic parallels between a container of spent fuel surrounded by bentonite and the Cigar Lake mineralization, locally invested with a partially oxidized clay halo made this an obvious location for modelling the barrier functions of the clay to surrounding groundwater flow, and the nature and movement of a redox front. A number of useful findings were made with respect to modelling processes that are of significance in the near field of a spent-fuel repository.

- Recent performance assessment work in the SKB-91 project has suggested that radionuclide releases are rather insensitive to groundwater fluxes in the rock around the near-field clay. The simple analytical model used at Cigar Lake to evaluate unretarded transport from the ore through the clay tends to support this suggestion; the role of the clay in controlling uranium release from the ore is considerably greater than the effect of flow variation in the sandstone host rock.

- It has been possible to apply a number of codes and databases often associated with performance assessment work (e.g., CHEQMATE, TRUCHN, HATCHES) to the Cigar Lake near-field. As noted earlier, none of these codes has actually been tested in this work, in the sense of being used predictively, but it has been possible to demonstrate their suitability for modelling this type of geochemical system, for example, by using them to replicate and, to some extent, to help explain some of the field observations. In addition, it has been possible to use the more complex coupled models to define the extent to which simpler analytical models can be used to describe processes in the same system.

- In general, confidence in the utility of all the models in describing near-field processes has been increased, although there remain many specific issues of uncertainty in the interpretation of such complex geochemical systems. It proved necessary to use both simplifying assumptions and a number of estimated parameter values, and the results did not always provide unambiguous interpretations; for example, even though substantial progress has been made at Poços de Caldas and Cigar Lake, redox-front propagation is not yet easily modelled, and the esentially unavoidable use of a geochemical equilibrium approach is well known to be an approximation with poorly quantifiable consequences. At present then, although these types of mass transport models shed considerable and increasing light on the near field, they must be treated cautiously if they are to be applied in a predictive fashion in a safety assessment.

4. SUMMARY OF RESULTS AND CONCLUSIONS

(J. Cramer and J. Smellie)

4.1 DATABASES AND CONCEPTUAL MODELS

The **geological** and **hydrogeological databases** for the Cigar Lake deposit consist mainly of the vast collection of information, data and reports collected and produced by the exploration and mining companies. A large amount of work was done on the geological and hydrogeological characterization of the site, including geological, geochemical, petrological, mineralogical, geophysical, hydrological and geotechnical studies, as well as some studies of the Quaternary geology. This work involved the drilling of over 200 boreholes, conducting in-hole measurements and experiments, installing tens of piezometers, carrying out pump tests and excavating a shaft and horizontal drifts. Additional hydrogeological data were also collected as part of this analog study.

The **mineralogical** and **lithogeochemical database** was compiled from the existing mineralogical and geochemical data available with the mining company, from a PhD study on the clay mineralogy and geochemistry in this deposit (Percival 1990), and from additional work carried out as part of the analog study.

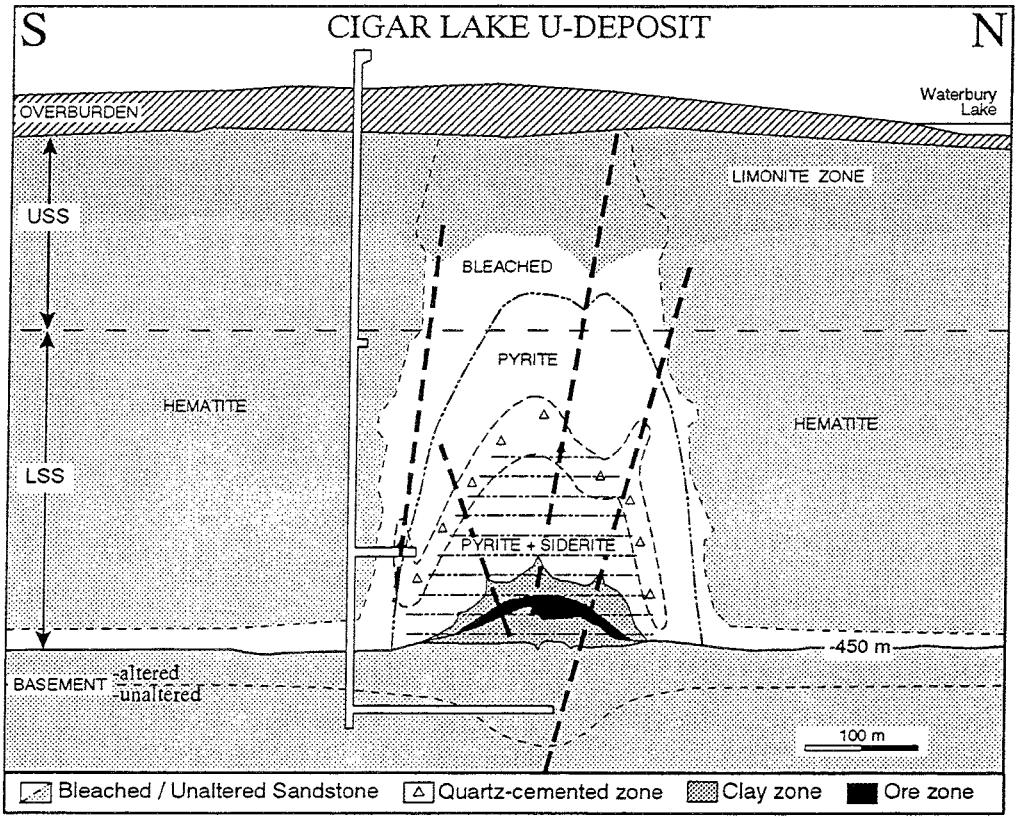

FIGURE 4.1 Schematic cross section through the Cigar Lake deposit showing the uranium mineralization and its host rocks, including the lithologic characteristics related to hydrothermal alteration and weathering. (USS= upper sandstone; LSS= lower sandstone).

The set of **reference groundwater compositions** was produced from an extensive hydrogeochemical database collected by AECL over a period of 7 years, during which time samples were collected regularly from surface- and groundwaters at the site. This carefully reviewed reference set was produced primarily for all the modelling activities of the project to provide representative compositions for all the lithological units and for the overburden.

The **conceptual geological model** is illustrated in the schematic cross section of Figure 4.1, which shows the various lithological, mineralogical and structural units in the deposit. This south-to-north cross section represents the East Zone, the 800-m-long part of the deposit containing the richest and largest uranium mineralization. Its extension toward the west, the West Zone, is about 1,200 m long, but contains only about one third of the total ore reserve and has a less-extensive alteration halo in the sandstones. Because much of the exploration and test-mining effort was focussed on the East Zone, the best data are available for this part of the deposit; therefore, the modelling has been concentrated here.

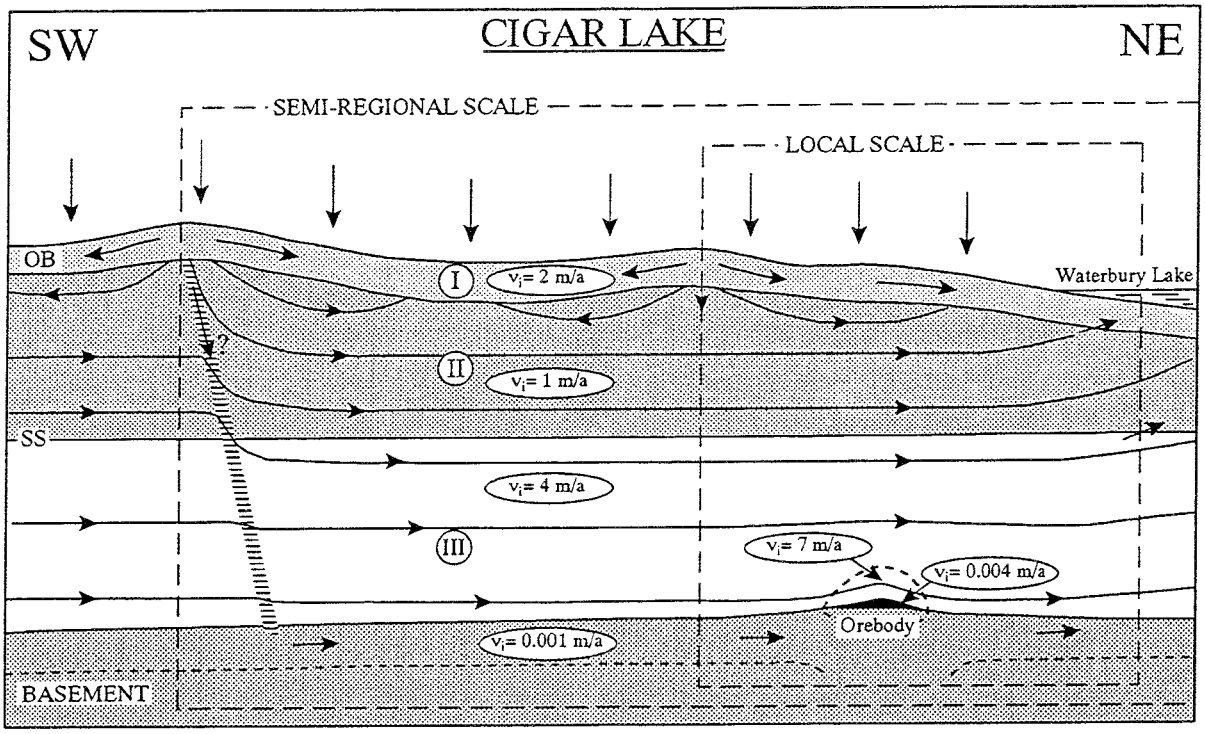

FIGURE 4.2 Schematic section through the Cigar Lake deposit showing the conceptual hydrogeologic model with three distinct flow regimes (I-III) and calculated particle velocities. An example of recharge along a fracture zone is schematically illustrated in the left side of the diagram. (OB= overburden, SS= sandstone).

Several conceptual hydrogeological models were already available at the onset of the AECL/SKB program. Further development of these models and analyses of existing data

were carried out, leading to the construction of 2D and 3D models both on a regional and local scale (Section 3.4). Maps of the hydraulic head and of particle velocities and tracks were produced, and sensitivity analyses were carried out on the boundary conditions, the geometry of the uranium mineralization and the material properties of the rocks.

The resulting **conceptual hydrogeological model** is illustrated by the schematic 2D section through the deposit, based on the 3D local model, in Figure 4.2. Three distinct flow regimes are shown: I) the local regime, restricted to the overburden; II) the intermediate regime, restricted to the Upper Sandstone unit; and III) the semi-regional regime, restricted to the Lower Sandstone unit. Some hydraulic interconnection occurs between each flow regime, primarily along faults or fracture zones. Also shown on the section in Figure 4.2 are the calculated particle velocities (v_i) for each lithologic unit. Note the very low velocities calculated for the clay and ore zones and for the regolith. Corresponding residence times for the clay and ore zones were calculated for particles released within the ore, and range between 18,000 and 85,000 a. These values correspond with residence times estimated from ^{36}Cl data for groundwaters from the ore zone.

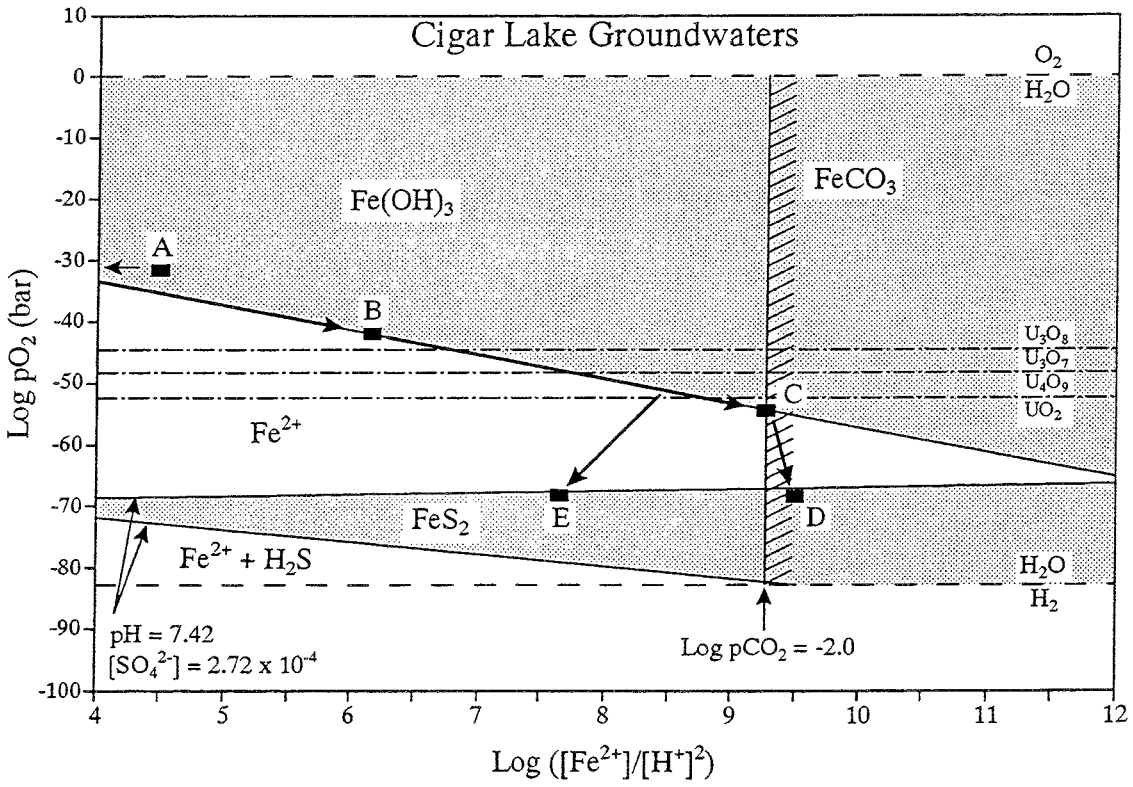

FIGURE 4.3 Redox diagram for water-rock interaction in the Cigar Lake deposit. Groundwater compositions evolve from A (overburden) to B (unaltered sandstone and limonite zone), to C (altered sandstone), to D/E (clay and ore zones). Semi-dashed lines represent stability boundaries for various solid uranium oxides. See text for further explanation.

The geochemistry and evolution of groundwaters at Cigar Lake are described in detail in Section 3.5. In general, the groundwaters in and around the uranium deposit are characterized by neutral to near-neutral pH (~6-8), by low contents of total dissolved solids (~60-240 mg/L), by decreasing redox potentials toward the ore zone (from about +0.25 to -0.25 V), and by overall low U content (usually «30 μg/L or $10^{-6.5}$ mol/L). Within the ore-zone groundwaters, marked increases in the contents of certain isotopes (e.g., ^{3}H and ^{36}Cl) are observed as a result of nuclear reactions occurring in situ.

The **conceptual hydrogeochemical model** for the evolution of groundwater compositions at Cigar Lake is illustrated by the redox diagram in Figure 4.3. This evolution is characterized by the interaction of the waters primarily with the clay and iron minerals in the rocks. Surface precipitation (rain and snow) reacts with illite and kaolinite, dissolving iron from various minerals in the overburden and producing a recharge water to the Upper Sandstone unit that is already equilibrated with the main clay minerals and is rich in iron (point **A** in Figure 4.3). Reaction of this oxidizing recharge water with the Upper Sandstone produces precipitation of ferrihydrites down to a depth of about 100 m, overprinting both the unaltered and bleached sandstone ("limonite" zone; **B** in Figure 4.3). Upon approaching the clay and ore zones of the deposit, subsequent reaction of the waters with Fe sulphides and siderite in the bleached sandstone reduces the oxidation potential of these waters (decreasing pO_2: **B→C→D/E** in Figure 4.3) to well within the UO_2 stability field. The redox-buffering capacity of the Fe sulphides in the ore and its host rocks plays an important role in maintaining reducing conditions, and thus preserves the stability of the uranium mineralization.

4.2 PERFORMANCE-ASSESSMENT-RELATED MODELLING

4.2.1 Thermodynamic codes and databases

Thermodynamic codes and their databases are tools used in the performance assessment of disposal concepts to provide two main types of chemical information: 1) solubility and 2) speciation of dissolved elements and radionuclides. The solubility of an element or radionuclide determines its release rate from a solid host phase under certain conditions, and the speciation of that element/radionuclide in solution provides information on its transport properties.

To test such codes, a series of "blind" predictions was carried out in a fashion similar to that described by Bruno et al. (1990). Compositions of representative groundwaters from the Cigar Lake deposit were used as input to predict the solubility and its limiting solid phase, and the speciation of U, Pu and other elements considered important in performance assessment. The codes and databases used include PHREEQE (Parkhurst et al. 1980), ZZ-HATCHES (Cross and Ewart 1991) and SKBPU (for Pu, Puigdomènech and Bruno 1991).

The results generally showed that the predicted solubilities are in reasonable agreement with the measured concentrations, in particular for those elements that have a good thermodynamic database (Section 3.9.2). Good agreement was found for U, Th, Ba and Cu. Limited success was found for Sr, Mo and As, mostly because of a lack of relevant thermodynamic data for the critical solubility-limiting phases, which resulted in the

concentration of the dissolved species being overpredicted. Similarly, the uncertainty in the redox potential for the Cr^{6+}/Cr^{3+} couple resulted in an underprediction of the concentration of the dissolved species. The analytical detection limits for Ni and Pb were insufficient to successfully predict their solubilities.

Further improvements to be considered for this evaluation exercise include a) a comparison of the thermodynamic databases used in each code, b) better detection limits for certain elements dissolved in the groundwaters, and c) measuring the speciation for the dissolved elements of interest.

4.2.2 Colloids, Organics and Microbes

Although theoretical considerations indicate that radionuclide mobility may be affected by the presence of particles (through sorption), dissolved organic compounds (through complexation) and microbial activity (through redox buffering), there is a very limited database on these processes in deep natural systems. The Cigar Lake deposit provides an opportunity to study these aspects in a deep natural system containing a relatively concentrated source of uranium and other radionuclides.

The **colloid studies** at Cigar Lake (Section 3.6; Vilks et al. 1988, 1993) were focussed on determining the concentration, size and composition of particles throughout the deposit, and on determining the trace-element and radionuclide sorption on the particles. Aspects of particle migration were addressed by determining particle-size distributions, looking for evidence of particle dispersion away from the ore zone, studying particle behaviour in a flow field, and assessing mechanisms of particle generation. The results of these studies include the following observations:

- In the case of reversible radionuclide sorption onto the particles, the average particle contents in the dilute Cigar Lake groundwaters are too low to have a significant impact on radionuclide migration.

- In the case of irreversible sorption, some radionuclides (e.g., U, Th, Ra) can remain fixed on particles for thousands of years (up to 8,000 a) and may thus contribute to radionuclide migration.

- A large portion of natural particles in Cigar Lake groundwaters are generated by erosion of fragments from minerals and alteration products from the host rock. Thus, particle concentrations are highest in friable rock and lowest in well-consolidated rock.

- The composition of groundwater particles in the ore zone is distinct from that in the host sandstone, indicating that the transport of particles from the ore through the clay zone has been negligible, and the mobilization of clay particles from the clay into the sandstone has not been important.

The studies at Cigar Lake lead to an overall conclusion that the role of colloids is not important in radionuclide migration, at least on a time scale of 10^4 a based on the 8,000-a-

old particles found in the ore zone waters.

The characterization of **organic compounds** in the Cigar Lake groundwaters (Section 3.7) included the determination of total organic carbon (TOC) in all waters, of volatile and solvent extractable organics and of humic compounds, and detailed characterization of fulvic acids (including ^{14}C ages). The results of these studies include the following observations:

- The TOC content in all surface and groundwaters is ≤ 2 mg/L, except in ore zone waters (up to ~ 11 mg/L). Volatile and solvent-extractable organics account for «10 % of the TOC (most of which are probably contaminants), and only 15 to 25 % of TOC are humic substances except in the altered sandstone (< 10 %) and in the ore zone (< 2 %).

- The humic fraction in all groundwaters consists largely of low-molecular-weight fulvic acid, with the oldest ^{14}C ages measured for humics from the ore zone (ranging up to 15,000 a).

- The abundance and complexing capacity of fulvic acids in all groundwaters is insufficient to have a significant influence on the speciation of either U^{4+} or U^{6+}.

From the studies at Cigar Lake, the overall conclusion on the role of organics is that the humics in the groundwaters are unlikely to play any significant role in either speciation or mobilization of uranium or any other actinide with a valency of ≥ 4.

Microbial studies on both water and rock samples from the Cigar Lake deposit (Section 3.7.4) were focussed on the identification and quantification of micro-organisms, and on evaluating the effect of microbial activity on the redox and uranium chemistry. The results of these studies include the following observations:

- Despite low nutrient contents in the groundwaters, micro-organisms are present in all groundwaters and seem capable of surviving in radiation fields.

- Anaerobe bacteria are, on average, about 10 times more abundant than aerobe bacteria, in agreement with the prevailing reducing chemical environment in the deposit.

- Sulphate-reducing, iron-related and denitrifying bacteria are common in both groundwaters and rocks from the most reducing parts of the deposit, and their mediation in redox reactions may contribute to the redox-buffering capacity of the system.

From the studies at Cigar Lake, the overall conclusion on the role of micro-organisms is that bacteria can survive in natural radiation fields and their activity may contribute toward maintaining a reducing chemical environment, thereby reducing the potential for dissolution and mobilization of redox-sensitive radionuclides.

4.2.3 UO_2 stability and Radiolysis

In both Canada and Sweden, the waste consists of used fuel made up of a crystalline UO_2 matrix that incorporates most of the fission and activation products from the nuclear reaction processes. The long-term stability of the UO_2 matrix under disposal conditions is thus of primary importance for the retention of both uranium and the contained nuclear reaction products inside the repository. The occurrence of "old" UO_2 (uraninite) minerals in the Cigar Lake deposit containing both natural-decay and natural-fission products provides an excellent opportunity for an analog study on UO_2 stability and on what controls this stability.

Canada and Sweden, in their respective performance assessment codes, have different models for the dissolution of the UO_2 matrix and the resulting release of radionuclides from the fuel waste. In Canada, the dissolution model is based on congruent dissolution of the UO_2 matrix through limited oxidation of UO_2 to U_4O_9-U_3O_7 (Johnson et al. 1994). Thus, the analog information being sought for this UO_2-dissolution model includes whether UO_2 is a stable phase and under what conditions, whether UO_2 has suitable low solubility, whether dissolution of UO_2 occurs congruently, and what the retention capability of UO_2 is for natural-decay and natural-fission products. In Sweden, the dissolution model is based on radiolysis-induced oxidation of UO_2 proceeding beyond the U_3O_7 stage (SKB 1992). When oxidation proceeds beyond U_3O_7, the corresponding change in the crystal structure strongly affects the release of radionuclides from the UO_2-U_3O_7 fuel matrix. Therefore, to further test the Swedish model, additional analog information would include evaluating the occurrence of radiolysis in the Cigar Lake deposit, its potential effects on UO_2 stability, and, in the case of dissolution, the predominant speciation of dissolved uranium.

Characterization studies of the uranium minerals from the Cigar Lake ore zone (Sunder et al. 1988, 1992) show that uraninite (natural UO_2) exposed to interaction with fluids and/or groundwaters has a surface-oxidation layer of micro-crystalline U_4O_9-U_3O_7, corresponding to U^{VI}/U^{IV} values in the range of 0.20 to 0.57 (as determined by XPS) and to dissolved-U concentrations of $< \sim 10^{-7}$ mol/L (as measured in groundwaters from the ore zone). This information indicates reducing conditions for the natural water-rock interaction, and corresponds to the low redox potentials measured in present-day groundwaters (Eh $< \sim 0.2$ V; Section 3.5.4). Thus, the dissolution, and therefore the stability, of UO_2 appears to be controlled by a thin surface layer of higher oxides (up to U_3O_7). This is supported by **a)** experimental work and theoretical considerations (e.g., Shoesmith and Sunder 1991; Garisto and Garisto 1986) showing that the oxidative dissolution rate of UO_2 does not become significant until it is oxidized beyond the $UO_{2.33}$ (U_3O_7) stage, and **b)** the predictive calculations (using measured groundwater compositions) of the uranium phases at equilibrium, which mostly give U_3O_7 with some overlap to U_4O_9 (see also Section 4.2.1).

Geological, geochronological and petrological information shows that the oxidation layers observed on exposed uraninite surfaces resulted from only a few discrete, major disturbances, of which the youngest can be dated at 293 Ma (Cumming and Krstic 1992). Thus, the composition of the uranium minerals observed in the ore zone today reflects the result of water-rock interaction over a period of millions of years. The composition of the

uraninites is characterized by a) $^{234}U/^{238}U$ and $^{230}Th/^{234}U$ activity ratios ranging between 0.98 and 1.00, and 1.05 and 1.11 respectively (Section 3.5.3), b) high contents of radiogenic Pb (Section 3.3.4; Cumming and Krstic 1992), and c) relatively high contents of ^{129}I and ^{239}Pu from naturally occurring nuclear reactions (Section 3.8.2). These three characteristics suggest both good retention of the isotopes in the natural-UO_2 matrix, and congruent dissolution of the matrix, at least over a period of 10^6 a.

The redox conditions of current water-rock interaction in the mineralized zones at Cigar Lake are controlled mainly by the Fe^{2+}/Fe^{3+} redox couple and are buffered by Fe-sulphides (pyrite/marcasite) and siderite (Section 3.5.4). The corresponding measured redox potentials of $< \sim 0.2$ V thus favour the solubility-controlled dissolution of UO_2, which is in agreement with calculated redox potentials of > 0.2 V (also using pyrite and siderite) required for oxidative dissolution of UO_2 (Section 3.9.3). This suggests that any radiolysis occurring in the Cigar Lake ore zone does not have a strong effect on the redox potential. In fact, calculations using SKB's current radiolysis models with a threshold redox potential of 0.12 V for UO_2 dissolution show that the Cigar Lake ore should have been totally oxidized within 18 to 170 Ma. As this is not the case, and as recent development of SKB's radiolysis models suggests, the 0.12-V threshold potential appears to be unreasonably low; the 0.2-V potential would allow a more realistic treatment of radiolysis effects. This is further supported by recent experimental work (Sunder et al. 1992) indicating that oxidative dissolution of UO_2 does not become important until the redox potential reaches values above -0.1 V versus SCE or +0.14 V versus SHE.

Model calculations for different radiolysis scenarios in the deposit were carried out (Section 3.8.4) to test a model for the formation of the red clay/ore contact. This model explained the red colouration (from precipitation of ferrihydrites) through scavenging of radiolysis-produced oxidants by dissolved Fe^{2+} in the ore-zone waters (Cramer 1986). Although the calculations confirm that products from α-radiolysis of water can oxidize dissolved Fe^{2+} to Fe^{3+}, it is uncertain whether the ferrihydrites (and hematite) in the clay/ore contact can be accounted for by this process. In fact, the initial model scenario, based on α-radiolysis, had to be revised to also consider γ-radiolysis when it was observed that most of the uranium ore is encapsulated inside the clay matrix of the ore zone. The alternate scenario includes groundwaters being subjected primarily to γ-radiation inside the more permeable, and more common, water-bearing horizons or fractures instead of the water having large areas of direct contact with the ore minerals as required for significant α-radiolysis.

The conclusions of the radiolysis modelling are that the effects of α- and/or γ-radiolysis are insufficient to cause significant oxidation of the UO_2, even when integrated over the lifetime of the deposit (Section 3.8.4). This is supported by the observations, mentioned earlier, that major dissolution and mobilization of uranium occurred since the ore was formed during distinct events in which the system underwent major perturbations. However, the extent of radiolysis taking place in the steady-state system of the ore zone is still an open question, and what causes the red oxidized clay/ore contact is also unresolved at this time. The established importance of dissolved Fe^{2+} as a fast oxidant-scavenger, combined with the measured high concentrations of dissolved H_2 in groundwaters from the ore zone (Section

3.5.4), suggest that, if radiolysis takes place locally and only on a minor scale, the natural system of clay and ferrous minerals can buffer the redox potential to maintain reducing conditions to well within the stability field of UO_2. Therefore, the net changes resulting from radiolysis are probably overestimated considerably in SKB's current performance assessment models based on radiolytic oxidation of UO_2 fuel waste.

4.2.4 Mass-transport modelling

One of the objectives for the detailed litho- and hydrogeochemical studies on the Cigar Lake deposit was to identify the occurrence and location of radionuclide migration from the mineralized zones. However, no evidence was found from studies of the ore-clay-altered sandstone sequence of significant radionuclide migration taking place, either currently or during the recent ~ 1-Ma history of the deposit. In contrast, active radionuclide migration may occur at shallower depths as the result of lateral groundwater flow through the limonitic and bleached sandstones (see Figures 4.1 and 4.2). To test this hypothesis, uranium-series data (Section 3.2.2) for rock samples from potential transport paths (i.e., fractures and obviously permeable horizons) in the ore, clay and altered sandstone units were obtained. The uranium-series data indicate that some mobilization of uranium, and possibly radium, has taken place, but only on a small, localized scale (i.e., both preferential removal and deposition of isotopes occur side by side). This is supported by the isotopic composition of the reducing groundwaters (from the permeable zones) in these rock units (Section 3.5.3), where high $^{234}U/^{238}U$ values likely result from α-recoil rather than from dissolution processes. Furthermore, the amounts of dissolved uranium and other radionuclides in groundwaters from either side of the clay zone can be compared to give concentration gradients across the clay zone that are positive, zero and negative. Thus, the general conclusion with regard to radionuclide migration at Cigar Lake is that any modelling of mass transport in the deposit must be considered as being only hypothetical.

Although mass transport is included in current performance assessment codes (e.g., SKB), there were no specific mass transport models available that could be directly tested in the Cigar Lake analog study. Therefore, a series of iterative, generic models had to be developed for potential mass-transport scenarios in the Cigar Lake deposit (Section 3.9.4). These generic models are based on the assumption that any potential radionuclide migration takes place from the ore zone through the clay zone to the aquifer in the altered sandstone (i.e., a positive concentration gradient across the clay zone). The models that were developed consider a range of scenarios for the source term and transport processes, including solubility-controlled and oxidative dissolution of UO_2, diffusion and advection, and coupling of mass-transport and geochemical processes. The results from this generic modelling include the following general conclusions:

- The extent of a uranium plume breaking through the clay/altered sandstone interface would not exceed 0.5 m into the altered sandstone.

- The one-dimensional modelling results are in good agreement with most measured parameters.

- At the dissolved-O_2 levels measured in the ore-zone waters, the modelling predicts that oxidation of the clay/ore contact over a distance of 1 m is reasonable.

- The low-permeability clay zone surrounding the mineralization is the most important parameter in limiting radionuclide mass transport.

4.3 CONCLUSIONS

The analog studies on the Cigar Lake uranium deposit have provided valuable information and insight on a number of performance assessment aspects common to the disposal concepts in both Canada and Sweden. The important general conclusions can be summarized as follows:

1- UO_2 dissolution and stability:
   - UO_2 is stable under reducing conditions over geological time;
   - little dissolution of UO_2 occurred during 100 Ma; and
   - congruent dissolution of UO_2 is controlled by surface alteration.

2- Clay sealing:
   - clay (in this case illite) can provide effective, long-term sealing;
   - illite is stable under suitable conditions over geological time; and
   - clay is an efficient barrier to radionuclide and colloid migration.

3- Colloids:
   - colloid and particle contents in groundwater are generally lowest in competent rock and highest in friable rock;
   - only a small fraction of radionuclides in water is attached to colloids;
   - colloids can be effectively sealed in by clay-rich rocks; and
   - colloids were not important in radionuclide migration at Cigar Lake, at least on a time scale of 10^4 a.

4- Organics and Microbes:
   - low humic contents in dilute water are unlikely to play a significant role in either speciation or mobilization of radionuclides;
   - microbes can survive in radiation fields, and they can mediate in redox control and buffering; and
   - organics and microbes are unlikely to adversely affect radionuclide migration in the near field.

5- Groundwater chemistry:
   - interactions with clay minerals control the bulk composition of groundwater;
   - redox geochemistry is strongly controlled and buffered by the iron and sulpur redox couples; and
   - the evolution of groundwater compositions can be predicted by existing geochemical codes.

6- Radiolysis:
   - radiolytic-oxidation models for UO_2 dissolution appear overly conservative in SKB's current PA code; and
   - dissolved Fe^{2+} is an important scavenger of radiolytic oxidants.

7- Radionuclide migration:
   - natural hydrologic barriers and appropriate geochemical conditions in a relatively open, natural system are effective in limiting radionuclide migration over any significant distance; and
   - clay sealing is an important barrier to radionuclide migration.

4.4 References

BRUNO, J., CROSS, J.E., EIKENBERG, J., McKINLEY, I.G., READ, D., SANDINO, A. and SELLIN, P. 1990. Testing of geochemical models in the Poços de Caldas analogue study. Svensk Kärnbränslehåntering AB Tech. Rep., **TR 90-20**.

CRAMER, J.J. 1986. A natural analog for a fuel waste disposal vault. In: 2nd International Conference on Radioactive Waste Management, Winnipeg, Sept. 1986. Can. Nucl. Soc. Proc., 697-702.

CROSS, J.E. and EWART, F.T. 1990. HATCHES - A thermodynamic database and management system. Radiochim. Acta, **52/53**, 421-422.

CUMMING, G.L. and KRSTIC, D. 1992. The age of unconformity-related uranium mineralization in the Athabasca Basin, northern Saskatchewan. Can. J. Earth Sci., **29**, 1623-1639.

GARISTO, N.C. and GARISTO, F. 1986. The dissolution of UO_2: a thermodynamic approach. Nucl. Chem. Waste Manag., **6**, 203-211.

JOHNSON, L.H., LENEVEU, D.M., SHOESMITH, D.W., OSCARSON, D.W., GRAY, M.N., LEMIRE, R.J. and GARISTO, N.C. 1994. The disposal of Canada's nuclear fuel wastes: The vault model for postclosure assessment. Atomic Energy of Canada Ltd. Rep., **AECL-10714, COG-93-4**.

PARKHURST, D.L., THORSTENSON, D.C. and PLUMMER, L.N. 1980. PHREEQE - a computer program for geochemical calculations. U.S. Geol. Surv. Water-Resour. Invest., **80-96** (revised 1985), 193p.

PERCIVAL, J.B. 1990. Clay mineralogy, geochemistry and partitioning of uranium within the alteration halo of the Cigar Lake uranium deposit, Saskatchewan, Canada. Carleton Univ., Ottawa, Canada. PhD Thesis, 343p.

PUIGDOMÈNECH, I. and BRUNO, J. 1991. Plutonium solubilities. Svensk Kärnbränslehåntering AB Tech. Rep., **TR 91-04**.

SHOESMITH, D.W. and SUNDER, S. 1991. An electrochemistry-based model for the dissolution of UO_2. Atomic Energy of Canada Ltd. Report, **AECL-10488**.

SKB 1992. Final disposal of spent nuclear fuel. SKB-91. Importance of bedrock for safety. Swedish Nuclear Fuel Waste Management Co., SKB Tech. Rep., **TR 92-20**.

SUNDER, S., TAYLOR, P. and CRAMER, J.J. 1988. XPS and XRD studies of uranium rich minerals from Cigar Lake, Saskatchewan. In: Proc. 11th Symp. Scientific Basis for Nuclear Waste Management. Mater. Res. Soc. Proc., **112**, 465-472.

SUNDER, S., CRAMER, J.J. and MILLER, N.H. 1992. X-Ray Photo-electron Spectroscopic study of uranium minerals from the Cigar Lake uranium deposit. In: Proc. 15th Symp. Scientific Basis for Nuclear Waste Management. Mater. Res. Soc. Proc., **257**, 449-457.

VILKS, P., CRAMER, J.J., SHEWCHUK, T.A. and LAROCQUE, J.P.A. 1988. Colloid and particulate matter studies in the Cigar Lake natural-analog program. Radiochimica Acta **44/45**, 305-310.

VILKS, P., CRAMER, J.J., BACHINSKI, D.B., DOERN, D.C. and MILLER, H.G. 1993. Studies of colloids and suspended particles in the Cigar Lake uranium deposit. Appl. Geochem., **8**, 605-616.

5. ACKNOWLEDGEMENTS

The natural analog studies at Cigar Lake were carried out as part of the research programs for the safe management of nuclear fuel wastes, conducted in Canada by AECL Research (AECL), in Sweden by the Swedish Nuclear Fuel and Waste Management Co. (SKB) and in the U.S.A. by the United States Department of Energy (USDOE).

The Canadian nuclear fuel waste management program is jointly funded by AECL Research and Ontario Hydro under the auspices of the CANDU Owners Group.

The Swedish nuclear fuel waste management program is jointly funded by the Swedish nuclear power utilities.

The study of the nuclear reaction product geochemistry by the Los Alamos National Laboratory is funded by the USDOE.

The natural analog studies at Cigar Lake were made possible through the generous cooperation and support of the Cigar Lake Mining Corp. (CLMC), which is jointly owned by Cameco Resources Ltd., Cogema Resources Inc., Idemitsu Uranium Exploration Canada Ltd., Corona Grande (a wholly owned subsidiary of Cogema Resources Inc.) and Korea Electric Power Corp..

The authors wish to thank CLMC's staff and owners for their cooperation, support and many fruitful discussions.

6. LIST OF CONTRIBUTORS

Name	Organization	Location
Ruben Aguilar	Los Alamos Nat. Lab.	Los Alamos, NM, USA
Bert Allard	Linköping University	Linköping, Sweden
Moses Attrep	Los Alamos Nat. Lab.	Los Alamos, NM, USA
Don Bachinski	AECL Research	Pinawa, MB, Canada
Jordi Bruno	MBT Tecnología Ambiental	Cerdanyola, Spain
Ignasi Casas	MBT Tecnología Ambiental	Cerdanyola, Spain
Neil Chapman	Intera	Melton Mowbray, UK
Hilbert Christensen	Studsvik Nuclear	Studsvik, Sweden
Jack Cornett	AECL Research	Chalk River, ON, Canada
Jan Cramer	AECL Research	Pinawa, MB, Canada
David Curtis	Los Alamos Nat. Lab.	Los Alamos, NM, USA
Paul Dixon	Los Alamos Nat. Lab.	Los Alamos, NM, USA
James Ephraim	Linköping University	Linköping, Sweden
Rodney Ewing	Univ. of New Mexico	Albuquerque, NM, USA
June Fabryka-Martin	Los Alamos Nat. Lab.	Los Alamos, NM, USA
A.J. Francis	Brookhaven Nat. Lab.	Upton, NY, USA
Janusz Janeczek	Univ. of New Mexico	Albuquerque, NM, USA
David Kettlewell	AECL Research	Pinawa, MB, Canada
Jinsong Liu	Royal Inst. of Technology	Stockholm, Sweden
Angus MacKenzie	SURRC	East Kilbride, Scotland
Hans Miller	AECL Research	Pinawa, MB, Canada
Ivars Neretnieks	Royal Inst. of Technology	Stockholm, Sweden
Wayne Nesbitt	Univ. of Western Ontario	London, ON, Canada
Jeanne Percival	Geological Survey of Canada	Ottawa, ON, Canada
Catharina Petterson	Linköping University	Linköping, Sweden
Fred Roensch	Los Alamos Nat. Lab.	Los Alamos, NM, USA
Don Rokop	Los Alamos Nat. Lab.	Los Alamos, NM, USA
John Smellie	Conterra AB	Uppsala, Sweden
Doug Stevenson	AECL Research	Pinawa, MB, Canada
Simcha Stroes-Gascoyne	AECL Research	Pinawa, MB, Canada
Sham Sunder	AECL Research	Pinawa, MB, Canada
Peter Taylor	AECL Research	Pinawa, MB, Canada
Peter Vilks	AECL Research	Pinawa, MB, Canada
Anders Winberg	Conterra AB	Mölndal, Sweden
Ji-Wei Yu	Royal Inst. of Technology	Stockholm, Sweden

List of SKB reports

Annual Reports

1977-78
TR 121
KBS Technical Reports 1 – 120
Summaries
Stockholm, May 1979

1979
TR 79-28
The KBS Annual Report 1979
KBS Technical Reports 79-01 – 79-27
Summaries
Stockholm, March 1980

1980
TR 80-26
The KBS Annual Report 1980
KBS Technical Reports 80-01 – 80-25
Summaries
Stockholm, March 1981

1981
TR 81-17
The KBS Annual Report 1981
KBS Technical Reports 81-01 – 81-16
Summaries
Stockholm, April 1982

1982
TR 82-28
The KBS Annual Report 1982
KBS Technical Reports 82-01 – 82-27
Summaries
Stockholm, July 1983

1983
TR 83-77
The KBS Annual Report 1983
KBS Technical Reports 83-01 – 83-76
Summaries
Stockholm, June 1984

1984
TR 85-01
Annual Research and Development Report 1984
Including Summaries of Technical Reports Issued during 1984. (Technical Reports 84-01 – 84-19)
Stockholm, June 1985

1985
TR 85-20
Annual Research and Development Report 1985
Including Summaries of Technical Reports Issued during 1985. (Technical Reports 85-01 – 85-19)
Stockholm, May 1986

1986
TR 86-31
SKB Annual Report 1986
Including Summaries of Technical Reports Issued during 1986
Stockholm, May 1987

1987
TR 87-33
SKB Annual Report 1987
Including Summaries of Technical Reports Issued during 1987
Stockholm, May 1988

1988
TR 88-32
SKB Annual Report 1988
Including Summaries of Technical Reports Issued during 1988
Stockholm, May 1989

1989
TR 89-40
SKB Annual Report 1989
Including Summaries of Technical Reports Issued during 1989
Stockholm, May 1990

1990
TR 90-46
SKB Annual Report 1990
Including Summaries of Technical Reports Issued during 1990
Stockholm, May 1991

1991
TR 91-64
SKB Annual Report 1991
Including Summaries of Technical Reports Issued during 1991
Stockholm, April 1992

1992
TR 92-46
SKB Annual Report 1992
Including Summaries of Technical Reports Issued during 1992
Stockholm, May 1993

Technical Reports
List of SKB Technical Reports 1994

TR 94-01
Anaerobic oxidation of carbon steel in granitic groundwaters: A review of the relevant literature
N Platts, D J Blackwood, C C Naish
AEA Technology, UK
February 1994

TR 94-02
Time evolution of dissolved oxygen and redox conditions in a HLW repository
Paul Wersin, Kastriot Spahiu, Jordi Bruno
MBT Technología Ambiental, Cerdanyola, Spain
February 1994

TR 94-03
Reassessment of seismic reflection data from the Finnsjön study site and prospectives for future surveys
Calin Cosma[1], Christopher Juhlin[2], Olle Olsson[3]
[1] Vibrometric Oy, Helsinki, Finland
[2] Section for Solid Earth Physics, Department of Geophysics, Uppsala University, Sweden
[3] Conterra AB, Uppsala, Sweden
February 1994